Synthesis, Structure, and Reactivity of New Palladium(III) Complexes

Dissertation Advisor: Professor Tobias Ritter Michael Glenn Campbell

Synthesis, Structure, and Reactivity of New Palladium(III) Complexes

Abstract

Palladium is one of the most common and versatile transition metals used in modern organometallic chemistry. The chemistry of palladium in its 0, +II, and +IV oxidation states is well-known; by comparison, the chemistry of palladium in its +III oxidation state is in its infancy. The work in this thesis involves the study of previously unknown Pd(III) complexes, including applications in materials chemistry and catalysis.

Chapter 1 describes the first examples of one-dimensional (1-D) wires supported by Pd–Pd bonds. Interest in 1-D metal chains has long been sustained by a fundamental curiosity about their optical and electrical properties because of their high anisotropy; in recent years, interest has also grown based on the potential utility of 1-D metal wires in applications such as nanotechnology, molecular sensing, and photovoltaic devices. We have developed a synthesis of solution-stable 1-D palladium wires upon oxidation of Pd(II) dimers, via self-assembly by Pd−Pd bond formation. The 1-D palladium wires described in this thesis represent the first examples of Pd(III) complexes that feature Pd–Pd bonds not supported by bridging ligands, as well as the longest known solution-stable 1-D metal chains. Additionally, we report the use of molecular control elements to alter supramolecular properties of the 1-D palladium wires, including Pd–Pd distances, porosity of the crystalline wire frameworks, and thin-film conductivity.

Chapter 2 describes the development and mechanistic investigation of a Pd(III)-catalyzed fluorination of arylboronic acid derivatives. Aryl fluorides are valuable molecules in pharmaceuticals and agrochemicals, but synthesis of functionalized aryl fluorides via C–F bond formation is challenging, and a metal-catalyzed fluorination of arylboronic acid derivatives had not been reported prior to this work. The Pd-catalyzed reaction presented here is operationally simple and amenable to multigram-scale synthesis. Evaluation of the reaction mechanism suggests a single-electron-transfer pathway, involving a Pd(III) intermediate that has been isolated and characterized.

TABLE OF CONTENTS

Acknowledgements

There are many people who deserve thanks for the help and support they have given me during my graduate studies, so I will begin by apologizing sincerely to anyone whose name I forgot to include. First I need to thank my advisor, Prof. Tobias Ritter. Tobias has not only given me interesting projects, but also allowed me a great deal of freedom to direct my own research, which has been both challenging and rewarding. While Tobias has always been forthcoming with advice, one of his greatest strengths as an advisor is that he is more than happy to have students disagree with him, and I have learned a great deal from disagreeing with Tobias (especially when I ended up being wrong in the end).

I have had the good fortune to work alongside so many talented and helpful people, a great many of whose names appear on the publications that resulted from the work described in this thesis. I have made my best effort to thank them indivudually throughout the Results and Discussion section, but I want to thank them all together here as well: Dave Powers, Jean Raynaud, Ping Xie, Anthony Mazzotti, Pingping Tang, Jennifer Murphy, Sarah Parker, Charles Reese, and Jonas Börgel. Eunsung Lee's experimental skills and positive attitude were a constant inspiration, and I have to thank him for teaching me everything I know about DFT. Michael Graham was a very talented undergraduate student that I had the pleasure of mentoring, and who contributed significantly to the Pd wires project. I also need to thank Greg Boursalian, Jochen Brandt, and Connie Neumann for many helpful and enjoyable discussions. The Ritter group has been a great place to work over the years, thanks in large part to the company of my colleagues past and present, so thanks to Gary, Jessica, Takeru, Allie, Johannes,

Greg, Heejun, Andrew, Ming, Erica, Filippo, Martin, and all of the other Ritter group alumni.

A few other people at Harvard deserve individual thanks: Dr. Shao-Liang Zheng has been an incredible resource for all things X-ray crystallography, and has taught me so many useful skills. Dr. Shaw Huang and Bill Collins have always been friendly and helpful, especially during the long hours of EPR troubleshooting when the darn helium cryostat just wouldn't work. Chris Perry has helped me ship fragile, air- and temperature-sensitive samples all over the world, and Robert at the LISE café has always been a friendly (though sarcastic) face during all of those much-needed coffee breaks.

My chemistry career began way back during my sophomore year of high scool, in Mary Fuller's CP Chemistry class. Ms. Fuller's excitement and enthusiasm about science has always been an inspiration. I have received an abundance of support and encouragement from Ms. Fuller, and I can honestly say that without her, I would not be where I am today. I was also lucky enough to have a wonderful undergraduate research advisor, Dr. Jesse More, who always gave honest advice, and made sure to send me off to grad school with good experimental techniques.

Last, but most importantly, thanks to my family for all of their love and support over the years. My parents, Glenn and Suzanne, have always given me encouragement and understanding, and I can't thank them enough. My girlfriend Weike gave me a good reason to leave lab early on some nights (sorry, Tobias!), and is so good at keeping me grounded. I'm not sure how I would have made it through grad school without her.

List of abbreviations:

Ac: Acetyl
Ag: silver
Ar: Aryl
bhq: benzo[*h*]quinoline
bpy: 2,2'-dipyridyl
Bu: Butyl
cat: Catalyst
CPE: controlled potential electrolysis
Cu: copper
CV: cyclic voltammetry
DCM: dichloromethane
DFT: density functional theory
DMF: *N*, *N*-Dimethylformamide
EPR: electron paramagnetic resonance
equiv: equivalent(s)
Fc: ferrocene
h: hour
Me: Methyl
MIDA: N-methyl-iminodiacetic acid
min: minute
MO: molecular orbital
NIR: near-infrared
NMR: nuclear magnetic resonance
Pd: palladium
Ph: Phenyl
pin: Pinacol
Py: Pyridine
TBA: tetra-n-butylammonium
TD-DFT: time-dependent density functional theory
TEMPO: 2,2,6,6-tetramethyl-1-piperidinyloxy radical
terpy: 2,2′:6′,2″-terpyridine
Tf: Trifluoromethanesulfonyl
TMS: trimethylsilyl
UV-vis: ultraviolet-visible

NOTE: Portions of this dissertation are reproduced, with permission, from the following publications.

1) **M.G. Campbell**, D.C. Powers, J. Raynaud, M.J. Graham, P. Xie, E. Lee, T. Ritter "Synthesis and structure of solution-stable one-dimensional palladium wires" *Nature Chem.* **2011**, *3*, 949–953.
2) A.R. Mazzotti‡, **M.G. Campbell**‡, P. Tang, J.M. Murphy, T. Ritter "Palladium(III)-Catalyzed Fluorination of Arylboronic Acid Derivatives" *J. Am. Chem. Soc.* **2013**, *135*, 14012–14015.
3) **M.G. Campbell**, S.-L. Zheng, T. Ritter "One-Dimensional Palladium Wires: Influence of Molecular Changes on Supramolecular Structure" *Inorg. Chem.* **2013**, *52*, 13295-13297.
4) **M.G. Campbell**, T. Ritter "Late-Stage Fluorination: From Fundamentals to Application" *Org. ProcessRes. Dev.* **2014**, *Submitted* (Invited Review).

Additional work performed during my Ph.D. studies, not included in this dissertation, has been published in:

1) J.B. Raynaud, **M.G. Campbell**, S.E. Parker, C.N. Reese, T. Ritter "A Practical Synthesis of COD Featuring a Well-Defined Iron Catalyst" *Submitted.*
2) J. Börgel‡, **M.G. Campbell**‡, T. Ritter "Revising the textbooks: d-orbital splitting diagrams for square planar transition metal complexes" *In Preparation.*

‡ Denotes equal author contributions.

INTRODUCTION

1. Palladium(III) Complexes[1]

The chemistry of palladium in its 0, +II, and +IV oxidation states is well-known;[2] by comparison, the chemistry of palladium in its +III oxidation state is in its infancy.[3] This section aims to provide an overview of structure and bonding concepts for Pd(III) complexes, and selected examples of stoichiometric and catalytic reactivity from organopalladium(III) complexes.

1.1 Mononuclear Palladium(III) Complexes

The first unambiguous structural characterization of coordination complexes that feature a d^7 Pd(III) center was reported in 1987 and 1988 (Fig. I.1).[4,5] While square planar and octahedral geometries are typically observed for d^8 Pd(II) and d^6 Pd(IV) complexes, respectively,[6] d^7 Pd(III) complexes are expected to exhibit a Jahn-Teller distorted octahedral geometry with an unpaired electron in a $4d_{z^2}$-based orbital (Fig. I.2).[7]

---

[1] Portions of this section have been adapted, with permission, from Powers, D. C.; Ritter, T. *Top Organomet Chem* **2011**, *503*, 129–156.

[2] Negishi, E.; ed. *Handbook of Organopalladium Chemistry for Organic Synthesis*; John Wiley & Sons, Inc.: New York, 2002; Vol. 1.

[3] Mirica, L. M.; Khusnutdinova, J. R. *Coord. Chem. Rev.* **2012**, *257*, 299–314.

[4] (a) Blake, A. J.; Holder, A. J.; Hyde, T. I.; Roberts, Y. V.; Lavery, A. J.; Schröder, M. *J. Organomet. Chem.* **1987**, *323*, 261-270. (b) Blake, A. J.; Holder, A. J.; Hyde, T. I.; Schröder, M. *J. Chem. Soc., Chem. Commun.* **1987**, 987-988. (c) Matsumoto, M.; Itoh, M.; Funahashi, S.; Takagi, H. D. *Can. J. Chem.* **1999**, *77*, 1638-1647.

[5] Blake, A. J.; Gordon, L. M.; Holder, A. J.; Hyde, T. I.; Reid, G.; Schröder, M. *J. Chem. Soc., Chem. Commun.* **1988**, 1452-1454.

[6] Albright, T. A. *Tetrahedron* **1982**, *38*, 1339-1388.

[7] Miessler, G. L.; Tarr, D. A. *Inorganic Chemistry*; 3rd ed.; Pearson Education, Inc.: Upper Saddle River, New Jersey, 2004.

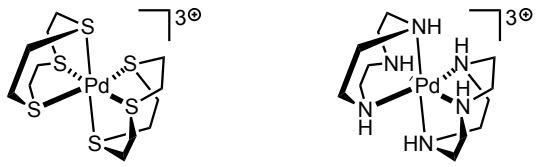

Figure I.1. The first strucurally characterized coordination complexes of Pd(III).

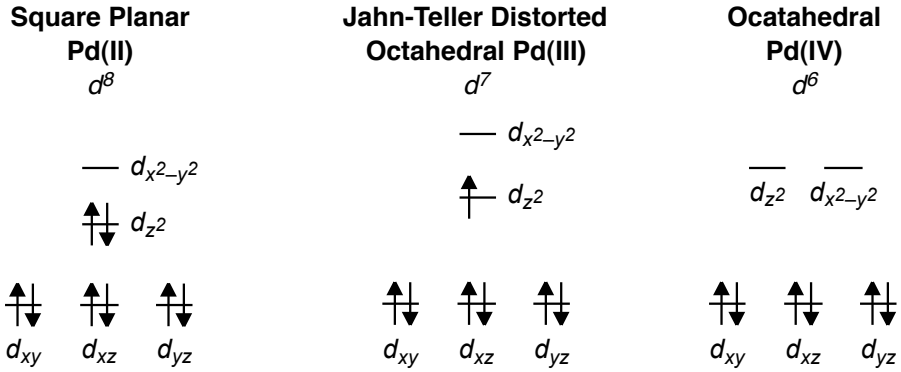

Figure I.2. Simplified molecular orbital diagrams for typical Pd(II), Pd(III), and Pd(IV) coordination complexes.

The first examples of well-defined mononuclear organopalladium(III) complexes were reported in 2010 by the Mirica group.[8] The macrocyclic tetradentate ligand N,N′-di-tert-butyl-2,11-diaza[3.3](2,6)pyridinophane ("N4") was used to prepare the square planar Pd(II) complexes (N4)Pd(II)MeCl, (N4)Pd(II)PhCl, and (N4)Pd(II)Me_2. The corresponding Pd(III) complexes were then accessed via either controlled potential electrolysis (CPE) or chemical oxidation with single-electron oxidants (Fig. I.3).

[8] Khusnutdinova, J. R.; Rath, N. P.; Mirica, L. M. *J. Am. Chem. Soc.* **2010**, *132*, 7303-7305.

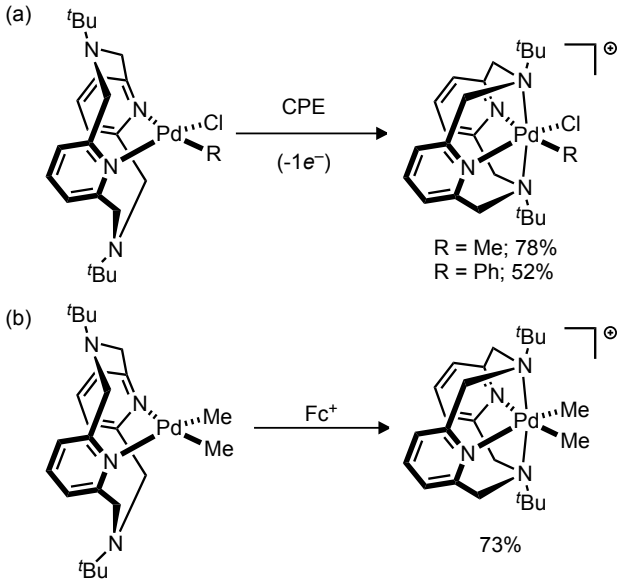

Figure I.3. Synthesis of the first well-defined organopalladium(III) complexes, via (a) electrochemical or (b) chemical oxidation.

Photolysis of $[(N4)Pd(III)MeCl]^+$ produced a mixture of ethane, methane, and methyl chloride, as well as an isolable Pd(II) product (Fig. I.4a). Addition of the radical scavenger TEMPO suppressed formation of the organic products, affording instead only TEMPO–Me (Fig. I.4b). These observations suggest a radical mechanism involving Pd–C bond homolysis from $[(N4)Pd(III)MeCl]^+$, and mechanistic studies including isotopic labeling experiments suggest the possibiliy of a reaction pathway involving reductive elimination from a transiently generated Pd(IV) intermediate.[9] In related studies, (N2S2)Pd(II)MeX complexes (N2S2 = 2,11-dithia[3.3](2,6)pyridinophane; X = Br or Cl) were synthesized, and ethane and Me–X were observed upon one-electron oxidation of the Pd(II) complexes.[10] For complexes with the N2S2 ligand, mechanistic studies

[9] Tang, F.; Qu, F.; Khusnutdinova, J. R.; Rath, N. P.; Mirica, L. M. *Dalton Trans.* **2012**, *41*, 14046.

[10] Luo, J.; Rath, N. P.; Mirica, L. M. *Organometallics* **2013**, *32*, 3343–3353.

suggested methyl group transfer/disproportionation from a short-lived Pd(III) species and subsequent reductive elimination from a Pd(IV) intermediate.

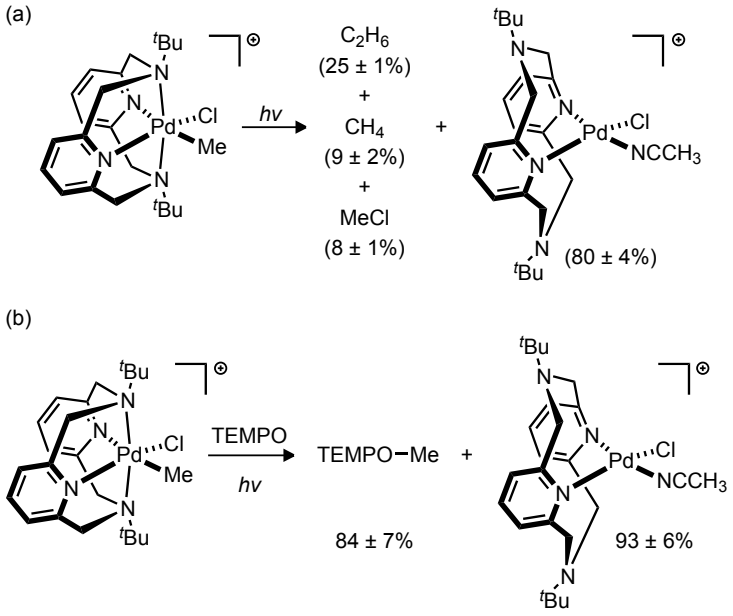

Figure I.4. (a) Formation of ethane, methane, and methyl chloride upon photolysis of $[(N4)Pd(III)MeCl]^{+}$, and (b) suppresion of organic product formation upon addition of TEMPO.

More recently, the Mirica group has also reported the aerobic oxidation of $(N4)Pd(II)Me_2$, affording ethane via the intermediacy of Pd(III) and Pd(IV) intermediates (Fig. I.5).[11] Mechanistic studies indicate that oxidation occurs through the formation of a Pd(III)-superoxide intermediate, and that C–C reductive elimination occurs from Pd(IV).[12,13]

[11] Khusnutdinova, J. R.; Rath, N. P.; Mirica, L. M. *J. Am. Chem. Soc.* **2012**, *134*, 2414–2422.

[12] Khusnutdinova, J. R.; Qu, F.; Zhang, Y.; Rath, N. P.; Mirica, L. M. *Organometallics* **2012**, *31*, 4627–4630.

[13] Tang, F.; Zhang, Y.; Rath, N. P.; Mirica, L. M. *Organometallics* **2012**, *31*, 6690–6696.

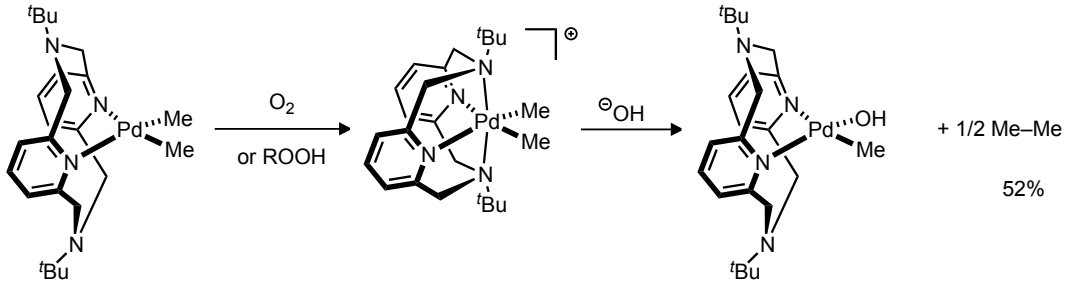

Figure I.5. Aerobic oxidation of (N4)Pd(II)Me_2, affording ethane via Pd(III) and Pd(IV) intermediates.

In 2011, a series of Pd(III) complexes were reported featuring the tridentate ligand N,N′,N″-trimethyl-1,4,7-triazacyclononane (Me_3tacn), in which the Pd(III) centers are bridged by a single μ^2 halide ligand (Fig. I.6).[14] The Pd(III) dimers could be readily accessed either by electrochemical oxidation of the corresponding Pd(II) complexes, or by stoichiometric combination of the appropriate Pd(II) and Pd(IV) precursors.

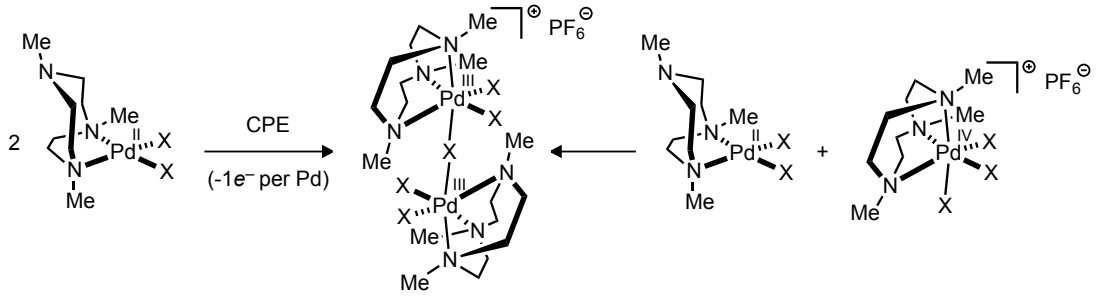

Figure I.6. Synthesis and structure of dipalladium(III) complexes featuring a single bridging halide ligand (X = Cl, Br).

1.2 Dinuclear Palladium(III) Complexes

When two square planar metal centers are held together in a face-to-face orientation, such as by bridging ligands, mixing of the metal-based d orbitals can occur to form a set

[14] Khusnutdinova, J. R.; Rath, N. P.; Mirica, L. M. *Angew. Chem. Int. Ed.* **2011**, *50*, 5532–5536.

of metal–metal bonding orbitals.[15] The metal–metal bonding interactions can be described in terms of a simplified MO diagram, as shown in Figure I.7. For a dimeric Pd(II) complex, full population of both the bonding and antibonding orbital sets results in a Pd–Pd bond order of zero.[16] One- and two-electron oxidation removes electrons from a σ^*_{Pd-Pd} orbital, resulting in Pd–Pd bond orders of 0.5 and 1, respectively.

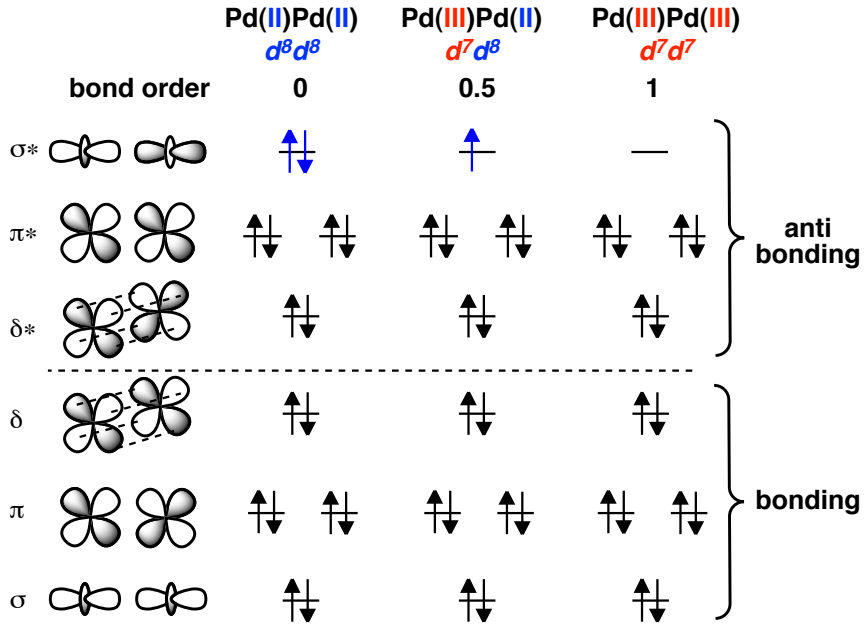

Figure I.7. Simplified MO diagram for Pd–Pd bonding interactions in a dimeric Pd complex.

Only a few examples of well-defined d^7d^8 dipalladium complexes have been reported, with average Pd oxidation state +2.5 and a Pd–Pd bond order of 0.5.[17] In 1988, Bear reported the EPR spectrum of an amidinate-bridged dinuclear Pd(2.5) complex, prepared

[15] Cotton, F. A.; Murillo, C. A.; Walton, R. A.; eds. *Multiple Bonds Between Metal Atoms*; 3rd ed.; Springer Science and Business Media, Inc.: New York, 2005.

[16] Cotton, F. A.; Matusz, M.; Poli, R.; Feng, X. *J. Am. Chem. Soc.* **1988**, *110*, 1144-1154.

[17] Berry, J. F.; Cotton, F. A.; Ibragimov, S. A.; Murillo, C. A.; Wang, X. *Inorg. Chem.* **2005**, *44*, 6129-6137.

by electrochemical oxidation of the corresponding Pd(II) dimer (Fig. I.8a).[18] In 2007, Cotton reported the first crystallographically characterized Pd(2.5) complex (Fig. I.8b).[19] Both complexes are paramagnetic and have EPR spectra consistent with a metal-based oxidation. The metal–metal distance in the crystallographically characterized Pd(2.5) dimer is 0.052 Å shorter than in the corresponding Pd(II) complex, consistent with a Pd–Pd bond order of 0.5.

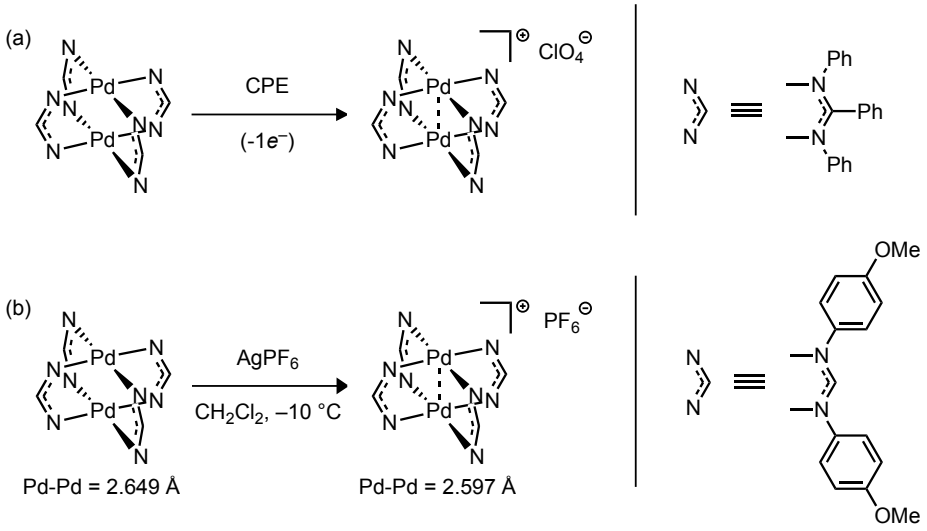

Figure I.8. Well-defined examples of dipalladium(2.5) complexes, with a Pd–Pd bond order of 0.5.

There are conflicting reports regarding the identity of the first dinuclear Pd(III) complex. In a 1993 review article, Umakoshi described the oxidation of a dinuclear Pd(II) complex in which the two Pd centers were bridged by four pyridine-2-thiloate ligands (Pd–Pd = 2.68 Å) to a dinuclear Pd(III) complex (Pd–Pd = 2.53 Å) with $PhICl_2$

[18] Yao, C. L.; He, L. P.; Korp, J. D.; Bear, J. L. *Inorg. Chem.* **1988**, *27*, 4389-4395.

[19] Berry, J. F.; Bill, E.; Bothe, E.; Cotton, F. A.; Dalal, N. S.; Ibragimov, S. A.; Kaur, N.; Liu, C. Y.; Murillo, C. A.; Nellutla, S.; North, J. M.; Villagrán, D. *J. Am. Chem. Soc.* **2007**, *129*, 1393-1401.

(Fig. 1.9a).[20,21] In 1998 Cotton reported the oxidation of $(hpp)_4Pd(II)$ with $PhICl_2$ (hpp = hexahydro-2*H*-pyrimido[1,2-*a*]pyrimidine), resulting in a Pd–Pd bond contraction from 2.55 Å to 2.39 Å (Fig. I.9b).[22] The dipalladium(III) complexes are diamagnetic, consistent with the formation of a spin-paired Pd–Pd σ bond.

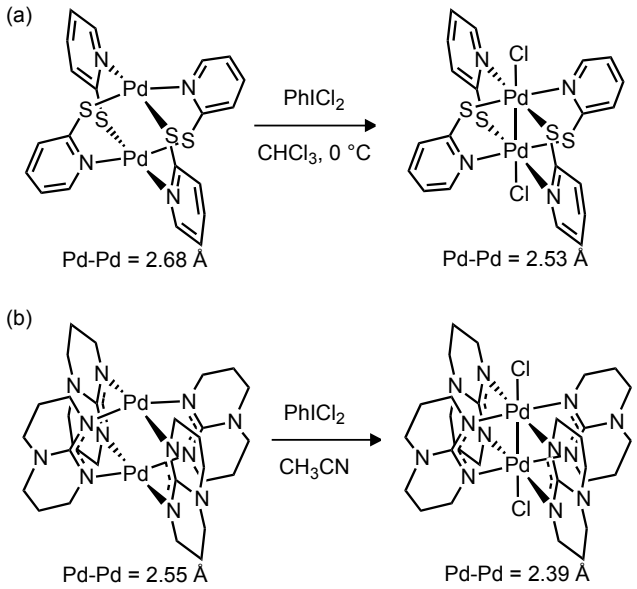

Figure I.9. The first reported dipalladium(III) complexes, with Pd–Pd single bonds.

Subsequently, Cotton *et al* published a series of stable organometallic Pd(III) complexes featuring a bridging metallated phosphine ligand (Fig. I.10).[23] More recently, the Ubeda group has reported an additional series of dipalladium(III) complexes featuring the metallated phosphine ligand shown in Figure I.10 and O,O-chelating ligands,[24] and

[20] (a) Umakoshi, K.; Kinoshita, I.; Ooi, S. *Inorg. Chim. Acta* **1987**, *127*, L41-L42. (b) Umakoshi, K.; Ichimura, A.; Kinoshita, I.; Ooi, S. *Inorg. Chem.* **1990**, *29*, 4005-4010.

[21] Umakoshi, K.; Sasaki, Y. *Adv. Inorg. Chem.* **1993**, *40*, 187-239.

[22] Cotton, F. A.; Gu, J.; Murillo, C. A.; Timmons, D. J. *J. Am. Chem. Soc.* **1998**, *120*, 13280-13281.

[23] Cotton, F. A.; Koshevoy, I. O.; Lahuerta, P.; Murillo, C. A.; Sanaú, M.; Ubeda, M. A.; Zhao, Q. *J. Am. Chem. Soc.* **2006**, *128*, 13674–13675.

[24] Ibáñez, S.; Estevan, F.; Hirva, P.; Sanaú, M.; Ubeda, M. A. *Organometallics* **2012**, *31*, 8098–8108.

the Vicente group has reported the first example of an Pd(III) dimer supported by a bridging acyclic diaminocarbene ligand.[25]

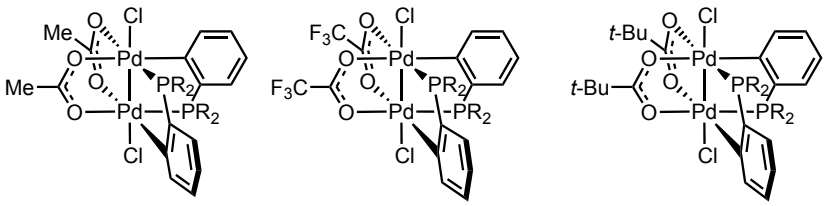

Figure I.10. Early examples of organometallic dipalladium(III) complexes (R = Ph).

In 2009, our group reported the first example of reductive elimination from a well-defined organopalladium(III) complex (Fig. I.11), and implicated such a transformation in Pd-catalyzed oxidative C–H functionalization reactions (*vide infra*, section 1.3).[26] It was shown through a combination of experimental and computational studies that metal–metal bonding in Pd(III) complexes could be used to lower activation barriers for difficult organometallic transformations.[27]

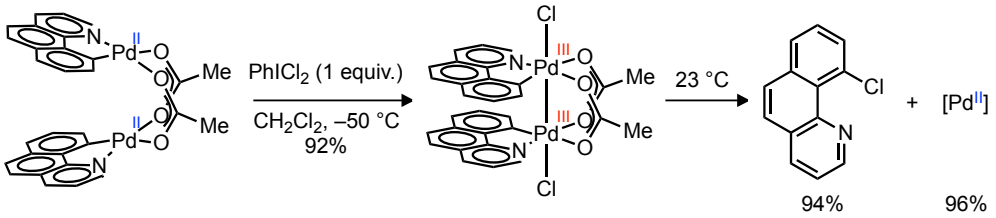

Figure I.11. Reductive elimination from a well-defined organopalladium(III) dimer.

1.3 Palladium(III) Complexes in Catalysis

While palladium complexes are ubiquitous as catalysts in modern organometallic chemistry,[2] the potential role of Pd(III) intermediates in catalysis has only recently been

[25] Martinez-Martinez, A.-J.; Chicote, M.-T.; Bautista, D.; Vicente, J. *Organometallics* **2012**, *31*, 3711–3719.

[26] Powers, D. C.; Ritter, T. *Nature Chemistry* **2009**, *1*, 302–309.

[27] Powers, D. C.; Benitez, D.; Tkatchouk, E.; Goddard, W. A., III; Ritter, T. *J. Am. Chem. Soc.* **2010**, *132*, 14092–14103.

studied.[1,3] There are few examples in which the intermediacy of Pd(III) complexes is postulated, and even fewer examples in which a Pd(III) intermediate has been observed or isolated.

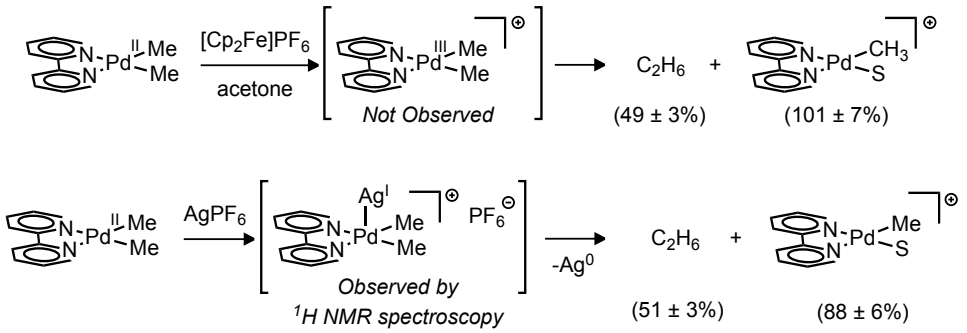

Figure I.12. Treatment of (bpy)Pd(II)Me_2 with Fc^+ or $AgPF_6$ affords ethane and a cationic Pd(II) product (S = acetone).

Pd-catalyzed oxidative C–H coupling reactions are frequently carried out in the presence of potential single-electron oxidants, such as Ag(I) salts.[28] Therefore, the possibility of one-electron oxidation of known Pd(II) intermediates to Pd(III) intermediates has been experimentally probed. The oxidatively induced reductive coupling of methyl ligands to afford ethane from a Pd(II) dimethyl complex was studied in 2009 by Mayer and Sanford.[29] Treatment of (bpy)Pd(II)Me_2 with ferrocenium hexafluorophosphate ($[Cp_2Fe]PF_6$; Fc^+), an outer-sphere, single-electron oxidant, led to the formation of ethane along with a cationic Pd(II) complex (Fig. I.12, top). Based on

[28] (a) Chen, X.; Goodhue, C. E.; Yu, J.-Q. *J. Am. Chem. Soc.* **2006**, *128*, 12634-12635. (b) Takahashi, M.; Masui, K.; Sekiguchi, H.; Kobayashi, N.; Mori, A.; Funahashi, M.; Tamaoki, N. *J. Am. Chem. Soc.* **2006**, *128*, 10930-10933. (c) Campeau, L. C.; Parisien, M.; Jean, A.; Fagnou, K. *J. Am. Chem. Soc.* **2006**, *128*, 581-590. (d) Stuart, D. R.; Villemure, E.; Fagnou, K. *J. Am. Chem. Soc.* **2007**, *129*, 12072-12073. (e) Cho, S. H.; Hwang, S. J.; Chang, S. *J. Am. Chem. Soc.* **2008**, *130*, 9254-9256. (f) Potavathri, S.; Dumas, A. S.; Dwight, T. A.; Naumiec, G. R.; Hammann, J. M.; DeBoef, B. *Tetrahedron Lett.* **2008**, *49*, 4050-4053. (g) Lebrasseur, N.; Larrosa, I. *J. Am. Chem. Soc.* **2008**, *130*, 2926-2927. (h) René, O.; Fagnou, K. *Org. Lett.* **2010**, *12*, 2116-2119.

[29] Lanci, M. P.; Remy, M. S.; Kaminsky, W.; Mayer, J. M.; Sanford, M. S. *J. Am. Chem. Soc.* **2009**, *131*, 15618-15620.

the electrochemical study of a closely related bis-mesityl Pd(II) complex,[30] the observed ethane formation was proposed to proceed via initial single-electron oxidation of (bpy)Pd(II)Me_2 to a Pd(III) intermediate. The chemistry of (bpy)Pd(II)Me_2 with $AgPF_6$ was also evaluated: treatment (bpy)Pd(II)Me_2 with $AgPF_6$ resulted in the immediate formation of an intermediate that was observed by ^{1}H NMR spectroscopy, which subsequently reacted to form ethane, Ag mirror, and a cationic Pd(II) product (Fig. I.12, bottom). The authors proposed that Ag(I) acts as an inner-sphere one-electron oxidant. Initial coordination of Ag(I) to Pd(II), followed by electron transfer, would furnish the proposed Pd(III) intermediate. Disproportionation of the Pd(III) intermediate to Pd(II) and Pd(IV) complexes, followed by reductive elimination from Pd(IV), would then generate the observed reaction products. Such a reaction pathway is analagous to the reactivity proposed by the Mirica group for isolated Pd(III)Me_2 complexes (*vide supra*, section 1.1).

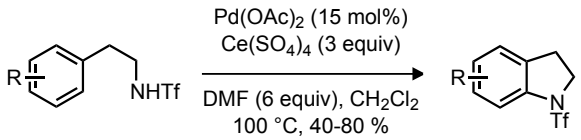

Figure I.13. Pd-catalyzed C–H amidation reported by Yu.

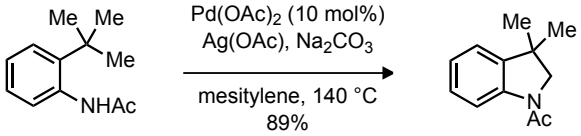

Figure I.14. Pd-catalyzed C–H amidation reported by Glorius.

[30] Klein, A.; Niemeyer, M. *Z. Anorg. Allg. Chem.* **2000**, *626*, 1191-1195.

In 2009, two reports disclosed the use of single-electron oxidants in intramolecular Pd-catalyzed C–H amidation reactions. Yu and coworkers described a Pd-catalyzed N-triflyl indoline synthesis from N-triflyl phenethylamines using single-electron oxidant $Ce(SO_4)_2$ (Fig. I.13).[31] The authors proposed that this reaction proceeds through initial oxidation of Pd(II) to Pd(III). Glorius and coworkers reported a Pd-catalyzed N-acyl indoline synthesis from N-acyl anilines in the presence of AgOAc (Fig. I.14).[32] While the authors favored a Pd(0)/Pd(II) catalysis cycle, they noted that the intermediacy of higher-valent Pd species could not be discounted given that AgOAc can serve as a single-electron oxidant.

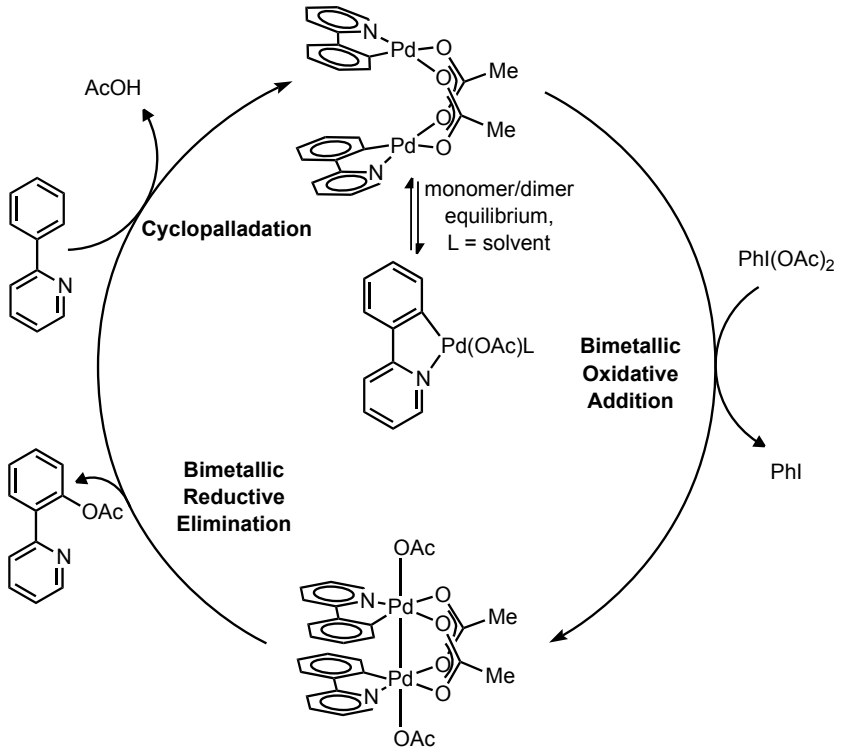

Figure I.15. Proposed bimetallic mechanism for Pd-catalyzed C–H acetoxylation, involving a dipalladium(III) intermediate that has been isolated and characterized.

[31] Mei, T.-S.; Wang, X.; Yu, J.-Q. *J. Am. Chem. Soc.* **2009**, *131*, 10806–10807.

[32] Neumann, J. J.; Rakshit, S.; Dröge, T.; Glorius, F. *Ang. Chem. Int. Ed.* **2009**, *48*, 6892-6895.

Beginning in 2009, work from our group has described the first examples of dimeric Pd(III) complexes with relevance to Pd-catalyzed oxidative C–H functionalization reactions, challenging the conventionally accepted mechanism for oxidative palladium catalysis via Pd(II)–Pd(IV) redox cycles.[26,33] Spectroscopically observed, and in some cases isolated, dipalladium(III) complexes have been implicated as relevant intermediates in a variety of C–X bond-forming catalytic reactions, including X = Cl, Br, O, and CF_3.[34,35,36,37] Kinetic and computational studies have demonstrated that the dipalladium core remains intact during both oxidative addition and reductive elimination, and that the the bimetallic reaction pathway is lower in energy as compared to a pathway involving mononuclear palladium intermediates.[27,38] A proposed mechanism for Pd-catalyzed C–H acetoxylation, involving bimetallic redox steps and an isolated Pd(III) intermediate, is shown in Figure I.15.

2. One-Dimensional Metal Wires

One-dimensional (1-D) metal chain compounds, featuring metal–metal interactions, have been studied for more than a century.[39] Interest in 1-D metal chains has long been sustained by a fundamental curiosity about their optical and electrical properties because of their high anisotropy. The 1960s and 1970s saw a flurry of research activity in 1-D metal compounds, fueled by a new theory of superconductivity put forth by W.A. Little

[33] Powers, D. C.; Ritter, T. *Acc. Chem. Res.* **2012**, *45*, 840–850.

[34] Powers, D. C.; Geibel, M. A. L.; Klein, J. E. M. N.; Ritter, T. *J. Am. Chem. Soc.* **2009**, *131*, 17050–17051.

[35] Powers, D. C.; Xiao, D. Y.; Geibel, M. A. L.; Ritter, T. *J. Am. Chem. Soc.* **2010**, *132*, 14530–14536.

[36] Powers, D. C.; Lee, E.; Ariafard, A.; Sanford, M. S.; Yates, B. F.; Canty, A. J.; Ritter, T. *J. Am. Chem. Soc.* **2012**, *134*, 12002–12009.

[37] Chuang, G. J.; Wang, W.; Lee, E.; Ritter, T. *J. Am. Chem. Soc.* **2011**, *133*, 1760–1762.

[38] Powers, D. C.; Ritter, T. *Organometallics* **2013**, *32*, 2042–2045.

[39] (a) Thomas, T. W.; Underhill, A. E. *Chem. Soc. Rev.* **1972**, *1*, 99−120. (b) Miller, J. S.; Epstein, A. J. *Prog. Inorg. Chem*. **1976**, *20*, 1−151. (c) Bera, J. K.; Dunbar, K. R. *Angew. Chem., Int. Ed*. **2002**, *41*, 4453− 4457.

in 1964.[40] Little's theory has never been experimentally verified or falsified, and predicts that 1-D conductors may, if they fulfill the correct requirements, exhibit superconductivity at or above room temperature. In recent years, interest in the field has been renewed based on the potential utility of 1-D metal wires in applications such as nanotechnology, molecular sensing, and photovoltaic devices.[41]

The brief review presented here will focus on 1-D metal wires that are supported by metal–metal bonds along the chain. A great deal of work has been done on 1-D chain compounds that do *not* fit this definition, and the interested reader is encouraged to explore the references provided below. In particular there are two categories of 1-D metal chain compounds, not reviewed here, that deserve mention: (1) ligand-supported extended metal atom chains (EMACs);[42,43] and (2) halogen-bridged metal chains, sometimes referred to as "shish-kebab polymers" or "coordination polymers."[44]

---

[40] (a) Little, W. A. *Phys. Rev. A* **1964**, *134*, 1416–1424. (b) Collman, J. P. *J. Polym. Sci., Part C.* **1970**, *29*, 133–155.

[41] (a) Swager, T. M. *Acc. Chem. Res*. **1998**, *31*, 201−207. (b) Frampton, M. J.; Anderson, H. L. *Angew. Chem., Int. Ed*. **2007**, *46*, 1028−1064. (c) Habas, S. E.; Platt, H. A. S.; van Hest, M. F. A. M.; Ginley, D. S. *Chem. Rev*. **2010**, *110*, 6571−6594. (d) Givaja, G.; Amo-Ochoa, P.; Gomez-García, C.J.; Zamora, F. *Chem.Soc.Rev*. **2011**, *41*, 115. (e) Mas-Balleste, R.; Castillo, O.; Sanz Miguel, P. J.; Olea, D.; Gomez-Herrero, J.; Zamora, F. *Eur. J. Inorg. Chem*. **2009**, *20*, 2885−2896. (f) Repko, A.; Cademartiri, L. *Can. J. Chem*. **2013**, *90*, 1032−1047. (g) Shaw, S.; Cademartiri, L. *Adv. Mater*. **2013**, DOI: 10.1002/ adma.201300850.

[42] For an excellent review on ligand-supported EMACs, see Berry, J. F. *Struct. Bond* **2010**, *136*, 1–28, and references therein.

[43] (a) Murahashi, T.; Mochizuki, E.; Kai, Y.; Kurosawa, H. *J. Am. Chem. Soc.* **1999**, *121*, 10660–10661. (b) Murahashi, T.; Shirato, K.; Fukushima, A.; Takase, K.; Suenobu, T.; Fukuzumi, S.; Ogoshi, S.; Kurosawa, H. *Nat. Chem.* **2012**, *4*, 52–58.

[44] (a) Collman, J. P.; McDevitt, J. T.; Yee, G. T.; Leidner, C. R.; McCullough, L. G.; Little, W. A.; Torrance, J. B. *Proc. Natl. Acad. Sci. U.S.A.* **1986**, *83*, 4581–4585. (b) Butler, L. G.; Zietlow, M. H.; Che, C. M.; Schaefer, W. P.; Sridhar, S.; Grunthaner, P. J.; Swanson, B. I.; Clark, R. J. H.; Gray, H. B. *J. Am. Chem. Soc.* **1988**, *110*, 1155–1162. (c) Calzolari, A.; Alexandre, S. S.; Zamora, F.; Di Felice, R. *J. Am. Chem. Soc.* **2008**, *130*, 5552–5562. (d) Givaja, G.; Amo-Ochoa, P.; Gómez-García, C. J.; Zamora, F. *Chem. Soc. Rev.* **2012**, *41*, 115–147.

2.1 Solution-Stable Oligomeric Chains

Interest in 1-D metal chain compounds began in 1908 with the discovery of a category of compounds now commonly referred to as the "Platinum Blues."[45] The platinum blues are a family of mixed-valence oligomeric chain compounds, supported by Pt–Pt bonds, and with an average Pt oxidation state between Pt(II) and Pt(III). Typically the Pt blues feature ammine ligands and bridging amidate ligands (Fig. I.16). In 1977 the first structural characterization of a Pt blue compound by X-ray crystallography was reported by Lippard *et al*.[46] The Pt blues are most frequently tetranuclear cationic chains,[47] and a few examples of octanuclear chains have been characterized.[48] Pt blues retain their oligomeric chain structure both in solution and in the solid state. This is an important, and typical, feature of the mixed-valence oligomeric chains reported to date: the same discrete chain length is preserved in solution and in the solid state. Tetranuclear Pt blue chains have not been reported to polymerize into longer metal–metal bonded chains upon crystallization.

---

[45] Hofmann, K. A.; Bugge, G. *Chem. Ber.* **1908**, *41*, 312–314.

[46] Barton, J. K.; Rabinowitz, H. N.; Szalda, D. J.; Lippard, S. J. *J. Am. Chem. Soc.* **1977**, *99*, 2827–2829.

[47] (a) Barton, J. K.; Best, S. A.; Lippard, S. J.; Walton, R. A. *J. Am. Chem. Soc.* **1978**, *100*, 3785–3788. (b) Barton, J. K.; Szalda, D. J.; Rabinowitz, H. N.; Waszczak, J. V.; Lippard, S. J. *J. Am. Chem. Soc.* **1979**, *101*, 1434–1441. (c) O'Halloran, T. V.; Roberts, M. M.; Lippard, S. J. *J. Am. Chem. Soc.* **1984**, *106*, 6427–6428. (d) O'Halloran, T. V.; Mascharak, P. K.; Williams, I. D.; Roberts, M. M.; Lippard, S. J. *Inorg. Chem.* **1987**, *26*, 1261–1270. (e) Matsumoto, K.; Watanabe, T. *J. Am. Chem. Soc.* **1986**, *108*, 1308–1309.

[48] (a) Sakai, K.; Matsumoto, K. *J. Am. Chem. Soc.* **1989**, *111*, 3074–3075. (b) Matsumoto, K.; Sakai, K.; Nishio, K.; Tokisue, Y.; Ito, R.; Nishide, T.; Shichi, Y. *J. Am. Chem. Soc.* **1992**, *114*, 8110–8118.

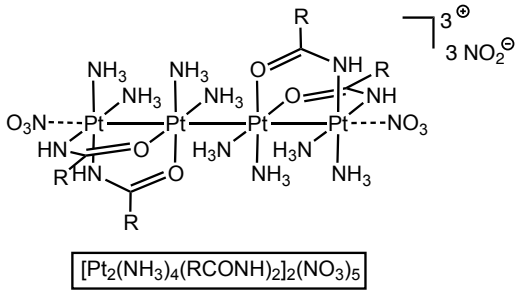

Figure I.16. Representative structure of a tetrameric "Platinum Blue" chain.

Along with the Pt blues, rhodium chain compounds are the most abundant examples of mixed-valence oligomers. Like the Pt blues, Rh oligomers feature a mixed d^7d^8 configuration of the metal centers, with an average oxidation state between Rh(I) and Rh(II). Typical ligands for mixed-valence Rh oligomers are bridging diisonitriles, such as 1,3-diisocyanopropane ("bridge") and 2,5-di-methyl-2,5-diisocyanohexane ("TMB") (Fig. I.17). Pioneering work in this area was performed by Gray and Mann, and in 1981 Gray reported the characterization of a well-defined chain containing 12 Rh atoms.[49] This dodecanuclear chain complex was the longest reported solution-stable 1-D metal chain at the time I began my Ph.D. research.[49d] Numerous related examples of mixed-valence Rh oligomers have subsequently been reported.[50] More recently, mixed-valence iridium oligomers (referred to as "Ir blues") have also been synthesized by Oro *et al*.[51]

---

[49] (a) Miskowski, V. M.; Sigal, I. S.; Mann, K. R.; Gray, H. B.l; Milder, S. J.; Hammond, G. S.; Ryason, P. R. *J. Am. Chem. Soc*. **1979**, *101*, 4384. (b) Sigal, I. S.; Mann, K. R.; Gray, H.B. *J. Am. Chem. Soc*. **1980**, *102*, 7252. (c) Mann, K. R.; DiPierro, M. J.; Gill, T. P. *J. Am. Chem. Soc*. **1980**, *102*, 3965. (d) Sigal, I. S.; Gray, H. B. *J. Am. Chem. Soc*. **1981**, *103*, 2220–2225.

[50] See the following reviews, and references therein: (a) Albers, M. O.; Robinson, D. J.; Coville, N. J. *Coord. Chem. Rev.* **1986**, *69*, 127. (b) Felthouse, T. R. *Prog. Inorg. Chem*. **1982**, *29*, 73.

[51] (a) Ciriano, M. A.; Sebastian, S.; Oro, L. A.; Tiripicchio, A.; Camellini, M. T.; Lahoz, F. J. *Angew. Chem. Int. Ed*. **1988**, *27*, 402. (b) Tejel, C.; Ciriano, M. A.; Oro, L. A. *Chem. Eur. J.* **1999**, *5*, 1131. (c) Tejel, C.; Ciriano, M. A.; Lopez, J. A.; Lahoz, F. J.; Oro, L. A. *Angew. Chem. Int. Ed.* **1998**, *37*, 1542. (d) Tejel, C.; Ciriano, M. A.; Villarroya, B. E.; Gelpi, R.; Lopez, J. A.; Lahoz, F. J.; Oro, L. A. *Angew. Chem. Int. Ed.* **2001**, *40*, 4084.

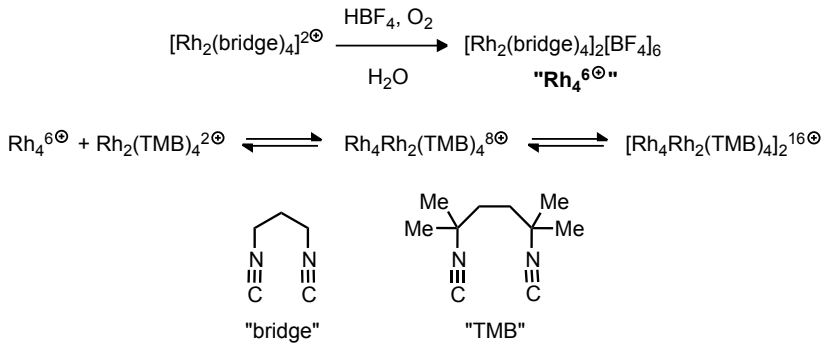

Figure I.17. Mixed-valence rhodium oligomers reported by Gray *et al*.

Synthesis of the mixed-valence d^7d^8 oligomers described above can typically be carried out by one of two procedures: combination of the correct ratio of d^7 and d^8 precursor compounds; or, partial oxidation of an appropriate d^7 precursor. Often the d^7 precursor is a dinuclear complex, such as the $[Rh_2(bridge)_4]^{2+}$ complex shown in Figure I.17. The use of dimeric building blocks as precursors is a common theme in 1-D metal chain synthesis, including the new work from our lab described in this thesis. Dinuclear complexes provide a powerful "templating" strategy, wherein the d_{z^2}-based orbitals involved in metal–metal bonding along the chain are already aligned within the dimer (see section 1.2 above).

2.2 Infinite 1-D Chains

There have been a number of reports of infinite mixed-valence d^7d^8 1-D chains of metal atoms, in the solid state, featuring metal–metal bonds. In contrast to the oligomeric chains discussed in the previous section, the infinite 1-D chains described here do not persist in solution. In all cases, the solid compounds are either highly insoluble, or dissolution in coordinating solvents results in dissociation of the chain into discrete mono- or dinuclear complexes. Historically the primary strategy for accessing infinite

1-D metal chains with metal–metal bonds has revolved around the use of mono- or dinuclear square planar transition metal complexes with sterically undemanding ligands, which often have a propensity to form "stacks" in the solid state (see section 2.3 below). Synthesis of the metal–metal bonded chains is then typically performed by either: (1) oxidation of crystalline compounds that feature "stacks" of pre-aligned metal complexes; or (2) polymerization of the building block complexes upon crystallization to form 1-D wires. In either case, the length of the 1-D wire is limited only by the size of the single crystal that is grown.

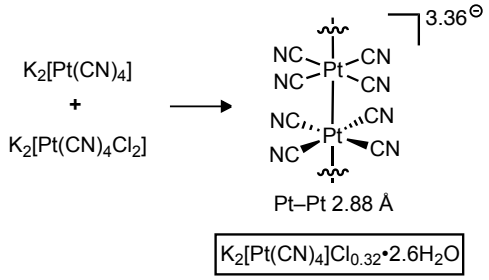

Figure I.18. Synthesis and structure of partially-oxidized tetracyanoplatinates ("Krogmann Salts").

Among the oldest infinite 1-D wires with metal–metal bonds are the partially-oxidized tetracyanoplatinates, known as "Krogmann Salts."[52] Complexes with the $[Pt(CN)_4]^{2-}$ anion were long known to crystallize in 1-D "stacks" with close Pt–Pt contacts (~3.1–3.5 Å),[53] and it was discovered that partial oxidative doping resulted in decreased Pt–Pt distances and increased electrical conductivity. Oxidative doping could be accomplished through co-crystallization of $K_2[Pt(CN)_4]$ and $K_2[Pt(CN)_4C1_2]$ in a 5:1 ratio, to give $K_2[Pt(CN)_4]Cl_{0.32}$•2.6 H_2O as needles with a metallic luster and a Pt–Pt

[52] Krogmann, K. *Angew. Chem. Int. Ed.* **1969**, *8*, 35–42, and references therein.

[53] (a) Bozorth, R. M.; Pauling, L. *Phys. Rev*. **1932**, *39*, 537. (b) Yamada, S. *Bull. Chem. Soc. Japan* **1951**, *24*, 125.

distance of 2.88 Å (Fig. I.18). A variety of related systems have also been reported, based on oxidative doping of $[M(C_2O_4)_2]^{2-}$ and $[M(dmg)_2]^{2-}$ complexes (dmg = dimethylglyoximato; M = Pt, Pd, Ni).[54,55] In many cases, the oxidative doping was performed simply by exposure of the crystalline M^{II} stacks to an oxidant such as Cl_2 gas.

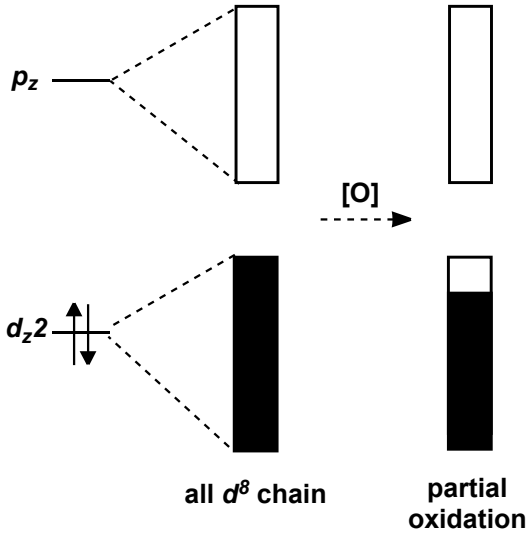

Figure I.19. Band structure model for partial oxidative doping of 1-D stacks.

The observation of poor electrical conductivity in the crystalline M^{II} stacks, along with improved conductivity upon oxidative doping, led to the development of a band structure model for 1-D metal chains, based on a simplified MO treatment (Fig. I.19).[39a] The orientation of the square-planar monomers in the 1-D stacks results in metal–metal interactions via overlap of the nd_{z2} and the (n+1)p_z orbitals on the metal centers. In the M^{II} stacks, with a d^8 configuration at the metal centers, the nd_{z2}-based orbitals are doubly occupied, resulting in a filled nd_{z2}-band in the 1-D band structure. The (n+1)p_z-based

[54] Krogmann, K.; Dodel, P. *Chem. Ber.* **1966**, *99*, 3402.

[55] (a) Godycki, L. E.; Rundle, R. E. *Acta Cryst.,* **1953**, *6*, 487. (b) Williams, D. E.; Wohlauer, G.; Rundle, R. E. *J. Am. Chem. Soc.* **1959**, *81*, 755. (c) Panattoni, C.; Frasson, E.; Zannetti, R. *Gazzetta* **1959**, *12*, 2132. (d) Banks, C. V.; Barnum, D. W. *J. Am. Chem. Soc.* **1958**, *80*, 4767. (e) Frasson, E.; Panattoni, C.; Zannetti, R. *Acta Cryst*. **1959**, *12*, 1027.

orbitals are unoccupied, resulting an an empty (n+1)p_z-band. The resulting band structure necessarily results in semiconducting or insulating behavior, due to the presence of a bandgap between the filled and unfilled bands. Partial oxidation of the d^8 metal chains, to give mixed-valence d^7d^8 chains, leads to improved electrical conductivity due to the generation of a partially-filled band.

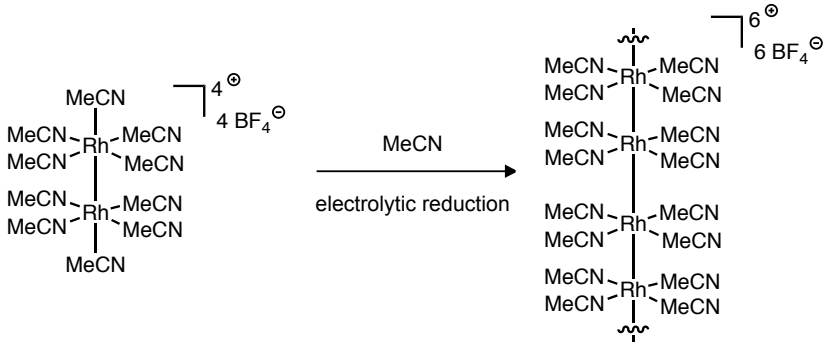

Figure I.20. Synthesis of an infinite 1-D Rh(1.5) chain by electrolytic reduction of a Rh(II) dimer.

In recent years, a new approach to infinite 1-D mixed-valence chains has been developed, based on polymerization of dinuclear precursors. The first example of such an approach came from the Dunbar group, who reported the synthesis of an infinite Rh(1.5) chain, $[\{Rh(CH_3CN)_4\}(BF_4)_{1.5}]_\infty$, obtained by slow electrolytic reduction of Rh(II) dimer $[Rh_2(CH_3CN)_{10}][BF_4]_4$ (Fig. I.20).[56] The Rh(1.5) chain exhibits alternating Rh–Rh bond distances of 2.8442(8) and 2.9277(8) Å, and single crystal electrical conductivity measurements showed semiconducting behavior.[57] Following the initial report by Dunbar, several other examples of infinite 1-D Rh chains have been reported via partial reduction of Rh(II) dimers featuring bridging carboxylate ligands, most

[56] Finniss, G. M.; Canadell, E.; Campana, C.; Dunbar, K. R. *Angew. Chem. Int. Ed.* **1996**, *35*, 2772–2774.

[57] Prater, M. E.; Pence, L. E.; Clérac, R.; Finniss, G. M.; Campana, C.; Auban-Senzier, P.; Jérome, D.; Canadell, E.; Dunbar, K. R. *J. Am. Chem. Soc.* **1999**, *121*, 8005–8016.

notably by Pruchnik *et al*.[58] In addition to electrolytic reduction, Pruchnik described chemical reduction of the dirhodium(II) precurors by refluxing in an alcohol solvent such as *i*PrOH under anaerobic conditions. The mixed-valence Rh chains display semiconducting behavior in all cases in which conductivity data has been reported. Cotton has also reported the synthesis of a mixed-valence Rh chain via solid state deposition of a mixture of $Rh_2(O_2CCF_3)_2(CO)_4$ and $Rh_2(O_2CCF_3)_4$ from the vapor phase.[59]

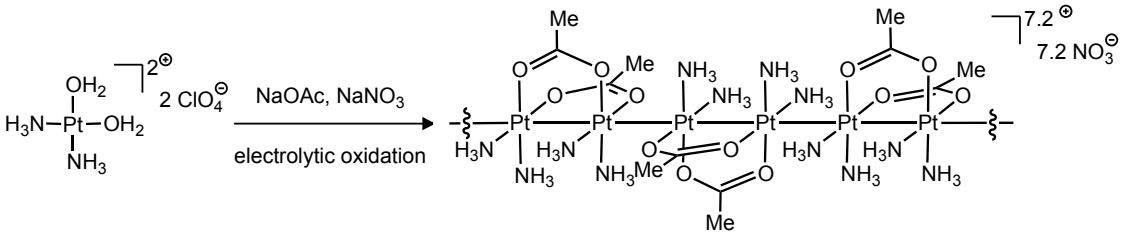

Figure I.21. Synthesis of 1-D mixed valence Pt chains, with average Pt(2.2) oxidation state, via slow electrolytic oxidation.

Slow controlled potential electrolysis has also been used by the Sakai group to prepare crystals of infinite mixed-valence Pt chains, via partial oxidation of acetate-bridged Pt(II) precursors (Fig. I.21).[60] Such 1-D Pt chains can be considered as extended analogs of the oligomeric Pt blues (*vide supra*), and are additionally stabilized by hydrogen bonding interactions between the ammine and acetate ligands of the dimeric building blocks.

---

[58] (a) Pruchnik, F. P.; Jakimowicz, P.; Ciunik, Z.; Stanislawek, K.; Oro, L. A.; Tejel, C.; Ciriano, M. A. *Inorg. Chem. Commun.* **2001**, *4*, 19–22. (b) Pruchnik, F. P.; Jutarska, A.; Ciunik, Z.; Pruchnik, M. *Inorganica Chimica Acta* **2004**, *357*, 3019–3026. (c) Lafolet, F.; Chardon-Noblat, S.; Duboc, C.; Deronzier, A.; Pruchnik, F. P.; Rak, M. *Dalton Trans.* **2008**, 2149. (d) Rak, M.; Pruchnik, F. P.; Ciunik, L. Z.; Lafolet, F.; Chardon-Noblat, S.; Deronzier, A. *Eur. J. Inorg. Chem.* **2009**, *2009*, 111–118.

[59] Cotton, F. A.; Dikarev, E. V.; Petrukhina, M. A. *J. Organomet. Chem*. **2000**, *596*, 130.

[60] (a) Sakai, K.; Takeshita, M.; Tanaka, Y.; Ue, T.; Yanagisawa, M.; Kosaka, M.; Tsubomura, T.; Ato, M.; Nakano, T. *J. Am. Chem. Soc.* **1998**, *120*, 11353–11363. (b) Sakai, K.; Ishigami, E.; Konno, Y.; Kajiwara, T.; Ito, T. *J. Am. Chem. Soc.* **2002**, *124*, 12088–12089.

2.3 Chains Supported by Metallophilic Interactions

There are several noteworthy examples of 1-D metal chains that are supported by metal–metal interactions that may not be considered formal metal–metal bonds, but are sufficiently strong to create 1-D chain structures in the solid state. Frequently such interactions between closed-shell d^8 or d^{10} metal centers are referred to as "metallophilic" interactions. For example, there are numerous reports of 1-D chains in the solid state based on monomeric Ag(I),[61] Au(I),[62] Ru(0),[63] and Os(0)[64] complexes. The closed-shell M^{II} stacks (M = Ni, Pd, Pt) that serve as precursors to the partially-oxidized chains discussed in section 2.2 may also be considered members of this category, although it is not always clear whether chain formation upon crystallization is due to metallophilic interactions or other crystal packing forces.

One case in which metallophilic interactions unambiguously result in 1-D chain formation is in d^8 Rh(I) complexes.[65] Cationic Rh(I) isocyanide complexes were studied by Gray and Mann in the 1970s, and were shown to oligomerize into at least trimetallic chains in MeCN solutions, while crystallization led to the isolation of discrete dirhodium(I) complexes (Fig. I.22, left).[66] The "metallophilicity" was explained by a

---

[61] Hou, L.; Li, D. *Inorg. Chem. Commun.* **2005**, *8*, 128–130.

[62] Zheng, S.-L.; Nygren, C. L.; Messerschmidt, M.; Coppens, P. *Chem. Commun.* **2006**, 3711.

[63] (a) Hastings, W. R.; Baird, M. C. *Inorg. Chem.* **1986**, *25*, 2913–2915. (b) Masciocchi, N.; Moret, M.; Cairati, P.; Ragaini, F.; Sironi, A. *J. Chem. Soc., Dalton Trans.* **1993**, 471. (c) Chardon-Noblat, S.; Deronzier, A.; Zsoldos, D.; Ziessel, R.; Haukka, M.; Pakkanen, T.; Ven l inen, T. *J. Chem. Soc., Dalton Trans.* **1996**, 2581. (d) Gerbaud, G.; Mouesca, J.-M.; Hediger, S.; Chardon-Noblat, S.; Lafolet, F.; Deronzier, A.; Bardet, M. *Phys. Chem. Chem. Phys.* **2010**, *12*, 15428.

[64] (a) Chardon-Noblat, S.; Deronzier, A.; Hartl, F.; van Slageren, J.; Mahabiersing, T. *Eur. J. Inorg. Chem.* **2001**, *2001*, 613–617. (b) Hartl, F.; Mahabiersing, T.; Chardon-Noblat, S.; Da Costa, P.; Deronzier, A. *Inorg. Chem.* **2004**, *43*, 7250–7258.

[65] Cotton, F. A.; Dikarev, E. V.; Petrukhina, M. A. *J. Chem. Soc., Dalton Trans.* **2000**, 4241–4243.

[66] (a) Mann, K. R.; Gordon, J. G.; Gray, H. B. *J. Am. Chem. Soc.* **1975**, *97*, 3553–3555. (b) Mann, K. R.; Lewis, N. S.; Williams, R.

symmetry-allowed mixing of $4d_{z^2}$ and $5p_z$ orbitals on the Rh centers,[66b] an explanation which was later extended to interactions in Pd(II) dimers,[67] and also to the Pd(III) chains described in this thesis (see Chapter 1.2 in the Results and Discussion section).

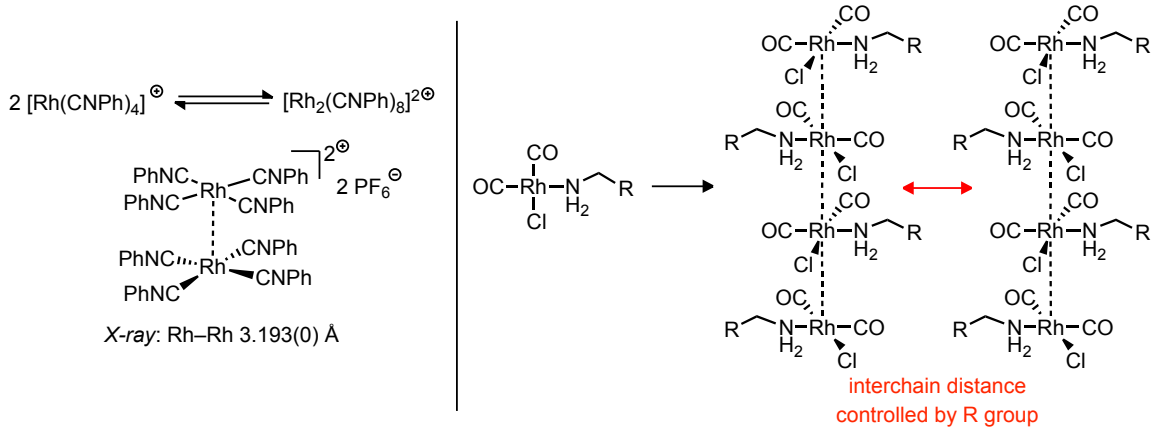

Figure I.22. Rh(I) monomers have been found to oligomerize in solution, and to sometimes form infinite 1-D chains in the solid state.

Based on DFT calculations, it has also been proposed that attractive London dispersion forces between commonly used phenyl isocyanide ligands may play a key role in aggregation of the cationic Rh(I) monomers.[68] However, recent examples of infinite Rh(I) chains based on $Rh(CO)_2Cl$(amine) building blocks clearly demonstrate that such ligand interactions are not necessary for chain formation (Fig. I.22, right).[69] The polymerization of the $Rh(CO)_2Cl$(amine) building blocks also represents a rare and valuable example of using rational synthesis to control the supramolecular properties of 1-D metal chains: based on varying the alkyl substituent on the amine ligand, the interchain distances and optical bandgap could by systematically varied in the solid state.

M.; Gray, H. B.; Gordon, J. G. *Inorg. Chem.* **1978**, *17*, 828–834.

[67] Bercaw, J. E.; Durrell, A. C.; Gray, H. B.; Green, J. C.; Hazari, N.; Labinger, J. A.; Winkler, J. R. *Inorg. Chem.* **2010**, *49*, 1801–1810.

[68] Grimme, S.; Djukic, J.-P. *Inorg. Chem.* **2011**, *50*, 2619–2628.

[69] Jang, K.; Jung, I. G.; Nam, H. J.; Jung, D.-Y.; Son, S. U. *J. Am. Chem. Soc.* **2009**, *131*, 12046–12047.

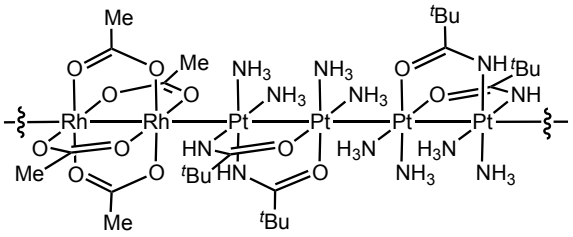

Figure I.23. Repeat unit of a 1-D chain formed through lewis acid/base interaction of Pt(II) and Rh(II) dimers.

Another strategy for 1-D metal chain formation without formal metal–metal bonds is the use of extended lewis acid/base interactions. A notable example that deserves individual mention is the co-crystallization of Pt(II) and Rh(II) dimers to give 1-D chains (Fig. I.23).[70] The d^7d^7 Rh(II) dimers have a Rh–Rh bond order of 1, while the d^8d^8 Pt(II) dimers have a Pt–Pt bond order of 0, and donation of $\sigma^*_{Pt–Pt} \rightarrow \sigma^*_{Rh–Rh}$ creates an extended metal–metal bonding structure along the chain. Extension of this methodology to include d^9 Cu(II) atoms along the chain has also been reported recently, providing access to heterotrimetallic 1-D chains with modified electronic structures.[71]

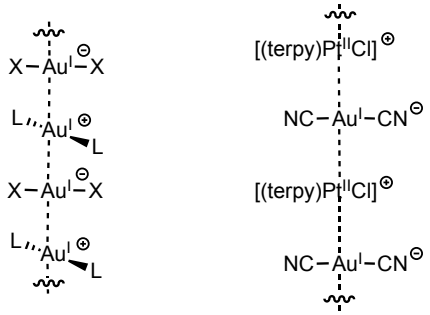

Figure I.24. Lewis acid/base "double salt" chains.

The lewis acid/base strategy for 1-D chain formation is often coupled with coulombic attraction between M^- lewis bases and M^+ lewis acids, to form what are commonly

[70] Uemura, K.; Ebihara, M. *Inorg. Chem.* **2011**, *50*, 7919–7921.

[71] Uemura, K.; Ebihara, M. *Inorg. Chem.* **2013**, *52*, 5535–5550.

referred to as "double salts" (Fig. I.24).[72] The M^- lewis base is frequently an $[AuX_2]^-$ anion, and the M^+ lewis acid can involve a variety of cations such as $Ag(I)^+$, $Tl(I)^+$, and $Pt(II)^+$.[73] One of the oldest examples of such a double salt chain is $[Pt(NH_3)_4][PtC1_4]$, known as Magnus' green salt.[74]

3. Palladium-Mediated and -Catalyzed Aryl C–F Bond Formation

In this section, a short overview will be presented on the role of Pd complexes in the synthesis of aryl fluorides via C–F bond formation. An in-depth review on metal-mediated and -catalyzed C–F bond formation is beyond the scope of this thesis; however, it will be necessary to provide appropriate context for the results presented in Chapter 2 of the Results and Discussion section. In particular, I wish to distinguish between two conceptually distinct approaches to C–F bond formaton, nucleophilic and electrophilic fluorination. For a more detailed treatment of modern fluorination reactions, please see several recent reviews written by our group and others.[75]

---

[72] For a good introduction to "double salt" chains, see Doerrer, L. H. *Dalton Trans.* **2010**, *39*, 3543, and references therein.

[73] Fernández, E. J.; Laguna, A.; López-de-Luzuriaga, J. M.; Monge, M.; Mendizabal, F. *J. Mol. Structure: THEOCHEM* **2008**, *851*, 121–126.

[74] (a) Cox, E. G.; Pinkard, F. W.; Wardlaw, W.; Preston, G. H. *J. Chem. Soc*. **1932**, 2527. (b) Atoji, M.; Richardson, J. W.; Rundle, R. E. *J. Am. Chem. Soc*. **1957**, *79*, 3017. (c) Martin, Jr., D. S.; Rush, R. M.; Kroening, R. F.; Fanwick, P. E. *Inorg. Chem.* **1973**, *12*, 301.

[75] (a) Brown, J. M.; Gouverneur, V. *Angew. Chem., Int. Ed*. **2009**, *48*, 8610. (b) Furuya, T.; Klein, J. E. M. N.; Ritter, T. *Synthesis* **2010**, 1804. (c) Furuya, T.; Kamlet, A. S.; Ritter, T. *Nature* **2011**, *473*, 470. (d) Liang, T.; Neumann, C. N.; Ritter, T. *Angew. Chem., Int. Ed*. **2013**, *52*, 8214.

3.1 Nucleophilic Fluorination

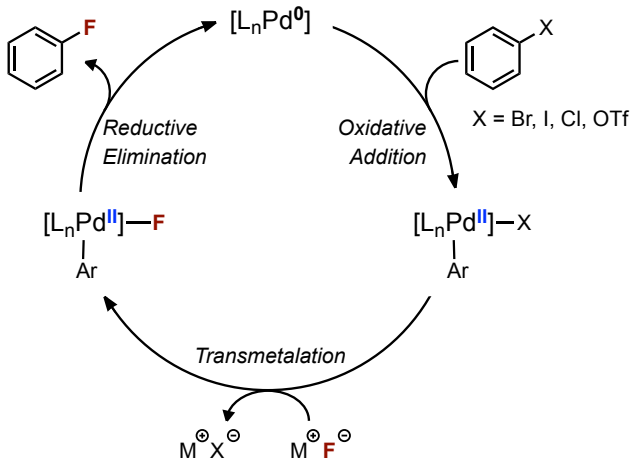

Figure I.25. General catalysis cycle for Pd-catalyzed nucleophilic arene fluorination.

Fluorination of an aryl halide (or pseudohalide), using anionic fluoride as the fluorine atom source, is referred to as *nucleophilic* fluorination. A general catalysis cycle for Pd-catalyzed nucleophilic fluorination is shown in Figure I.25, and is typical of a Pd-catalysis approach for C–X cross-coupling reactions.[76] Metal-catalyzed nucleophilic arene fluorination is challenging for several reasons. The C–F bond-forming step, reductive elimination, is difficult due to the strength and high polarization of metal–fluorine bonds.[77,78] This problem is not unique to nucleophilic arene fluorination, but can potentially be especially difficult from a Pd(II) center as compared to a Pd(IV) center (*vide infra*, section 3.2).[79] Furthermore, reductive elimination must be faster than competing non-productive side reactions, such as hydrolysis of the metal–fluorine bond.

---

[76] deMeijere, A. & Diederich, F. (eds) *Metal-Catalyzed Cross-Coupling Reactions* (Wiley, 2004).

[77] Grushin,V. V. *Acc. Chem. Res.* **2010**, *43*, 160–171.

[78] Shannon, R. D. *Acta Crystallogr. A* **1976**, *32*, 751–767.

[79] Yandulov, D. V.; Tran, N. T. *J. Am. Chem. Soc*. **2007**, *129*, 1342–1358.

The transmetalation step, which forms the Pd–F bond prior to reductive elimination, can also be problematic: due to its electronegativity and small anionic radius, fluoride can form strong hydrogen bonds with, for example, water, alcohols, amines and amides.[80] Extensive hydrogen-bonding renders the fluoride anion significantly less nucleophilic, which can slow down or prevent the transmetalation step from occuring. When hydrogen-bond donors are meticulously excluded, such as by extensive drying of the fluoride salt, fluoride is a better nucleophile, but also basic, which can lead to undesired side reactions.

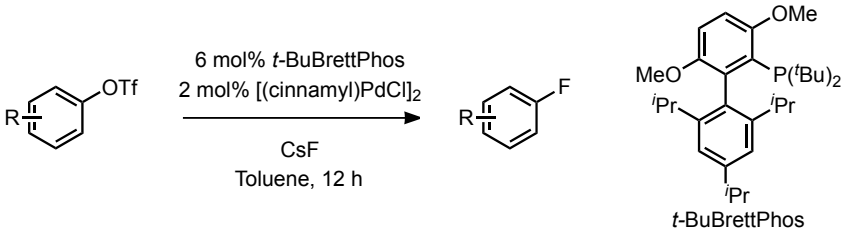

Figure I.26. Pd-catalyzed nucleophilic fluorination of aryl triflates.

In 2009, the Buchwald group reported the first successful Pd-catalyzed nucleophilic fluorination reaction, using aryl triflates (Fig. I.26).[81] Use of the bulky monodentate phosphine ligand *t*-BuBrettPhos was crucial for success, reflecting the need for reductive elimination from a three-coordinate, T-shaped Pd(II) complex.[79] For a few substrates, undesired constitutional isomers were formed as by-products when para-electron-donating or meta-electron-withdrawing groups were present. The isomers potentially arise from a competing benzyne pathway, owing to high reaction temperatures and dried, basic fluoride. The reaction must be performed under anhydrous conditions, and

[80] Emsley, J. *Chem. Soc. Rev*. **1980**, *9*, 91–124.

[81] (a) Watson, D. A.; Su, M.; Teverovskiy, G.; Zhang, Y.; Garcia-Fortanet, J.; Kinzel, T.; Buchwald, S. L. *Science* **2009**, *325*, 1661–1664. (b) Noël, T.; Maimone, T. J.; Buchwald, S. L. *Angew. Chem. Int. Ed.* **2011**, *50*, 8900–8903.

substrates with protic functional groups were not demonstrated to undergo fluorination. Further investigation of the reaction mechanism indicated that the *t*-BuBrettPhos ligand was undergoing arylation via C–C bond formation, and that this *in situ* ligand modification was important for the catalytic fluorination reaction.[82] Most recently, the Buchwald group reported an improved Pd(0) pre-catalyst for nucleophilic fluorination of aryl triflates, providing improved yields for electron-rich substrates and heterocycle-containing aryl triflates.[83]

3.2 Electrophilic Fluorination

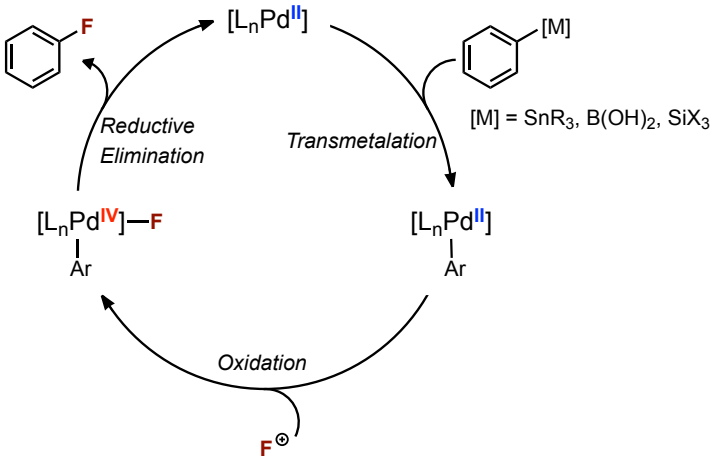

Figure I.27. General catalysis cycle for Pd-catalyzed electrophilic arene fluorination.

Fluorination of an aryl metal reagent, using an electrophilic fluorinating reagent as both the oxidant and the fluorine atom source, is referred to as *electrophilic* fluorination. A general catalysis cycle for Pd-catalyzed electrophilic fluorination is shown in Figure I.27. In contrast to nucleophilic fluorination, the Pd–F bond is formed upon oxidation of

[82] Maimone, T. J.; Milner, P. J.; Kinzel, T.; Zhang, Y.; Takase, M. K.; Buchwald, S. L. *J. Am. Chem. Soc.* **2011**, *133*, 18106–18109.

[83] Lee, H. G.; Milner, P. J.; Buchwald, S. L. *Org. Lett.* **2013**, *15*, 5602–5605.

an arylpalladium(II) complex with an electrophilic fluorinating reagent, and C–F reductive eliminaton proceeds from a high-valent Pd(IV) complex. A selection of representative electrophilic fluorinating reagents is shown in Figure I.28.

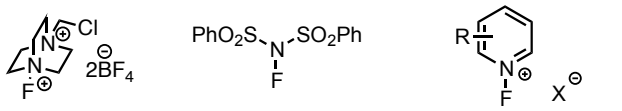

Selectfluor® **NFBS** **N-Fluoropyridinium Salts**

Figure I.28. Commonly used electrophilic fluorinating reagents.

In 2008, our group reported the first example of well-defined carbon–fluorine reductive elimination to form aryl fluorides from a transition metal complex.[84] A Pd-mediated electrophilic fluorination sequence was carried out, in which a range of arylboronic acids were converted into the corresponding aryl fluorides using electrophilic fluorinating reagent Selectfluor® (Fig. I.29). Experimental and computational investigations support a concerted C–F reductive elimination mechanism from an arylpalladium(IV) fluoride: dissociation of one oxygen atom of the tridenate pyridyl-sulfonamide ligand gives a five-coordinate Pd(IV) complex that readily undergoes C–F reductive elimination (Fig. I.29).[85] Reductive elimination from an arylpalladium(IV) fluoride was subsequently used by our lab to enable the synthesis of new [^{18}F]aryl fluorides for applications in positron emission tomography (PET).[86] Prior to the work described in this thesis, extension of this Pd-mediated methodolgy to a Pd-catalyzed

[84] Furuya, T.; Kaiser, H. M.; Ritter, T. *Angew. Chem. Int. Ed.* **2008**, *47*, 5993–5996.

[85] (a) Furuya, T.; Ritter, T. *J. Am. Chem. Soc.* **2008**, *130*, 10060–10061. (b) Furuya, T.; Benitez, D.; Tkatchouk, E.; Strom, A. E.; Tang, P.; Goddard, W. A., III; Ritter, T. *J. Am. Chem. Soc.* **2010**, *132*, 3793–3807.

[86] (a) Lee, E.; Kamlet, A. S.; Powers, D. C.; Neumann, C. N.; Boursalian, G. B.; Furuya, T.; Choi, D. C.; Hooker, J. M.; Ritter, T. *Science* **2011**, *334*, 639–642. (b) Brandt, J. R.; Lee, E.; Boursalian, G. B.; Ritter, T. *Chem. Sci.* **2014**, *5*, 169–179.

fluorination of arylboronic acid derivatives had not been reported – slow transmetallation of the arene from boron to palladium resulted in destructive side reactions under Pd-catalyzed conditions.

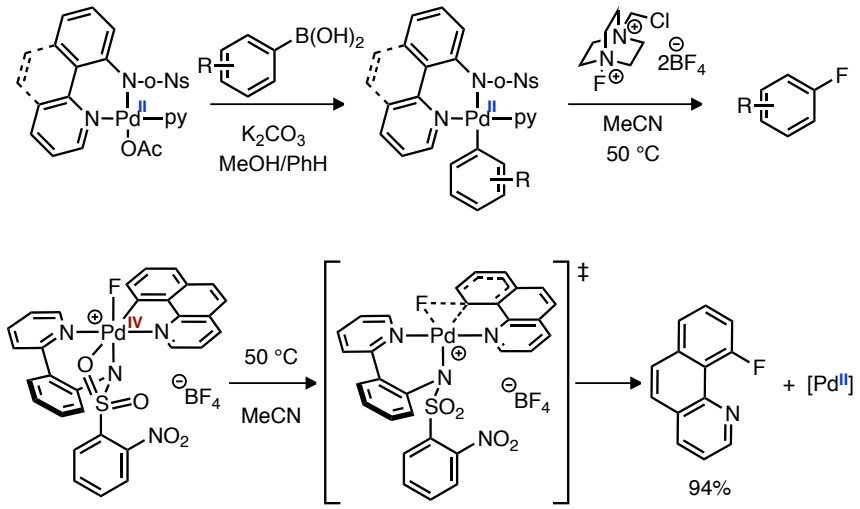

Figure I.29. Pd-mediated electrophilic fluorination of arylboronic acids, and well-defined C–F reductive elimination from a Pd(IV) fluoride complex featuring a hemi-labile pyridyl-sulfonamide ligand to promote reductive elimination via a five-coordinate transition state.

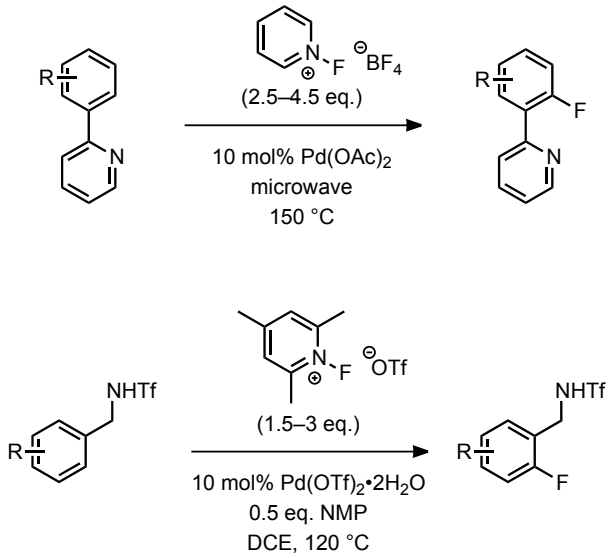

Figure I.30. Pd-catalyzed electrophilic fluorination of aryl C–H bonds.

Work towards Pd-catalyzed electrophilic fluorination of aryl C–H bonds has also been developed. In 2006, the Sanford group reported that arene substrates bearing coordinating directing groups, such as 2-phenylpyridine, can undergo Pd-catalyzed C–H fluorination using an N-fluoropyridinum reagent (Fig. I.30, top).[87] The Yu group seubsequently reported a related transformation from N-benzyltriflamide derivatives (Fig. I.30, bottom).[88] Selective C–H fluorination of arenes that do not bear coordinating directing groups has not yet been reported, but would be a powerful advance for the field of fluorination.

[87] Hull, K. L.; Anani, W. Q.; Sanford, M. S. *J. Am. Chem. Soc.* **2006**, *128*, 7134–7135.

[88] Wang, X.; Mei, T. S.; Yu, J.-Q. *J. Am. Chem. Soc.* **2009**, *131*, 7520–7521.

RESULTS AND DISCUSSION

Chapter 1: One-Dimensional Palladium Wires

This chapter describes the synthesis, structure, and electronic properties of solution-stable, one-dimensional palladium wires. The Pd wires described herein are self-assembled via Pd–Pd bonds upon oxidation of dimeric Pd(II) building blocks. One-dimensional Pd wires featuring Pd–Pd bonds had not been reported prior to our work. For a background discussion on Pd–Pd bond formation via oxidation of Pd(II) dimers, please see the Introduction section.

1.1 Discovery of a Pd(III) Wire[1]

Organopalladium(III) complexes that feature Pd–Pd bonds are uncommon and to date have primarily been limited to discrete dipalladium complexes.[2] Since 2009 our laboratory has investigated the previously unknown role of dipalladium(III) complexes in catalysis.[3] We reported the synthesis of dipalladium(III) complexes by the oxidation of dipalladium(II) complexes (e.g. **1.1** → **1.2**) and their ability to undergo facile carbon–heteroatom reductive elimination (Fig. 1.1, top).[4] Our interest in utilizing metal–metal bonding to reduce activation barriers in catalysis led us to investigate carbon–fluorine bond formation from dipalladium(III) fluoride complexes such as **1.3** (Fig. 1.1, bottom).

[1] The initial discovery of a Pd(III) wire was made by Dr. David Powers, a former graduate student in the Ritter group, during his studies on C–X reductive elimination from dipalladium(III) complexes. I thank Dave for his contributions to the work described in this section, on the synthesis and characterization of the first Pd(III) wire.

[2] (a) Powers, D. C.; Ritter, T. *Top Organomet Chem* **2011**, *503*, 129–156. (b) Mirica, L. M.; Khusnutdinova, J. R. *Coord. Chem. Rev.* **2012**, *257*, 299–314.

[3] See Powers, D. C.; Ritter, T. *Acc. Chem. Res.* **2012**, *45*, 840–850, and references therein.

[4] Powers, D. C.; Ritter, T. *Nat. Chem.* **2009**, *1*, 302–309.

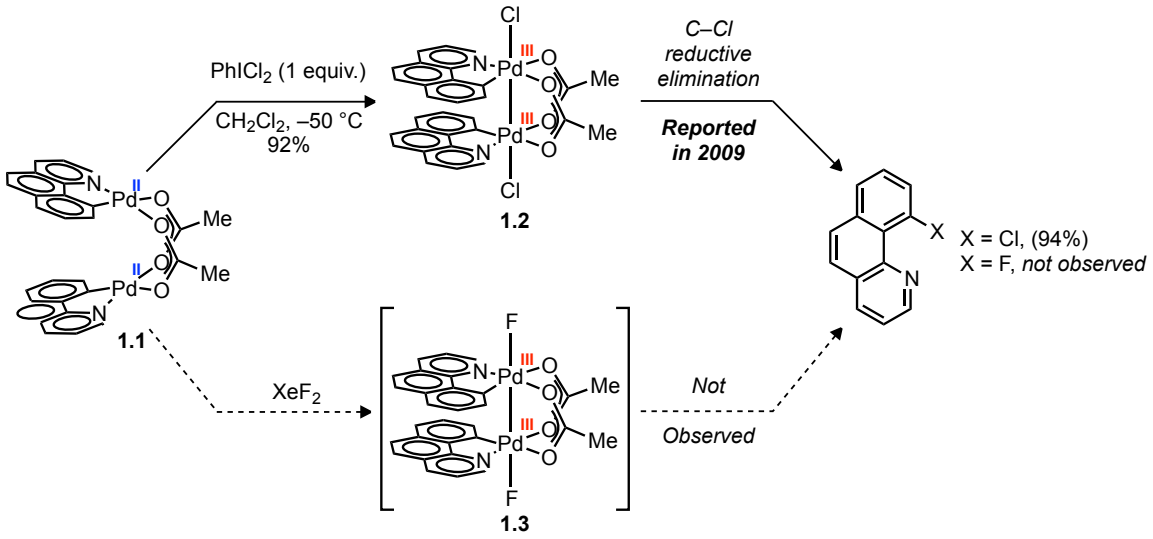

Figure 1.1. Two-electron oxidation of dimeric Pd(II) complex **1.1** gave dipalladium(III) dichloride **1.2**, which subsequently underwent carbon–chlorine reductive elimination. Carbon–fluorine reductive elimination from the analogous putative dipalladium(III) difluoride complex **1.3** was not observed.

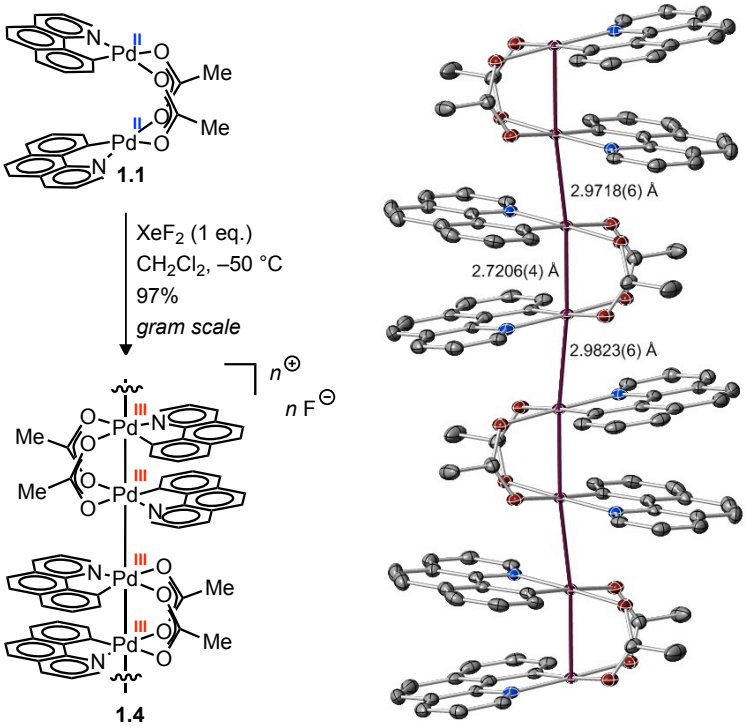

Figure 1.2. Synthesis and X-ray structure of 1-D Pd(III) wire **1.4**, with Pd–Pd distances labeled. X-ray structure drawn with 50% probability ellipsoids, H-atoms are omitted for clarity.

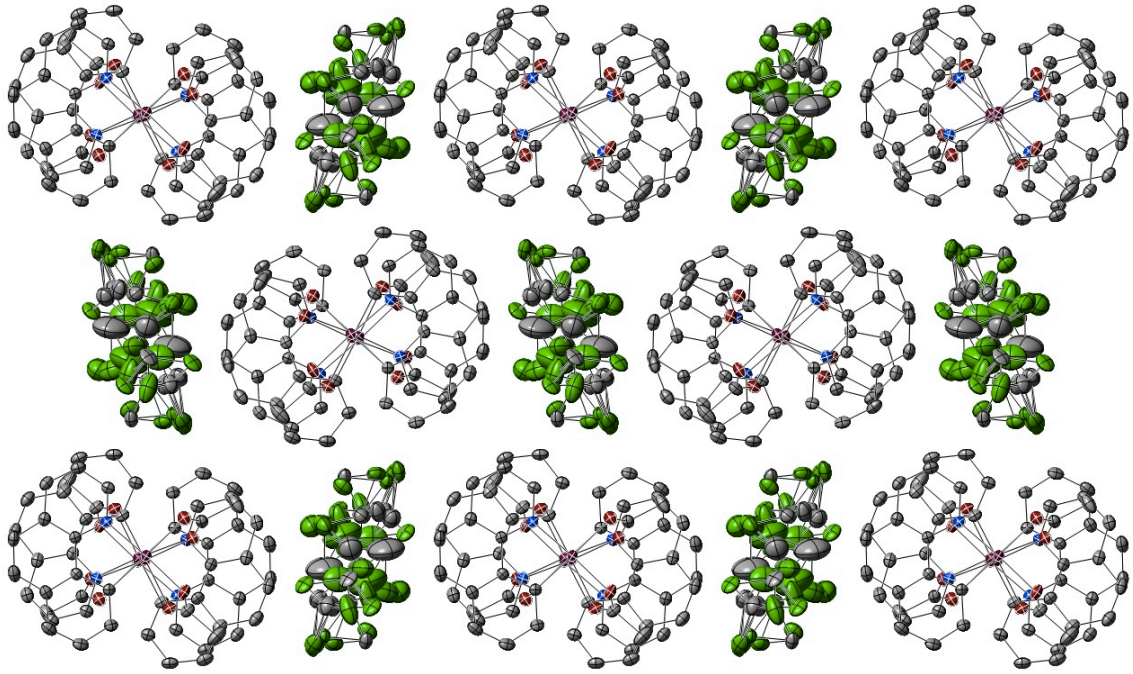

Figure 1.3. X-ray structure of **1.4** viewed down the Pd–Pd axis, showing collinear columns of infinite palladium chains with disordered CH_2Cl_2 in the channels between columns. X-ray structure drawn with 50% probability ellipsoids, H-atoms are omitted for clarity.

Unexpectedly, when **1.3** was targeted we observed the self-assembly of solution-stable 1-D polymers with a backbone of metal–metal bonds. Treatment of a solution of **1.1** in CH_2Cl_2 at –50 °C with XeF_2 (1.0 equiv.) led to an immediate colour change from pale yellow to dark red. Crystallization afforded thermally sensitive, dark-red needles of **1.4** as infinite chains of cationic Pd(III) nuclei with non-coordinated fluoride anions (Fig. 1.2). In the crystal packing of **1.4**, adjacent polycationic wire strands are collinear and the voids between the chains are occupied by disordered fluoride counteranions and solvent (Fig. 1.3). As a result of the high level of disorder in the voids, the fluoride anions were not located in the crystal structure of **1.4**. Therefore, the presence of fluoride in a 1:1 Pd:F ratio was established chemically by the treatment of **1.4** with trimethylsilyl chloride: both trimethylsilyl fluoride and Pd(III) dichloride **1.2** were observed in 96%

yield, which confirmed the assigned molecular formula and the Pd(III) oxidation state in **1.4** (eq. 1.1).

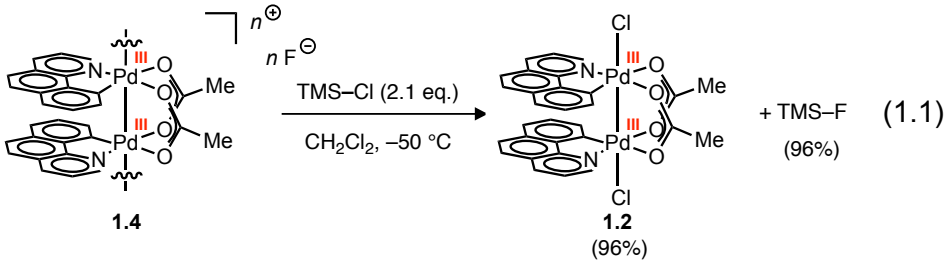

Crystals of Pd(III) difluoride **1.3** were isolated alongside crystals of **1.4** (Fig. 1.4), but redissolved crystals of both **1.3** and **1.4** displayed identical solution spectral features that indicated extended chain structures. Thermal decomposition of solutions of **1.4** did not provide observable C–F reductive elimination. The data suggest that fluoride coordination to palladium in **1.4** is reversible and disfavoured in solution.

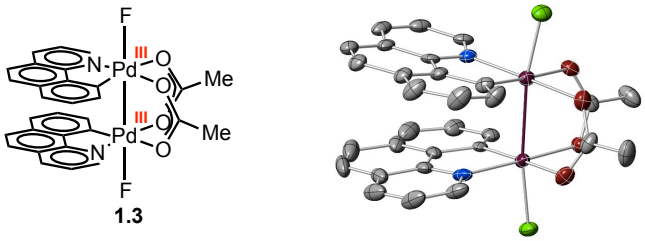

Figure 1.4. X-ray structure of Pd(III) difluoride **1.3**. X-ray structure drawn with 50% probability ellipsoids, H-atoms are omitted for clarity.

The acetate-bridged Pd–Pd distance in **1.4** is 2.72 Å (0.12 Å shorter compared to that in **1.1**), as expected for the oxidation of Pd(II) to Pd(III) with concurrent metal–metal bond formation.[4] The short interdimer Pd–Pd distances (average 2.98 Å) are consistent with unbridged Pd–Pd bonds. Previously, palladium had not been observed to form 1-D complexes with unsupported metal–metal bonds in any oxidation state; additionally, **1.4**

is the first 1-D metal wire with all metal atoms in a d^7 configuration.[5] Molecular wires with an all-d^7 configuration have been postulated to exhibit unique conductive properties.[6] All previous examples of 1-D chains supported by metal–metal bonding interactions are mixed-valence d^7–d^8 systems or closed-shell d^8 or d^{10} chains.[7]

1.2 Discussion of Pd–Pd Bonding in 1-D Pd(III) Chains

In dipalladium complexes such as Pd(II) dimer **1.1** and dipalladium(III) dichloride **1.2**, the Pd–Pd bonding interactions can be described by a simplified molecular orbital (MO) diagram based on overlap of the metal-based orbitals, as described in the Introduction section. For example, oxidation of **1.1** by $PhICl_2$ to give **1.2** removes two electrons from the Pd–Pd σ* antibonding orbital (HOMO), resulting in a Pd–Pd single bond in **1.2** (*vide supra*, Fig. 1.1).

For 1-D chains based on Pd(III) dimers, the primary interaction will be along the z-axis, via the Pd d_{z^2}-based MOs – in this case the σ and σ* orbitals of the dimeric units. A simplified MO description involving only d_{z^2}-based Pd orbitals is shown in Figure 1.5a, for the interaction of two dipalladium(III) units to form a tetrameric chain. Both the bonding (Ψ_1) and antibonding (Ψ_2) orbitals formed by interaction of the σ MOs will be fully occupied, which does not result in a net bonding interaction between the two dimeric units.

---

[5] Shortly after our initial report of 1-D Pd(III) wires, Oh *et al* reported data that suggests the formation of an all-d^7 Ru(I) chain in the solid state, but structural characterization was not reported. See: Oh, S. P.; Chor, B. Y.; Fan, W. Y.; Li, Y.; Leong, W. K. *Organometallics* **2011**, *30*, 6774–6777.

[6] Miller, J. S.; Epstein, A. J. *Prog. Inorg. Chem.* **1976**, *20*, 1–151.

[7] Please see the Introduction section for a review of previously reported 1-D metal chains.

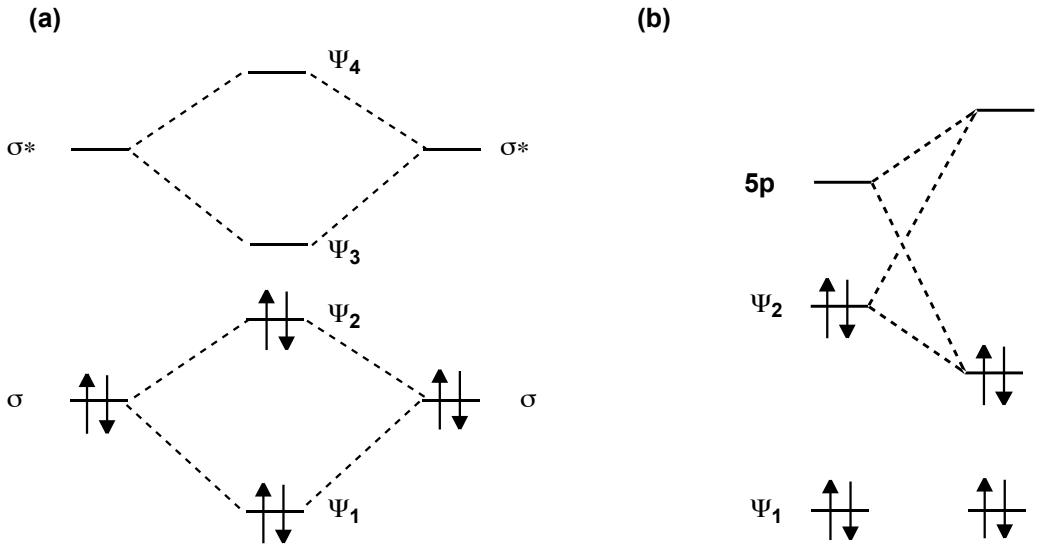

Figure 1.5. (a) Qualitative molecular orbital diagram for Pd–Pd bonding in a tetrameric Pd(III) chain. (b) Symmetry-allowed mixing with Pd 5p orbital, resulting in a net Pd–Pd bonding interaction.

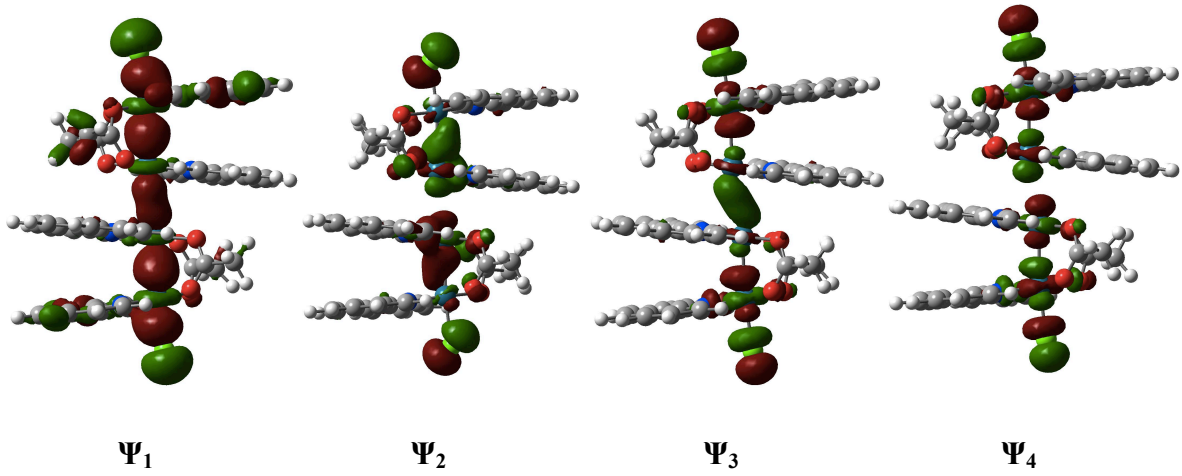

Figure 1.6. Graphical depiction of the Pd–Pd bonding orbitals in a tetrameric Pd(III) chain, as described in Figure 1.5. Orbital images were generated from single-point DFT calculation (B3PW91) of a hypothetical Pd(III) tetramer, based on truncating the crystal structure of **1.4** with apical chloride ligands.

Symmetry-allowed mixing of d orbitals with vacant, higher-lying p and s orbitals on the metals can play a role in metal–metal bonding interactions. Metal–metal bonding through $d_{z^2}/p_z/s$ hybridization is proposed to occur in dipalladium(II) complexes such as

1.1,[8] as well as oligomeric Rh(I) chains.[9] We propose that this orbital hybridization may play a role in stabilizing the unsupported Pd–Pd bonds in the 1-D Pd(III) wires described in this work. The Ψ_2 (antibonding) orbital mixes with the $5p_z$ orbitals on the Pd atoms to a greater extent than the bonding Ψ_1 orbital, due to a closer match in orbital energies. The overall effect is an increase in the bonding interaction between dimeric units relative to the antibonding interaction, stabilizing the unsupported Pd–Pd bonds along the 1-D chain (Fig. 1.5b).

1.3 Establishment of Solution Stability

Pd(III) wire **1.4** is soluble in CH_2Cl_2 and spectroscopic methods, including ^1H and ^{19}F NMR, EPR, and UV-vis/NIR spectroscopy, are consistent with solution-stable extended chain structures. UV-vis/NIR absorption spectra of dilute solutions of **1.4** show a NIR absorption centred around 1,000 nm (Fig. 1.7). The absorption is consistent with solution-stable extended metal chains in which the metal atoms are in electronic communication through metal–metal bonds.[10] In contrast, discrete Pd(III) dimers, such as **1.2**, do not absorb in the NIR region.[4] The NIR absorption of **1.4** displays a concentration-dependent red shift that indicates longer chain lengths in solution at higher concentrations,[11] which is also supported by light-scattering measurements (*vide infra*).

---

[8] Bercaw, J. E.; Durrell, A. C.; Gray, H. B.; Green, J. C.; Hazari, N.; Labinger, J. A.; Winkler, J. R. *Inorg. Chem.* **2010**, *49*, 1801–1810.

[9] Mann, K. R.; Lewis, N. S.; Williams, R. M.; Gray, H. B.; Gordon, J. G. *Inorg. Chem.* **1978**, *17*, 828–834.

[10] (a) Matsumoto, K.; Sakai, K.; Nishio, K.; Tokisue, Y.; Ito, R.; Nishide, T.; Shichi, Y. *J. Am. Chem. Soc.* **1992**, *114*, 8110–8118. (b) O'Halloran, T. V.; Roberts, M. M.; Lippard, S. J. *J. Am. Chem. Soc.* **1984**, *106*, 6427–6428.

[11] (a) Nocera, D. G. *Acc. Chem. Res.* **1995**, *28*, 209–217. (b) Sigal, I. S.; Gray, H. B. *J. Am. Chem. Soc.* **1981**, *103*, 2220–2225.

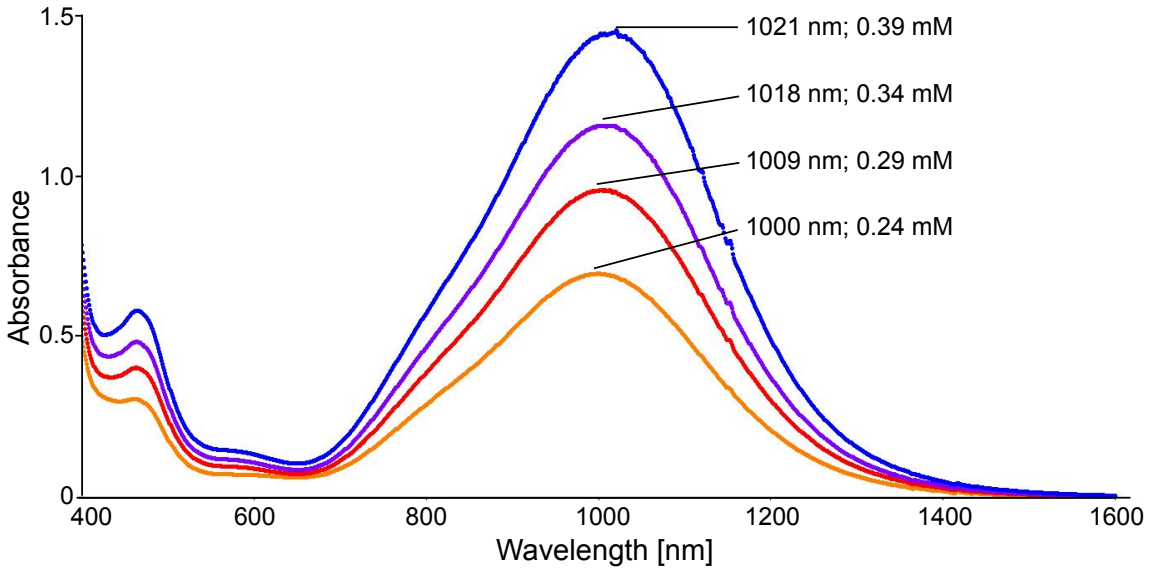

Figure 1.7. UV-vis/NIR absorption spectrum of Pd(III) wire **1.4**, showing a concentration-dependent red shift of the NIR absorption (concentration given in terms of [Pd])

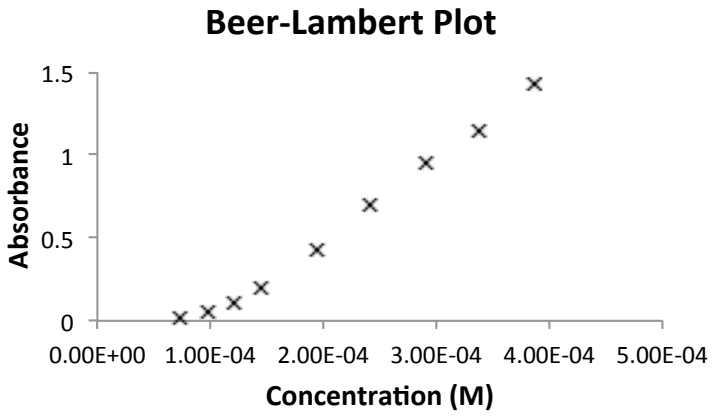

Figure 1.8. Beer-Lambert plot for the absorption maximum at 1,000 nm in Figure 1.7.

Static and dynamic light scattering (SLS/DLS) measurements were used to probe the solution-state supramolecaur structure of Pd(III) wire **1.4**, and show that **1.4** exists as extended rod-like structures in solution with an average calculated length of 350 nm,

which corresponds to more than 600 palladium centres per wire.[12] SLS and DLS measurements led to hydrodynamic radius (R_H) and gyration radius (R_G) values of 63 and 107 nm respectively for Pd(III) wire **1.4** (Figs. 1.9-1.10). The corresponding R_G/R_H ratios is 1.70, which is consistent with the theoretical value for rod-like structures (1.732).[13] The average calculated length of these structures is 350 nm in CH_2Cl_2 solutions, indicating approximately 600 Pd atoms in length based on the average Pd–Pd bond length obtained from the X-ray structure of **1.4** (2.85 Å). The calculated second Virial coefficient A_2 is negative, indicative of an auto-associative system, and consistent with macromolecules prone to crystallization in CH_2Cl_2.[14] The correlation between molar mass and the object length obtained by SLS suggests the possibility that individual wire strands associate in solution to form bundles. To a first approximation, based on average length and assuming simple bundles with perfect overlap of the strands, an aggregation number of 19 can be calculated.

[12] Special thanks to Dr. Jean Raynaud, a former postdoctoral researcher in the Ritter group, for his invaluable contributions to the light scattering measurements. Jean and I performed the measurements together, and Jean performed the data analysis. Additional thanks to Prof. Seth Fraden (Physics Department, Brandeis University) for generously allowing us to use his group's optical bench for the light scattering measurements.

[13] Ruggiero, A. *et al. Proc. Natl. Acad. Sci.* **2010**, *107*, 12369-12374.

[14] Zhang, W. *et al*. *Macromolecules* **2004**, *37*, 2924-2929

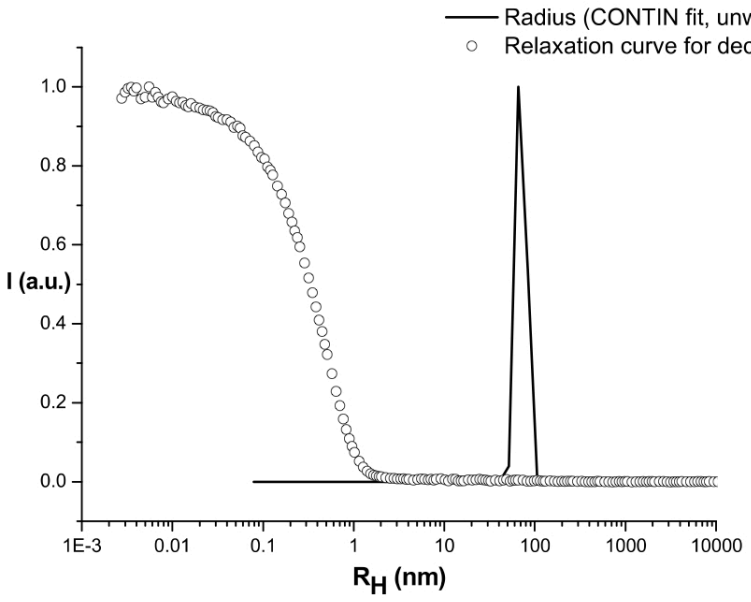

Figure 1.9. DLS measurement at 90° for a 0.3 mg/mL sample of **1.4** in CH_2Cl_2. (I is normalized intensity, and R_H is hydrodynamic radius).

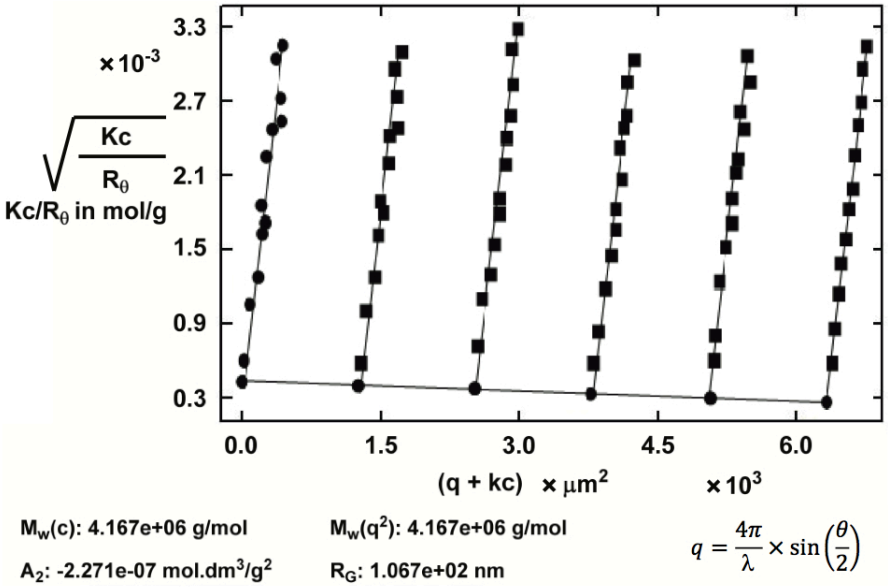

Figure 1.10. Berry Plot obtained from SLS measurements between 30 and 150° for **1.4** with a concentration range from 0.1 to 0.3 mg/mL. The extrapolation of the Berry plot at θ=0 and c=0 gives a molar mass of 4.2×10^6 g/mol, a R_G of 107 nm and a second Virial coefficient (A_2) of -2.3×10^{-7} mol•L/g^2.

1.4 Effect of Molecular Changes on Supramolecular Structure

The solution-phase self-assembly of Pd(III) wire **1.4** allowed us to explore the effect of molecular changes on the resulting supramolecular structure of the 1-D Pd wire. While interest in 1-D wires has grown in recent years based on potential applications in fields such as nanotechnology, molecular sensing, and photovoltaic devices, a major shortcoming in the field of 1-D metal wire research has been the inability to access wires with systematically varied structures, in order to determine the relationship between the structure and properties. Therefore, a primary goal of our work was to establish the concept of molecular control over wire properties. Due to the modular nature of the dipalladium(II) building blocks, we aimed to explore the effect on wire strucutre and properties upon variation of:

- Pd oxidation state,
- counteranion,
- bridging ligand, and
- cyclometallated ligand.

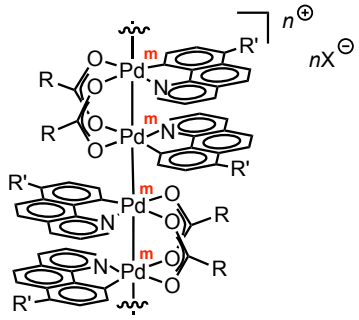

Control of Pd oxidation state was effected simply through variation in stoichiometry in the oxidation of Pd(II) dimer **1.1**: Pd(2.5) wire **1.5** was prepared by treatment of **1.1** with XeF_2 (0.5 equiv.) under identical conditions to those used for the preparation of **1.4**. Only two other complexes that contain Pd(2.5) have been reported, both of which exist as discrete dinuclear complexes.[15] Crystals of **1.5** are dark-red needles that can exceed 1 cm

[15] (a) Yao, C. L.; He, L. P.; Korp, J. D.; Bear, J. L. *Inorg. Chem.* **1988**, *27*, 4389-4395. (b) Berry, J. F.; Bill, E.; Bothe, E.; Cotton, F. A.; Dalal, N. S.; Ibragimov, S. A.; Kaur, N.; Liu, C. Y.; Murillo, C. A.; Nellutla, S.; North, J. M.; Villagrán, D. *J. Am. Chem. Soc.* **2007**,

in length, and X-ray crystallographic analysis showed an infinite 1-D chain structure analogous to that of **1.4**, with one fluoride counteranion for every two palladium nuclei (Fig. 1.11).

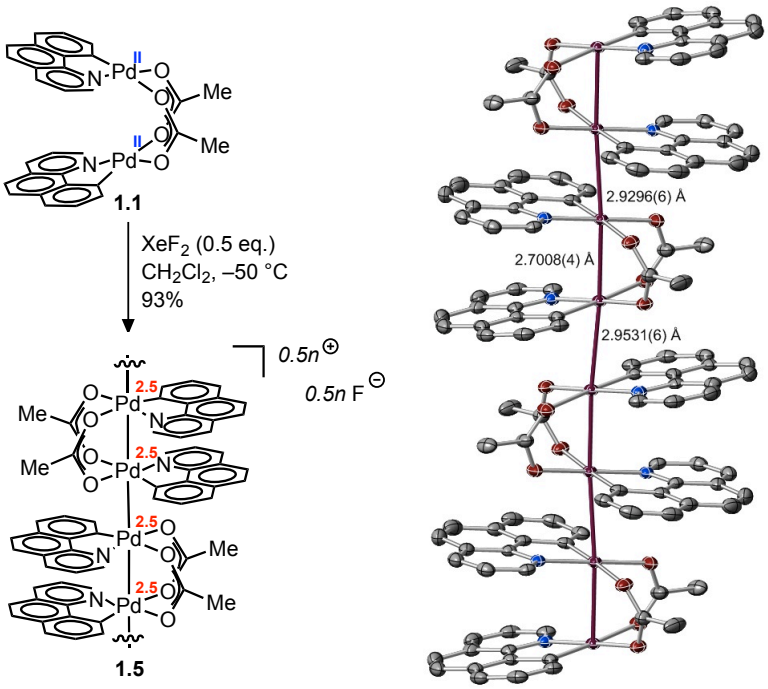

Figure 1.11. Synthesis and X-ray structure of 1-D Pd(2.5) wire **1.5**, with Pd–Pd distances labeled. X-ray structure drawn with 50% probability ellipsoids, H-atoms are omitted for clarity.

At 100 K, the acetate-bridged Pd–Pd distance in **1.5** is 0.02 Å shorter than that in **1.4**, while the unbridged distances are, on average, 0.04 Å shorter in **1.5**. The shorter Pd–Pd distances may be accounted for by a decrease in coulombic repulsion between palladium centres in **1.5** as compared to **1.4**.[15b] Pd(2.5) wire **1.5** crystallizes in the space group $P2_1/c$, with the same supramolecular structure as Pd(III) wire **1.4**, in which the collinear chains are separated by 1-D channels containing disordered CH_2Cl_2 solvent and fluoride anions (Fig. 1.3). While the change in oxidation state from Pd(III) to Pd(2.5) had little

129, 1393-1401.

impact on the structural features of the 1-D Pd wires, the abiliy to control oxidation state was found to be important for modifying the thin-film condictive properties of the 1-D wires (*vide infra*).

We were able to take advantage of the solution stability of Pd(III) wire **1.4** to perform anion metathesis and examine the effect of the counteranion on the wire structure. The addition of $AgPF_6$ to a CH_2Cl_2 solution of Pd(III) wire **1.4** resulted in the immediate precipitation of dark blue solids. Slow diffusion of a Et_2O solution of $AgPF_6$ into a CH_2Cl_2 solution of **1.4** at −35 °C resulted in the growth of dark blue needle crystals, which were insoluble in CH_2Cl_2. X-ray crystallographic analysis revealed Pd(III) wire **1.6**, in which one-third of the fluoride counteranions in **1.4** are replaced with hexafluorophosphate (PF_6^-) anions (Fig. 1.12).

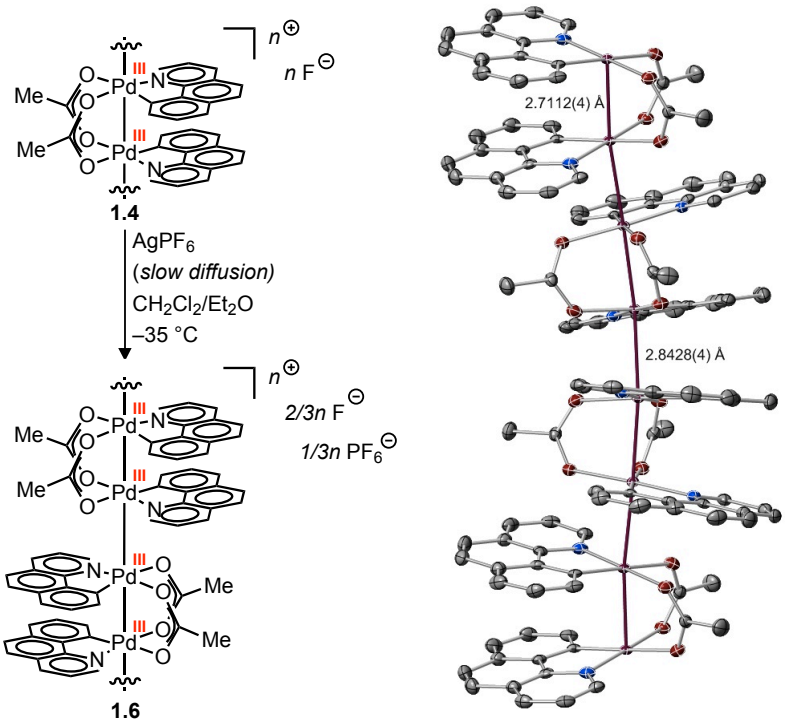

Figure 1.12. Synthesis and X-ray structure of 1-D Pd(III) wire **1.6**, with Pd–Pd distances labeled. X-ray structure drawn with 50% probability ellipsoids, H-atoms are omitted for clarity.

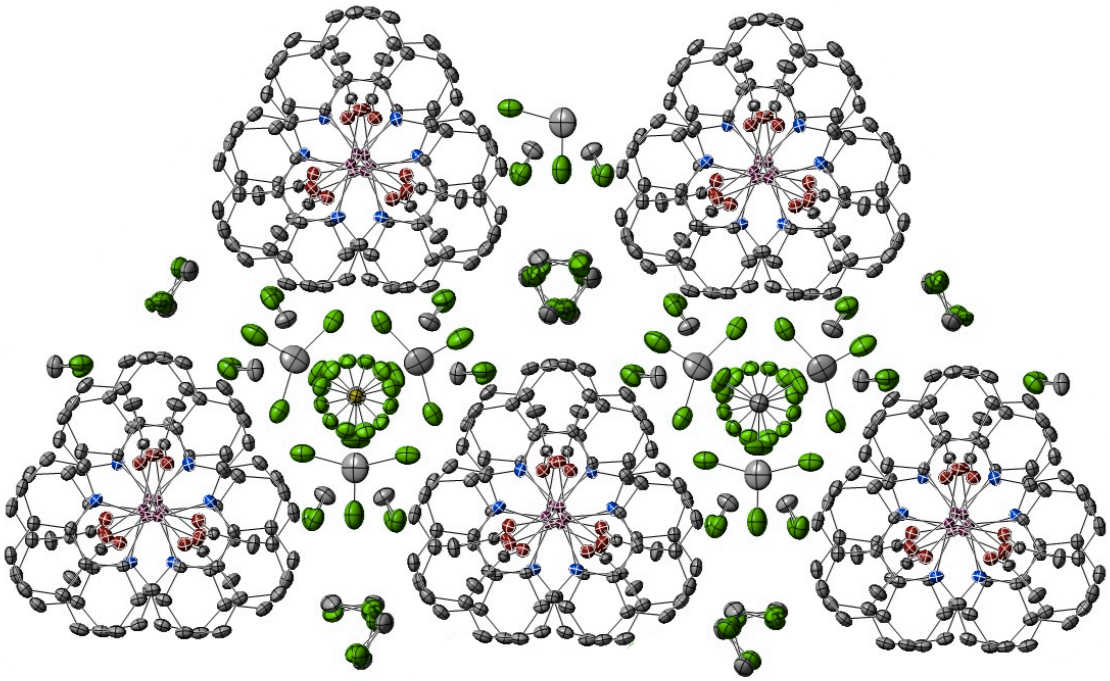

Figure 1.13. X-ray structure of **1.6** viewed down the Pd–Pd axis, showing collinear columns of infinite palladium chains with disordered counteranions and CH_2Cl_2 in the channels between columns. X-ray structure drawn with 50% probability ellipsoids, H-atoms are omitted for clarity.

Counteranion substitution has a pronounced effect on the solid-state structure: while palladium wires **1.4** and **1.5** with all-fluoride counteranions crystallize in the space group $P2_1/c$, featuring a 2-fold screw axis, Pd(III) wire **1.6** crystallizes in the space group *R32*, featuring a 3-fold screw axis (Fig. 1.13). The change in crystal packing is accompanied by a significant decrease in the Pd−Pd distance between dimeric units. As shown in Figure 1.12, the interdimer Pd−Pd distance in **1.6** is 0.1316(4) Å shorter than the average interdimer Pd−Pd distance in **1.4**. Variations in metal−metal distance can be a key factor in altering the electrical conductivity and optical properties of 1-D metal wires.[16] We were unable to obtain electrical conductivity measurements for the 1-D palladium wire

[16] (a) Georgiev, V. P.; McGrady, J. E. *J. Am. Chem. Soc.* **2011**, *133*, 12590–12599. (b) Jang, K.; Jung, I. G.; Nam, H. J.; Jung, D.-Y.; Son, S. U. *J. Am. Chem. Soc.* **2009**, *131*, 12046–12047.

crystals described in this thesis because of thermal and atmospheric instability, resulting in decomposition upon attempted electrode attachment.[17]

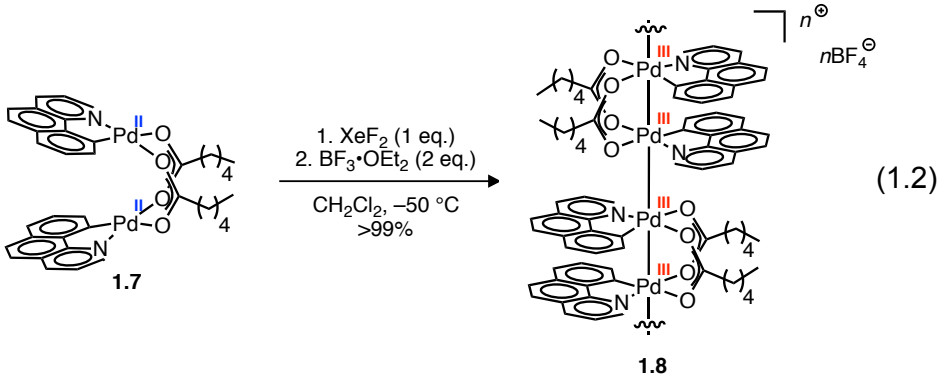

(1.2)

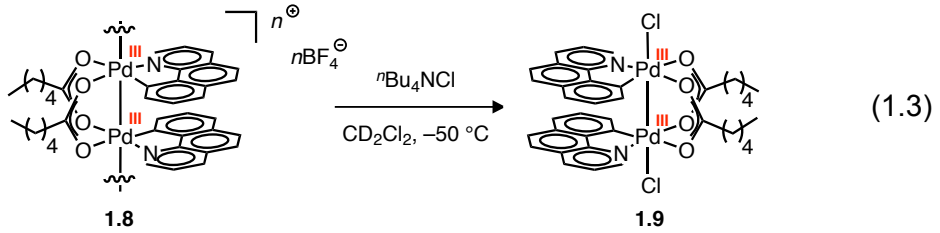

(1.3)

We also sought to examine the effect of counteranion on the solution-state structure of the 1-D wires. Because the spectroscopic data suggest that in fluoride binding to Pd is reversible in solutions of Pd(III) wire **1.4**, we hypothesized that replacing the fluoride anions with more weakly-coordinating anions may result in increased solution-state chain length. However, as described above, treatment of a CH_2Cl_2 solution of Pd(III) wire **1.4** with $AgPF_6$ results in precipiatation, and no 1-D Pd chains are observed in solution. We were able to use substitution of the bridging acetate ligands with hexanoate ligands as a synthetic handle to increase solubility. Treatment of dipalladium(II) complex **1.7** (an analog of complex **1.1** with bridging hexanoate ligands) with 1.0 equivalents of XeF_2 followed by 2.0 equivalents of BF_3•OEt_2 gave Pd(III) wire **1.8**, with weakly-coordinating

[17] We hypothesize that decomposition of Pd wire single crystals upon electrode attachment may also be due in part to evaporation of solvent from the interchain channels, resulting in collapse of the crystalline framework. The crystals were observed to become brittle and lose their shiny appearance after removal from the solvent of crystallization, if not held at low temperature.

tetrafluoroborate (BF_4^-) anions (eq. 1.2). The Pd(III) oxidation state of **1.8** was established by treatment with TBACl to afford discrete Pd(III) dimer **1.9**, the identity of which was confirmed via independent synthesis (eq. 1.3).

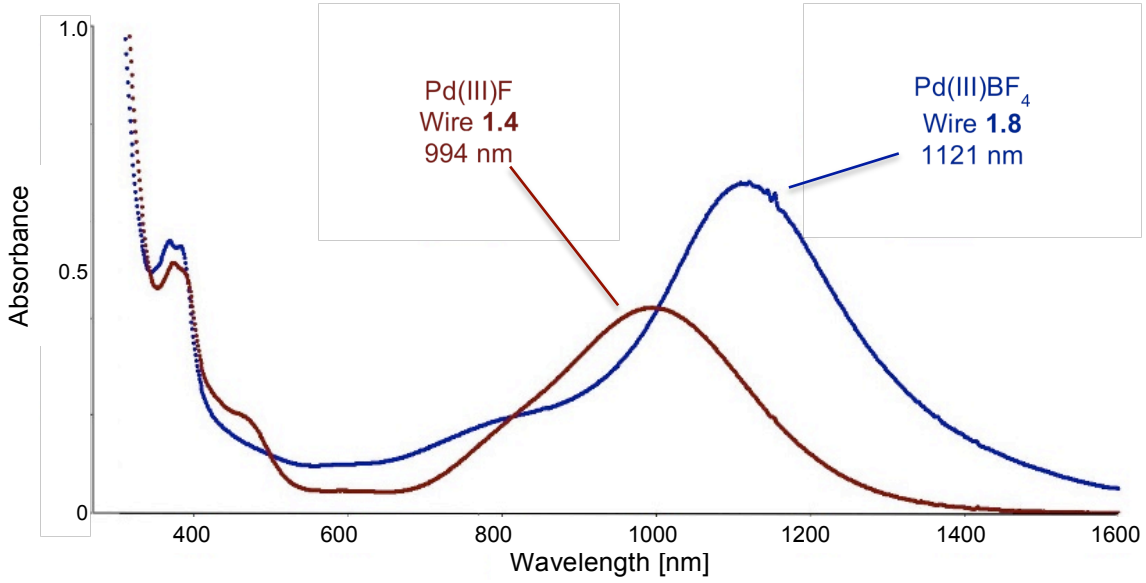

Figure 1.14. Spectra of Pd(III) wires **1.4** and **1.8** at identical concentrations with respect to palladium. The NIR absorbance displayed a red shift of 127 nm when fluoride counteranions were replaced by weakly coordinating BF_4^- anions.

Solutions of **1.8** are deep blue in color, and the NIR absorption observed for **1.8** is red-shifted by 127 nm as compared to **1.4** at identical concentrations with respect to Pd, indicating increased chain length (Fig. 1.14). In longer chains, optical bandgap decreases, which results in a red shift of the observed absorption. SLS/DLS measurements show an average chain length in solution of 750 nm (400 nm longer than for **1.4**), corresponding to approximately 1,300 Pd per wire. The longest solution-stable metal chain with assigned length that had been reported prior to our work contains 12 metal atoms.[11b]

In general, we found that wire formation is highly sensitive to the nature of the supporting ligand scaffold: the presence of bridging carboxylate ligands with small substituents, such as acetate, seems to be particularly important for wire formation. While substitution of the bridging acetate ligands in **1.1** with linear aliphatic carboxylates such as *n*-hexanoate is tolerated, as described above, Pd(II) dimers featuring sterically more demanding carboxylates were not found to give 1-D wires upon oxidation.

Modification of the cyclometallated ligand also proved challenging, but was found to have a dramatic impact on suparamolecular structure. Pd(II) dimer **1.10**, featuring the 7-chlorobenzo[*h*]quinolyl ligand, gave 1-D palladium wire **1.11**, with an average Pd oxidation state of +2.5, upon treatment with 0.5 equivalents of XeF_2 in CH_2Cl_2 at −50 °C (Fig. 1.15). Pd(2.5) wire **1.11** crystallizes as red needles in the space group $P\bar{3}c1$. X-ray crystallographic analysis is consistent with a 2:1 Pd/F ratio in **1.11**, which, along with spectroscopic data, supports an average +2.5 oxidation state for Pd.[18] As with palladium wires **1.4** and **1.5**, in the solid-state structure of **1.11**, adjacent palladium dimers are oriented at 180° with respect to one another. The interdimer Pd−Pd distance in **1.11** is 2.9053(8) Å, which is slightly shorter than that observed for Pd(2.5) wire **1.5** and Pd(III) wire **1.4**. Attempts to access an isostructural wire with a Pd oxidation state of +III resulted only in the isolation of discrete, fluoride-capped Pd(III) dimer **1.12** upon crystallization (Fig. 1.16). Other attempted modifications of the cyclometalated benzo[*h*]quinolyl ligand of **1.1** did not result in the observable formation of 1-D palladium wires.

[18] While Dr. Shao-Liang Zheng deserves thanks for all of the help he gave me regarding X-ray crystallography, his contributions to the structure determination of **1.11** were particularly valuable.

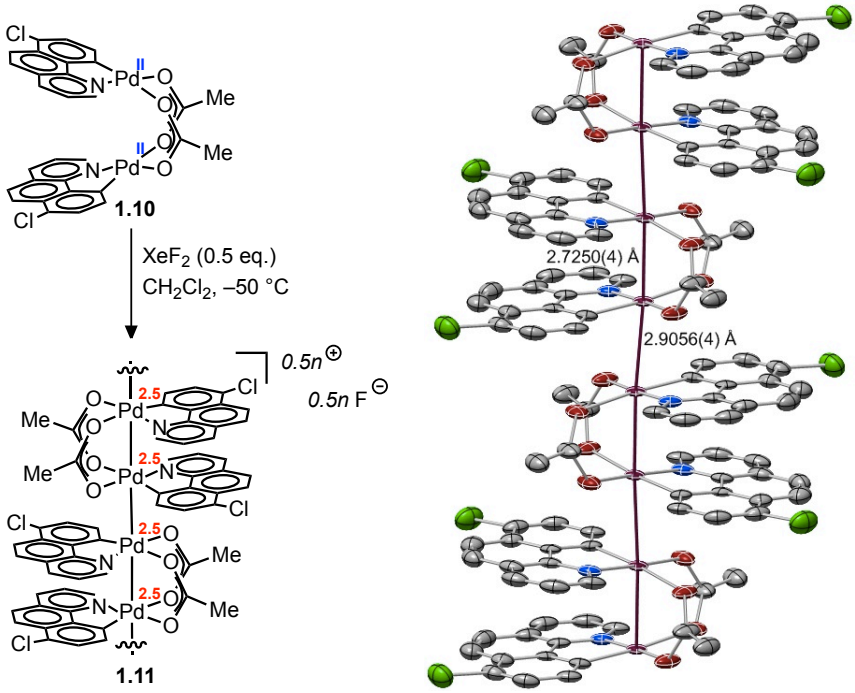

Figure 1.15. Synthesis and X-ray structure of 1-D Pd(2.5) wire **1.11**, with Pd–Pd distances labeled. X-ray structure drawn with 50% probability ellipsoids, H-atoms are omitted for clarity.

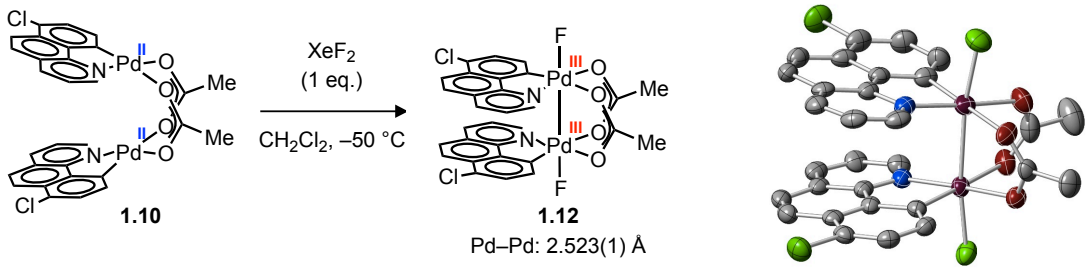

Figure 1.16. Synthesis and X-ray structure of Pd(III) chloride dimer **1.12**. X-ray structure drawn with 50% probability ellipsoids, H-atoms are omitted for clarity.

A unique feature of the solid-state structure of **1.11** is the presence of large 1-D pores, organized by the chloride substituent on the cyclometalated ligand (Figs. 1.17-1.18). Crystals of Pd(2.5) wire **1.11** display two distinct pore sizes, with diameters of 15.2 and 9.2 Å, while Pd(2.5) wire **1.5** displays a uniform pore diameter of 10.2 Å. Remarkably, the 15.2-Å-diameter pores of **1.11** appear to be largely empty in single crystals: the

difference map shows only weak, highly delocalized residual electron density peaks inside the 15.2-Å-diameter pores, which are not strong enough to support the assignment of solvent molecules or ions. The disordered fluoride anions and CH_2Cl_2 solvent molecules are found to occupy the 9.2-Å-diameter pores, stabilized by possible C–H···X hydrogen-bonding interactions, including C_{bhq}–H···Cl, C_{bhq}–H···F, and Cl_2HC–H···F (bhq = benzo[*h*]quinolyl ligand). The possibility for such stabilizing interactions is absent in the 15.2-Å-diameter pores because of the Cl atoms of the cyclometalated ligand that line the channel. Highly porous nanostructured materials featuring 1-D metal chains are potentially useful for porous electrodes and molecular sensors, and the ability to tune the pore size is of particular value.[19]

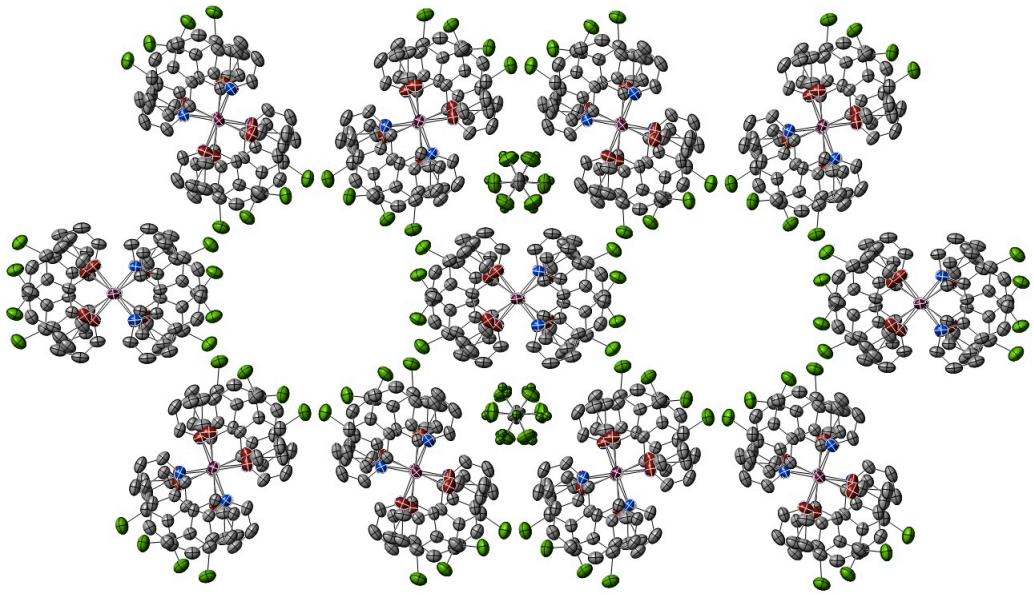

Figure 1.17. X-ray structure of **1.11** viewed down the Pd–Pd axis, showing collinear columns of infinite palladium chains with disordered fluoride anions and CH_2Cl_2 in the channels between columns. X-ray structure drawn with 50% probability ellipsoids, H-atoms are omitted for clarity.

[19] (a) Mas-Balleste, R.; Castillo, O.; Sanz Miguel, P. J.; Olea, D.; Gomez-Herrero, J.; Zamora, F. *Eur. J. Inorg. Chem*. **2009**, *20*, 2885–2896. (b) D'Alessandro, D. M.; Kanga, J. R. R.; Caddy, J. S. *Aust. J. Chem*. **2011**, *64*, 718–722.

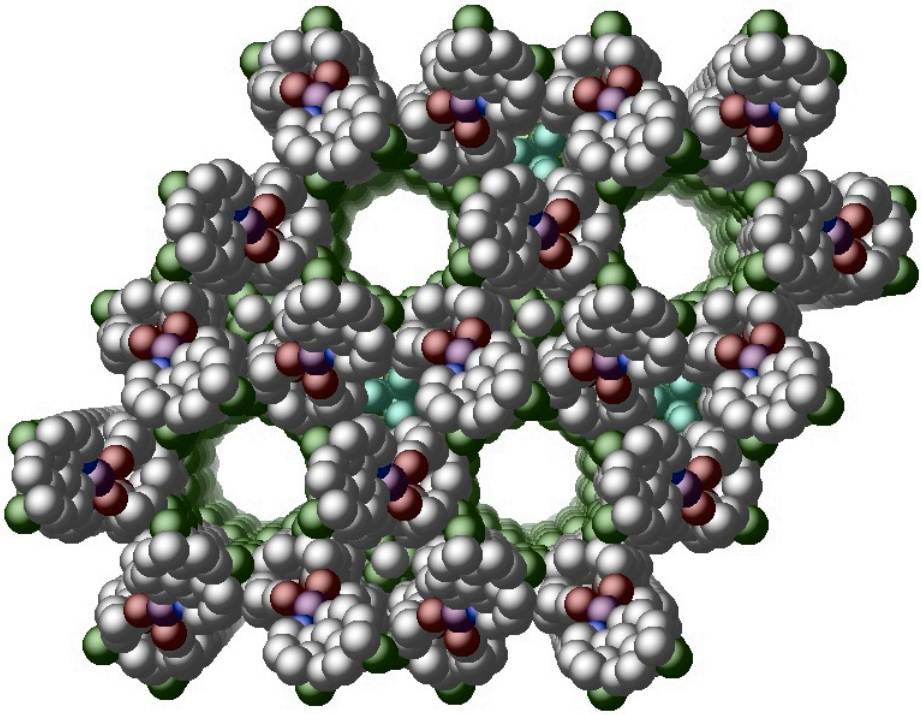

Figure 1.18. Space-filling projection of the X-ray structure of **1.11**, viewed down the Pd–Pd axis, showing empty pores lined by the chloride substituents on the cyclometallated ligands.

Solutions of **1.11** and **1.12** display broad near-IR absorbances around 1000 nm that are nonlinear with concentration, consistent with the presence of solution-stable 1-D metal chains (Figure 1.19). The spectroscopic data indicate that in CH_2Cl_2 solutions Pd(III) dimer **1.12** is in equilibrium with 1-D Pd(III) chains; however, fluoride coordination to palladium appears to be favored in the solid state. In contrast to Pd(2.5) wire **1.11**, solutions of **1.12** display additional absorbances at 642 and 468 nm, which are also nonlinear with concentration. These absorbances are likely due to the equilibrium with discrete Pd(III) dimer **1.12**, which is supported by TD-DFT calculations. All known Pd(III) dimers display characteristic absorption features in the range of 400−650 nm.[2b]

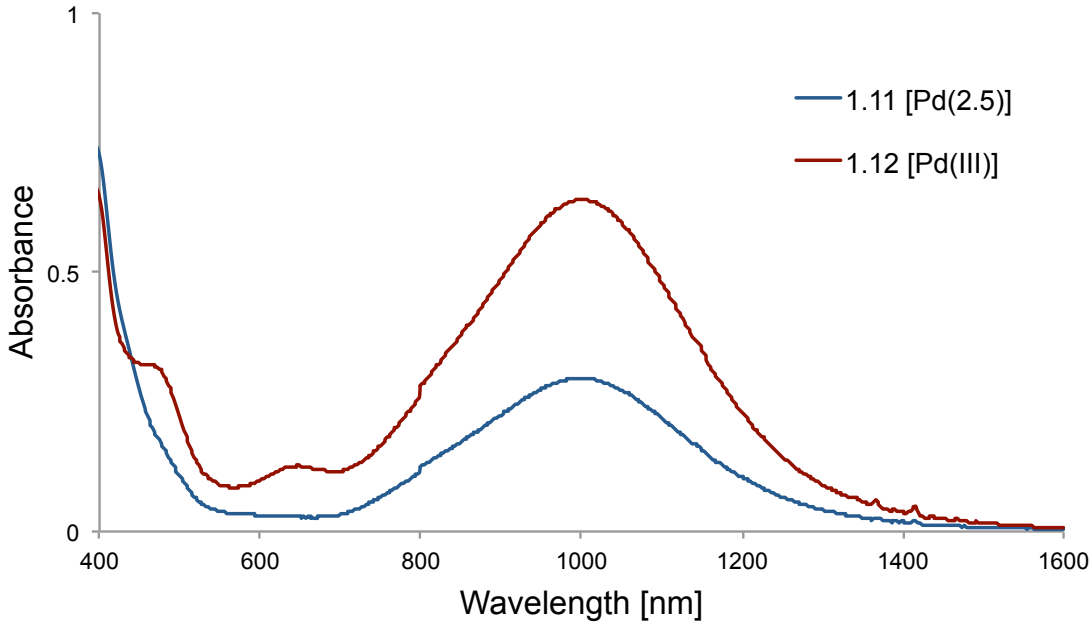

Figure 1.19. UV−vis/near-IR absorbance spectra of **1.11** and **1.12** (CH_2Cl_2, 5 °C, 2.6×10^{-4} M in [Pd]).

1.5 Effect of Molecular Changes on Conductivity

A molecular wire that retains its 1-D polymeric structure in solution can be valuable for the construction of devices with molecular wires,[20] but most reported examples of 1-D metal chains supported by metal–metal bonds were synthesized and studied exclusively in the solid state. To demonstrate the capability for solution processing, we used drop casting to assess thin-film conductivity by four-point probe measurements.[21] Films deposited from a solution of Pd(III) wire **1.4** behaved as a semiconductor, displaying increasing conductance with increasing temperature in the range of 150–280 K. A bandgap of 1 eV was calculated from linear fitting of ln(conductance) versus

[20] (a) Frampton, M. J. & Anderson, H. L. *Angew. Chem. Int. Ed.* **2007**, *46*, 1028–1064. (b) Habas, S. E., Platt, H. A. A., van Hest, M. F. A. M. & Ginley, D. S.. *Chem. Rev.* **2010**, *110*, 6571–6594. (c) Roncali, J. *Chem. Rev.* **1997**, *97*, 173–205.

[21] Thanks to Dr. Ping Xie, a former postdoctoral researcher in the Lieber group, for his contributions to the thin-film conductivity measurements. Ping fabricated a custom four-point probe device for me, loaned me the necessary equipment to perform the measurements, and taught me how to analyze the conductivity data.

1/temperature (Fig. 1.20). By comparison, a film of dipalladium(III) complex **1.2** behaved as an insulator across the measured temperature range. For Pd(III) wire **1.8** with BF_4^- counteranions, thin-film conductivity measurements show a bandgap of 0.7 eV: 0.3 eV lower in energy than the bandgap measured for **1.4** (Fig. 1.21). The lower electrical bandgap for thin films of **1.8** as compared to that of **1.4** is consistent with the observed red shift in NIR absorption (Fig. 1.14). The ability to modify bandgap in semiconducting polymers is valuable for applications such as photovoltaic devices.[19c]

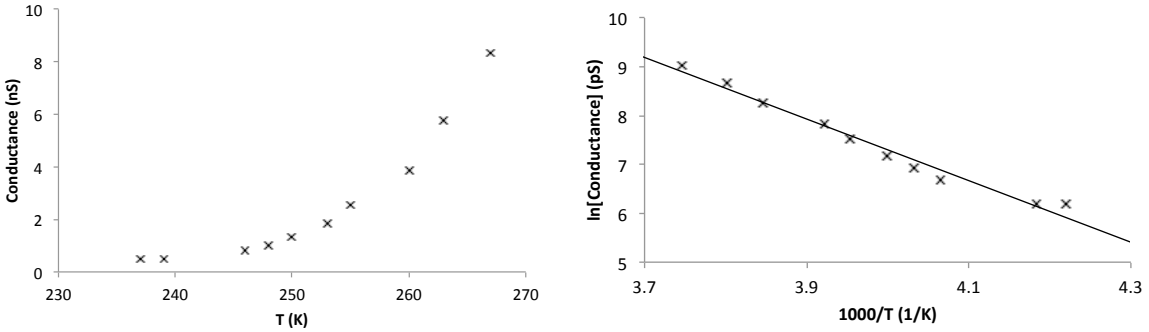

Figure 1.20. (*left*) Temperature-dependent thin-film conductivity for Pd(III)F wire **1.4.** (*right*) Plot of ln[conductance] (pS) versus inverse temperature (1,000 K^{-1}) for a film of **1.4**, which behaves as a semiconductor. Bandgap was calculated as 1 eV. Data points were obtained from linear fitting of I/V curves at each temperature.

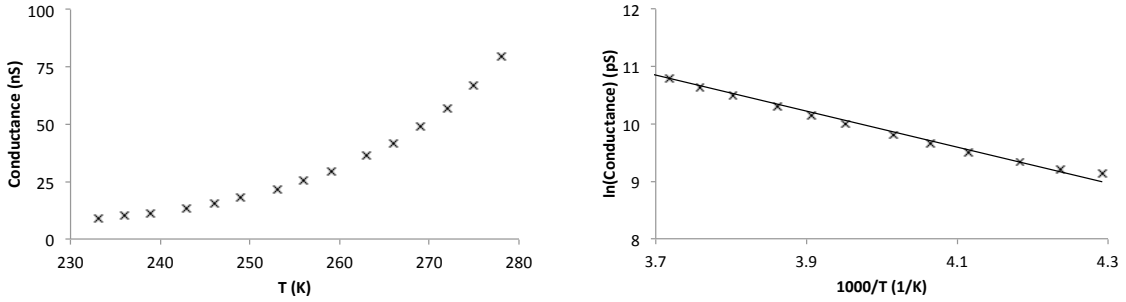

Figure 1.21. (*left*) Temperature-dependent thin-film conductivity for Pd(III)BF_4 wire **1.8.** (*right*) Plot of ln[conductance] (pS) versus inverse temperature (1,000 K^{-1}) for a film of **1.8**, which behaves as a semiconductor. Bandgap was calculated as 0.7 eV. Data points were obtained from linear fitting of I/V curves at each temperature.

The change in bandgap from **1.4** to **1.8** demonstrates that controlled molecular changes can influence the conductive properties of polymer films of 1-D palladium wires. In addition to the adjustment of bandgap through counteranion substitution, modification of electronic properties was effected through variation in the palladium oxidation state. In contrast to semiconducting films of Pd(III) wire **1.4** (Fig. 1.20), thin-film conductivity measurements of Pd(2.5) wire **1.5** show that a metal to insulator transition occurs at around 200 K (Fig. 1.22). Previously, a metallic state had not been observed for any polymer composed of 1-D metal wires.

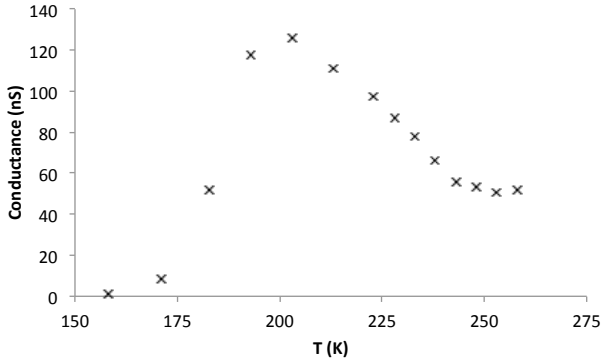

Figure 1.22. Temperature-dependent thin-film conductivity for Pd(2.5)F wire **1.5**, showing a metal to insulator transition around 200 K. Data points were obtained from linear fitting of I/V curves at each temperature.

As the supramolecular structure within the thin film of **1.5** is not known, the cause of the metal to insulator transition cannot be assigned as of yet. One-dimensional conductors are subject to Peierls distortion, in which the conductive electrons are no longer delocalized at low temperature, causing insulating behaviour.[22] Variable-temperature X-ray analysis of crystals of **1.5** did not show an apparent structural

[22] Peierls, R. E. *Quantum Theory of Solids* (Oxford University Press, 1955).

transition in the range of 15 to 250 K.[23] Conductivity measurements of single crystals of **1.5** have been unsuccessful to date because of crystal instability, but measurements of single crystals or single molecules could help to understand the effect of palladium oxidation state and molecular structure on wire conductivity.

[23] Thanks to Dr. Yu-Sheng Chen, the Advanced Photon Source at Argonne National Laboratory, for his assistance in acquiring the 15 K X-ray structure of **1.5**.

Chapter 2: Palladium(III)-Catalyzed Fluorination of Arylboronic Acid Derivatives

In recent years, there has been a dramatic increase in the number of available methods for the installation of fluorine and fluorine-containing functional groups into organic molecules. However, the development of practical carbon–fluorine bond forming reactions to provide aryl fluorides still remains as one of the most challenging transformations in the field of fluorination. This chapter describes the development of a palladium-catalyzed fluorination of arylboronic acid derivatives, which allows for an operationally simple, multi-gram-scale synthesis of functionalized aryl fluorides. A metal-catalyzed fluorination of arylboronic acid derivatives had not been reported prior to this work.[1] Evaluation of the reaction mechanism suggests a single-electron-transfer pathway, involving a Pd(III) intermediate that has been isolated and characterized.

2.1 Palladium-Catalyzed Fluorination of Aryl Trifluoroborates[2]

We have recently developed a palladium-catalyzed fluorination of aryl trifluoroborates, using commercially-available electrophilic fluorinating reagent Selectfluor® and terpyridyl Pd(II) complex **2.1** as a pre-catalyst (Scheme 2.1). Complex **2.1** has been prepared in one step from $Pd(OAc)_2$, terpyridine (terpy), and HBF_4 on decagram scale, and all reagents used in the catalytic fluorination reaction including **2.1**

[1] Several metal-mediated flurorination reactions of arylboronic acid derivatives have been reported, using Pd, Ag, and Cu. See: (a) Furuya, T.; Kaiser, H. M.; Ritter, T. *Angew. Chem., Int. Ed*. **2008**, *47*, 5993. (b) Furuya, T.; Ritter, T. *Org. Lett*. **2009**, *11*, 2860. (c) Fier, P. S.; Luo, J.; Hartwig, J. F. *J. Am. Chem. Soc*. **2013**, *135*, 2552. (d) Ye, Y.; Sanford, M. S. *J. Am. Chem. Soc*. **2013**, *135*, 4648.

[2] Much of the credit for the work described in this section belongs to Dr. Jennifer Murphy and Dr. Pingping Tang, former postdoctoral researchers in the Ritter group, and Anthony Mazzotti, a current graduate student in the Ritter group. Jennifer and Pingping were the first to identify the catalyst system described in Scheme 2.1; Anthony optimized the reaction conditions and performed all of the work pertaining to the substrates in Table 2.1.

are stable to air and moisture. The reaction can be performed in an open flask, and is effective for milligram to at least multi-gram scale synthesis of aryl fluorides, which are readily isolated. Inseparable side products from protodeborylation were not observed for the majority of substrates: protodeborylation is a common problem for fluorination reactions of arylboronic acid derivatives.[1c,d]

Scheme 2.1. Palladium-Catalyzed Fluorination of Aryl Trifluoroborates[a]

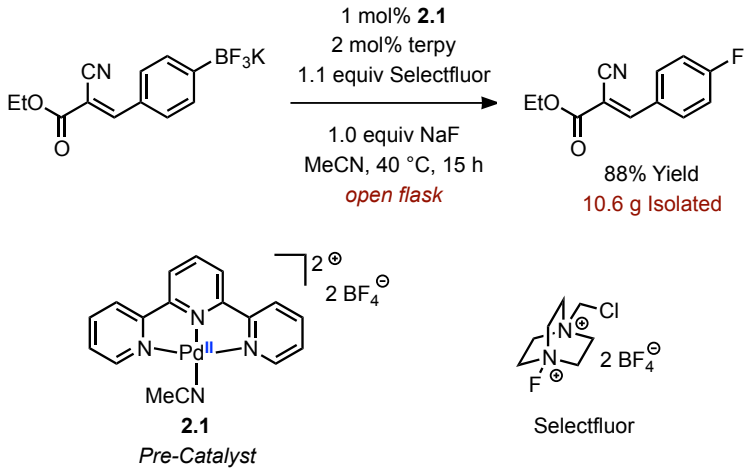

[a] terpy = 2,2′:6′,2″-terpyridine

As shown in Table 2.1, a wide variety of aryl trifluoroborates can be fluorinated, including both electron-rich and electron-poor arenes. DMF was found to be the optimal solvent for most electron-rich and electron-neutral arenes, while acetonitrile typically provided higher yields for arenes with electron-withdrawing substituents. Ketones, primary amides, carboxylic acids, esters, alcohols, basic heterocycles, aryl bromides, and *ortho*, *ortho'*-disubstitution are tolerated in the reaction.

Table 2.1. Fluorination of Aryl Trifluoroborates[a]

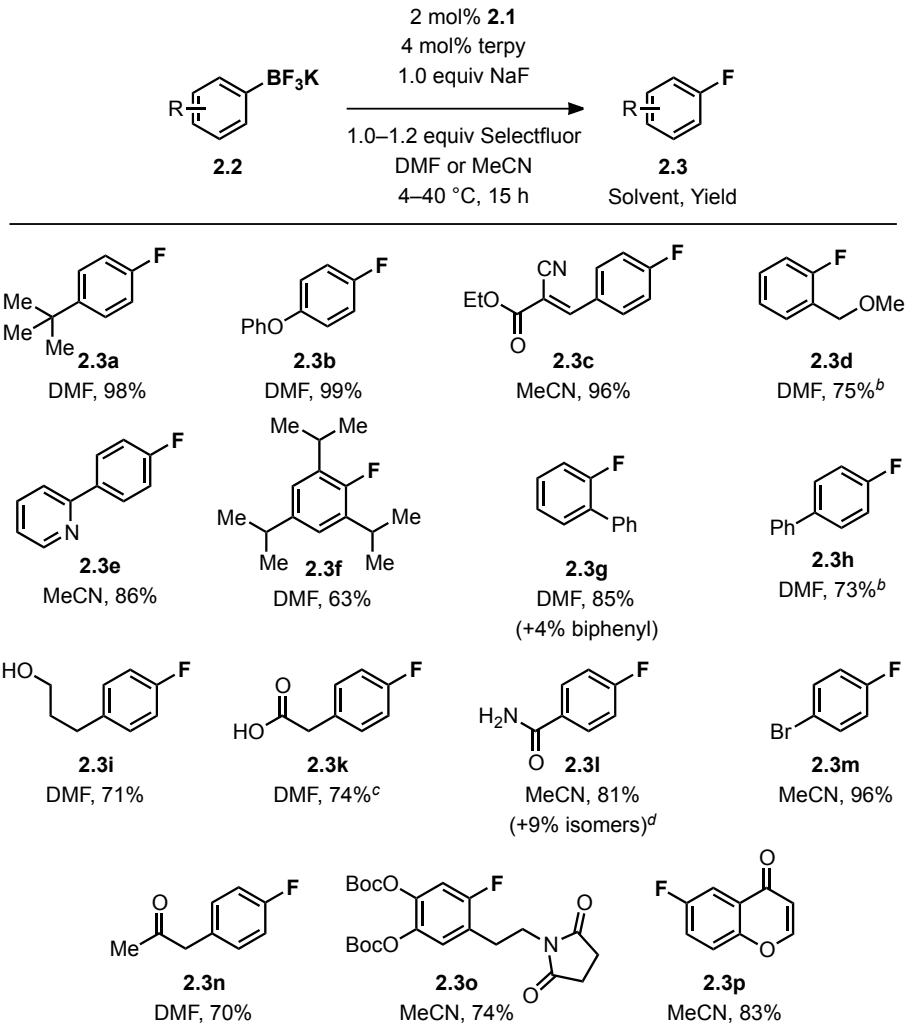

[a] Yields refer to isolated material of ≥98% purity unless otherwise noted. [b] No NaF was used. [c] 5 mol% **2.1** and 10 mol% terpy were used. [d] 9% of a mixture of constitutional isomers (ortho- and meta-fluorobenzamide).

Competing formation of constitutional isomers is a challenge for metal-catalyzed fluorination reactions.[3] Such impurities are usually difficult to separate from the desired aryl fluoride product. The majority of the aryl fluorides shown in Table 2.1 were isolated cleanly, with ≥98% purity. In particular, electron-rich aryl trifluoroborates generally did

[3] (a) Watson, D. A.; Su, M.; Teverovskiy, G.; Zhang, Y.; Garcia- Fortanet, J.; Kinzel, T.; Buchwald, S. L. *Science* **2009**, *325*, 1661. (b) Noel, T.; Maimone, T. J.; Buchwald, S. L. *Angew. Chem., Int. Ed*. **2011**, *50*, 8900. (c) Maimone, T. J.; Milner, P. J.; Kinzel, T.; Zhang, Y.; Takase, M. K.; Buchwald, S. L. *J. Am. Chem. Soc*. **2011**, *133*, 18106.

not react to form inseparable side products. Substrates with electron-withdrawing substituents are more likely to give constitutional isomers and diflurorinated products along with the expected aryl fluoride product (typically ≤10%): substrate **2.2l** is a representative example, which reacts to form **2.3l** along with 9% of ortho- and meta-fluorobenzamide. Other electron-poor substrates such as **2.2c** provided clean isolated product. The Pd-catalyzed fluorination reaction is ineffective for fluorination of heterocycles, and arenes bearing methoxy substituents gave significant amounts of side products resulting from demethylation.

2.2 Generality of Palladium-Catalyzed Fluorination

A variety of commercially available Pd(II) salts can be used in the fluorination reaction, as shown in Table 2.2. In general, palladium salts with less coordinating anions gave the highest yields. Anion metathesis using $NaBF_4$ as an additive resulted in higher yields for pre-catalysts with coordinating anions such as acetate. Palladium salts with halide anions were not suitable pre-catalysts for the fluorination reaction. Ultimately, we found **2.1** to be the most convenient pre-catalyst because no additive was needed, and due to its robust stability toward air and moisture as compared to $[Pd(MeCN)_4][BF_4]_2$. Complex **2.1** can be stored on the benchtop under ambient conditions without observable decomposition or decrease in catalytic reactivity for at least six months.

Table 2.2. Effectiveness of Other Palladium Pre-Catalysts[a]

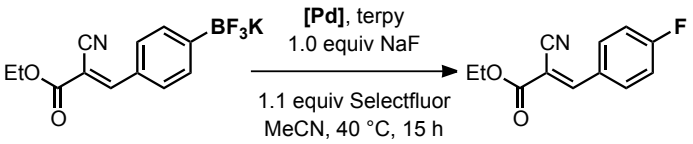

[Pd]	Additive	Yield
2.1	*none*	96%
2.4	*none*	95%
$[Pd(MeCN)_4][BF_4]_2$	*none*	95%
$Pd(OAc)_2$	$NaBF_4$ (2.0 equiv)	91%[b]
$Pd(O_2CCF_3)_2$	$NaBF_4$ (1.0 equiv)	91%

[a] 2 mol% [Pd] and 4 mol% terpy were used. Yields refer to isolated, purified material. [b] 5 mol% $Pd(OAc)_2$ and 10 mol% terpy were used.

Scheme 2.2. Palladium-Catalyzed Fluorination of Various Arylboronic Acid Derivatives

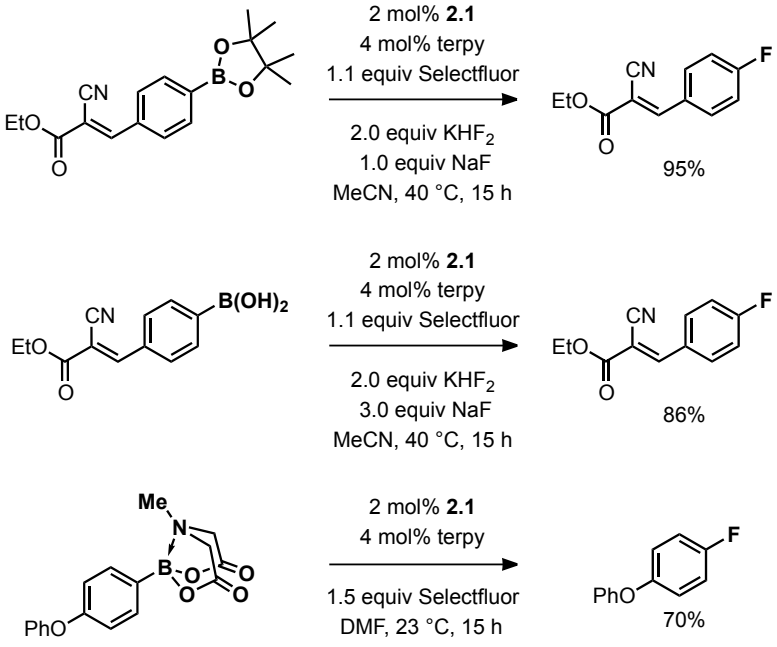

To highlight the reaction's practical utility, we have demonstrated that other common arylboron reagents are viable substrates. *In situ* formation of aryl trifluoroborates via addition of a mixture of NaF and KHF_2 allowed for efficient fluorination of pinacol boronic esters and arylboronic acids (Scheme 2.2). The ability to directly use a variety of

arylboronic acid derivatives, without the need for prior isolation of the aryl trifluoroborate, allows for fluorination of a greater range of starting materials.

We observed that MIDA esters of electron-rich arylboronic acids can also undergo Pd-catalyzed fluorination, albeit in lower yield and requiring a larger amount of Selectfluor (Scheme 2.2). No aryl fluoride product was obtained when either NaF or KHF_2 was added, suggesting that fluorination proceeds without formation of the aryl trifluoroborate. MIDA esters of electron-poor arylboronic acids did not afford product. The direct fluorination of MIDA boronates, in the absence of exogenous fluoride anion, indicates a mechanism in which the fluorine atom involved in C–F bond formation is derived from Selectfluor, rather than added fluoride anion.

2.3 Identification of Palladium(III) Intermediate

When Pd(II) pre-catalyst **2.1** was treated with one equivalent of terpyridine, followed by one equivalent of Selectfluor, a color change from orange to deep red occurred.[4] The color persisted in MeCN, and crystallization afforded red needles of Pd(III) complex **2.4** in 62% yield (Scheme 2.3). The structure of **2.4** was determined by X-ray crystallography; however, the high degree of disorder in the X-ray structure of **2.4** prevented satisfactory determination of the metric parameters and the Pd oxidation state. We were able to obtain a higher quality X-ray structure by co-crystallization of **2.4** with $NaBF_4$, affording **2.4•NaBF$_4$** as dark red prisms. The Pd cation of **2.4•NaBF$_4$** exhibits a Jahn-Teller distorted octahedral geometry, indicative of a d^7 Pd(III) center (Scheme 2.3). In the solid state, **2.4** is stable for months under ambient conditions. Pd(III) complex **2.4**

[4] This observation was first made by Anthony Mazzotti, and deserves acknowledgement as the starting point for all of the mechanistic work that follows.

is a chemically competent catalyst in the fluorination reaction (see Table 2.2), and was not observed to react with aryl trifluoroborates in the absence of Selectfluor, consistent with the mechanism shown in Figure 2.4 (*vide infra*). Additionally, **2.4** was not observed to react further when treated with additional Selectfluor, suggesting that a Pd(IV) intermediate is not accessible under the fluorination reaction conditions.

Scheme 2.3. Synthesis and X-ray Structure of Pd(III) Intermediate 2.4[a]

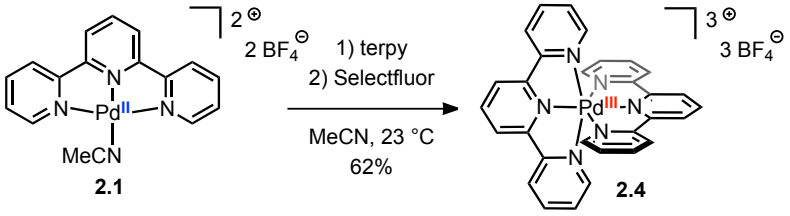

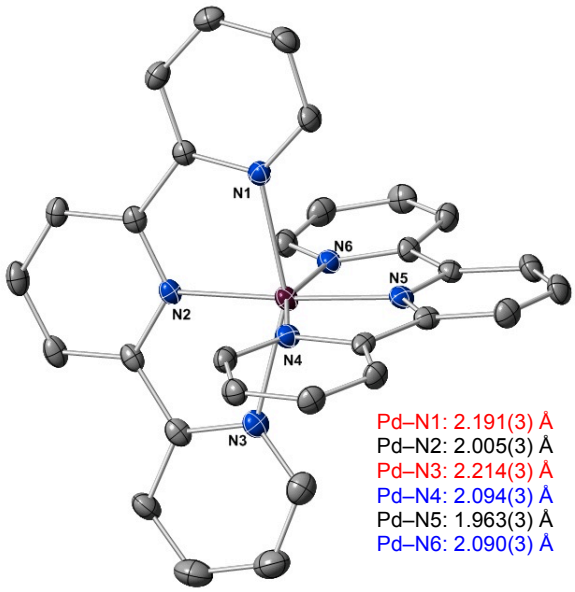

[a] X-ray structure of **2.4•NaBF$_4$** shown with 50% elipsoids; H-atoms, counteranions, and solvent molecules omitted for clarity.

The Jahn-Teller distorted octahedral geometry and the metric parameters of the terpyridine ligands for **2.4** are consistent with a d^7 configuration at Pd with an unpaired electron in a d_{z^2}-based orbital, rather than a ligand-centered radical, which is also supported by DFT calculations. The DFT-calculated α-HOMO of **2.4** is depicted in

Figure 2.1, and shows that the unpaired electron resides in an orbital that is is primarily of d_{z^2} parentage with respect to palladium and antibonding between palladium and the apical pyridyl ligands. EPR spectra of single cystals of **2.4** display isotropic spectra at both 298 K (g = 2.082) and 77 K (g = 2.089), with no observable spectral features due to hyperfine coupling or Jahn-Teller distortion (Fig. 2.2). We hypothesize that the lack of features observed in the EPR spectra may be due to a fluxional Jahn-Teller distortion at the temperatures at which the spectra were measured: fluxional Jahn-Teller distortion is well-precedented for cationic bis-terpyridyl transition metal complexes.[5]

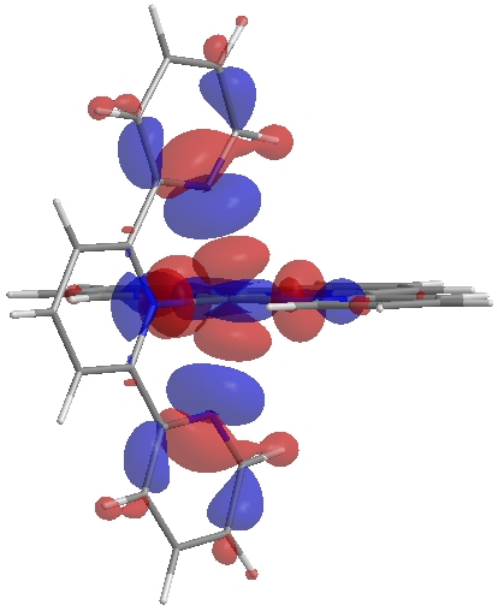

Figure 2.1. DFT-calculated α-HOMO of **2.4** (M06).

[5] (a) Folgado, J. V.; Henke, W.; Allmann, R.; Stratemeier, H.; Beltran-Porter, D.; Rojo, T.; Reinen, D. *Inorg. Chem.* **1990**, *29*, 2035–2042. (b) Mack, K.; Wünsche von Leupoldt, A.; Förster, C.; Ezhevskaya, M.; Hinderberger, D.; Klinkhammer, K. W.; Heinze, K. *Inorg. Chem.* **2012**, *51*, 7851–7858.

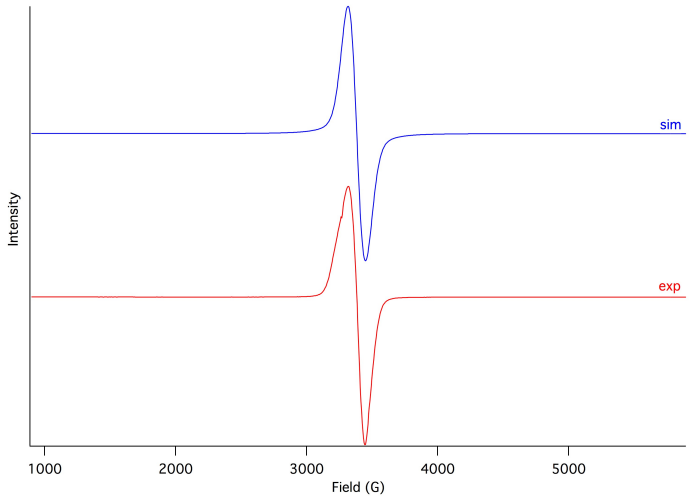

Figure 2.2. EPR spectrum of **2.4** (single crystals, 298 K), with simulated spectrum (g = 2.082).

The solution-state identity of Pd(III) complex **2.4** was also established in MeCN. EPR analysis of a frozen MeCN solution of **2.4** (77 K) shows an identical spectrum to single crystals of **2.4**. Solutions of **2.4** display a magnetic moment of μ_{eff} = 1.74 μB (23 °C, Evans method), which is close to the predicted spin-only value for a complex containing one unpaired electron (1.73 μB).[6] UV-vis/NIR spectra of **2.4** display characteristic features that futher confirm the d^7 electronic structure (Fig. 2.3).[7] Absorption bands were observed at 419 and 1002 nm, which were assigned as $\pi_{terpy} \rightarrow d_{z^2}$ and $d_{z^2} \rightarrow d_{x^2-y^2}$ transitions, respectively, using TD-DFT calculations.

[6] Drago, R. S. *Physical Methods for Chemists* (Saunders College Publishing, 1992).

[7] Mirica, L. M.; Khusnutdinova, J. R. *Coord. Chem. Rev.* **2012**, *257*, 299–314.

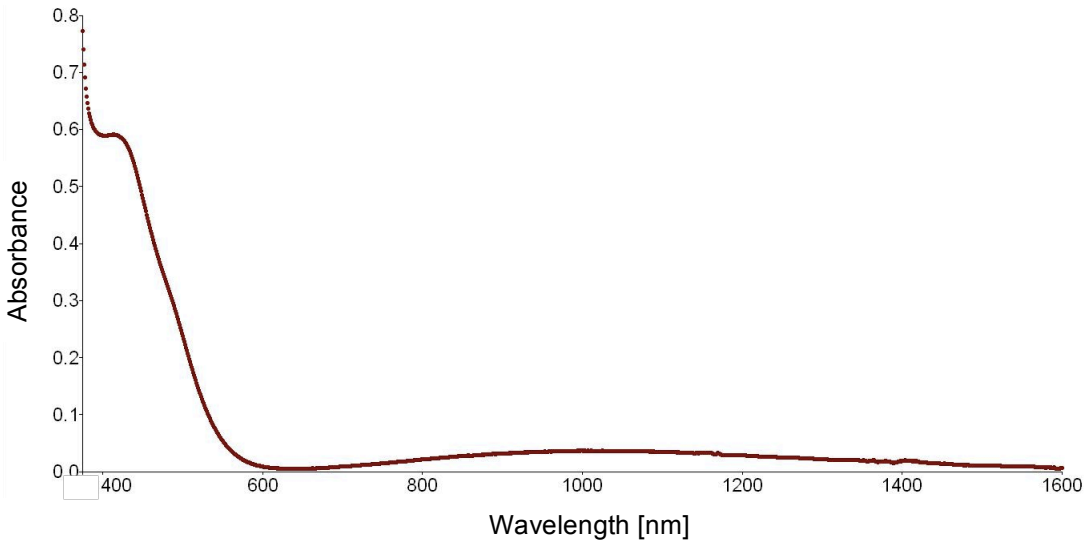

Figure 2.3. UV-vis/NIR spectrum of **2.4** (MeCN solution, 298 K).

2.4 Kinetic Studies and Evaluation of Reaction Mechanism[8]

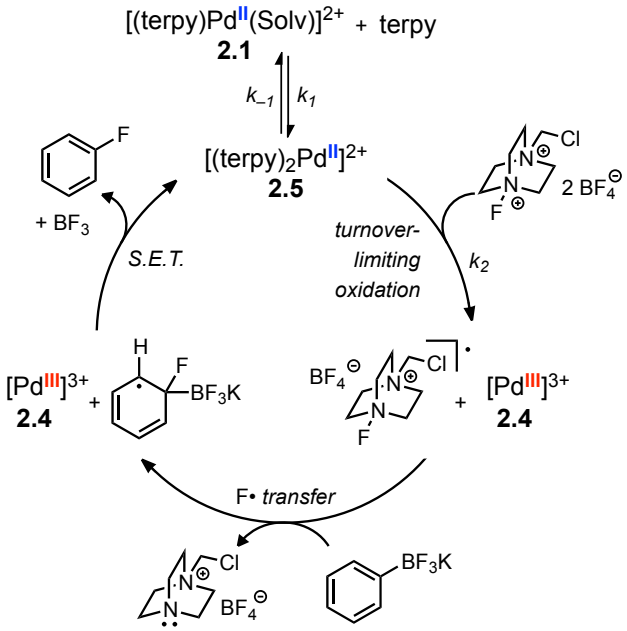

Figure 2.4. Proposed mechanism for Pd-catalyzed fluorination.

[8] Thanks to Dr. Jochen Brandt, a former postdoctoral researcher in the Ritter group, and Greg Boursalian, a current graduate student in the Ritter group, for many helpful discussions regarding mechanism and kinetic analysis.

We propose that the Pd-catalyzed fluorination reaction proceeds via an outer-sphere pathway, involving Pd(III) intermediate **2.4**. A mechanism that is consistent with the experimental data, as described below, is shown in Figure 2.4: first, turnover-limiting oxidation of a bis-terpyridyl Pd(II) complex (**2.5**) by Selectfluor affords Pd(III) **2.4** and a Selectfluor radical cation; F• transfer from the Selectfluor radical cation to an aryl trifluoroborate forms the C–F bond and generates a delocalized radical; finally, S.E.T. from the radical to **2.4** regenerates **2.5**, and provides a delocalized cation, which converts to the aryl fluoride with loss of BF_3. The generated BF_3 can react with fluoride anion or adventitious water, which may be why the addition of one equivalent of NaF typically increases the yield of aryl fluoride.

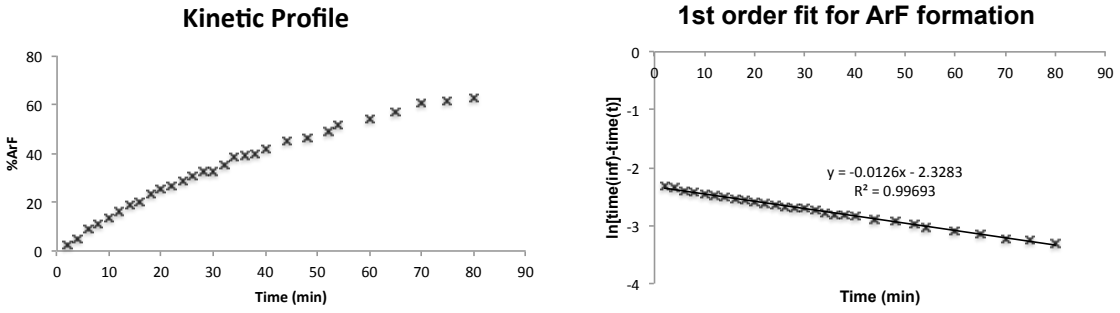

Figure 2.5. Kinetic profile of Pd-catalyzed fluorination reaction, displaying first-order behavior.

Aryl fluoride formation displayed a well-behaved first-order kinetics throughout the course of the catalytic reaction, and no induction period was observed (Fig. 2.5). Therefore, we were able to experimentally determine the rate law using initial rate kinetics, by monitoring aryl fluoride formation via ^{19}F NMR spectroscopy. The reaction displays first-order kinetic dependence on the palladium catalyst, saturation kinetics with

respect to terpyridine, zero-order dependence on aryl trifluoroborate, and a non-integer kinetic order of 1.4 with respect to Selectfluor (Figs. 2.6-2.9).

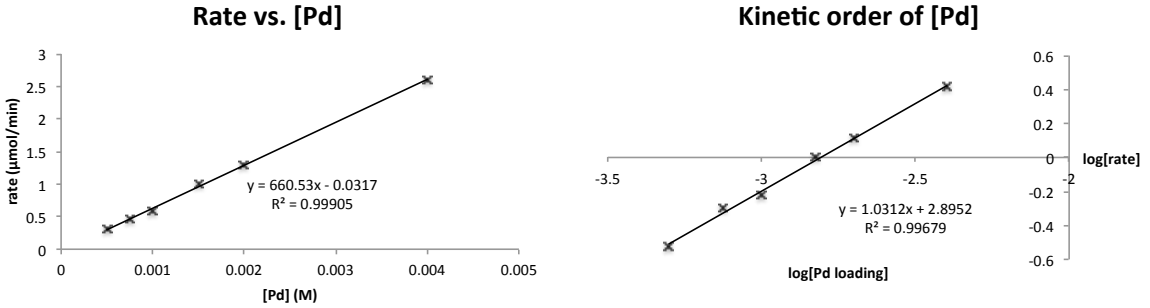

Figure 2.6. Determination of kinetic order of 1 with respect to Pd.

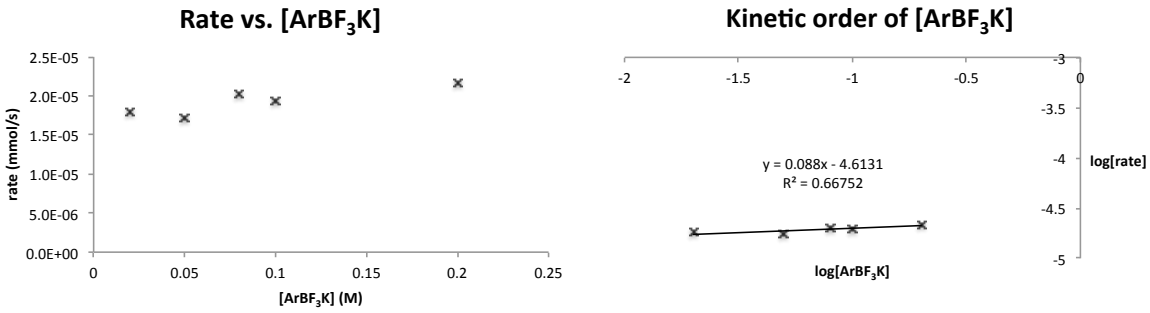

Figure 2.7. Determination of kinetic order of 0 with respect to aryl trifluoroborate.

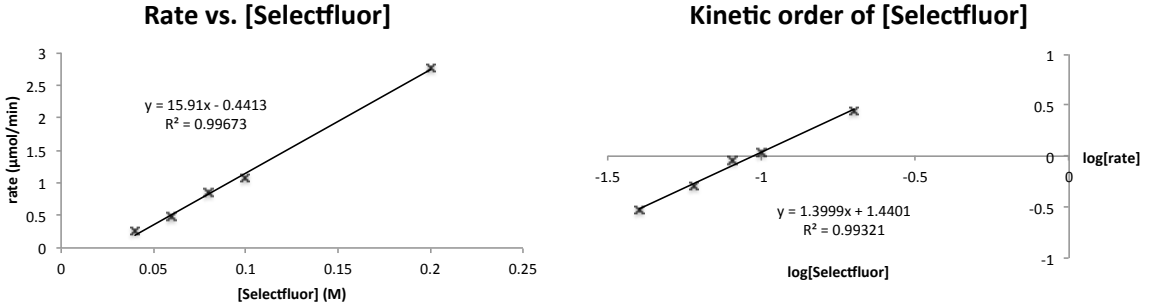

Figure 2.8. Determination of kinetic order of 1.4 with respect to Selectfluor.

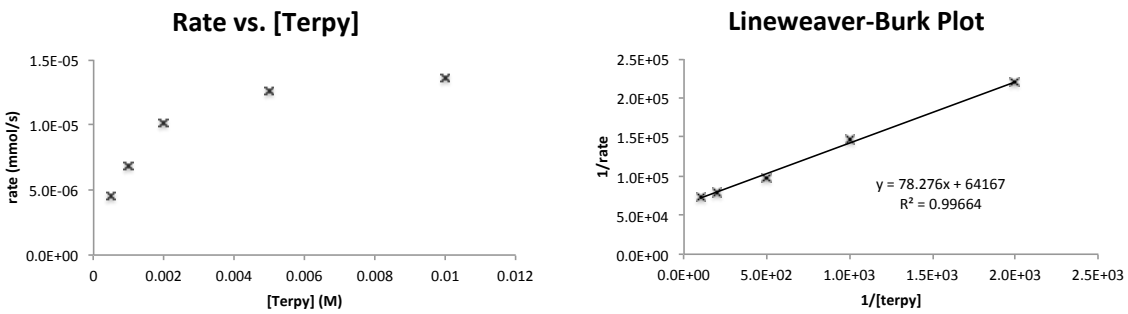

Figure 2.9. Determination of saturation kinetics with respect to terpyridine, and Lineweaver-Burk plot.

Based on the obtained kinetics data, oxidation of the palladium catalyst by Selectfluor is turnover-limiting during catalysis. The saturation behavior observed for terpyridine, along with *in situ* ^{1}H NMR spectroscopy of the reaction mixture (Figs. 2.10-2.12), indicates a catalyst resting state consisting of an off-cycle equilibrium between bis-terpyridyl Pd(II) complex **2.5** and a terpyridyl Pd(II) solvento complex (e.g. **2.1**). In DMF, the equilibrium of **2.5** with **2.1** and free terpyridine is rapid, with a measured binding constant of $K_a = 3\times10^3$.

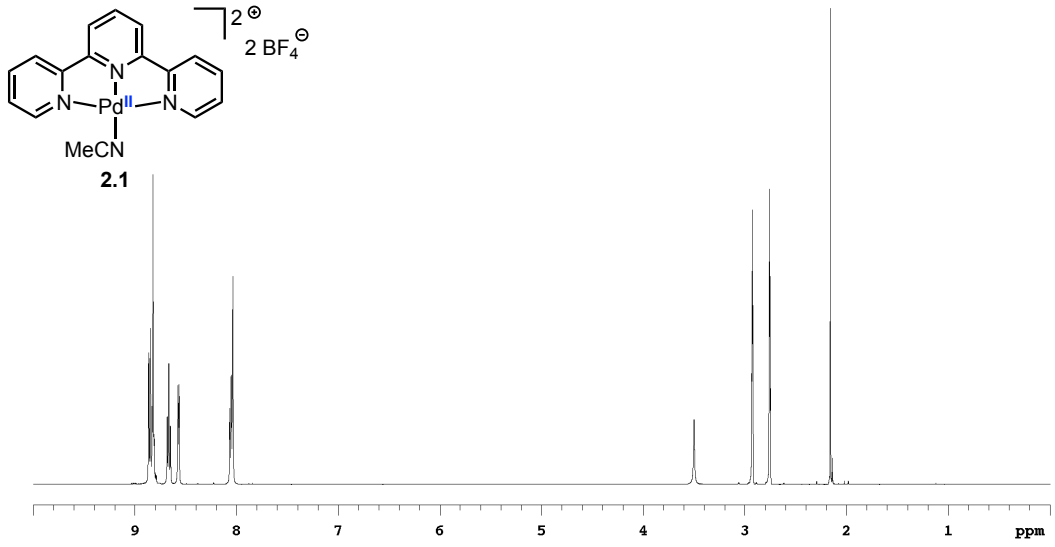

Figure 2.10. ^{1}H NMR spectrum of **2.1**. DMF-d_7, 500 MHz, 23 °C

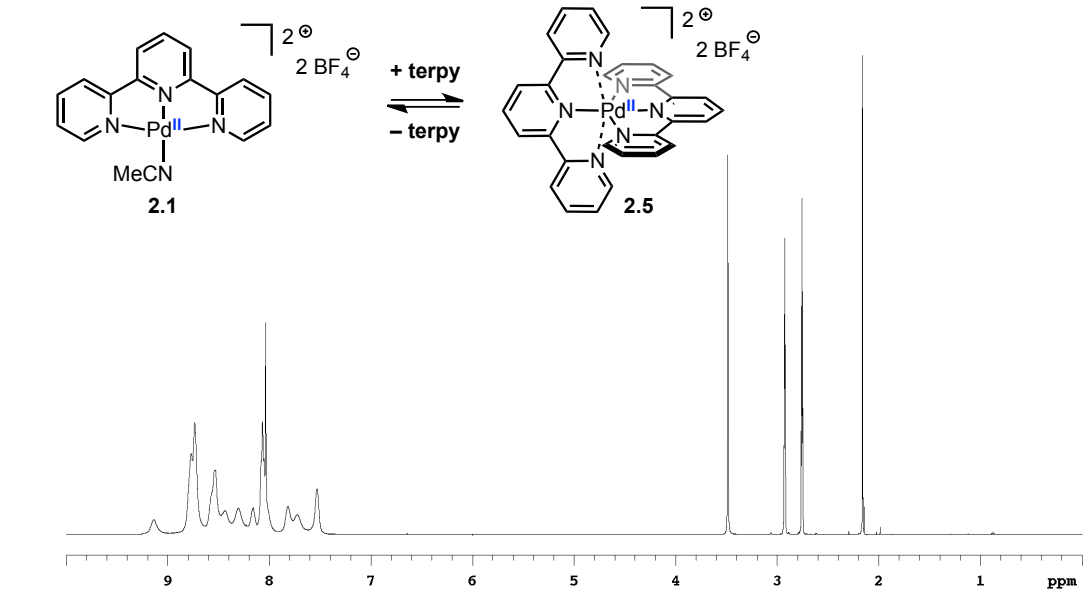

Figure 2.11. ^{1}H NMR spectrum of **2.1** with added terpyridine. DMF-d_7, 500 MHz, 23 °C

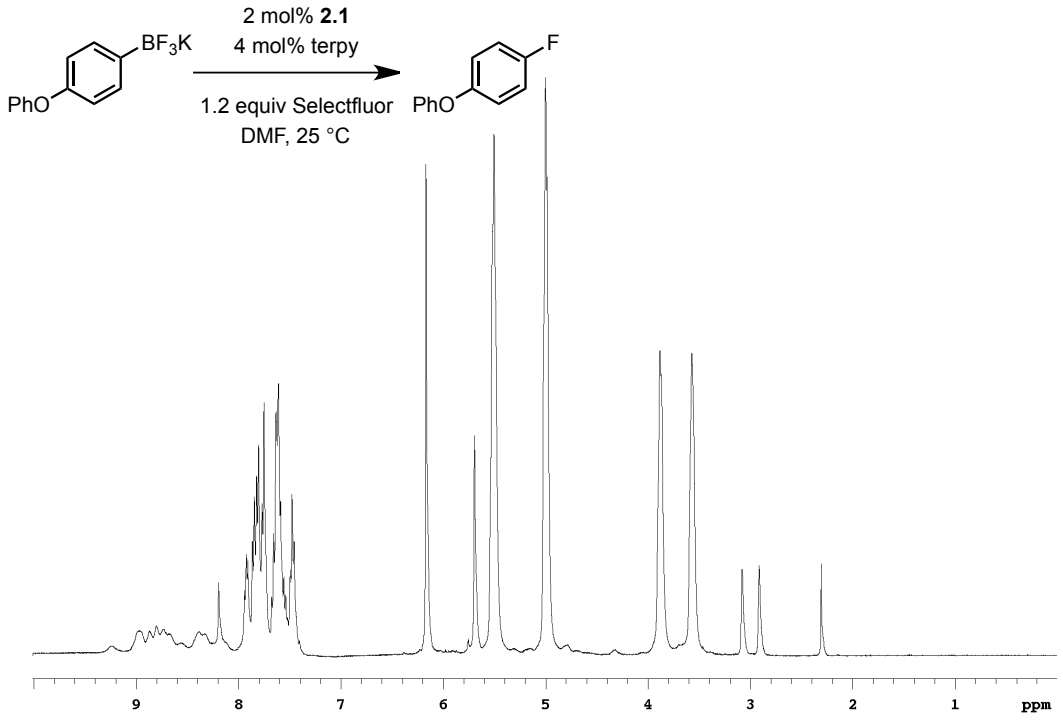

Figure 2.12. *In situ* ^{1}H NMR spectrum of Pd-catalyzed fluorination reaction. DMF-d_7, 400 MHz, 23 °C

The observation of a non-integer kinetic order for Selectfluor (1.4) suggests that Selectfluor also participates in a rapid equilibrium with **2.5**, prior to turnover-limiting oxidation. Electrochemical studies support this hypothesis, and provide additional insight into the oxidation step: cyclic voltammetry (CV) of Pd(III) complex **2.4** shows that oxidation of Pd(II) complex **2.5** to Pd(III) **2.4** does not occur via outer-sphere single electron transfer (Fig. 2.13). Additionally, Pd(III) complex **2.4** is observed to undergo a reversible one-electron oxidation to the Pd(IV) cation at a potential of 1.17 V (vs Fc/Fc^{+}). This potential is not accessible under the reaction conditions of the Pd-catalyzed fluorination, and therefore we believe that the intermediacy of Pd(IV) during catalysis is unlikely. It has been notoriously difficult to accurately measure or calculate the reduction potential of Selectfluor:[9] the reduction potential of Selectfluor has been measured at –40 mV vs SCE (–199 mV vs Fc/Fc^{+}),[10] but this value is inconsistent with the observed chemical reactivity.[11] A better estimate has been provided by chemical means: it has been demonstrated that Selectfluor is capable of oxidizing bromide ion to elemental bromine (690 mV vs Fc/Fc^{+}), but not of oxidizing chloride ion to elemental chlorine (980 mV Fc/Fc^{+}).[10] The inability to oxidize chloride ion provides an upper limit for the oxidation potential of Selectfluor at 980 mV, well below the observed Pd(III)/Pd(IV) redox couple at 1.17 V.

[9] Serguchev, Y. A.; Ponomarenko, M. V.; Lourie, L. F.; Fokin, A. A. *J. Phys. Org. Chem.* **2010**, *24*, 407–413.

[10] Gilicinski, A. G.; Pez, G. P.; Syvret, R. G.; Lal, G. S. *J. Fluor. Chem.* **1992**, *59*, 157–162.

[11] Nyffeler, P. T.; Dur n, S. G.; Burkart, M. D.; Vincent, S. P. P.; Wong, C.-H. *Angew. Chem. Int. Ed.* **2005**, *44*, 192–212.

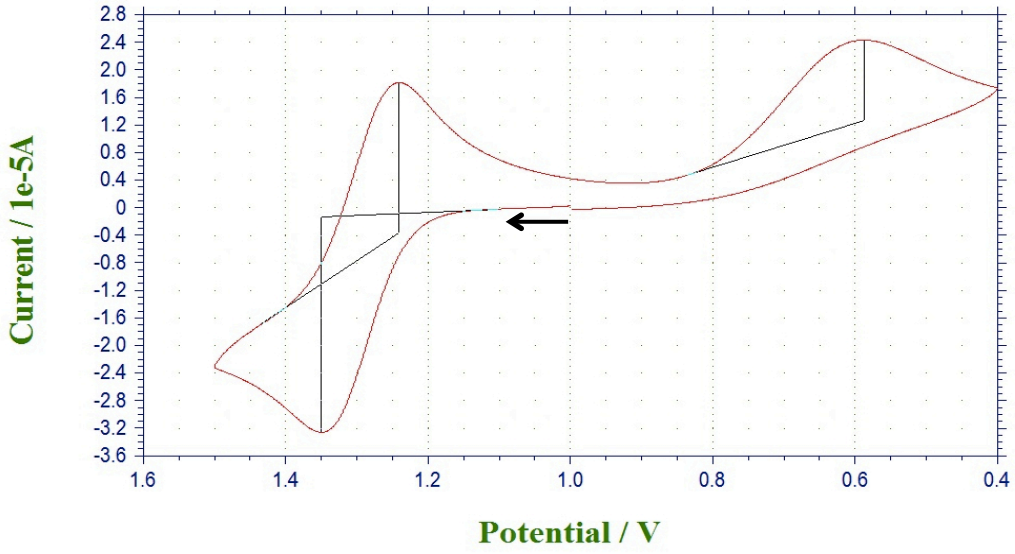

Figure 2.13. CV of Pd(III) complex **2.4**. The reversible oxidation wave at 1.17 V (vs Fc/Fc^{+}) is assigned as the Pd(III)/Pd(IV) redox couple while the irreversible reduction wave at 460 mV (vs. Fc/Fc^{+}) is assigned as the Pd(III)/Pd(II) redox couple.

$$\text{rate} = \frac{d[\text{ArF}]}{dt} = k_2[\text{Selectfluor}][\mathbf{2.5}]$$

Applying steady state approximation:

$$\frac{d[\mathbf{2.5}]}{dt} = 0 = k_1[\mathbf{2.1}][\text{terpy}] - k_{-1}[\mathbf{2.5}] - k_2[\text{Selectfluor}][\mathbf{2.5}]$$

$$= k_1([\text{Pd}]_0 - [\mathbf{2.5}])[\text{terpy}] - k_{-1}[\mathbf{2.5}] - k_2[\mathbf{2.5}][\text{Selectfluor}]$$

$$\left([\text{Pd}]_0 = \text{total concentration of Pd} = [\mathbf{2.1}] + [\mathbf{2.5}]\right)$$

$$k_1[\text{Pd}]_0[\text{terpy}] = k_1[\mathbf{2.5}][\text{terpy}] + k_{-1}[\mathbf{2.5}] + k_2[\mathbf{2.5}][\text{Selectfluor}]$$

$$k_1[\text{Pd}]_0[\text{terpy}] = [\mathbf{2.5}](k_1[\text{terpy}] + k_{-1} + k_2[\text{Selectfluor}])$$

$$[\mathbf{2.5}] = \frac{k_1[\text{Pd}]_0[\text{terpy}]}{k_{-1} + k_2[\text{Selectfluor}] + k_1[\text{terpy}]}$$

$$\text{rate} = \frac{k_1k_2[\text{Pd}]_0[\text{terpy}][\text{Selectfluor}]}{k_{-1} + k_2[\text{Selectfluor}] + k_1[\text{terpy}]}$$

if $k_{-1} + k_1[\text{terpy}] >> k_2[\text{Selectfluor}]$, then

$$\boxed{\text{rate} = \frac{k_1k_2[\text{Pd}][\text{Selectfluor}][\text{terpy}]}{k_{-1} + k_1[\text{terpy}]}}$$

Figure 2.14. Derivation of the rate law for the mechanism proposed in Figure 2.4.[12]

[12] Due to k_1/k_{-1} being a fast equilibrium, and k_2 being the rate of the turnover-limiting step, assuming $k_{-1} + k_1[\text{terpy}] >> k_2[\text{Selectfluor}]$

The proposed mechanism shown in Figure 2.4 would require zero-order dependence on the aryl trifluoroborate, first-order dependence on palladium, saturation behavior with respect to terpyridine, and first-order dependence on Selectfluor (rate law derivation given in Fig. 2.14). If the kinetic of 1.4 with respect to Selectfluor, along with the electrochemical data, is taken into account, the mechanism proposed in Figure 2.4 can be updated to include an equilibrium between Pd(II) **2.5** and Selectfluor to give a steady-state adduct prior to turnover-limiting oxidation.[13] If such an adduct (**A**) is incorporated into the proposed mechanism, a rate law can be derived that is consistent with all measured data (Fig. 2.15). The specific mode of interaction between the palladium catalyst and Selectfluor is unclear at this point, but is likely critical to the success of the fluorination reaction; we speculate that the fluxional binding of terpyridine in **2.5** is important to the observed reactivity (*vide infra*).

---

is reasonable, and consistent with the measured data.

[13] An additional empirical observation supports the formation of an intermediate between **2.5** and Selectfluor prior to turnover-limiting oxidation: in the stoichiometric reaction to form Pd(III) complex **2.4** (Scheme 2.3), a rapid color change from orange (**2.5**) to yellow is first observed, followed by a darkening of the reaction mixture to give a red color (**2.4**). I postulate that the short-lived yellow intermediate may be an adduct between **2.5** and Selectfluor. Freeze-quenching of the reaction mixture allowed for EPR analysis of the yellow solution (77 K), which showed no EPR signal. Freeze quenching after longer reaction times (as the yellow color darkens to red) results in the observation of an EPR spectrum attributable to Pd(III) **2.4**. This observation also supports our conclusion that oxidation of **2.5** to **2.4** does not proceed via outer-sphere SET, based on analysis of the electrochemical data.

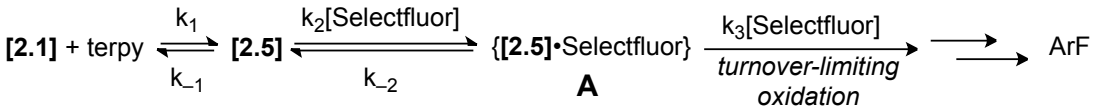

$$\text{rate} = \frac{d[\text{ArF}]}{dt} = k_3[\text{Selectfluor}][\mathbf{A}]$$

Applying steady state approximation for **A**:

$$\frac{d[\mathbf{A}]}{dt} = 0 = k_2[\mathbf{2.5}][\text{Selectfluor}] - k_{-2}[\mathbf{A}] - k_3[\text{Selectfluor}][\mathbf{A}]$$

$$[\mathbf{A}] = \frac{k_2[\mathbf{2.5}][\text{Selectfluor}]}{k_{-2} + k_3[\text{Selectfluor}]}$$

Applying steady state approximation for **2.5**:

$$\frac{d[\mathbf{2.5}]}{dt} = 0 = k_1[\mathbf{2.1}][\text{terpy}] - k_{-1}[\mathbf{2.5}] - k_2[\text{Selectfluor}][\mathbf{2.5}]$$

$$\left([\text{Pd}]_0 = \text{total concentration of Pd} = [\mathbf{2.1}] + [\mathbf{2.5}]\right)$$

$$[\mathbf{2.5}] = \frac{k_1[\text{Pd}]_0[\text{terpy}]}{k_{-1} + k_2[\text{Selectfluor}] + k_1[\text{terpy}]}$$

Incorporating [**2.5**] into [**A**]:

$$[\mathbf{A}] = \underbrace{\left(\frac{k_2[\text{Selectfluor}]}{k_{-2} + k_3[\text{Selectfluor}]}\right)}_{\approx k_{-2}} \bullet \left(\frac{k_1[\text{Pd}]_0[\text{terpy}]}{k_{-1} + k_2[\text{Selectfluor}] + k_1[\text{terpy}]}\right)$$

$$[\mathbf{A}] = \frac{k_1k_2[\text{Pd}]_0[\text{terpy}][\text{Selectfluor}]}{k_{-1}k_{-2} + k_2k_{-2}[\text{Selectfluor}] + k_1k_{-2}[\text{terpy}]}$$

$$\boxed{\text{rate} = \frac{k_1k_2k_3[\text{Pd}]_0[\text{terpy}][\text{Selectfluor}]^2}{k_{-1}k_{-2} + k_2k_{-2}[\text{Selectfluor}] + k_1k_{-2}[\text{terpy}]}}$$

Figure 2.15. Derivation of a rate law which is consistent with all obtained data for the Pd-catalyzed fluorination reaction.

In order to consider the possibility of an adduct between the Pd(II) catalyst and Selectfluor, it is necessary to examine the structure of Pd(II) complex **2.5**, formed upon binding of terpyridine to pre-catalyst **2.1**. It is challenging to characterize the structure of **2.5** due to rapid equilibria in solution (*vide supra*). Crystallization from a mixture of **2.1** and terpyridine affords compound **2.6**, the structure of which was determined using X-ray crystallography (Scheme 2.4). However, the data indicate that **2.6** is not the structure of

the initial adduct between **2.1** and terpyridine, and is not relevant to the Pd-catalyzed fluorination reaction.

Scheme 2.4. Synthesis of 2.6, and X-ray structures of 2.1 and 2.6[a]

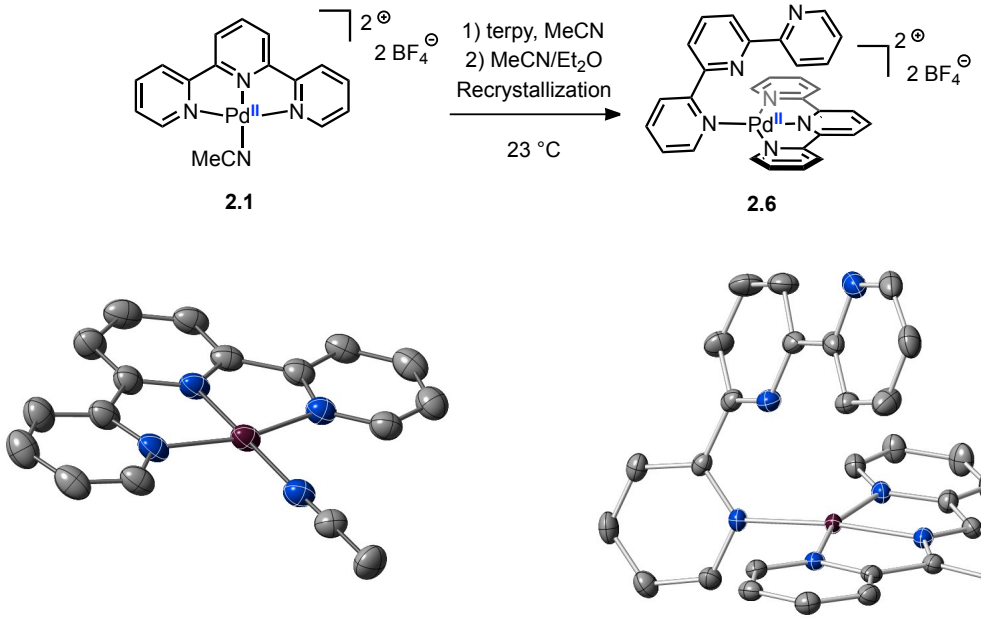

[a] X-ray structures are shown with 50% elipsoids; H-atoms, counteranions, and solvent molecules omitted for clarity.

Scheme 2.5. Demonstration of Chemical Incompetence of Pd(II) Complex 2.6 in the Fluorination of Aryl Trifluoroborates

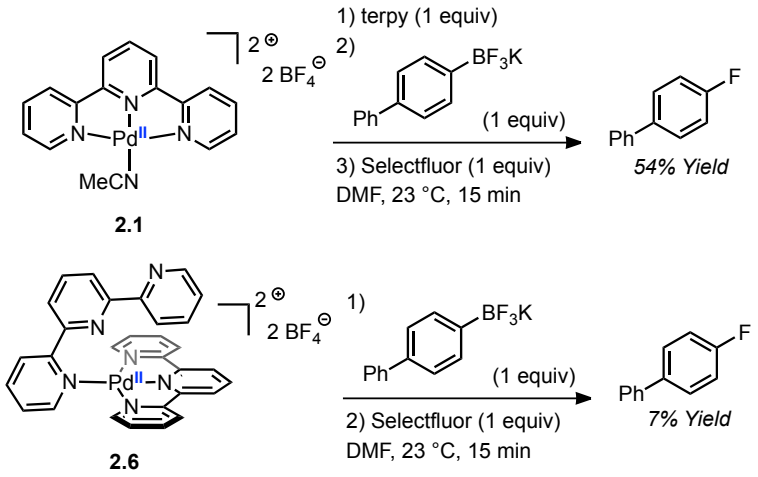

When the reactivity of isolated **2.6** was compared with a freshly prepared solution of **2.1** and terpyridine, it was found that **2.6** is not chemically competent in the fluorination of aryl trifluoroborates with Selectfluor (Scheme 2.5). Additionally, **2.6** does not react with Selectfluor to form Pd(III) complex **2.4**. We propose that the structure of the initial adduct between **2.1** and terpyridine is pseudo-octahedral complex **2.5**, which converts to **2.6** upon crystallization. The observed reactivity is summarized in Scheme 2.6, in which **2.6** is a thermodynamically more stable product than **2.5**, but is not relevant in the catalytic fluorination reaction with Selectfluor.

Scheme 2.6. Reactivity of Bis-Terpyridyl Pd(II) Complexes 2.5 and 2.6 with Selectfluor

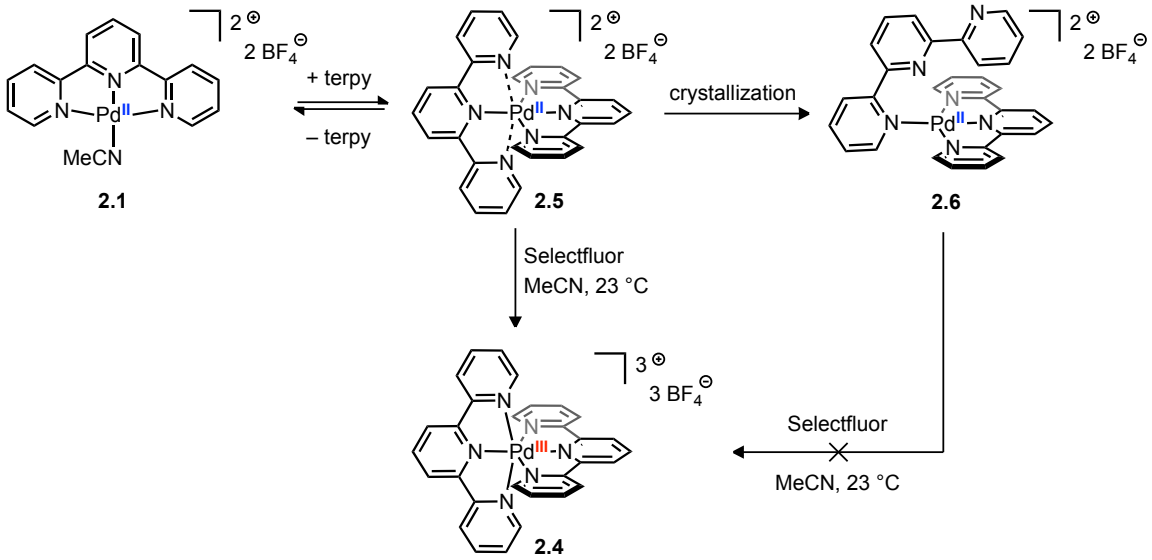

DFT calculations are consistent with the observed chemical reactivity difference between **2.5** and **2.6**: the optimized structure of **2.5** displays a psedudo-octahedral geometry, in which the apical pyridyl ligands are rotated away from the *z*-axis to avoid interaction with the filled d_{z^2} orbital on Pd. The calculated HOMO is primarily of d_{z^2} parentage with respect to Pd, and antibonding with respect to the apical pyridyl ligands. Removal of one electron from this orbital via oxidation would be expected to give a

distorted octahedral d^7 Pd(III) complex (e.g. **2.4**), as is indeed observed when **2.5** is treated with terpyridine and Selectfluor. The optimized structure of **2.6** has a calculated HOMO which is primarily based on the π-system of the monodentate terpyridine ligand: this is consistent with the observation that **2.6** is not oxidized to Pd(III) **2.4** (Fig. 2.16). The calculations indicate that **2.6** is thermodynamically favored by 2.3 kcal/mol as compared to **2.5**. Based on the observed reactivity, however, we believe that **2.5** is not kinetically accessible during the Pd-catalyzed fluorination reaction.

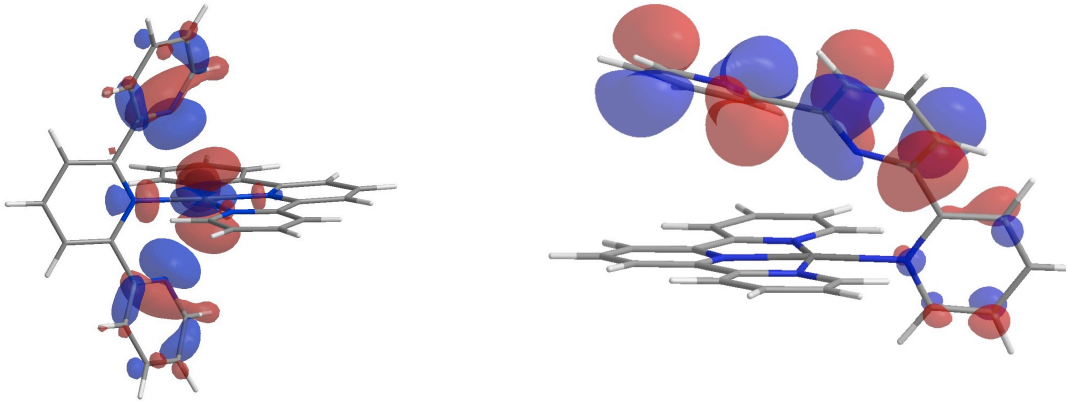

Calculated HOMO of **2.5** Calculated HOMO of **2.6**

Figure 2.16. DFT calculated HOMOs of Pd(II) complexes **2.5** and **2.6** (M06).

The observation of turnover-limiting oxidation during catalysis prevents us from studying the C–F bond forming step via kinetic analysis. We postulate that C–F bond formation occurs via one of two pathways after initial oxidation of **2.5** by Selectfluor: (1) direct F• transfer to the aryl trifluoroborate; or, (2) S.E.T. from the aryl trifluoborate to the Selectfluor radical cation, to afford a radical cation, followed by nucleophilic attack of fluoride (Scheme 2.7, top). In both cases, one-electron oxidation of the resulting radical by Pd(III) **2.4** would afford product and regenerate Pd(II) **2.5**. We carried out an isotopic labeling experiment to distinguish between the two pathways, in which the

fluorination reaction was performed in the presence of exogenous [^{18}F]fluoride.[14] Aryl fluoride formation proceeded in 72% yield, but no incorporation of the ^{18}F label was observed (Scheme 2.7, bottom). While the S.E.T./fluoride attack pathway via a tight solvent cage mechanism cannot be rigorously excluded, the absence of ^{18}F incorporation suggests the F• transfer pathway for C–F bond formation.

Scheme 2.7. Potential Pathways for C–F Bond Formation, and Isotopic Labeling Experiment

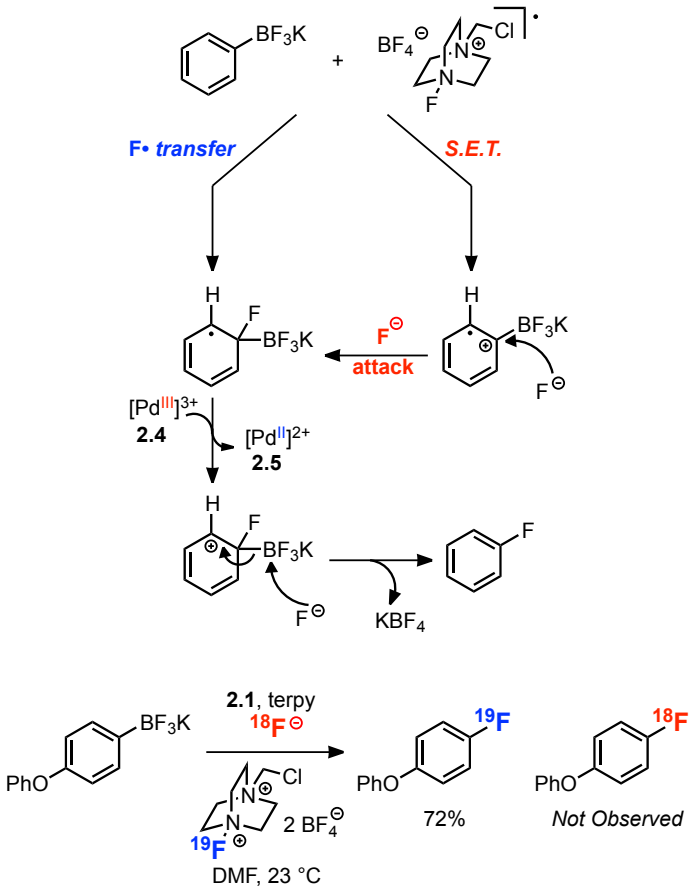

In previously reported metal-mediated or -catalyzed arene fluorination reactions, including our group's palladium- and silver-mediated fluorination of arylboronic acids, carbon–fluorine bond formation is proposed to occur via reductive elimination from an

[14] Thanks to Constanze Neumann, a graduate student in the Ritter group, for performing the radiochemistry experiments.

aryl–metal fluoride complex.[1a,b] The palladium-catalyzed fluorination reaction presented here is unusual in that it seems to proceed without the formation of organopalladium intermediates, yet provides high levels of selectivity.

CONCLUSION

While palladium has long been recognized as one of the most useful and versatile transition metals in homogeneous and heterogeneous catalysis, the burgeoning field of Pd(III) chemistry demonstrates that there is significant untapped potential for new reactivity. The development of fundametally new reactivity is often necessary in order to address unsolved problems in chemistry, and the study of transition metal complexes with unusual electronic structures can be a powerful approach for discovering new reactivity. It is my hope that the work in this thesis provides a demonstration of such an approach, and that my results may be useful for guiding future development of new and better chemistry.

In the 1-D Pd wires project, it was shown that Pd–Pd bonding between Pd(III) centers allowed for synthesis of the longest known solution-stable 1-D metal chain. The solution stability allows not only for device fabrication via thin-film coating, but also allows for facile modification of wire structure, resulting in changes in supramolecular structure and properties. Such a degree of rational molecular control over 1-D wire structure had not been reported prior to our work. While the thermal and atmospheric instability of the 1-D Pd wires described in this thesis prevents their use as functional materials in any practical application, I hope that the synthetic methodology we have developed can inspire new approaches to 1-D metal wires with rationally tailored properties. Additionally, the discovery of strong metal–metal bonding between Pd(III) centers suggests that all-d^7 chains of other metals, such as Ru(I), may be worthy synthetic targets.

I believe that the Pd(III)-catalyzed fluorination project also provides significant opportunity for the development of new reactivity. The mode of interaction between

Selectfluor and the Pd(II) catalyst is not currently well-understood, but seems to allow for mild and selective F• transfer via a previously unappreciated mechanistic pathway. Further development and understanding of this reactivity could ultimately allow for the design of an improved Pd catalyst system that facilitates C–H fluorination via F• transfer, without the need for pre-functionalized substrates such as arylboronic acid derivatives.

EXPERIMENTAL

Materials and Methods

Reactions were carried out under ambient atmosphere unless otherwise noted. Purified compounds were dried under high vacuum (0.01–0.05 Torr). Yields refer to purified and spectroscopically pure compounds. Thin layer chromatography (TLC) was performed using EMD TLC plates pre-coated with 250 μm thickness silica gel 60 F_{254} plates and visualized by fluorescence quenching under UV light and $KMnO_4$ stain. Flash chromatography was performed using silica gel (230-400 mesh) purchased from Silicycle Inc. Melting points were measured on a Thomas Scientific Uni-Melt capillary melting point apparatus. All melting points were measured in open capillaries and are uncorrected. NMR spectra were recorded on either a Varian Unity/Inova 600 spectrometer operating at 600 MHz for ^{1}H acquisitions, a Varian Unity/Inova 500 spectrometer operating at 500 MHz and 125 MHz for ^{1}H and ^{13}C acquisitions, respectively, or a Varian Mercury 400 spectrometer operating at 400 HMz and 375 MHz for ^{1}H and ^{19}F acquisitions, respectively. Chemical shifts are reported in ppm with the solvent resonance as the internal standard (^{1}H: $CDCl_3$, δ 7.26; CD_2Cl_2, δ 5.32; $(CD_3)_2SO$, δ 2.50; CD_3CN, δ 1.94; $(CD_3)_2CO$, δ 2.05), (^{13}C: $CDCl_3$, δ 77.16; CD_2Cl_2, δ 53.84; CD_3CN, δ 1.32, $(CD_3)_2SO$, δ 39.52; $(CD_3)_2CO$, δ 29.84, 206.26).[1] Data is reported as follows: s = singlet, br = broad, d = doublet, t = triplet, q = quartet, quin = quintet, m =

[1] Fulmer, G. R.; Miller, A. J. M.; Sherden, N. H.; Gottlieb, H. E.; Nudelman, A.; Stoltz, B. M.; Bercaw, J. E.; Goldberg, K. I. *Organometallics* **2010**, *29*, 2176-2179.

multiplet; coupling constants in Hz; integration. All deuterated solvents were purchased from Cambridge Isotope Laboratories. Solution-state magnetic susceptibility measurements were obtained using the Evans method[2] and are reported as follows: (field strength, solvent, temperature): μ_{eff} (concentration in mg/mL). EPR spectra were recorded on a Bruker ElexSys E500 EPR spectrometer operating at X-band frequency (9 GHz). UV-vis/NIR spectra were measured on a PerkinElmer Lambda 750 spectrophotometer. Electrochemical measurements were made using a CH Instruments Model 600E Series Electrochemical Analyzer/Workstation with a glassy carbon working electrode, a Pt wire counterelectrode, and a non-aqueous Ag/Ag^+ reference electrode. High-resolution mass spectra were obtained using an Agilent ESI-TOF (6210) mass spectrometer or a Bruker q-TOF Maxis Impact mass spectrometer. LC/MS data were obtained using a Shimadzu LCMS-2020.

Reagents and Solvents: All chemicals were used as received unless otherwise noted. $Pd(OAc)_2$ was purchased from Strem. $HBF_4 \cdot OEt_2$ was purchased from Alfa Aesar. 1-Chloromethyl-4-fluoro-1,4-diazoniabicyclo[2.2.2]octane bis(tetrafluoroborate) (Selectfluor) and 2,2′:6′,2″-terpyridine (terpy) were purchased from Strem or SigmaAldrich. XeF_2 was purchased from Matrix Scientific. Benzo[h]quinoline was obtained from TCI America. Trimethylsilyl chloride and boron trifluoride etherate were obtained from Alfa Aesar and distilled before use.

For the reactions described in Chapter 1, anhydrous solvents were obtained either by filtration through drying columns[3] (Et_2O, pentane, CH_2Cl_2) on an mBraun system or by distillation over sodium (benzene, hexanes). For the reactions described in Chapter 2,

[2] Evans, D. F. *J. Chem. Soc.* **1959**, 2003–2005.

[3] Pangborn, A. B.; Giardello, M. A.; Grubbs, R. H.; Rosen, R. K.; Timmers, F. J. *Organometallics* **1996**, *15*, 518.

DMF was ACS Reagent grade, purchased from SigmaAldrich; MeCN was ACS grade, purchased from BDH. These solvents were used as received without further purification.

Experimental Procedures and Compound Characterization for Chapter 1[4]

Benzo[*h*]quinolinyl Palladium Acetate Dimer (1.1)[5]

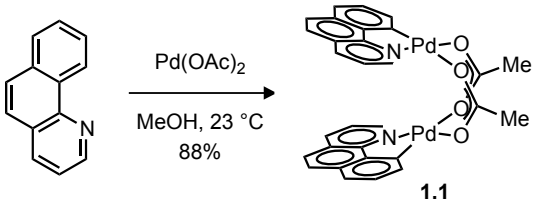

1.1

To benzo[*h*]quinoline (1.00 g, 5.58 mmol, 1.00 equiv) in MeOH (75 mL) at 23 ºC was added $Pd(OAc)_2$ (1.25 g, 5.58 mmol, 1.00 equiv). After eight hours, the precipitate was isolated by filtration and washed sequentially with MeOH (50 mL) and Et_2O (50 mL) to afford 1.68 g of the title compound as a yellow solid (88% yield).

NMR spectroscopy: ^{1}H-NMR (500 MHz, $CDCl_3$, 23 ºC, δ): 7.82 (dd, J = 5.0 Hz, 1.1 Hz, 2H), 7.44 (dd, J = 8.0 Hz, 1.1 Hz, 2H), 7.25–7.20 (m, 6H), 7.09 (dd, J = 6.9 Hz, 1.1 Hz, 2H), 6.99 (d, J = 8.7 Hz, 2H), 6.48 (dd, J = 8.0 Hz, 5.0 Hz, 2H), 2.38 (s, 6H). ^{13}C-NMR (125 MHz, $CDCl_3$, 23 ºC, δ): 182.25, 152.92, 148.60, 148.52, 139.74, 135.00, 132.18, 128.71, 127.59, 127.42, 124.70, 122.62, 121.81, 119.51, 24.92. These spectroscopic data correspond to the reported data in reference 4. UV-VIS Spectroscopy

[4] I thank Dave Powers, Jean Raynaud, and Ping Xie for their contributions to the experiments described herein. Please see the footnotes throughout Chapter 1 for details of each of their individual contributions.

[5] Dick, A. R., Hull , K. L. & Sanford, M. S. *J. Am. Chem. Soc.* **2004**, *126*, 2300–2301.

(CH_2Cl_2, 23 ˚C): 377 nm (ε = 2.39 × 10^3 M^{-1} cm^{-1}); 346 nm (ε = 2.30 × 10^3 M^{-1} cm^{-1}). Mass Spectrometry: LRMS-APCI (m/z): calcd for [$C_{30}H_{22}N_2O_4Pd_2^+$]: 687.97; found: 686.0. X-ray data for **1.1** has been deposited in the CCDC under reference numbers 705005 (Needle morphology) and 832191 (prismatic morphology).

[Pd(bhq)Cl(OAc)]$_2$ (1.2)

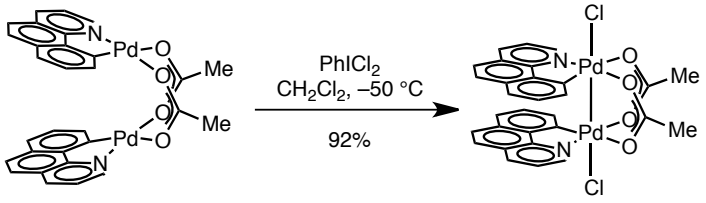

1.1 **1.2**

All manipulations were carried out in a dry box under a N_2 atmosphere. To benzo[*h*]quinolinyl palladium acetate dimer (**1.1**) (72.0 mg, 0.105 mmol, 1.00 equiv) in CH_2Cl_2 (2.5 mL) at –50 ˚C was added $PhICl_2$ (28.8 mg, 0.105 mmol, 1.00 equiv.). The pale yellow solution became dark red-brown immediately upon addition. After stirring at –50 ˚C for 10 minutes, solvent was removed *in vacuo*. The residue was washed with cold Et_2O (–50 ˚C) three times. The remaining solid was dried under vacuum to afford 73.1 mg of the title compound as a dark red solid (92% yield.). X-ray quality crystals were obtained after 24 hours by layering a concentrated CH_2Cl_2 solution with pentane at –35˚C.

NMR Spectroscopy: When the ^{1}H NMR spectrum is obtained at –10 ºC , fluxional acetate exchange with chloride leads to two distinct acetate signals (at 2.70 and 1.58 ppm, respectively). ^{1}H-NMR (500 MHz, CD_2Cl_2, –10 ºC, δ): 7.83 (d, *J* = 4.3 Hz, 2H), 7.71 (d, *J* = 7.8 Hz, 2H), 7.49 (dd, *J* = 7.3 Hz, *J* = 7.3 Hz, 2H), 7.42 (d, *J* = 7.3 Hz, 2H), 7.37 (d, *J*

= 8.8 Hz, 2H), 7.22 (d, *J* = 7.8 Hz, 2H), 7.18 (d, *J* = 8.8 Hz, 2H), 6.85 (dd, *J* = 6.5 Hz, *J* = 6.5 Hz, 2H), 2.70 (s, 4H), 1.58 (s, 2H). When the ^{1}H NMR spectrum is obtained at –50 ºC , fluxional acetate exchange with chloride has not occurred and thus only one acetate signal (bridging position; 2.69 ppm) is observed. ^{1}H-NMR (500 MHz, CD_2Cl_2, –50 ºC, δ): 7.71 (bs, 2H), 7.58 (d, *J* = 7.8 Hz, 2H), 7.45 (dd, *J* = 7.3 Hz, *J* = 7.3 Hz, 2H), 7.35 (d, *J* = 7.8 Hz, 2H), 7.22 (d, *J* = 8.8 Hz, 2H), 7.18 (d, *J* = 7.8 Hz, 2H), 7.03 (d, *J* = 8.3 Hz, 2H), 6.71 (bs, 2H), 2.69 (s, 6H). UV-VIS Spectroscopy (CH_2Cl_2, 0 ˚C): 583 nm (ε = 1.12 × 10^3 M^{-1} cm^{-1}); 415 nm (ε = 9.70 × 10^3 M^{-1} cm^{-1}). Thermal instability prevented both meaningful mass spectrometry as well as elemental analysis from being obtained. ^{13}C NMR could not be obtained due to low solubility of **2** at temperatures at which **2** is stable. X-ray data for **1.2** has been deposited in the CCDC under reference number 705506.

Palladium(III) Wire 1.4

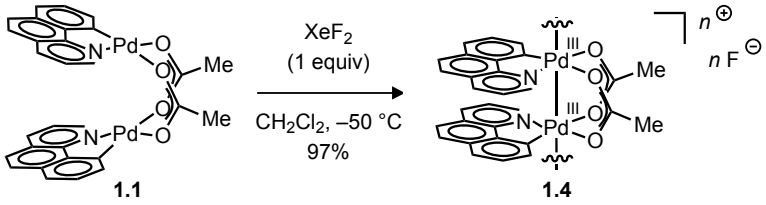

All manipulations were carried out in a dry box under a N_2 atmosphere. Benzo[*h*]quinolinyl palladium acetate dimer (**1.1**) (21 mg, 3.1 × 10^{-5} mol, 1.0 equiv) was dissolved in 1.0 mL CH_2Cl_2 at –50 ˚C. XeF_2 (5.3 mg, 3.1 × 10^{-5} mol, 1.0 equiv) was added as a solid in one portion. The yellow solution immediately became a dark red-brown suspension. After stirring for five minutes at –50 ˚C, solvent was removed *in vacuo* at –50 °C. The residue was washed with Et_2O (1.0 mL) at –50 ˚C. The Et_2O was

decanted, and the residue was dried *in vacuo* (approx. 50 mTorr) at –50 °C to afford 22 mg of the title compound (97% yield) as a dark red solid.

NMR Spectroscopy: ^{1}H-NMR (500 MHz, CD_2Cl_2, –10 ºC, δ): 7.87 (d, J = 5.1 Hz, 2H), 7.71 (d, J = 7.7 Hz, 2H), 7.47–7.40 (m, 4H), 7.35 (d, J = 8.4 Hz, 2H), 7.27 (d, J = 7.0 Hz, 2H), 7.15 (d, J = 8.8 Hz, 2H), 6.86 (dd, J = 4.8 Hz, J = 4.8 Hz, 2H), 2.72 (s, 6H). ^{19}F-NMR (375 MHz, CD_2Cl_2, –10 ºC, δ): –170.4 (br s). UV-VIS Spectroscopy (CH_2Cl_2, 0 ˚C): 1021 nm (absorbance at this wavelength is non-linear with concentration); 464 nm (absorbance at this wavelength is non-linear with concentration); 376 nm ($\varepsilon = 2.47 \times 10^3$ M^{-1} cm^{-1}). Thermal instability prevented both meaningful mass spectrometry as well as elemental analysis from being obtained. ^{13}C NMR signals were not observed.

X-ray quality crystals of **1.4** were obtained as follows: at –50 ˚C, a solution of approximately 20 mg of **1.4** in 1.0 mL CH_2Cl_2 was filtered through glass wool into two 2.0 mL plastic vials at –50 ˚C. Pre-cooled pentane (–50 ˚C) was carefully layered on top of the solution containing **1.4**. The vials were stored at –35 ˚C for 24 hours, at which point red needle crystals of **1.4** were observed. Redissolved crystals of **1.4** in CD_2Cl_2 displayed ^{1}H and ^{19}F NMR spectra that were identical to freshly prepared samples of **1.4**. X-ray data for **1.4** has been deposited in the CCDC under reference number 841654.

When solutions of **1.4** were crystallized in plastic vials, red block crystals we also observed alongside the needle crystals of **1.4**. X-ray analysis of these blocks revealed dipalladium(III) difluoride compound **1.3**. Redissolved crystals of **1.3** displayed solution state spectral data that was consistent with the presence of **1.4**, rather than **1.3**, in solution. X-ray data for **1.3** has been deposited in the CCDC under reference number 841653.

Reaction of 1.4 with TMSCl

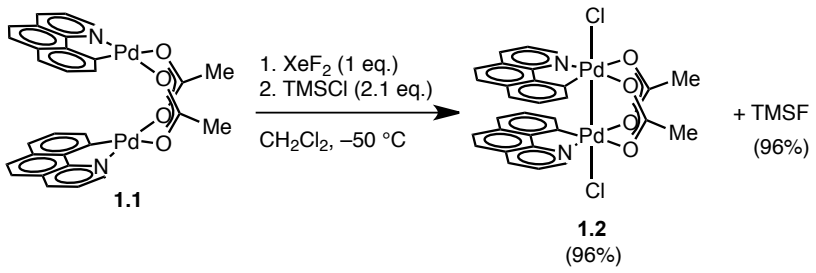

Determination of Yield of TMSF:

All manipulations were carried out in a dry box under a N_2 atmosphere. Benzo[*h*]quinolinyl palladium acetate dimer (**1.1**) (21 mg, 3.1×10^{-5} mol, 1.0 equiv) was dissolved in 1.0 mL CH_2Cl_2 at −50 ˚C. XeF_2 (5.3 mg, 3.1×10^{-5} mol, 1.0 equiv) was added as a solid in one portion. The yellow solution immediately became a dark red-brown suspension. After 10 minutes, TMSCl (8.1 μL, 6.4×10^{-5} mol, 2.1 equiv) was added in one portion. The reaction was stirred for an additional 10 minutes before 1-fluoro-3-nitrobenzene (3.0 μL, 2.8×10^{-5} mol, 0.90 equiv) was added as a standard to allow the yield of TMSF to be determined (96% yield) by ^{19}F NMR with relaxation delay set to 60 s. ^{19}F spectrum used in this determination can be found in the 'Spectroscopic Data' section.

NMR Spectroscopy for TMSF: ^{1}H-NMR (400 MHz, CD_2Cl_2, 23 ºC, δ): 0.21 (d, J = 8.8 Hz, 9H). ^{19} F-NMR (375 MHz, CD_2Cl_2, 23 ºC, δ): –160.3. ^{29}Si-NMR (80 MHz, CD_2Cl_2, 23 ºC, δ) 31.3 (d, J = 273 Hz).

Determination of Yield of **1.2**:

All manipulations were carried out in a dry box under a N_2 atmosphere. Benzo[*h*]quinolinyl palladium acetate dimer (**1.1**) (71.4 mg, 1.04×10^{-4} mol, 1.00 equiv)

was dissolved in 1.5 mL CH_2Cl_2 at −50 ˚C. XeF_2 (17.6 mg, 1.04×10^{-4} mol, 1.00 equiv) was added as a solid in one portion. After 10 minutes, TMSCl (27.0 μL, 2.13×10^{-4} mol, 2.05 equiv) was added in one portion. The reaction was stirred for an additional 10 minutes before all volatiles were removed *in vacuo* at −50 ˚C. The residue was triturated with 3 mL Et_2O at −50 ˚C. The residue was dried under vaccuum to afford 75.4 mg of the title compound (96% yield). Spectroscopic data were in agreement with an authentic sample of **1.2**, the preparation of which is described above.

Observation of both TMSF and **1.2** in 96% yield confirms the average Pd oxidation state of +III in **1.4**.

Palladium(2.5) Wire 1.5

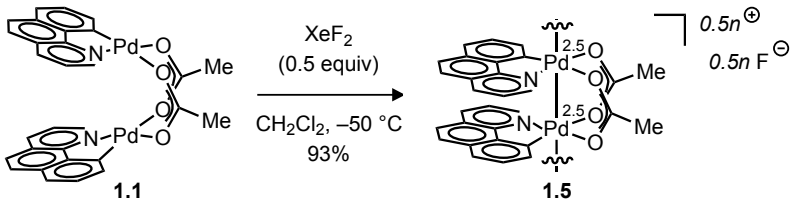

All manipulations were carried out in a dry box under a N_2 atmosphere. Benzo[*h*]quinolinyl palladium acetate dimer (**1.1**) (20. mg, 2.9×10^{-5} mol, 1.0 equiv) was dissolved in 1.0 mL CH_2Cl_2 at −50 ˚C. XeF_2 (2.5 mg, 1.5×10^{-5} mol, 0.50 equiv) was added as a solid in one portion. The yellow solution immediately became dark red-brown. After stirring for five minutes at −50 ˚C, solvent was removed *in vacuo*. The residue was triturated with pentane (2 × 1 mL) at −50 ˚C. The pentane was decanted, and the residue was dried *in vacuo* (approx. 50 mTorr) at −50 °C to afford 19 mg of the title compound (93% yield) as a dark red-brown solid.

NMR Spectroscopy: ^{1}H NMR (400 MHz, CD_2Cl_2, –25 °C, δ): 7.85 (d, J = 5.9 Hz, 2H), 7.73 (d, J = 8.8 Hz, 2H), 7.47–7.17 (m, 10H), 6.85 (br, 2H), 2.71 (s, 6H). ^{19}F NMR (375 MHz, CD_2Cl_2, –25 °C, δ): –213.2 (br s, $h_{1/2}$ = 440 Hz). UV-Vis Spectroscopy (CH_2Cl_2, 0 °C): 991 nm (absorbance at this wavelength is non-linear with concentration); 374 nm (ε = 2.29 × 10^3 $M^{-1}cm^{-1}$); 345 nm (ε = 2.27 × 10^3 $M^{-1}cm^{-1}$). Thermal instability prevented both meaningful mass spectrometry as well as elemental analysis from being obtained. ^{13}C NMR signals were not observed.

X-ray quality crystals of **1.5** were obtained as follows: at –50 °C, 0.5 mL of a 10 mg/mL solution of **1.5** in CH_2Cl_2 was filtered through glass wool into a 2.0 mL plastic vial. Pentane (1.5 mL, pre-cooled to –50 °C) was carefully layered on top of the solution containing **1.5**. The vial was stored at –35 °C for 24 hours, at which point long, red needle crystals of **1.5** were observed. Redissolved crystals of **1.5** in CD_2Cl_2 displayed ^{1}H and ^{19}F NMR spectra identical to freshly prepared **1.5**. X-ray data for **1.5** has been deposited in the CCDC under reference number 846179.

Pd(III) Wire 1.6

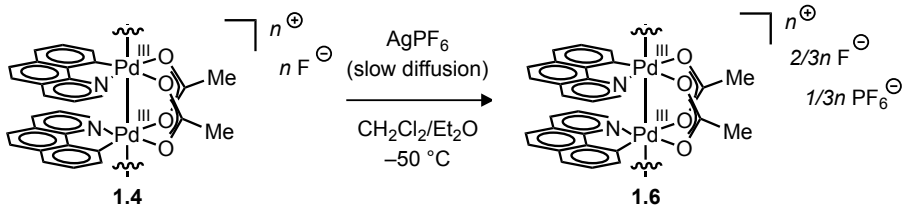

1.4 1.6

All manipulations were carried out in a dry box under a N_2 atmosphere. A 10 mg/mL solution of Pd(III) Wire **1.4** (0.5 mL) at –50 °C was divided into three glass tubes (6 × 50 mm), pre-cooled to –50 °C. The solution of **1.4** was layered with a small amount of benzene (~50 μL), which was allowed to freeze into a solid wafer. On top of the frozen

benzene was layered an 8 mg/mL solution of $AgPF_6$ in Et_2O, pre-cooled to –50 °C (optimal results were obtained when the ratio of solutions of **1.4**:$AgPF_6$ was approximately 1:5). The tubes were capped and stored at –35 °C for three days, at which point dark blue needle crystals were observed. X-ray crystallographic analysis of these crystals revealed Pd(III) wire **1.6**. X-ray data for **1.6** has been deposited in the CCDC under reference number 952240.

Crystals of the title compound were insoluble in non-coordinating solvents such as CD_2Cl_2, therefore we were unable to obtain meaningful solution-state spectroscopic data of the 1-D wires. Attempts to redissolve crystals of **1.6** in coordinating solvents such as CD_3CN led to decomposition.

Benzo[*h*]quinolinyl Palladium Chloride Dimer (1.S1)[6]

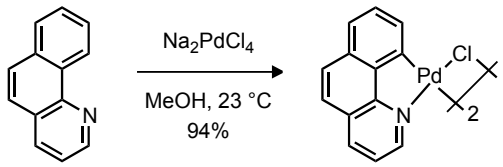

1.S1

To Na_2PdCl_4 (1.00 g, 3.40 mmol, 1.00 equiv) in MeOH (40 mL) at 23 °C was added benzo[*h*]quinoline (609 mg, 3.40 mmol, 1.00 equiv). After stirring for three hours, the tan solids were isolated by filtration, washed sequentially with H_2O (50 mL) and MeOH (50 mL), and dried under a stream of air to give 1.03 g of the title compound (94% yield).

NMR Spectroscopy: ^{1}H NMR (500 MHz, DMSO-d_6, 23 ºC, δ): 9.44 (d, J = 4.5 Hz, 1H), 8.72 (br), 8.67 (d, J = 7.5 Hz, 1H), 8.61 (br), 8.22 (d, J = 7.0 Hz, 1H), 7.91 (d, J =

[6] Hartwell, G. E.; Lawrence, R. V.; Smas, M. J. *J. Chem. Soc. Chem. Comm.* **1970**, 912.

9.0 Hz, 1H), 7.86–7.74 (m, 3H), 7.73 (br), 7.60 (br), 7.53 (dd, J = 7.5 Hz, J = 7.0, 1H), 7.38 (br). ^{13}C NMR (125 MHz, DMSO-d_6, 23 ºC, δ): 153.9, 152.2, 150.7, 150.6, 148.0, 141.7, 139.9, 134.4, 130.8, 129.6, 129.4, 127.5, 125.1, 124.4, 123.0, 122.9. Note: The ^{1}H and ^{13}C NMR spectra are more complicated than would be expected from structure **1.S1**, probably due to the presence of solvated adducts. The title compound is not soluble in non-coordinating solvents.

Silver Hexanoate (1.S2)

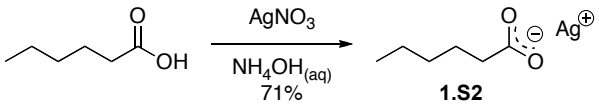

1.S2

Hexanoic acid (2.00 mL, 16.0 mmol, 1.00 equiv) was added to a 1.0 M aqueous ammonia solution (16.0 mL). To this mixture was added a solution of $AgNO_3$ (2.71 g, 16.0 mmol, 1.00 equiv) in H_2O (20 mL) with vigorous stirring, causing the formation of a white precipitate. The precipitate was isolated by filtration, washed with H_2O (50 mL), and dried under vacuum to give 2.52 g of the title compound as a white solid (71% yield). The crude product was stored in the dark and used without further purification.

Benzo[*h*]quinolinyl Palladium Hexanoate Dimer (1.7)

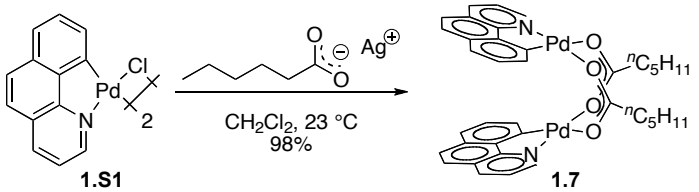

1.S1 **1.7**

To benzo[*h*]quinolinyl palladium chloride dimer (**1.S1**) (100. mg, 0.156 mmol, 1.00 equiv) in CH_2Cl_2 (8 mL) at 23 °C was added silver hexanoate (**1.S2**) (175 mg, 0.781

mmol, 5.00 equiv). After stirring for two hours, the reaction mixture was filtered through a short pad of celite, and the filtrate was concentrated *in vacuo* to give a thick yellow oil. Trituration with Et_2O (2 × 2 mL) gave 127 mg of the title compound (98% yield) as a bright yellow solid.

NMR Spectroscopy: ^{1}H NMR (500 MHz, $CDCl_3$, 23 ºC, δ): 7.81 (d, J = 4.9 Hz, 2H), 7.44 (d, J = 7.8 Hz, 2H), 7.23 (d, J = 4.9 Hz, 4H), 7.20 (t, J = 6.8 Hz, 2H), 7.08 (d, J = 6.8 Hz, 2H), 6.98 (d, J = 8.8 Hz, 2H), 6.46 (dd, J = 7.8 Hz, J = 4.9 Hz, 2H), 2.58 (t, J = 7.3 Hz, 4H), 1.85 (m, 4H), 1.50-1.39 (m, 8H), 0.99 (t, J = 7.3 Hz, 6H). ^{13}C NMR (125 MHz, $CDCl_3$, 23 ºC, δ): 184.8, 153.0, 148.7, 148.6, 139.8, 134.9, 132.2, 128.7, 127.5, 127.4, 124.7, 122.6, 121.7, 119.5, 38.3, 31.8, 26.5, 22.6, 14.2. Anal: calcd for $C_{38}H_{38}N_2O_4Pd_2 \bullet H_2O$: C, 55.82; H, 4.93; N, 3.43; found: C, 55.80; H, 4.63; N, 3.51.

Palladium(III) Tetrafluoroborate Wire (1.8)

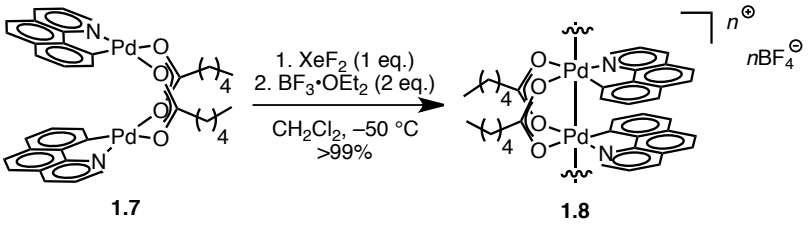

1.7 **1.8**

All manipulations were carried out in a dry box under a N_2 atmosphere. Benzo[*h*]quinolinyl palladium hexanoate dimer (**1.7**) (20. mg, 2.4 × 10^{-5} mol, 1.0 equiv) was dissolved in 2.0 mL CH_2Cl_2 at −50 ˚C. XeF_2 (4.1 mg, 2.4 × 10^{-5} mol, 1.0 equiv) was added as a solid in one portion. The yellow solution immediately became dark red-brown. After stirring for five minutes at −50 ˚C, $BF_3 \bullet OEt_2$ (6.1 μL, 4.8 × 10^{-5} mol, 2.0 equiv) was added in one portion. The reaction was stirred for one hour, at which point

the solution color was deep blue. The reaction mixture was then placed under high vacuum at –50 °C for several hours, giving 24 mg of the title compound as a dark blue solid (>99% yield).

NMR Spectroscopy: ^{1}H NMR (400 MHz, CD_2Cl_2 –25 ºC, δ): 7.70-5.65 (br m), 2.64-1.91 (br), 1.65-0.57 (br m). ^{19}F NMR (375 MHz, CD_2Cl_2, –25 ºC, δ): -152.4 (s). UV-Vis Spectroscopy (CH_2Cl_2, 0 °C): 1043–1133 nm (λ_{max} for this absorbance exhibits a strong concentration-dependent red shift); 470 nm ($\varepsilon = 7.74 \times 10^2$ $M^{-1}cm^{-1}$); 384 nm ($\varepsilon = 3.24 \times 10^3$ $M^{-1}cm^{-1}$); 367 nm ($\varepsilon = 3.34 \times 10^3$ $M^{-1}cm^{-1}$). Thermal instability prevented both meaningful mass spectrometry as well as elemental analysis from being obtained. ^{13}C NMR signals were not observed due to signal broadness.

Reaction of 1.8 with ^{n}Bu$_4$NCl

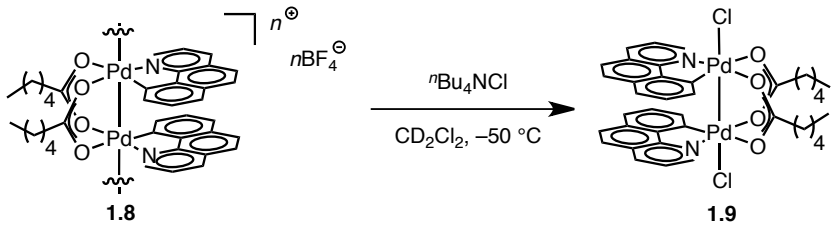

1.8 **1.9**

All manipulations were carried out in a dry box under a N_2 atmosphere. To 10 mg of **1.8** (pre-prepared, as described above) in 1 mL CD_2Cl_2 at –50 °C was added ^{n}Bu$_4$NCl (6.7 mg, 2.4×10^{-5} mol, 2.0 equiv) as a solid in one portion. The dark blue solution quickly became dark red-brown. Pd(III) dichloride (**1.9**) was observed, and spectroscopic data of the crude reaction mixture were in agreement with an authentic sample of **1.9**, the preparation of which is described below.

Observation of **1.9** as the reaction product confirms the average Pd oxidation state of +III in complex **1.8**.

Benzo[*h*]quinolinyl Palladium(III) Chloride Dimer (1.9)

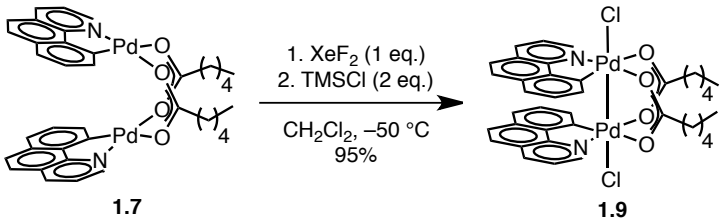

All manipulations were carried out in a dry box under a N_2 atmosphere. Benzo[*h*]quinolinyl palladium hexanoate dimer (**1.7**) (10. mg, 1.2×10^{-5} mol, 1.0 equiv) was dissolved in 1.0 mL CH_2Cl_2 at −50 ˚C. XeF_2 (2.1 mg, 1.2×10^{-5} mol, 1.0 equiv) was added as a solid in one portion. The yellow solution immediately became dark red-brown. After stirring for five minutes at −50 ˚C, TMSCl was added as a 10% v/v solution in CH_2Cl_2 (32 μL, 2.4×10^{-5} mol, 2.0 equiv), and the reaction mixture was stirred an additional five minutes. Concentration of the reaction mixture *in vacuo* afforded 10.3 mg of the title compound as a dark red solid (95% yield).

NMR Spectroscopy: ^{1}H NMR (500 MHz, CD_2Cl_2, –30 °C, δ): 7.71 (d, J = 5.5 Hz, 2H), 7.59 (d, J = 8.5 Hz, 2H), 7.42 (t, J = 8.0 Hz, 2H), 7.33 (d, J = 8.0 Hz, 2H), 7.23 (d, J = 8.5 Hz, 2H), 7.14 (d, J = 7.5 Hz, 2H), 7.04 (d, J = 9.0 Hz, 2H), 6.74 (dd, J = 7.5 Hz, J = 5.5 Hz, 2H), 2.87 (t, J = 7.8 Hz, 4H), 1.97 (m, 4H), 1.48 (m, 8H), 0.99 (t, J = 6.8 Hz, 6H). ^{13}C NMR (125 MHz, CD_2Cl_2, –30 °C, δ): 190.7, 155.4, 148.8, 148.6, 137.0, 135.9, 133.8, 131.0, 128.2, 127.0, 126.3, 124.75. 124.66, 122.4, 38.7, 32.2, 26.6, 23.0, 14.5. UV-Vis Spectroscopy (CH_2Cl_2, 0 °C): 582 nm ($\varepsilon = 8.14 \times 10^2$ $M^{-1}cm^{-1}$); 413 nm ($\varepsilon = 7.58 \times 10^3$

$M^{-1}cm^{-1}$). Thermal instability prevented both meaningful mass spectrometry as well as elemental analysis from being obtained.

7-Nitrobenzo[*h*]quinoline (1.S3)[7,8]

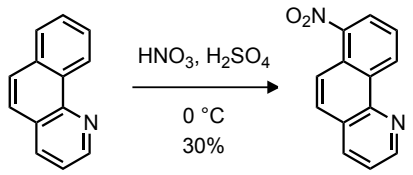

1.S3

Benzo[*h*]quinoline (5.00 g, 27.9 mmol, 1.00 equiv) was dissolved in conc. H_2SO_4 (10 mL) at 23 ºC. The reaction mixture was cooled to 0 ºC and a mixture of conc. H_2SO_4 (3.3 mL) and HNO_3 (5.3 mL) (prepared with cooling) was added drop-wise over 20 min. The reaction mixture was stirred at 0 °C for 15 min and was subsequently poured onto water (300 mL) with vigorous stirring, causing the precipitation of yellow solids. The precipitate was filtered, dried, and purified by chromatography on silica gel eluting with a gradient from CH_2Cl_2/hexanes 1:1 (v/v) to 100% CH_2Cl_2, affording 1.88 g of the title compound as a pale yellow solid (30% yield).

R_f = 0.78 (CH_2Cl_2). NMR Spectroscopy: ^{1}H NMR (500 MHz, $CDCl_3$ 25 ºC, δ): 9.65 (d, *J* = 8.0 Hz, 1H), 9.03 (dd, *J* = 4.5 Hz, *J* = 2.0 Hz, 1H), 8.43 (d, *J* = 9.5 Hz, 1H), 8.32 (dd, *J* = 7.5 Hz, *J* = 1.0 Hz, 1H), 8.21 (dd, *J* = 8.0 Hz, *J* = 1.5 Hz, 1H), 7.88 (d, *J* = 9.0 Hz, 1H), 7.77 (dd, *J* = 8.0 Hz, *J* = 8.0 Hz, 1H), 7.61 (dd, *J* = 8.0 Hz, *J* = 4.5 Hz, 1H). ^{13}C NMR (125 MHz, $CDCl_3$, 25 ºC, δ): 149.9, 146.9, 145.3, 135.9, 132.9, 130.4, 129.0,

[7] Barltrop, J. A.; MacPhee, K. E. *J. Chem. Soc.* **1952**, 638–642.

[8] Furuya, T.; Benitez, D.; Tkatchouk, E.; Strom, A. E.; Tang, P.; Goddard, W. A., III; Ritter, T. *J. Am. Chem. Soc.* **2010**, *132*, 3793–3807.

125.9, 125.6, 125.6, 125.1, 123.0, 121.3. Mass Spectrometry: HRMS-FIA (m/z): Calcd for $[C_{13}H_9N_2O_2]^+$ ($[M+H]^+$), 225.06585. Found, 225.06650. These spectroscopic data correspond to the reported data in reference 8.

7-Aminobenzo[*h*]quinoline (1.S4)[8]

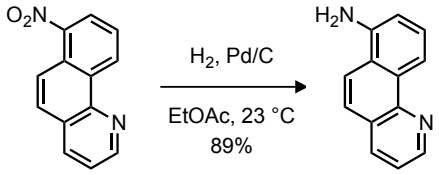

1.S3 **1.S4**

To 7-nitrobenzo[*h*]quinoline (**1.S3**) (810 mg, 3.61 mmol, 1.00 equiv) in EtOAc (36 mL) at 23 ºC was added 10% Pd/C (361 mg). H_2 gas (1 atm) was introduced using a balloon and the reaction mixture was stirred for 1 hour at 23 ºC. The reaction mixture was filtered through a pad of celite and the filtrate was concentrated to afford 628 mg of the title compound as a brown solid (89% yield).

R_f = 0.30 (CH_2Cl_2). NMR Spectroscopy: ^{1}H NMR (500 MHz, $CDCl_3$, 23 ºC, δ): 8.99 (dd, *J* =4.0 Hz, *J* = 1.5 Hz, 1H), 8.79 (d, *J* = 8.5 Hz, 1H), 8.13 (dd, *J* = 8.0 Hz, 1.5 Hz, 1H), 7.82 (d, *J* = 9.0 Hz, 1H), 7.62 (d, *J* = 9.5 Hz, 1H), 7.54 (dd, *J* = 7.5 Hz, *J* = 7.5 Hz, 1H), 7.49 (dd, *J* = 8.0 Hz, *J* = 4.5 Hz, 1H), 7.02 (dd, *J* = 7.5 Hz, *J* = 1.0 Hz, 1H), 4.19 (br s, 2H). ^{13}C NMR (125 MHz, $CDCl_3$, 25 ºC, δ): 146.8, 146.7, 142.4, 135.7, 132.5, 127.5, 126.1, 124.0, 122.4, 121.7, 120.5, 115.3, 113.5. Mass Spectrometry: HRMS-FIA (m/z): Calcd for $[C_{13}H_{11}N_2]^+$ ($[M+H]^+$), 195.09222. Found, 195.09235. These spectroscopic data correspond to the reported data in reference 8.

7-Chlorobenzo[*h*]quinoline (1.S5)[8]

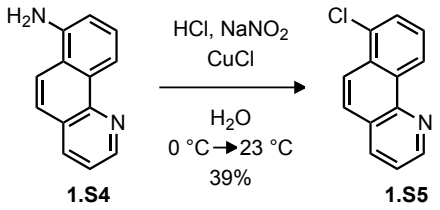

1.S4 **1.S5**

7-Aminobenzo[*h*]quinoline (**1.S4**) (188 mg, 0.968 mmol, 1.00 equiv) was dissolved in 2N HCl (5.6 mL) at 0 ºC. To the reaction mixture was added a solution of $NaNO_2$ (80.1 mg, 1.16 mmol, 1.20 equiv) in H_2O (1.5 mL) drop-wise. The reaction mixture was stirred for 30 min at 0 ºC and a solution of CuCl (95.8 mg, 0.968 mmol, 1.00 equiv) in conc. HCl (2.4 mL) was added drop-wise over 2 min. The reaction mixture was allowed to slowly warm to 23 ºC with further stirring for 3 hours before saturated aqueous $NaHCO_3$ (~15 mL) was added to adjust pH to ~7. To the reaction mixture was added CH_2Cl_2 (20 mL) and the phases were separated. The aqueous layer was extracted with CH_2Cl_2 (2 × 20 mL). The combined organic phases were washed with brine (20 mL) and dried (Na_2SO_4). The filtrate was concentrated *in vacuo* and the residue was purified by chromatography on silica gel eluting with CH_2Cl_2/hexanes 2:1 (v/v) to afford 81.0 mg of the title compound as a pale-yellow solid (39% yield).

R_f = 0.79 (CH_2Cl_2). NMR Spectroscopy: ^{1}H NMR (500 MHz, $CDCl_3$ 25 ºC, δ): 9.26 (d, *J* = 8.5 Hz, 1H), 9.02 (dd, *J* = 4.5 Hz, *J* = 2.0 Hz, 1H), 8.27 (d, *J* = 9.5 Hz, 1H), 8.19 (dd, *J* = 8.0 Hz, *J* = 2.0 Hz, 1H), 7.79–7.76 (m, 2H), 7.64 (dd, *J* = 8.5 Hz, *J* = 8.5 Hz, 1H), 7.55 (dd, *J* = 8.0 Hz, *J* = 4.5 Hz, 1H). ^{13}C NMR (125 MHz, $CDCl_3$, 25 ºC, δ): 149.3, 146.1, 135.9, 133.1, 131.9, 130.8, 128.6, 127.0, 126.5, 126.2, 123.4, 123.4, 122.3. Mass

Spectrometry: HRMS-FIA (m/z): Calcd for $[C_{13}H_9ClN]^+$ ($[M+H]^+$), 214.04235. Found, 214.04200. These spectroscopic data correspond to the reported data in reference 8.

7-Chlorobenzo[*h*]quinolinyl Palladium Acetate Dimer (1.10)[9]

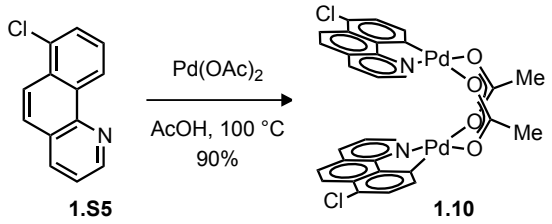

1.S5 **1.10**

To 7-chlorobenzo[*h*]quinoline (**1.S5**) (29 mg, 0.14 mmol, 1.0 equiv) and $Pd(OAc)_2$ (31 mg, 0.14 mmol, 1.0 equiv) in a 4 mL glass vial was added acetic acid (1.5 mL). The vial was sealed with a teflon-lined cap, and the reaction mixture was heated at 100 °C with stirring. After 15 minutes, the reaction mixture was cooled to 23 °C, and the solvent was removed *in vacuo*. The resulting residue was triturated with Et_2O (2 × 1 mL) and then dried *in vacuo* (approx. 10 mTorr) to give 47 mg of the title compound as a yellow solid (90% yield) in a 14:1 ratio of isomers (7-chlorobenzo[*h*]quinolinyl ligands head to tail vs. head to head).

NMR Spectroscopy: ^{1}H-NMR (600 MHz, $CDCl_3$, 23 °C, δ): Major Isomer : 7.92 (d, J = 5.1 Hz, 2H), 7.67 (d, J = 8.2 Hz, 2H), 7.59 (d, J = 8.9 Hz, 2H), 7.16 (d, J = 7.9 Hz, 2H), 7.14 (d, J = 8.9 Hz, 2H), 6.91 (d, J = 7.8 Hz, 2H), 6.74 (dd, J = 8.1 Hz, J = 5.1 Hz, 2H), 2.37 (s, 6H). Minor Isomer : 8.12 (d, J = 5.1 Hz, 2H), 7.77 (d, J = 7.9 Hz, 2H), 7.00 (d, J = 7.8 Hz, 2H), 6.96 (dd, J = 7.8, J = 5.3 Hz, 2H), 6.68 (d, J = 7.9 Hz, 2H). ^{13}C-NMR (125 MHz, CD_2Cl_2, 23 °C, δ): Major Isomer: 182.4, 152.5, 149.0, 146.6, 140.3, 135.3, 129.3,

[9] Powers, D. C.; Benitez, D.; Tkatchouk, E.; Goddard, W. A., III; Ritter, T. *J. Am. Chem. Soc.* **2010**, *132*, 14092–14103.

129.2, 127.3, 126.2, 125.2, 124.1, 124.1, 120.7, 24.9. UV-VIS Spectroscopy (CH_2Cl_2, 23 °C): 384 nm ($\varepsilon = 4.58 \times 10^3$ M^{-1} cm^{-1}); 291 nm ($\varepsilon = 1.98 \times 10^4$ M^{-1} cm^{-1}). Mass Spectrometry: LRMS-FIA (m/z): calcd for $[C_{13}H_7ClNPd + C_2H_3N]^+$, 358.9562. Found, 358.9580. These spectroscopic data correspond to the reported data in reference 9.

Pd(2.5) Wire 1.11

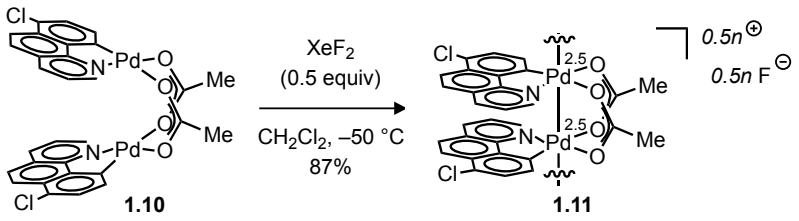

All manipulations were carried out in a dry box under a N_2 atmosphere. 7-Chlorobenzo[*h*]quinolinyl palladium acetate dimer (**1.10**) (8.5 mg, 1.1×10^{-2} mmol, 1.0 equiv) was dissolved in 1 mL CH_2Cl_2 at −50 °C, and then XeF_2 (1.0 mg, 5.9×10^{-3} mmol, 0.50 equiv) was added as a solid in one portion. The yellow solution immediately became deep red. The reaction mixture was stirred for 5 minutes, and then the solvent was evaporated *in vacuo*, maintaining a temperature of –50 °C. The residue was triturated with pentane (2 × 0.5 mL, pre-cooled to –50 °C), and then dried *in vacuo* (approx. 50 mTorr) at –50 °C to afford 7.6 mg of the title compound as a dark red-brown solid (87% yield).

NMR Spectroscopy: ^{1}H NMR (400 MHz, CD_2Cl_2 –25 ºC, δ): 7.47 (br s), 7.29–7.08 (m), 2.31 (br s), 2.30–2.10 (br m). ^{19}F NMR (375 MHz, CD_2Cl_2, –25 ºC, δ): 210.8 (br s). UV-VIS Spectroscopy (CH_2Cl_2, 23 °C): 988 nm (absorbance at this wavelength is non-linear with concentration); 380 nm ($\varepsilon = 2.93 \times 10^3$ M^{-1} cm^{-1}). Thermal instability

prevented both meaningful mass spectrometry as well as elemental analysis from being obtained. ^{13}C NMR signals were not observed.

As a note, the ^{1}H NMR spectrum for Pd(2.5) wire **1.11** displays very weak, broad signals that suggest a high degree of paramagnetism. This is in contrast to the ^{1}H NMR spectrum of Pd(2.5) wire **1.5**, which displays more well-behaved signals. Such a discrepancy suggests that alteration of the supporting ligand scaffold may also affect the degree of electronic communication between the dipalladium units of the 1-D Pd wires in solution.

X-ray quality crystals of **1.11** were grown as follows: 1 mL of a solution of **1.11** (8 mg/mL) in CH_2Cl_2 at –50 °C was filtered through glass wool into a 2 mL plastic vial. Pentane (1 mL, pre-cooled to –50 °C) was carefully layered on top of the solution. The vial was stored at –35 °C for 24 hours, at which point red needle crystals of the title compound were observed. X-ray data for **1.11** has been deposited in the CCDC under reference number 952241.

[(7-Cl-bhq)Pd(OAc)F]$_2$ (1.12)

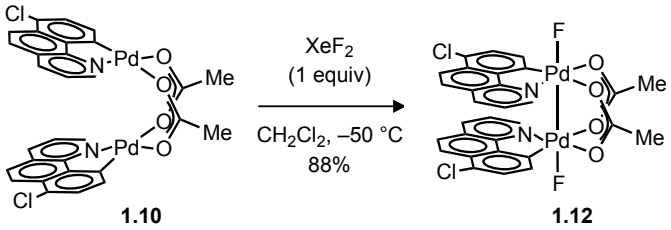

1.10 1.12

All manipulations were carried out in a dry box under a N_2 atmosphere. 7-Chlorobenzo[*h*]quinolinyl palladium acetate dimer (**1.10**) (8.9 mg, 1.2×10^{-2} mmol, 1.0 equiv) was dissolved in 1 mL CH_2Cl_2 at –50 °C. XeF_2 (2.0 mg, 1.2×10^{-2} mmol, 1.0 equiv) was added as a solid in one portion. The yellow solution immediately became

deep red. After stirring for five minutes at –50 °C, the solvent was removed the solvent was evaporated *in vacuo*, maintaining a temperature of –50 °C. The residue was triturated with pentane (2 × 1 mL, pre-cooled to –50 °C), and then dried *in vacuo* (approx. 50 mTorr) at –50 °C to afford 8.3 mg of the title compound as a dark red-brown solid (88% yield).

NMR Spectroscopy: ^{1}H NMR (400 MHz, CD_2Cl_2 –25 ºC, δ): 7.98 (d, J = 4.4 Hz, 2H), 7.91 (d, J = 8.1 Hz, 2H), 7.63 (d, J = 9.5 Hz, 2H), 7.46 (d, J = 8.1 Hz, 2H), 7.32 (d, J = 8.8 Hz, 2H), 7.15 (d, J = 8.8 Hz, 2H), 7.09 (t, J = 6.2 Hz, 2H), 2.71 (s, 6H). ^{19}F NMR (375 MHz, CD_2Cl_2, –25 ºC, δ): 210.8 (br s). UV-VIS Spectroscopy (CH_2Cl_2, 23 °C): 1002 nm (absorbance at this wavelength is non-linear with concentration); 642 nm (absorbance at this wavelength is non-linear with concentration); 468 nm (absorbance at this wavelength is non-linear with concentration); 395 nm ($\varepsilon = 2.61 \times 10^3$ M^{-1} cm^{-1}); 380 nm ($\varepsilon = 2.75 \times 10^3$ M^{-1} cm^{-1}). Thermal instability prevented both meaningful mass spectrometry as well as elemental analysis from being obtained. ^{13}C NMR signals were not observed due to low solubility at temperatures at which **1.12** is stable.

The broadness of the ^{19}F NMR signal observed for **1.12**, along with the non-linear absorbances at 468, 642, and 1002 nm, suggest that fluoride coordination to Pd is fluxional in solutions of **1.12**, and that Pd(III) chain species are accessible in solution. However, fluoride coordination to Pd seems to be strongly favored in the solid state, and only discrete Pd(III) dimer **1.12** was observed upon crystallization.

X-ray quality crystals of **1.12** were grown as follows: At –50 °C, 0.5 mL of a 10 mg/mL solution of **1.12** in CH_2Cl_2 was filtered through glass wool into a 2.0 mL plastic vial. Pentane (1.5 mL, pre-cooled to –50 °C) was carefully layered on top of the solution.

The vial was stored at –35 °C for 24 hours, at which point dark crystals were observed. X-ray data for **1.12** has been deposited in the CCDC under reference number 952242.

Light Scattering Measurements

Dynamic Light Scattering (DLS) and Static Light Scattering (SLS) experiments were performed using an ALV laser goniometer, which consisted of a 35 mW HeNe linear polarized laser with a wavelength of 632.8 nm and an ALV-5000/EPP Multiple Tau digital correlator with 125 ns initial sampling time. Samples were kept at constant temperature (3 °C) during all the experiments. The accessible scattering angle range was 30° to 150°, and the dynamic measurements were carried out at 90°. Aliquots of the samples (2 mL in a 10 mm diameter cylindrical glass cell) were immersed in a filtered toluene bath. The data acquisition was done with the ALV-Correlator Control software[10], and the counting time for dynamic measurements was fixed for each sample at 120 s. CONTIN fits were used to obtain the hydrodynamic radius (R_H) values from the relaxation curves of decay time[8]. For analysis of SLS data, the differential refractive index increment dn/dc of the Pd molecular wires was measured over a concentration range of 0.1-1 mg/mL by means of a differential refractometer (Optilab T-rEX) operating at a wavelength of 658 nm and at 3 °C. Values of 0.114 and 0.128 mL/g for dn/dc were obtained for **1.4** and **1.8** respectively. The ALVstat software[8] was used to fit and plot the data obtained from light scattering and to access the gyration radius (R_G), second Virial coefficient (A_2) and average molar mass in weight (M_W).

DLS and SLS measurements led to hydrodynamic radius (R_H) and gyration radius (R_G) values of 63 and 107 nm respectively for Pd(III) fluoride wire (**1.4**), and 123 and

[10] Sanson, C.; Schatz, C.; Le Meins, J.-F.; Brûlet, A.; Soum, A.; Lecommandoux, S. *Langmuir* **2009**, *26*, 2751-2760

221 nm respectively for Pd(III) tetrafluoroborate wire (**1.8**). The corresponding R_G/R_H ratios are 1.70 (**1.4**) and 1.80 (**1.8**) which are both consistent with the theoretical value for rod-like structures (1.732)[11]. The average calculated lengths of these structures are 350 nm (**1.4**) and 750 nm (**1.8**) in solution in dichloromethane, indicating approximately 600 (**1.4**) and 1300 (**1.8**) Pd atoms in length based on the average Pd–Pd bond length obtained from the x-ray crystal structure of **1.4** (2.85 Å). The calculated second Virial coefficients A_2 are negative in both cases, indicative of auto-associative systems, and consistent with macromolecules prone to crystallization in dichloromethane[12]. The correlation between molar mass and the object length obtained by SLS suggests the possibility that individual wire strands associate in solution to form bundles. To a first approximation, based on average length and assuming simple bundles with perfect overlap of the strands, aggregation numbers of 19 (**1.4**) and 26 (**1.8**) can be calculated.

As a control, measurements were also performed with dipalladium(II) complex **1.1** and the discrete dipalladium(III) complex **1.2**. Both of these dipalladium complexes showed no scattering under the experimental conditions.

Berry Plot[11]:

The basic relationship used to obtain the molar mass and R_G radius for dilute solutions is the equation:

$$\frac{R_\theta}{Kc} = M_w \times P(\theta) - 2A_2 {M_w}^2 \times P^2(\theta) \times c + \cdots$$

[11] Ruggiero, A. *et al. Proc. Natl. Acad. Sci.* **2010**, *107*, 12369-12374.

[12] Zhang, W. *et al*. *Macromolecules* **2004**, *37*, 2924-2929

where Rθ is the Rayleigh ratio, which is directly proportional to the ratio between the scattered intensity at angle θ and the incident intensity. K is an optical constant, c the concentration (in weight) of the scattering species, M_w the weight average molar mass, A_2 the second Virial coefficient, and P(θ) the particle scattering function. In the following calculations, the concentration is assumed to be sufficiently low to neglect the terms containing the higher Virial coefficients.

$$\boldsymbol{K = \frac{4\pi}{\lambda_0} \times \frac{n_0^2}{N_A} \times \left(\frac{dn}{dc}\right)^2}$$

K is the optical constant, λ_0 is the wavelength of the laser used for LS, n_0 is the solvent refractive index for the analyzed sample, and $\lambda = \lambda_0/n_0$. N_A is the Avogadro constant and dn/dc is the variation of the refractive index of the sample with concentration.

For the Berry method, the square root of the expression used in the Zimm method[11], $(Kc/R\theta)^{1/2}$ is plotted on the ordinate to represent the variation of the scattered intensity as a function of the angle and factoring the concentration of the samples[13]. The Berry method is recommended for large objects in solution which have a tendency to aggregate. Its overall accuracy is higher than both Debye's and Zimm's when objects with $R_H > 50$ nm are considered.

The function becomes, in the case of the Berry method:

$$\boldsymbol{\sqrt{\frac{Kc}{R_\theta}} = \sqrt{\frac{1}{M_w} + \frac{16 \times \pi^2}{3 \times \lambda^2} \times \frac{1}{M_w} \times \langle R_G \rangle^2 \times \sin^2\left(\frac{\theta}{2}\right)}}$$

[13] Andersson, M.; Wittgren, B.; Wahlund, K.-G. *Anal. Chem.* **2003**, *75*, 4279-4291 [and references herein].

The intercept with the ordinate is $1/M^{1/2}$ and the slope is:

$$\frac{\partial\sqrt{\frac{R_\theta}{Kc}}}{\partial \sin^2\left(\frac{\theta}{2}\right)} = \frac{1}{2} \times \frac{\frac{16\times\pi^2}{3\times\lambda^2}\times\frac{1}{M_w}\times\langle R_G\rangle^2}{\sqrt{\frac{1}{M_w}+\frac{16\times\pi^2}{3\times\lambda^2}\times\frac{1}{M_w}\times\langle R_G\rangle^2\times\sin^2\left(\frac{\theta}{2}\right)}}$$

which simplifies to $8\pi^2\langle R_G\rangle^2/(3\pi^2M^{1/2})$ at $\sin^2(\theta/2) = 0$.

However, at higher θ, and when the scattering objects have dimensions approaching the wavelength of analysis (λ), the correction factor P(θ) has to be used.

In the case of rod-like structures:

$$\mathbf{P(\theta)} = \frac{\mathbf{2}}{\mathbf{x^2}} \times [\mathbf{x}\times\mathbf{sin(2x)} - \mathbf{1} + \mathbf{cos(x)}]$$

$$\text{with } x^2 = 12q^2R_G^2$$

This correction factor is implemented in the ALVstat software used to fit and plot the data obtained from static light scattering[8,11].

Thin-film Conductivity Measurements

Details of Device Fabrication and Measurement Setup

Four 1 mm-long, 320 μm wide probes with 40 μm spacing were defined on top of 600 nm SiO_2 coated Si wafer by electron-beam lithography. 95 nm thick Au with 5nm Cr adhesion layer was thermally evaporated to form the metal probes. Four probes were wire-bonded to a home-made print-circuit board. The four-point-probe device was connected to the electrical measurement system, which consisted of the following components:

DAQ: PCI-MIO-16XE-10 (AD/DA Card) + BNC-2090 Adaptor (the BNC connector) from National Instrument

Current Amplifier: DL1211 from DL Instruments

Voltage Amplifier: SR560 low-noise voltage preamplifier from Stanford Research

Measurement Procedure

All manipulations were carried out in a dry box under a N_2 atmosphere. The four-point probe device was cooled to –50 °C, and then a thin film of each sample was applied by iterative 2 μL additions of a 10 mg/mL CH_2Cl_2 solution of the Pd wires (pre-cooled to –50 °C), until sufficient contact with the electrodes was achieved (generally ~5 additions). After application of each 2 μL drop, the solvent was evaporated by passing a light N_2 stream over the device to give the thin film. Temperature-dependent conductivity measurements were performed starting at low temperature, and taking repeated measurements as the sample warmed, monitoring the device temperature using a digital temperature probe. For measurements below –50 °C, it was important to cool slowly to avoid cracking of the films.

Conductance values were obtained by linear fitting of I/V curves at each temperature. Measurements were conducted in duplicate or triplicate. Resistivity values for the Pd wires could not be calculated because thermal instability of the samples prevented accurate measurements of film thickness. For bandgap calculation of Pd(III) wires **1.4** and **1.8**, values were averaged from multiple runs. Below –50 °C, both **1.4** and **1.8** showed no conductivity, and bandgap was calcluated from the region that displayed activated behavior.

As a control, measurements were also performed on thin films of dipalladium(II) complex **1.1** and the discrete dipalladium(III) complex **1.2**. Both of these dipalladium complexes behaved as insulators under the experimental conditions.

Experimental Procedures and Compound Characterization for Chapter 2

I. Synthesis and Characterization of Palladium Complexes

[(terpy)Pd(MeCN)][BF_4]$_2$ (2.1)

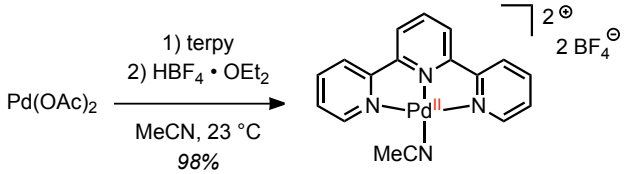

2.1

To $Pd(OAc)_2$ (5.00 g, 20.4 mmol, 1.00 equiv) in MeCN (250 mL) at 23 ºC was added terpy (4.77 g, 20.4 mmol, 1.00 equiv). The reaction mixture was stirred for 20 minutes, affording a pink/orange slurry. To this slurry was added HBF_4•OEt_2 (6.05 mL, 7.20 g, 41.9 mmol, 2.05 equiv) via syringe. The reaction mixture was stirred vigorously for 30 min, at which point a suspension of tan solids was observed. The solids were collected by filtration and washed with Et_2O (100 mL). Further precipitation was observed from the filtrate at this point, and the precipitate was collected by a second filtration. The combined solids were washed with additional Et_2O (50 mL), and then dried under vacuum to afford 10.8 g of the title compound as a pale tan solid (98% yield).

X-ray quality crystals were grown as follows: a saturated solution of **2.1** in MeCN was prepared by dissolving approximately 5 mg of **2.1** in 1 mL MeCN at 23 °C, and filtering over a celite plug to remove any remaining solids. A 4 mL glass vial containing the solution was placed, uncapped, into a 20 mL glass vial containing approximately 4 mL of Et_2O. The 20 mL vial was capped, and vapor diffusion of Et_2O into the MeCN solution of **2.1** at 23 °C gave orange crystals after 24 hours.

mp: 273–275 °C (decomp). NMR spectroscopy: ^{1}H-NMR (400 MHz, CD_3CN, 23 ºC, δ): 8.57 (d, J = 5.6 Hz, 2H), 8.51 (t, J = 8.2 Hz, 1H), 8.43 (t, J = 7.8 Hz, 2H), 8.34 (d, J = 8.0 Hz, 2H), 8.28 (d, J = 8.4 Hz, 2H), 7.84 (td, J = 6.6 Hz, 1.5 Hz, 2H), 1.96 (s, 3H). ^{1}H-NMR (400 MHz, dmso-d_6, 23 ºC, δ): 8.67–8.60 (m, 5H), 8.54–8.49 (m, 4H), 7.92 (td, J = 6.8 Hz, 1.0 Hz, 2H), 2.06 (s, 3H). ^{13}C-NMR (125 MHz, dmso-d_6, 23 ºC, δ): 157.0, 155.2, 150.5, 143.5, 143.2, 129.0, 125.5, 124.7, 118.1, 1.2. ^{19}F-NMR (375 MHz, CD_3CN, 23 ºC, δ): –151.7 (s). UV-VIS Spectroscopy (DMF, 23 ˚C): 526 nm (ε = 144 M^{-1} cm^{-1}); 367 nm (ε = 1.16 × 10^4 M^{-1} cm^{-1}); 349 nm (ε = 1.29 × 10^4 M^{-1} cm-1); 333 nm (ε = 1.07 × 104 M-1 cm-1). FT-IR Spectroscopy (neat, cm^{-1}): 2323, 1606, 1574, 1483, 1452, 1323, 1029, 828, 781, 724, 517. Anal: calcd for $C_{17}H_{14}B_2F_8N_4Pd$: C, 36.83; H, 2.55; N, 10.11; found: C, 37.11; H, 2.56; N, 9.97. X-ray data for **2.1** has been deposited in the CCDC under reference number 935776.

The acetonitrile ligand in **2.1** is displaced by either CD_3CN or dmso-d_6 upon dissolution; as a result, free CH_3CN is observed in the ^{1}H and ^{13}C NMR spectra (^{13}C-NMR signals were not observed in CD_3CN due to low solubility). Compound **2.1** is poorly soluble in non-coordinating solvents. Accordingly, the solution structures corresponding to the NMR data reported above should be considered as:

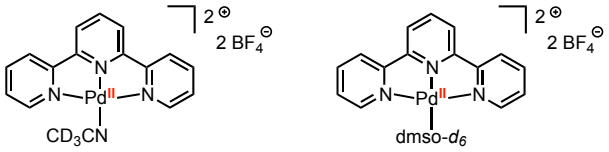

[(terpy)$_2$Pd][BF$_4$]$_3$ (2.4)

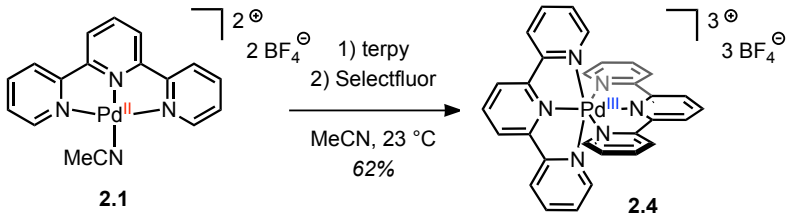

To a suspension of [(terpy)Pd(MeCN)][BF$_4$]$_2$ (**2.1**) (250. mg, 0.451 mmol, 1.00 equiv) in MeCN (10 mL) at 23 ºC was added terpy (105 mg, 0.451 mmol, 1.00 equiv) and the mixture was stirred for 1 minute, affording a homogeneous orange solution. To this solution was added Selectfluor (168 mg, 0.474 mmol, 1.05 equiv), and the reaction mixture was stirred vigorously at 23 °C for 20 minutes, at which point a homogeneous deep red solution was observed. The solution was transferred to a 20 mL glass vial, and the vial was placed, uncapped, into a jar containing approximately 50 mL of Et$_2$O. The jar was capped, and vapor diffusion of Et$_2$O into the MeCN solution at 23 °C resulted in the growth of large red needle crystals after 24 hours. The following purification procedure was performed to remove residual Selectfluor and TEDA-BF$_4$: the supernatant from crystallization was decanted, and the crystallized material was dissolved in MeCN (15 mL), filtered over a celite plug, and crystallized again by vapor diffusion of Et$_2$O (50 mL) into the MeCN solution. The supernatant from crystallization was decanted, and the crystallized material was again dissolved in MeCN (15 mL), filtered over a celite plug, and crystallized once more by vapor diffusion of Et$_2$O (50 mL) into the MeCN solution.

The final batch of crystals was isolated and dried under vacuum to afford 233 mg of the title compound as deep red needle crystals (62% yield). Crystals grown in this manner were found to be suitable for X-ray diffraction.

mp: 220 °C (decomp). NMR Spectroscopy: ^{19}F-NMR (375 MHz, CD_3CN, 23 ºC, δ): –151.3 (s). UV-VIS Spectroscopy (MeCN, 23 ˚C): 1002 nm ($\varepsilon = 95.9\ M^{-1}\ cm^{-1}$); 419 nm ($\varepsilon = 1.52 \times 10^3\ M^{-1}\ cm^{-1}$); 340 nm ($\varepsilon = 2.36 \times 10^4\ M^{-1}\ cm^{-1}$). Magnetic susceptibility (500 MHz, CD_3CN, 23 ºC): $\mu_{eff} = 1.74\ \mu_B$ (14.3 mg/mL). FT-IR Spectroscopy (neat, cm^{-1}): 3102, 1603, 1502, 1479, 1315, 1245, 1026, 780, 644, 519. Anal: calcd for $C_{30}H_{22}B_3F_{12}N_6Pd$: C, 43.24; H, 2.66; N, 10.08; found: C, 43.05; H, 2.51; N, 9.85. ^{1}H-NMR and ^{13}C-NMR signals were not observed. X-ray data for **2.4** has been deposited in the CCDC under reference number 935777.

Crystallization of $[(terpy)_2Pd][BF_4]_3 \cdot [NaBF_4]$ (2.4•$NaBF_4$)

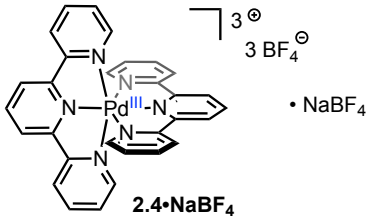

Due to the high level of disorder in the X-ray crystal structure of $[(terpy)_2Pd][BF_4]_3$ (**2.4**), we felt that this structure was not suitable to satisfactorily determine the structural metrics or Pd oxidation state. Therefore, compound **2.4** was derivatized as its $NaBF_4$ adduct, which allowed us to unambiguously characterize the Pd(III) cation.

To a solution of **2.4** (15. mg, 0.018 mmol, 1.0 equiv) in MeCN (1 mL) was added $NaBF_4$ (4.0 mg, 0.036 mmol, 2.0 equiv). The mixture was allowed to stir for 30 minutes at 23 °C, and was then transferred to a 4 mL glass vial. The vial was placed, uncapped,

into a 20 mL glass vial containing approximately 4 mL of Et_2O. The 20 mL vial was capped, and vapor diffusion of Et_2O into the MeCN solution at 23 °C gave dark red plate crystals of **2.4•NaBF$_4$** after 24 hours, which were suitable for X-ray analysis. X-ray data for **2.4•NaBF$_4$** has been deposited in the CCDC under reference number 935778.

Solutions prepared by dissolving crystals of **2.4•NaBF$_4$** in MeCN displayed spectroscopic properties (^{19}F-NMR, UV-vis/NIR, EPR) identical to **2.4**.

Crystallization of [(terpy)$_2$Pd][BF$_4$]$_2$ (2.6)

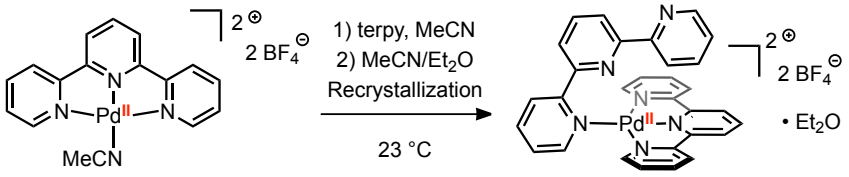

2.1 **2.6**

To a suspension of [(terpy)Pd(MeCN)][BF$_4$]$_2$ (**2.1**) (20. mg, 0.036 mmol, 1.0 equiv) in MeCN (1 mL) at 23 ºC was added terpy (8.4 mg, 0.036 mmol, 1.0 equiv), and the mixture was stirred for 5 minutes, affording an orange solution. The mixture was transferred to a 4 mL glass vial, and the vial was placed, uncapped, into a 20 mL glass vial containing approximately 4 mL of Et_2O. The 20 mL vial was capped, and vapor diffusion of Et_2O into the MeCN solution at 23 °C resulted in the growth of orange/yellow crystals after 24 hours, which were suitable for X-ray diffraction.

mp: 260–266 °C (decomp). NMR spectroscopy: ^{1}H-NMR (400 MHz, CD_3CN, 23 ºC, δ): 8.8 (br s), 8.5–7.8 (br m), 7.5 (br s). ^{19}F-NMR (375 MHz, CD_3CN, 23 ºC, δ): –151.9 (s). UV-VIS Spectroscopy (MeCN, 23 °C): 526 nm (ε = 102 M^{-1} cm^{-1}); 364 nm (ε = 1.15 × 10^4 M^{-1} cm^{-1}); 347 nm (ε = 1.08 × 10^4 M^{-1} cm^{-1}); 331 nm (ε = 7.52 × 10^3 M^{-1} cm^{-1}). FT-

IR Spectroscopy (neat, cm^{-1}): 3086, 1605, 1563, 1451, 1321, 1249, 1028, 771 520. Anal: calcd for $C_{30}H_{22}B_2F_8N_6Pd \bullet 0.5\ Et_2O$: C, 49.01; H, 3.45; N, 10.75; found: C, 49.06; H, 3.27; N, 10.73. ^{13}C-NMR signals were not observed due to low solubility of **2.6**. The broad ^{1}H-NMR signals suggest fluxional behavior, likely due to rotation of the unligated pyridyl groups on the NMR timescale. X-ray crystallographic analysis, along with the ^{1}H-NMR spectrum of crystals of **2.6** dissolved in CD_3CN, shows that compound **2.6** crystallizes with Et_2O as a solvent of crystallization (1:1 ratio of **2.6**:Et_2O). X-ray data for **2.6** has been deposited in the CCDC under reference number 935779.

II. Synthesis and Characterization of Non-Commerically Available Starting Materials[14]

Potassium 4-*tert*-butylphenyl trifluoroborate (2.2a)

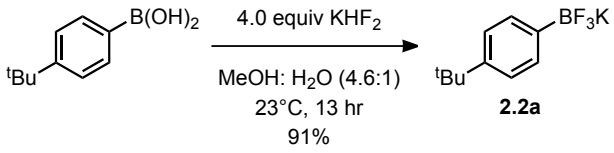

To a vigorously stirred suspension of 4-*tert*-butylphenylboronic acid (1.00 g, 5.62 mmol, 1.00 equiv) in methanol (25 mL, c = 0.2 M) was added a solution of potassium bifluoride (1.76 g, 22.5 mmol, 4.00 equiv) in water (5 mL) at 23 °C. The reaction mixture was stirred for 13 hours at 23 °C and then concentrated *in vacuo* to afford a colorless solid that was further dried at 80 °C at 100 mtorr. The solid was stirred in refluxing acetone (50 mL) and the hot supernatant was filtered through celite. The

[14] Anthony Mazzotti is acknowledged for performing the majority of the experimental work for the compounds described in the following two sections.

product was further extracted with acetone (2 × 50 mL) at 23 °C and the supernatant was filtered through celite. The combined filtrates were concentrated *in vacuo* to afford the title compound (1.22 g, 5.09 mmol, 91% yield) as a colorless crystalline solid.

NMR Spectroscopy: ^{1}H NMR (500 MHz, acetone-d_6, 23 °C, δ): 7.39 (d, J = 8.0 Hz, 2H), 7.13 (d, J = 7.6 Hz, 2H), 1.25 (s, 9H). ^{13}C NMR (125 MHz, DMSO-d_6, 23 °C, δ): 146.9, 131.1, 122.9, 33.9, 31.4. ^{19}F NMR (375 MHz, acetone-d_6, 23 °C, δ): –143.1 (bs). HRMS-FIA(m/z) calcd for $C_{10}H_{13}BF_3K$ $[M–K]^-$, 201.1070; found, 201.1070.

Potassium 4-phenoxyphenyl trifluoroborate (2.2b)

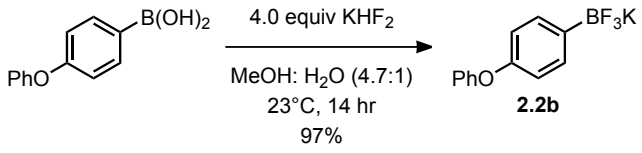

To a vigorously stirred suspension of 4-phenoxyphenylboronic acid (15.0 g, 70.1 mmol, 1.00 equiv) in methanol (280 mL, c = 0.3 M) was added a solution of potassium bifluoride (21.9 g, 280 mmol, 4.00 equiv) in water (60 mL) at 23 °C. The reaction mixture was stirred for 14 hours at 23 °C and then concentrated *in vacuo* to afford a colorless solid that was further dried at 80 °C at 100 mtorr. The solid was suspended in acetone (1 × 180 mL, 4 × 60 mL), stirred vigorously, and the supernatant was filtered through celite. The combined filtrates were concentrated *in vacuo* to afford the title compound (18.7 g, 67.8 mmol, 97% yield) as a colorless crystalline solid.

NMR Spectroscopy: ^{1}H NMR (500 MHz, acetone-d_6, 23 °C, δ): 7.48 (d, J = 8.2 Hz, 2H), 7.31-7.27 (m, 2H), 7.00 (tt, J = 7.4, 1.0 Hz, 1H), 6.91-6.89 (m, 2H), 6.78-6.77 (m, 2H). ^{13}C NMR (125 MHz, acetone-d_6, 23 °C, δ): 159.5, 155.5, 133.8, 133.8, 130.3, 122.9,

118.4, 118.4. ^{19}F NMR (375 MHz, acetone-d_6, 23 °C, δ): –143.1 (bs). HRMS-FIA(m/z) calcd for $C_{12}H_9BF_3OK$ [M–K]$^-$, 237.0706; found, 237.0712.

Potassium (*E*)-4-(2-cyano-2-ethoxycarbonylvinyl)phenyl trifluoroborate (2.2c)

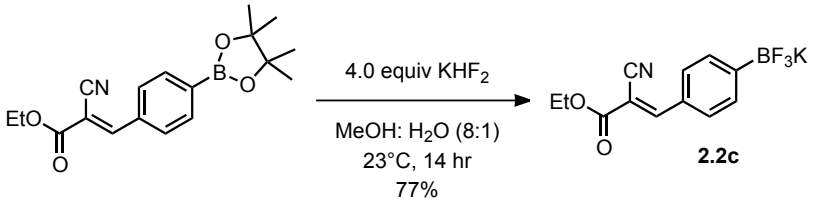

To a vigorously stirred suspension of [(*E*)-4-(2-cyano-2-ethoxycarbonylvinyl)phenyl]boronic acid pinacol ester (25.0 g, 76.4 mmol, 1.00 equiv) in methanol (560 mL, c = 0.1 M) was added a solution of potassium bifluoride (23.9 g, 306 mmol, 4.00 equiv) in water (70 mL) at 23 °C. The reaction mixture was stirred for 14 hours at 23 °C and then concentrated *in vacuo* to afford a colorless solid that was further dried at 80 °C at 100 mtorr. The solid was suspended in acetone (1 × 500 mL, 4 × 100 mL), stirred vigorously, and the supernatant was filtered through celite. The combined filtrates were concentrated *in vacuo* to afford a colorless solid. The solid was purified by the following procedure: the solid was dissolved in refluxing acetone (300 mL) and the solution was allowed to cool to 23 °C. Pentane (300 mL) was layered on top of the cooled acetone solution at 23 °C. Slow diffusion of the pentane into the acetone solution resulted in the growth of colorless crystals, which were isolated by filtration. The colorless crystals were dissolved in refluxing acetone (300 mL) and the hot solution was filtered through celite. The filtrate was concentrated *in vacuo* to afford a colorless solid. The solid was purified by crystallization using the layering procedure detailed above to afford the title compound (18.1 g, 58.9 mmol, 77% yield) as a colorless crystalline solid.

NMR Spectroscopy: ^{1}H NMR (600 MHz, DMSO-d_6, 23 °C, δ): 8.27 (s, 1H), 7.83 (d, J = 7.9 Hz, 2H), 7.51 (d, J = 8.0 Hz, 2H), 4.29 (q, J = 7.1 Hz, 2H), 1.29 (d, J = 14.2 Hz, 3H). ^{13}C NMR (125 MHz, DMSO-d_6, 23 °C, δ): 162.4, 156.3, 132.2, 129.4, 128.4, 116.1, 99.5, 62.1, 14.0. ^{19}F NMR (375 MHz, acetone-d_6, 23 °C, δ): –144.6 (bs). HRMS-FIA(m/z) calcd for $C_{12}H_{10}BF_3NO_2K$ [M–K]$^-$, 268.0764; found, 268.0770.

[(*E*)-4-(2-cyano-2-ethoxycarbonylvinyl)phenyl]boronic acid (2.S1)

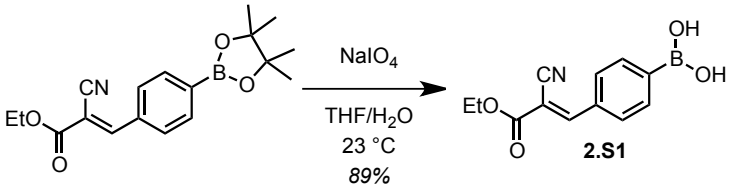

A 50 mL round-bottom flask was charged with [(*E*)-4-(2-cyano-2-ethoxycarbonylvinyl)phenyl]boronic acid pinacol ester (1.00 g, 3.06 mmol, 1.00 equiv), followed by THF (6 mL) and H_2O (6 mL) at 23 ºC. To this mixture was added $NaIO_4$ (1.96 g, 9.18 mmol, 3.00 equiv), and the reaction mixture was stirred for 1 hour at 23 °C, affording a thick white slurry. To this slurry was added 1.0 N HCl (10 mL), and the mixture was allowed to stir for an additional 4 hours. The reaction mixture was transferred to a separatory funnel, and the product was extracted from the aqueous mixture with EtOAc (4 × 50 mL). The combined organic phases were washed with brine (2 × 50 mL), dried over Na_2SO_4, filtered, and concentrated under vacuum to give an off-white solid. The solid was triturated with hexanes (2 × 30 mL), and then dried under vacuum to afford 668 mg of the title compound as an off-white solid (89% yield).

NMR spectroscopy: ^{1}H-NMR (400 MHz, dmso-d_6, 23 ºC, δ): 8.37 (s, 1H), 8.31 (br s, 2H), 7.99–7.91 (m, 4H), 4.30 (q, J = 7.2 Hz, 2H), 1.29 (t, J = 7.0 Hz, 3H). ^{13}C-NMR

(125 MHz, dmso-d_6, 23 ºC, δ): 161.8, 155.1, 140.3, 134.6, 132.5, 129.6, 115.6, 102.9, 62.4, 14.0. Mass Spectrometry: HRMS (ESI-TOF) (m/z): Calcd for $[C_{12}H_{12}BNO_4 + Na]^+$, 268.0757. Found, 268.0744.

The ^{1}H-NMR spectrum of **2.S1** in dmso-d_6 displays a minor set of aromatic peaks, the presence of which are concentration-dependent, corresponding to the boroxine of **2.S1**: arylboronic acids are well known to equilibrate with the boroxine form in solution.[15] The presence of the boroxine did not have an observable impact on the Pd-catalyzed fluorination of **2.S1** (*vide infra*).

Potassium 2-(methoxymethyl)phenyl trifluoroborate (2.2d)

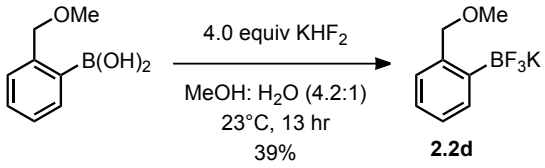

To a vigorously stirred suspension of 2-(methoxymethyl)phenylboronic acid (1.00 g, 6.02 mmol, 1.00 equiv) in methanol (25 mL, c = 0.2 M) was added a solution of potassium bifluoride (1.88 g, 24.1 mmol, 4.00 equiv) in water (6 mL) at 23 °C. The reaction mixture was stirred for 13 hours at 23 °C and then concentrated *in vacuo* to afford a colorless solid that was further dried at 80 °C at 100 mtorr. The solid was stirred in refluxing acetone (3 × 50 mL) and the hot supernatant was filtered through celite. The combined filtrates were concentrated *in vacuo* to afford the title compound (535 mg, 2.35 mmol, 39% yield) as a colorless crystalline solid.

[15] Hall, D.G. Boronic Acids: Preparation and Applications in Organic Synthesis and Medicine. Wiley-VCH 2005. doi: 10.1002/3527606548

NMR Spectroscopy: ^{1}H NMR (600 MHz, acetone-d_6, 23 °C, δ): 7.51 (d, J = 7.1 Hz, 1H), 7.24 (d, J = 7.5 Hz, 1H), 7.01 (td, J = 7.4, 1.4 Hz, 1H), 6.96 (t, J = 7.2 Hz, 1H), 4.68 (s, 2H), 3.29 (s, 3H). ^{13}C NMR (125 MHz, acetone-d_6, 23 °C, δ): 142.2, 133.0, 133.0, 126.9, 126.2, 126.0, 74.9, 57.6. ^{19}F NMR (375 MHz, acetone-d_6, 23 °C, δ): –140.2 (bs). HRMS-FIA(m/z) calcd for $C_8H_9BF_3OK$ [M–K]$^-$, 189.0706; found, 189.0706.

Potassium 4-(pyridin-2-yl)phenyl trifluoroborate (2.2e)

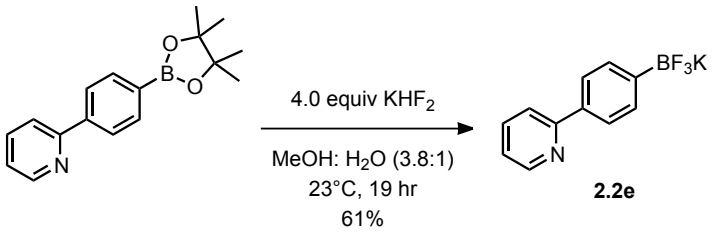

To a vigorously stirred suspension of 4-(pyridine-2-yl)phenylboronic acid pinacol ester (1.00 g, 3.56 mmol, 1.00 equiv) in methanol (15 mL, c = 0.2 M) was added a solution of potassium bifluoride (1.11 g, 14.2 mmol, 4.00 equiv) in water (4 mL) at 23 °C. The reaction mixture was stirred for 19 hours at 23 °C and then concentrated *in vacuo* to afford a yellow solid that was further dried at 80 °C at 100 mtorr. The solid was stirred in refluxing acetone (4 × 30 mL) and the hot supernatant was filtered through celite. The combined filtrates were concentrated *in vacuo* to afford a yellow solid. The solid was purified by the following procedure: the solid was dissolved in refluxing acetone (10 mL) and the solution was allowed to cool to 23 °C. Layering of pentane (10 mL) on top of the cooled acetone solution at 23 °C resulted in the growth of yellow crystals, which were isolated by filtration of the suspension. This layering procedure was

repeated twice more to afford the title compound (563 mg, 2.16 mmol, 61% yield) as a colorless crystalline solid.

NMR Spectroscopy: ^{1}H NMR (600 MHz, acetone-d_6, 23 °C, δ): 8.58 (dq, J = 4.8, 1.2 Hz, 1H), 7.86 (d, J = 7.7 Hz, 2H), 7.82 (dt, J = 8.4, 1.2 Hz, 1H), 7.76 (td, J = 7.7, 1.9 Hz, 1H), 7.58 (d, J = 8.0 Hz, 2H), 7.19 (ddd, J = 7.3, 4.8, 1.1 Hz, 1H). ^{13}C NMR (125 MHz, acetone-d_6, 23 °C, δ): 159.0, 150.2, 137.3, 137.2, 132.8, 135.6, 122.2, 120.4. ^{19}F NMR (375 MHz, acetone-d_6, 23 °C, δ): –143.4 (bs). HRMS-FIA(m/z) calcd for $C_{11}H_8BF_3NK$ $[M–K]^-$, 222.0709; found, 222.0710.

Potassium 2-biphenyl trifluoroborate (2.2g)

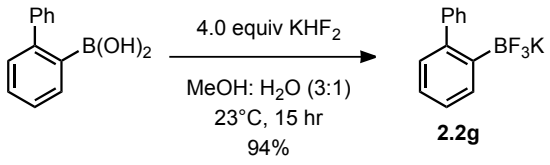

To a vigorously stirred suspension of 2-biphenylboronic acid (250 mg, 1.26 mmol, 1.00 equiv) in methanol (3 mL, c = 0.4 M) was added a solution of potassium bifluoride (394 mg, 5.05 mmol, 4.00 equiv) in water (1 mL) at 23 °C. The reaction mixture was stirred for 15 hours at 23 °C and then concentrated *in vacuo* to afford a colorless solid that was further dried at 80 °C at 100 mtorr. The solid was suspended in acetone (3 × 20 mL), stirred vigorously, and the supernatant was filtered through celite. The combined filtrates were concentrated *in vacuo* to afford the title compound (310 mg, 1.19 mmol, 94% yield) as a colorless crystalline solid.

NMR Spectroscopy: ^{1}H NMR (600 MHz, acetone-d_6, 23 °C, δ): δ 7.70 (dd, J = 6.2, 2.5 Hz, 1H), 7.54-7.52 (m, 2H), 7.25-7.22 (m, 2H), 7.16-7.13 (m, 1H), 7.10-7.06 (m, 2H),

7.04-7.01 (m, 1H). ^{13}C NMR (125 MHz, DMSO-d_6, 23 °C, δ): 146.0, 145.3, 133.0, 133.0, 129.2, 128.8, 126.8, 125.3, 125.1, 125.0. ^{19}F NMR (375 MHz, acetone-d_6, 23 °C, δ): –136.5 (bs). HRMS-FIA(m/z) calcd for $C_{12}H_9BF_3K$ [M–K]$^-$, 221.0757; found, 221.0761.

Potassium 4-biphenyl trifluoroborate (2.2h)

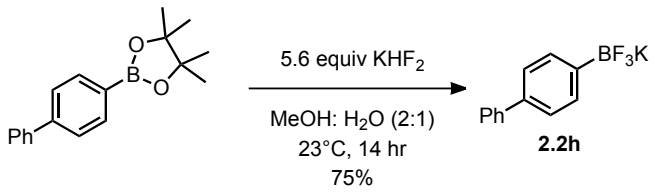

To a vigorously stirred suspension of 4-biphenylboronic acid pinacol ester (1.00 g, 3.57 mmol, 1.00 equiv) in methanol (10 mL, c = 0.4 M) was added a solution of potassium bifluoride (1.56 g, 20.0 mmol, 5.60 equiv) in water (5 mL) at 23 °C. The reaction mixture was stirred for 14 hours at 23 °C and then concentrated *in vacuo* to afford a colorless solid that was further dried at 80 °C at 100 mtorr. The solid was suspended in water (40 mL) and the suspension was filtered. The filter cake was washed with methanol (2 × 40 mL), diethyl ether (40 mL), and pentane (40 mL). The residue was dried under vacuum to afford the title compound (699 mg, 2.69 mmol, 75% yield) as a colorless crystalline solid.

NMR Spectroscopy: ^{1}H NMR (600 MHz, DMSO-d_6, 23 °C, δ): 7.59 (dd, J = 8.2, 1.1 Hz, 2H), 7.42-7.37 (m, 6H), 7.28 (tt, J = 7.3, 1.1 Hz, 1H). ^{13}C NMR (125 MHz, DMSO-d_6, 23 °C, δ): 141.5, 136.9, 132.0, 128.8, 126.6, 126.3, 124.7. ^{19}F NMR (375 MHz, DMSO-d_6, 23 °C, δ): –141.1. HRMS-FIA(m/z) calcd for $C_{12}H_9BF_3K$ [M–K]$^-$, 221.0757; found, 221.0761.

Potassium 4-(3-hydroxypropyl)phenyl trifluoroborate (2.2i)

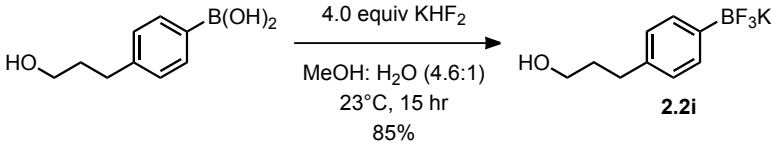

To a vigorously stirred suspension of 4-(3-hydroxypropyl)phenylboronic acid (1.00 g, 5.56 mmol, 1.00 equiv) in methanol (23 mL, c = 0.2 M) was added a solution of potassium bifluoride (1.74 g, 22.2 mmol, 4.00 equiv) in water (5 mL) at 23 °C. The reaction mixture was stirred for 15 hours at 23 °C and then concentrated *in vacuo* to afford a colorless solid that was further dried at 80 °C at 100 mtorr. The solid was stirred in refluxing acetone (4 × 20 mL) and the hot supernatant was filtered through celite. The combined filtrates were concentrated *in vacuo* to afford the title compound (1.14 g, 4.72 mmol, 85% yield) as a colorless crystalline solid.

NMR Spectroscopy: ^{1}H NMR (600 MHz, acetone-d_6, 23 °C, δ): 7.37 (d, J = 7.7 Hz, 2H), 6.94 (d, J = 7.5 Hz, 2H), 3.55-3.52 (m, 2H), 3.41 (t, J = 5.3 Hz, 1H), 2.57 (t, J = 7.7 Hz, 2H), 1.79-1.74 (m, 2H). ^{13}C NMR (125 MHz, DMSO-d_6, 23 °C, δ): 138.4, 131.4, 126.4, 60.4, 34.7, 31.7. ^{19}F NMR (375 MHz, acetone-d_6, 23 °C, δ): –142.9 (bs). HRMS-FIA(m/z) calcd for $C_9H_{11}BF_3OK$ $[M–K]^-$, 203.0862; found, 203.0862.

Potassium 4-(carboxymethyl)phenyl trifluoroborate (2.2k)

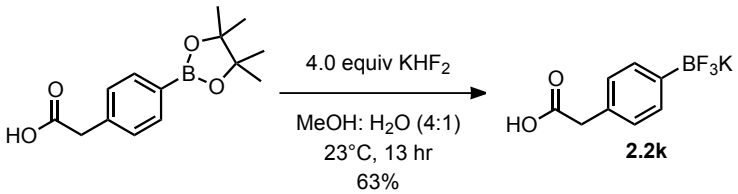

To a vigorously stirred suspension of 4-(carboxymethyl)phenylboronic acid pinacol ester (1.00 g, 3.82 mmol, 1.00 equiv) in methanol (16 mL, c = 0.2 M) was added a solution of potassium bifluoride (1.19 g, 15.3 mmol, 4.00 equiv) in water (4 mL) at 23 °C. The reaction mixture was stirred for 13 hours at 23 °C and then concentrated *in vacuo* to afford a yellow solid that was further dried at 80 °C at 100 mtorr. The solid was purified by continuous soxhlet extraction for 72 hours with acetone (200 mL). The filtrate was concentrated *in vacuo* and the residue was triturated with diethyl ether (3 × 10 mL) to afford the title compound (577 mg, 2.38 mmol, 63% yield) as a colorless crystalline solid.

NMR Spectroscopy: ^{1}H NMR (600 MHz, DMSO-d_6, 23 °C, δ): 12.38 (s, 1H), 7.23 (d, J = 7.7 Hz, 1H), 6.95 (d, J = 7.5 Hz, 1H), 3.38 (s, 1H). ^{13}C NMR (125 MHz, DMSO-d_6, 23 °C, δ): 173.4, 131.5, 131.3, 127.2, 41.3. ^{19}F NMR (375 MHz, DMSO-d_6, 23 °C, δ): –140.9. HRMS-FIA(m/z) calcd for $C_8H_7BF_3O_2K$ $[M–K]^-$, 203.0498; found, 203.0496.

Potassium 4-bromophenyl trifluoroborate (2.2m)

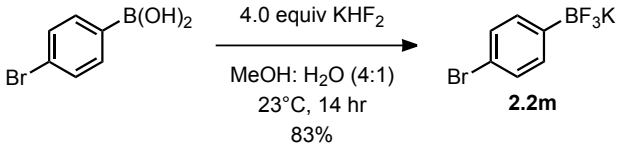

To a vigorously stirred suspension of 4-bromophenylboronic acid (1.00 g, 4.98 mmol, 1.00 equiv) in methanol (20 mL, c = 0.2 M) was added a solution of potassium bifluoride (1.56 g, 19.9 mmol, 4.00 equiv) in water (5 mL) at 23 °C. The reaction mixture was stirred for 14 hours at 23 °C and then concentrated *in vacuo* to afford a colorless solid that was further dried at 80 °C at 100 mtorr. The solid was suspended in acetone (4 × 25 mL), stirred vigorously, and the supernatant was filtered through celite. The combined

filtrates were concentrated *in vacuo* to afford the title compound (1.09 g, 4.15 mmol, 83% yield) as a colorless crystalline solid.

NMR Spectroscopy: ^{1}H NMR (600 MHz, DMSO-d_6, 23 °C, δ): 7.28-7.20 (m, 2H). ^{13}C NMR (125 MHz, acetone-d_6, 23 °C, δ): 134.6, 129.9, 119.7. ^{19}F NMR (375 MHz, acetone-d_6, 23 °C, δ): –143.8 (bs). HRMS-FIA(m/z) calcd for $C_6H_4BBrF_3L$ $[M–K]^-$, 222.9548; found, 222.9547.

Potassium 4-(2-oxopropyl)phenyl trifluoroborate (2.2n)

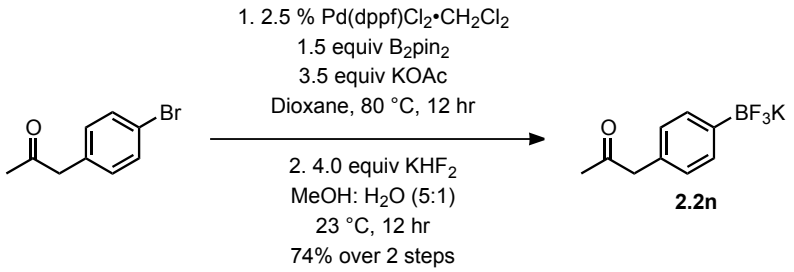

To a flame-dried Schlenk tube was added bis(pinacolato)diboron (3.58 g, 14.1 mmol, 1.5 equiv) and potassium acetate (3.22 g, 32.9 mmol, 3.5 equiv). The Schlenk tube was evacuated and backfilled with dinitrogen (process repeated three times). Dioxane (40 mL anhydrous, degassed) was added followed by 1-(4-bromophenyl)propan-2-one (2.00 g, 9.39 mmol, 1.00 equiv). The reaction mixture was submitted to two freeze-pump-thaw cycles, followed by the addition of [1,1'-bis(diphenylphosphino)ferrocene]dichloropalladium complex in dichloromethane (192 mg, 0.235 mmol, 0.025 equiv). The reaction mixture was submitted to another freeze-pump-thaw cycle and heated at 80 °C for 12 hours. The reaction was allowed to cool to 23 °C and water (30 mL) was added dropwise under a dinitrogen atmosphere. The reaction mixture was transferred to separatory funnel and the aqueous layer was extracted

with dichloromethane (3 × 30 mL). The combined organic layers were dried over magnesium sulfate, filtered, and concentrated *in vacuo* to afford an orange oil. The residue was purified by chromatography on silica gel eluting with a solvent mixture of hexanes/dichloromethane (1:4 (v/v)) to afford a yellow oil (3.48 g) containing 4-(2-oxopropyl)phenylboronic acid pinacol ester (2.37 g, 9.10 mmol, 97% yield), dioxane, and pinacol. The purity of the residue was determined by integration of the ^{1}H NMR spectrum of the mixture. This mixture was carried through to the next reaction without further purification.

The yellow oil obtained from the previous step was diluted with methanol (40 mL, c = 0.2). To this vigorously stirred solution was added a solution of potassium bifluoride (2.84 g, 36.4 mmol, 4.00 equiv) in water (8 mL) at 23 °C. The reaction mixture was stirred for 12 hours at 23 °C and then concentrated *in vacuo* to afford a yellow solid that was further dried at 80 °C at 100 mtorr. The solid was stirred in refluxing acetone (3 × 150 mL) and the hot supernatant was filtered through celite. The filtrate was concentrated *in vacuo* and the residue was triturated with tetrahydrofuran (5 × 12 mL) to afford the title compound (1.65 g, 6.89 mmol, 74% yield for 2 steps) as a colorless crystalline solid.

NMR Spectroscopy: ^{1}H NMR (600 MHz, DMSO-d_6, 23 °C, δ): 7.26 (d, J = 7.7 Hz, 2H), 6.91 (d, J = 7.5 Hz, 2H), 3.57 (s, 2H), 2.04 (s, 3H). ^{13}C NMR (125 MHz, DMSO-d_6, 23 °C, δ): 206.8, 131.6, 131.1, 127.5, 50.2, 29.0. ^{19}F NMR (375 MHz, DMSO-d_6, 23 °C, δ): –141.0 (bs). HRMS-FIA(m/z) calcd for $C_9H_9BF_3OK$ $[M–K]^-$, 201.0706; found, 201.0705.

Protected dopamine (2.S2)

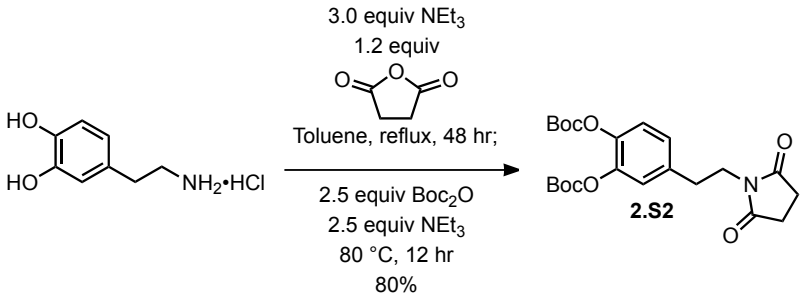

To a vigorously stirred suspension of dopamine hydrochloride (5.00 g, 26.4 mmol, 1.00 equiv) in toluene (100 mL, 0.3 M) was added triethylamine (10.9 mL, 79.1 mmol, 3.00 equiv) and succinic anhydride (3.17 g, 31.6 mmol, 1.20 equiv) at 23 °C. The reaction mixture was stirred for 48 hours at reflux and allowed to cool to 23 °C. Boc anhydride (15.2 mL, 65.9 mmol, 2.50 equiv) and triethylamine (9.11 mL, 65.9 mmol, 2.50 equiv) were added to the reaction mixture at 23 °C. The reaction mixture was stirred for 12 hours at 80 °C, allowed to cool to 23 °C, and then transferred to a separatory funnel. The organic layer was washed with brine (3 × 50 mL). The combined aqueous layers were extracted with ethyl acetate (50 mL). The combined organic layers were dried over magnesium sulfate, filtered, and concentrated *in vacuo*. The residue was purified by chromatography on silica gel eluting with a solvent mixture of hexanes/ethyl acetate (1:1 (v/v)) to afford the title compound (9.15 g, 21.0 mmol, 80% yield) as a colorless crystalline solid.

R_f = 0.37 (hexanes/ethyl acetate 1:1 (v/v)). NMR Spectroscopy: ^{1}H NMR (600 MHz, $CDCl_3$, 23 °C, δ): 7.17 (d, J = 8.3 Hz, 1H), 7.11 (dd, J = 8.3, 2.0 Hz, 1H), 7.08 (d, J = 2.0 Hz, 1H), 3.73 (dd, J = 8.5, 7.0 Hz, 2H), 2.88 (t, J = 7.7 Hz, 2H), 2.65 (s, 4H), 1.54 (s, 9H), 1.53 (s, 9H). ^{13}C NMR (125 MHz, $CDCl_3$, 23 °C, δ): 177.0, 150.6, 150.6, 142.2,

141.1, 136.1, 126.6, 123.5, 123.0, 83.6, 83.5, 39.3, 32.6, 27.9, 27.5, 27.5. HRMS-FIA(m/z) calcd for $C_{22}H_{29}NO_8$ $[M+NH_4]^+$, 453.2231; found, 453.2246.

Aryl iodide 2.S3

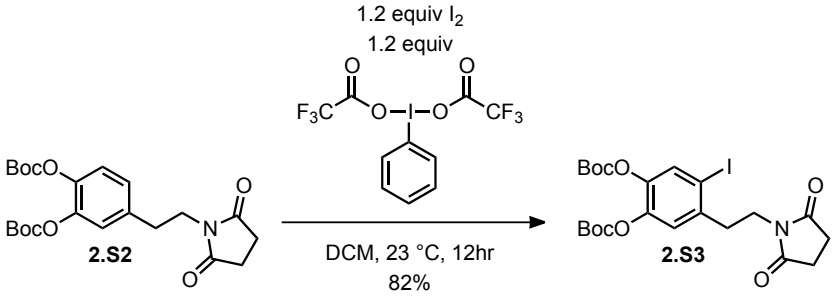

To a vigorously stirred solution of [bis(trifluoroacetoxy)iodo]benzene (2.15 g, 4.99 mmol, 1.20 equiv) and iodine (1.27 g, 4.99 mmol, 1.20 equiv) in dichloromethane (80 mL, c = 0.06 M) was added compound **2.S2** (1.81 g, 4.16 mmol, 1.00 equiv) at 23 °C. The reaction mixture was stirred for 12 hours at 23 °C, followed by the addition of a saturated aqueous sodium thiosulfate solution (approx. 30 mL) at 23 °C. The reaction mixture was transferred to a separatory funnel and extracted with dichloromethane (3 × 40 mL). The combined organic layers were dried over magnesium sulfate, filtered, and concentrated *in vacuo*. The residue was purified by chromatography on silica gel eluting with a solvent mixture of hexanes/ethyl acetate (2:1 (v/v)) to afford the title compound (1.90 g, 3.39 mmol, 82% yield) as a yellow oil.

R_f = 0.43 (hexanes/ethyl acetate 1:1 (v/v)). NMR Spectroscopy: ^{1}H NMR (600 MHz, $CDCl_3$, 23 °C, δ): 7.67 (s, 1H), 7.05 (s, 1H), 3.77 (t, *J* = 7.2 Hz, 2H), 3.01 (t, *J* = 7.1 Hz, 2H), 2.65 (s, 4H), 1.52 (s, 18H). ^{13}C NMR (125 MHz, $CDCl_3$-d_6, 23 °C, δ): 177.1, 150.4, 150.2, 142.5, 141.3, 138.9, 133.5, 124.0, 94.7, 84.1, 84.1, 37.8, 37.5, 28.0, 27.6, 27.5. HRMS-FIA(m/z) calcd for $C_{22}H_{28}INO_8$ $[M+NH_4]^+$, 579.1198; found, 579.1204.

Aryl trifluoroborate 2.2o

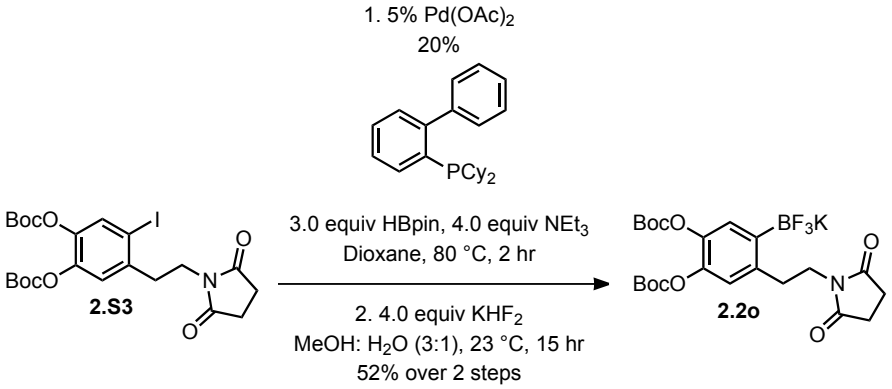

To a flame-dried Schlenk tube was added aryl iodide **2.S3** (1.00 g, 1.78 mmol, 1.00 equiv). The Schlenk tube was evacuated and backfilled with dinitrogen (process repeated three times). Dioxane (5 mL anhydrous, degassed) was added followed by triethylamine (985 μL, 7.13 mmol, 4.00 equiv) and pinacolborane (775 μL, 5.35 mmol, 3.00 equiv). The reaction mixture was submitted to three freeze-pump-thaw cycles, followed by the addition of palladium acetate (20.0 mg, 89.1 μmol, 0.0500 equiv) and (2-biphenyl)dicyclohexylphosphine (125 mg, 356 μmol, 0.200 equiv). The reaction mixture was submitted to another freeze-pump-thaw cycle and heated to 80 °C for 2 hours. The reaction was allowed to cool to 23 °C and a saturated aqueous ammonium chloride solution (5 mL) was added dropwise under a dinitrogen atmosphere. The reaction mixture was transferred to a separatory funnel and the aqueous layer was extracted with ethyl acetate (3 × 20 mL). The combined organic layers were dried over magnesium sulfate, filtered, and concentrated *in vacuo*. The residue was purified by chromatography on silica gel eluting with a solvent mixture of hexanes/ethyl acetate (3:1 (v/v)) to afford a yellow oil (1.00 g).

An aliquot of the yellow oil obtained in the previous step (400 mg) was diluted with methanol (3 mL). To this vigorously stirred solution was added a solution of potassium bifluoride (223 mg, 2.85 mmol, 4.00 equiv) in water (1 mL) at 23 °C. The reaction mixture was stirred for 18 hours at 23 °C and then concentrated *in vacuo* to afford a yellow solid that was further dried at 80 °C at 100 mtorr. The solid was suspended in acetone (4 × 20 mL), stirred vigorously, and the supernatant was filtered through celite. The combined filtrates were concentrated *in vacuo* to afford a yellow solid. The solid was purified by the following procedure: the solid was dissolved in acetone (4 mL) and the resulting solution was layered with pentane (15 mL). Slow diffusion of pentane into the acetone solution afforded colorless crystals, which were isolated and dried under vacuum to give the title compound (200 mg, 370 μmol, 52% yield over 2 steps) as a colorless crystalline solid.

NMR Spectroscopy: ^{1}H NMR (600 MHz, DMSO-d_6, 23 °C, δ): 7.08 (s, 1H), 6.76 (s, 1H), 3.57 (t, J = 7.3 Hz, 2H), 2.88 (t, J = 7.3 Hz, 2H), 2.58 (s, 4H), 1.46 (s, 18H). ^{13}C NMR (125 MHz, DMSO-d_6, 23 °C, δ): 177.5, 150.7, 150.6, 140.2, 139.5, 138.9, 125.6, 121.7, 82.8, 82.6, 31.6, 27.9, 27.2. ^{19}F NMR (375 MHz, DMSO-d_6, 23 °C, δ): –138.9 (bs). HRMS-FIA(m/z) calcd for $C_{22}H_{28}BF_3NO_8K$ [M–K]$^-$, 502.1870; found, 502.1879.

Potassium 4-oxo-4*H*-chromen-6-yl trifluoroborate (2.2p)

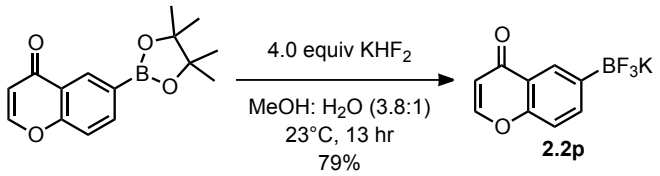

To a vigorously stirred suspension of 4-oxo-4*H*-chromen-6-ylboronic acid pinacol ester (1.00 g, 3.68 mmol, 1.00 equiv) in methanol (15 mL, c = 0.2 M) was added a solution of potassium bifluoride (1.15 g, 14.7 mmol, 4.00 equiv) in water (4 mL) at 23 °C. The reaction mixture was stirred for 13 hours at 23 °C and then concentrated *in vacuo* to afford an orange solid that was further dried at 80 °C at 100 mtorr. The solid was purified by continuous soxhlet extraction for 40 hours with acetone (250 mL). Subsequently, the hot extract was filtered through celite, which was rinsed with hot acetone (3 × 20 mL). The filtrate was concentrated *in vacuo* and the residue was triturated with tetrahydrofuran (4 × 5 mL) to afford the title compound (732 mg, 2.90 mmol, 79% yield) as a colorless crystalline solid.

NMR Spectroscopy: ^{1}H NMR (600 MHz, DMSO-d_6, 23 °C, δ): 8.18 (d, J = 6.0 Hz, 1H), 8.02 (s, 1H), 7.72 (d, J = 8.0 Hz, 1H), 7.34 (d, J = 8.1 Hz, 1H), 6.24 (d, J = 5.9 Hz, 1H). ^{13}C NMR (125 MHz, DMSO-d_6, 23 °C, δ): 177.3, 156.2, 155.0, 137.8, 127.0, 127.0, 122.9, 115.7, 112.1. ^{19}F NMR (375 MHz, acetone-d_6, 23 °C, δ): –143.4. HRMS-FIA(m/z) calcd for $C_9H_5BF_3O_2$ $[M–K]^-$, 213.0342; found, 213.0340.

III. Synthesis and Characterization of Aryl Fluorides

1-(*tert*-Butyl)-4-fluorobenzene (2.3a)

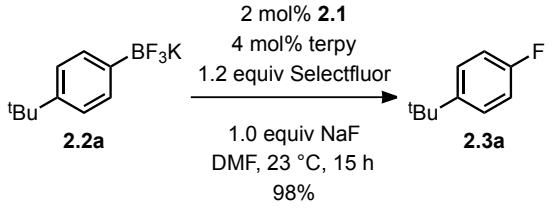

2.2a **2.3a**

To a mixture of palladium precatalyst **2.1** (7.8 mg, 14 μmol, 0.020 equiv), terpy (6.5 mg, 28 μmol, 0.040 equiv), aryl trifluoroborate **2.2a** (168 mg, 700 μmol, 1.00 equiv), Selectfluor (298 mg, 840 μmol, 1.20 equiv), and sodium fluoride (29.4 mg, 700 μmol, 1.00 equiv) was added dimethylformamide (7.0 mL, 0.1 M) at 23 °C. The reaction mixture was stirred for 15 hours at 23 °C and then transferred to a separatory funnel. Pentane (20 mL) was added and the organic layer was washed with a 5% aqueous lithium chloride solution (3 × 20 mL). The organic layer was dried over sodium sulfate. The organic layer was filtered through silica gel (approx. 20 g) eluting with pentane (approx. 200 mL) and concentrated *in vacuo* at 0 °C to afford a colorless oil (166 mg) containing the title compound (105 mg, 687 μmol, 98% yield), water, and pentane. The remaining solvent was not removed from the sample due to volatility of the product. The solvent content of the residue was determined by integration of the ^{1}H NMR spectrum of the mixture. Azeotropic evaporation of the trace solvent with $CDCl_3$ was performed prior to ^{1}H and ^{13}C NMR characterization.

R_f = 0.79 (pentane). NMR Spectroscopy: ^{1}H NMR (600 MHz, $CDCl_3$, 23 °C, δ): 7.35–7.32 (m, 2H), 6.99–6.95 (m, 2H), 1.31 (s, 9H). ^{13}C NMR (125 MHz, $CDCl_3$, 23 °C, δ): 160.9 (d, J = 242 Hz), 146.7 (d, J = 1.8 Hz), 126.7 (d, J = 7.3 Hz), 114.6 (d, J = 20.0 Hz), 34.3, 31.5. ^{19}F NMR (375 MHz, $CDCl_3$, 23 °C, δ): –121.7. HRMS-FIA(m/z) calcd for $C_{10}H_{13}F$ $[M–CH_3]^+$, 137.0761; found, 137.0760.

1-Fluoro-4-phenoxybenzene (2.3b)

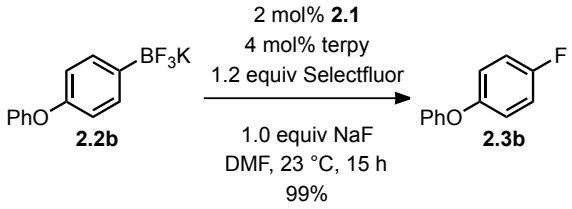

To a mixture of palladium precatalyst **2.1** (7.8 mg, 14 μmol, 0.020 equiv), terpy (6.5 mg, 28 μmol, 0.040 equiv), aryl trifluoroborate **2.2b** (193 mg, 700 μmol, 1.00 equiv), Selectfluor (298 mg, 840 μmol, 1.20 equiv), and sodium fluoride (29.4 mg, 700 μmol, 1.00 equiv) was added dimethylformamide (7.0 mL, 0.1 M) at 23 °C. The reaction mixture was stirred for 15 hours at 23 °C and then transferred to a separatory funnel. Pentane (20 mL) was added and the organic layer was washed with a 5% aqueous lithium chloride solution (20 mL). The aqueous layer was extracted with pentane (3 × 20 mL). The combined organic layers were dried over sodium sulfate, filtered, and concentrated *in vacuo* at 0 °C to afford a colorless oil. The residue was purified by chromatography on silica gel eluting with pentane to afford a colorless oil (142 mg) containing the title compound (99.2 mg, 700 μmol, >99% yield), water, pentane, diethyl ether, and acetone. The remaining solvent was not removed from the sample due to volatility of the product. The solvent content of the residue was determined by integration of the ^{1}H NMR spectrum of the mixture. Azeotropic evaporation of the trace solvent with $CDCl_3$ was performed prior to ^{1}H and ^{13}C NMR characterization.

R_f = 0.35 (pentane). NMR Spectroscopy: ^{1}H NMR (600 MHz, $CDCl_3$, 23 °C, δ): 7.34–7.31 (m, 2H), 7.09 (tt, J = 7.4, 1.0 Hz, 1H), 7.05–7.01 (m, 2H), 7.00–6.97 (m, 4H). ^{13}C NMR (125 MHz, $CDCl_3$, 23 °C, δ): 158.8 (d, J = 240 Hz), 157.7, 152.9, 129.8, 123.1,

120.5 (d, J = 8.3 Hz), 118.2, 116.3 (d, J = 23.8 Hz). ^{19}F NMR (375 MHz, $CDCl_3$, 23 °C, δ): –123.2. HRMS-FIA(m/z) calcd for $C_{12}H_9FO$ $[M]^+$, 188.0632; found, 188.0633.

(*E*)-Ethyl 2-cyano-3-(4-fluorophenyl)acrylate (2.3c) (milligram scale)

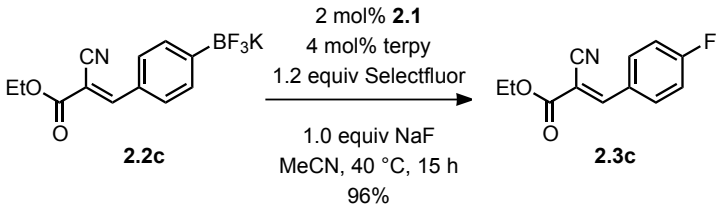

To a mixture of palladium precatalyst **2.1** (4.4 mg, 8.0 μmol, 0.020 equiv), terpy (3.7 mg, 16 μmol, 0.040 equiv), aryl trifluoroborate **2.2c** (123 mg, 400 μmol, 1.00 equiv), Selectfluor (170 mg, 480 μmol, 1.20 equiv), and sodium fluoride (16.8 mg, 400 μmol, 1.00 equiv) was added acetonitrile (4.0 mL, 0.1 M) at 23 °C. The reaction mixture was stirred for 15 hours at 40 °C, allowed to cool to 23 °C, and then transferred to a separatory funnel, rinsing the reaction vial with additional acetonitrile (2 × 4 mL). Pentane (20 mL) was added and the organic layer was washed with water (20 mL). The aqueous layer was extracted with pentane (5 × 20 mL). The combined organic layers were dried over sodium sulfate, filtered, and concentrated *in vacuo* to afford a colorless solid. The solid was purified by chromatography on silica gel eluting with a solvent mixture of pentane/Et_2O (17:3 (v/v)) to afford the title compound (84.5 mg, 385 μmol, 96% yield) as a colorless crystalline solid. Purity of the product was confirmed via ^{1}H and ^{19}F NMR spectroscopy. The spectra were identical to those obtained from the large-scale reaction below.

(*E*)-Ethyl 2-cyano-3-(4-fluorophenyl)acrylate (2.3c) (decagram scale).

To a mixture of palladium precatalyst **2.1** (307 mg, 554 μmol, 0.010 equiv), terpy (258 mg, 1.11 mmol, 0.040 equiv), aryl trifluoroborate **2.2a** (17.0 g, 55.4 mmol, 1.00 equiv), Selectfluor (23.5 g, 66.4 mmol, 1.20 equiv), and sodium fluoride (2.32 g, 55.4 mmol, 1.00 equiv) were added to a round-bottom flask (200 mL), followed by acetonitrile (55.4 mL, 1.0 M) at 23 °C. An air-cooled reflux condenser was fitted to the round bottom flask. The reaction mixture was stirred for 15 hours open to air at 40 °C, allowed to cool to 23 °C, and then transferred to a separatory funnel, rinsing the reaction vial with additional acetonitrile (2 × 50 mL). Pentane (250 mL) was added and the organic layer was washed with water (350 mL). The aqueous layer was extracted with dichloromethane (4 × 300 mL). The combined organic layers were extracted with brine (500 mL), dried over sodium sulfate, filtered, and concentrated *in vacuo* to afford a yellow solid. The solid was purified by chromatography on silica gel eluting with a solvent mixture of pentane/Et_2O (9:1 (v/v)) to afford the title compound (10.6 g, 48.6 mmol, 88% yield) as a colorless crystalline solid.

R_f = 0.38 (pentane/Et_2O 9:1 (v/v)). NMR Spectroscopy: ^{1}H NMR (500 MHz, $CDCl_3$, 23 °C, δ): 8.21 (s, 1H), 8.05–8.01 (m, 2H), 7.22–7.17 (m, 2H), 4.39 (q, *J* = 7.1 Hz, 2H), 1.40 (t, *J* = 7.2 Hz, 3H). ^{13}C NMR (125 MHz, $CDCl_3$, 23 °C, δ): 165.2 (d, *J* = 256 Hz), 162.2, 153.2, 133.4 (d, *J* = 9.1 Hz), 127.7 (d, *J* = 3.6 Hz), 116.5 (d, *J* = 21.9 Hz), 115.3, 102.4 (d, *J* = 2.8 Hz), 62.6, 14.0. ^{19}F NMR (375 MHz, $CDCl_3$, 23 °C, δ): –106.0. HRMS-FIA(m/z) calcd for $C_{12}H_{10}FNO_2$ $[M+H]^+$, 220.0768; found, 220.0769.

1-Fluoro-2-(methoxymethyl)benzene (2.3d)

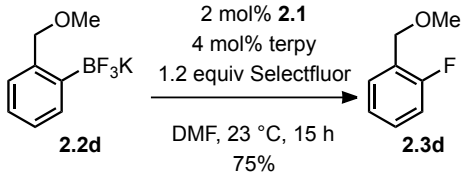

To a mixture of palladium catalyst **2.1** (7.8 mg, 14 μmol, 0.020 equiv) and terpy (6.5 mg, 28 μmol, 0.040 equiv) was added dimethylformamide (7.0 mL, 0.1 M) at 23 °C. This suspension was swirled for approx. 20 seconds until it became homogenous. This solution was transferred via syringe to a mixture of aryl trifluoroborate **2.2d** (160 mg, 700 μmol, 1.00 equiv) and Selectfluor (298 mg, 840 μmol, 1.20 equiv). The reaction mixture was stirred for 15 hours at 23 °C and then transferred to a separatory funnel. Pentane (20 mL) was added and the organic layer was washed with a 5% aqueous lithium chloride solution (1 × 20 mL, 2 × 10 mL). The organic layer was dried over sodium sulfate. The organic layer was filtered through silica gel (approx. 20 g) eluting with a solvent mixture of pentane/Et_2O (9:1 (v/v), approx. 200 mL) and concentrated *in vacuo* at 0 °C to afford a yellow oil (86.3 mg) containing the title compound (74.0 mg, 528 μmol, 75% yield), water, diethyl ether, and pentane. The remaining solvent was not removed from the sample due to volatility of the product. The solvent content of the residue was determined by integration of the ^{1}H NMR spectrum of the mixture. Azeotropic evaporation of the trace solvent with $CDCl_3$ was performed prior to ^{1}H and ^{13}C NMR characterization. The ^{1}H NMR and LRMS data correspond to the data reported in reference 16.[16] High resolution mass spectrometry could only identify [(M+H)-F],

[16] Ortiz, B.; Walls, F.; Yuste, F.; Barrios, H.; Sanchez-Obregon, R. Pinelo, L. *Synth. Commun.* **1993**, 23(6), 749-756.

therefore low resolution mass spectrometry was used to confirm the molecular ion of the title compound.

R_f = 0.67 (pentane/Et_2O 9:1 (v/v)). NMR Spectroscopy: ^1H NMR (500 MHz, $CDCl_3$, 23 °C, δ): 7.41 (t, *J* = 7.0 Hz, 1H), 7.28 (q, *J* = 7.5 Hz, 1H), 7.14 (t, *J* = 7.0 Hz, 1H), 7.05 (t, *J* = 9.0 Hz, 1H), 4.53 (s, 2H), 3.42 (s, 3H). ^{13}C NMR (125 MHz, $CDCl_3$, 23 °C, δ): 160.8 (d, *J* = 246 Hz), 130.0 (d, *J* = 3.6 Hz), 129.3 (d, *J* = 8.3 Hz), 125.2 (d, *J* = 14.6 Hz), 124.0 (d, *J* = 3.6 Hz), 115.2 (d, *J* = 21.9 Hz), 68.0 (d, *J* = 3.6 Hz), 58.3. ^{19}F NMR (375 MHz, $CDCl_3$, 23 °C, δ): –122.2. LRMS-FIA(m/z) calcd for C_8H_9FO $[M]^+$, 140.1; found, 140.1. HRMS-FIA(m/z) calcd for C_8H_9FO [(M+H)-F], 123.0760; found, 123.0756.

2-(4-Fluorophenyl)pyridine (2.3e)

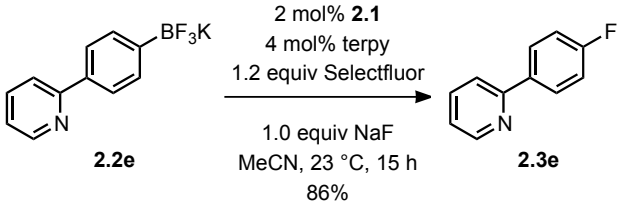

To a mixture of palladium precatalyst **2.1** (5.5 mg, 10 μmol, 0.020 equiv), terpy (4.7 mg, 20 μmol, 0.040 equiv), aryl trifluoroborate **2.2e** (131 mg, 500 μmol, 1.00 equiv), Selectfluor (213 mg, 600 μmol, 1.20 equiv), and sodium fluoride (21.0 mg, 500 μmol, 1.00 equiv) was added acetonitrile (5.0 mL, 0.1 M) at 23 °C. The reaction mixture was stirred for 15 hours at 23 °C and then transferred to a separatory funnel, rinsing the reaction vial with additional acetonitrile (2 × 4 mL). Pentane (20 mL) was added and the organic layer was washed with water (20 mL). The aqueous layer was extracted with pentane (6 × 20 mL). The combined organic layers were dried over sodium sulfate, filtered, and concentrated *in vacuo* to afford a yellow solid. The solid was purified by

chromatography on silica gel eluting with a solvent mixture of pentane/Et_2O (4:1 (v/v)) to afford a colorless solid (78.0 mg) containing the title compound (74.9 mg, 432 μmol, 86% yield), water, and pentane. The remaining solvent was not removed from the sample due to volatility of the product. The solvent content of the residue was determined by integration of the ^1H NMR spectrum of the mixture. Azeotropic evaporation of the trace solvent with $CDCl_3$ was performed prior to ^1H and ^{13}C NMR characterization.

R_f = 0.41 (pentane/diethyl ether 4:1 (v/v)). NMR Spectroscopy: ^1H NMR (600 MHz, $CDCl_3$, 23 °C, δ): 8.68 (ddd, *J* = 4.8, 1.7, 0.9 Hz, 1H), 7.98 (q, *J* = 7.5 Hz, 2H), 7.75 (td, *J* = 7.7, 1.8 Hz, 1H), 7.23 (ddd, *J* = 7.4, 4.8, 1.1 Hz, 1H), 7.18–7.14 (m, 2H). ^{13}C NMR (125 MHz, $CDCl_3$, 23 °C, δ): 163.4 (d, *J* = 249 Hz), 156.4, 149.6, 136.7, 135.5, 128.6 (d, *J* = 7.3), 122.0, 120.1, 115.6 (d, *J* = 20.0 Hz). ^{19}F NMR (375 MHz, $CDCl_3$, 23 °C, δ): –116.2. HRMS-FIA(m/z) calcd for $C_{11}H_8FN$ $[M+H]^+$, 174.0714; found, 174.0722.

2-Fluoro-1,3-5-triisopropylbenzene (2.3f)

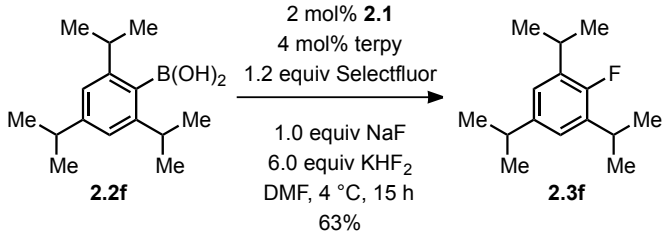

To a mixture of palladium precatalyst **2.1** (7.8 mg, 14 μmol, 0.020 equiv), terpy (6.5 mg, 28 μmol, 0.040 equiv), arylboronic acid **2.2f** (175 mg, 700 μmol, 1.00 equiv), Selectfluor (298 mg, 840 μmol, 1.20 equiv), sodium fluoride (29.4 mg, 700 μmol, 1.00 equiv), and potassium bifluoride (328 mg, 4.20 mmol, 6.00 equiv) at 4 °C was added cold

dimethylformamide (7.0 mL, 0.1 M) at 4 °C. The reaction mixture was stirred for 15 hours at 4 °C and then transferred cold to a separatory funnel. Pentane (20 mL) was added and the organic layer was washed with a 5% aqueous lithium chloride solution (20 mL). The aqueous layer was extracted with pentane (3 × 20 mL). The combined organic layers were dried over sodium sulfate, filtered, and concentrated *in vacuo* at 0 °C to afford a yellow oil. The residue was purified by preparative thin layer chromatography on silica gel eluting with perfluorohexanes to afford a colorless oil (148 mg) containing the title compound (98.6 mg, 443 μmol, 63% yield), water, pentane, and dichloromethane. The remaining solvent was not removed from the sample due to volatility of the product. The solvent content of the residue was determined by integration of the ^{1}H NMR spectrum of the mixture. Azeotropic evaporation of the trace solvent with $CDCl_3$ was performed prior to ^{1}H and ^{13}C NMR characterization.

R_f = 0.10 (perfluorohexanes). NMR Spectroscopy: ^{1}H NMR (600 MHz, $CDCl_3$, 23 °C, δ): 6.91 (d, *J* = 6.8 Hz, 2H), 3.22 (hept, *J* = 6.9 Hz, 2H), 2.86 (hept, *J* = 7.1 Hz, 1H), 1.26 (d, *J* = 7.0 Hz, 12H), 1.24 (d, *J* = 6.9 Hz, 6H). ^{13}C NMR (125 MHz, $CDCl_3$, 23 °C, δ): 156.6 (d, *J* = 240 Hz), 143.8 (d, *J* = 3.6 Hz), 134.5 (d, *J* = 15.4 Hz), 122.2 (d, *J* = 5.5 Hz), 33.9, 27.4 (d, *J* = 2.6 Hz), 24.3, 22.8. ^{19}F NMR (375 MHz, $CDCl_3$, 23 °C, δ): –133.4. HRMS-FIA(m/z) calcd for $C_{15}H_{23}F$ $[M]^+$, 222.1778; found, 222.1773.

2-Fluoro-1,1'-biphenyl (2.3g)

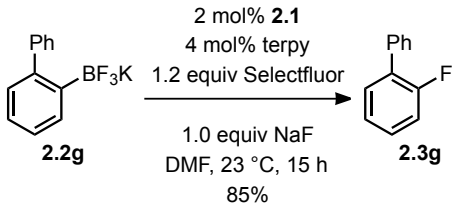

To a mixture of palladium catalyst **2.1** (7.8 mg, 14 μmol, 0.020 equiv) and terpy (6.5 mg, 28 μmol, 0.040 equiv) was added dimethylformamide (7.0 mL, 0.1 M) at 23 °C. This suspension was swirled for approx. 20 seconds until it became homogenous. This solution was transferred via syringe to a mixture of aryl trifluoroborate **2.2g** (182 mg, 700 μmol, 1.00 equiv), Selectfluor (298 mg, 840 μmol, 1.20 equiv), and sodium fluoride (29.4 mg, 700 μmol, 1.00 equiv). The reaction mixture was stirred for 15 hours at 23 °C and then transferred to a separatory funnel. Pentane (20 mL) was added and the organic layer was washed with a 5% aqueous lithium chloride solution (20 mL). The aqueous layer was extracted with pentane (4 × 20 mL). The combined organic layers were dried over sodium sulfate. The organic layer was filtered through silica gel (approx. 20 g) eluting with pentane (approx. 200 mL) and concentrated *in vacuo* at 0 °C to afford a colorless solid (106.6 mg) containing the title compound (102 mg, 592 μmol, 85% yield) and biphenyl (4.6 mg, 29.8 μmol, 4% yield). Purity of the residue was determined by integration of the ^{1}H NMR spectrum of the mixture.

R_f = 0.62 (pentane). NMR Spectroscopy: ^{1}H NMR (600 MHz, $CDCl_3$, 23 °C, δ): 7.57–7.54 (m, 2H), 7.46–7.43 (m, 3H), 7.39 (tt, *J* = 7.5, 1.4 Hz, 1H), 7.32 (dddd, *J* = 8.2, 7.3, 5.2, 1.9 Hz, 1H), 7.21 (td, *J* = 7.5, 1.2 Hz, 1H), 7.16 (ddd, *J* = 10.8, 8.2, 1.2 Hz, 1H). ^{13}C NMR (125 MHz, $CDCl_3$, 23 °C, δ): 159.7 (d, *J* = 247 Hz), 135.8, 130.7 (d, *J* = 3.6 Hz), 129.1 (d, *J* = 5.3 Hz), 129.0 (d, *J* = 2.8 Hz), 128.9 (d, *J* = 8.3 Hz), 128.4, 127.6, 124.3 (d, *J* = 3.6 Hz), 116.0 (d, *J* = 22.8 Hz). ^{19}F NMR (375 MHz, $CDCl_3$, 23 °C, δ): –121.1. HRMS-APCI(m/z) calcd for $C_{12}H_9F$ $[M]^+$, 172.0683; found, 172.0688.

4-Fluoro-1,1'-biphenyl (2.3h)

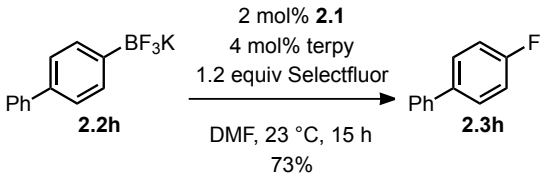

To a mixture of palladium catalyst **2.1** (7.8 mg, 14 μmol, 0.020 equiv) and terpy (6.5 mg, 28 μmol, 0.040 equiv) was added dimethylformamide (7.0 mL, 0.1 M) at 23 °C. This suspension was swirled for approx. 20 seconds until it became homogenous. This solution was transferred via syringe to a mixture of aryl trifluoroborate **2.2h** (182 mg, 700 μmol, 1.00 equiv) and Selectfluor (298 mg, 840 μmol, 1.20 equiv). The reaction mixture was stirred for 15 hours at 23 °C and then transferred to a separatory funnel. Pentane (20 mL) was added and the organic layer was washed with a 5% aqueous lithium chloride solution (20 mL). The aqueous layer was extracted with pentane (4 × 20 mL). The combined organic layers were dried over sodium sulfate. The organic layer was filtered through silica gel (approx. 20 g) eluting with pentane (approx. 200 mL) and concentrated *in vacuo* at 0 °C to afford the title compound (88.4 mg, 513 μmol, 73% yield) as a colorless crystalline solid.

R_f = 0.62 (pentane). NMR Spectroscopy: ^{1}H NMR (600 MHz, $CDCl_3$, 23 °C, δ): 7.56–7.53 (m, 4H), 7.45–7.42 (tm, J = 7.8 Hz, 2H), 7.36–7.33 (m, 1H), 7.15–7.11 (m, 2H). ^{13}C NMR (125 MHz, $CDCl_3$, 23 °C, δ): 162.4 (d, J = 246 Hz), 140.2, 137.3 (d, J = 3.6 Hz), 128.8, 128.6 (d, J = 8.3 Hz), 127.2, 127.0, 115.6 (d, J = 21.9 Hz). ^{19}F NMR (375 MHz, $CDCl_3$, 23 °C, δ): –118.9. HRMS-FIA(m/z) calcd for $C_{12}H_9F$ $[M]^+$, 172.0683; found, 172.0685.

3-(4-Fluorophenyl)propan-1-ol (2.3i)

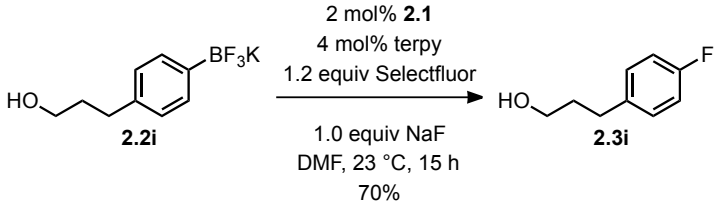

To a mixture of palladium precatalyst **2.1** (5.5 mg, 10 μmol, 0.020 equiv), terpy (4.7 mg, 20 μmol, 0.040 equiv), aryl trifluoroborate **2.2i** (121 mg, 500 μmol, 1.00 equiv), Selectfluor (213 mg, 600 μmol, 1.20 equiv), and sodium fluoride (21.0 mg, 500 μmol, 1.00 equiv) was added dimethylformamide (5.0 mL, 0.1 M) at 23 °C. The reaction mixture was stirred for 15 hours at 23 °C and then transferred to a separatory funnel. Diethyl ether (20 mL) was added and the organic layer was washed with a 5% aqueous lithium chloride solution (20 mL). The aqueous layer was extracted with diethyl ether (2 × 20 mL). The combined organic layers were dried over sodium sulfate, filtered, and concentrated *in vacuo* at 0 °C to afford a yellow oil. The residue was purified by chromatography on silica gel eluting with a solvent mixture of pentane/Et_2O (11:9 (v/v)) to afford a colorless oil (97.2 mg) containing the title compound (54.7 mg, 355 μmol, 71% yield), water, pentane, diethyl ether, and dichloromethane. The remaining solvent was not removed from the sample due to volatility of the product. The solvent content of the residue was determined by integration of the ^1H NMR spectrum of the mixture. Azeotropic evaporation of the trace solvent with $CDCl_3$ was performed prior to ^1H and ^{13}C NMR characterization. The ^1H and ^{13}C NMR spectroscopic data correspond to the data reported in reference 5.[17] High resolution mass spectrometry could only identify

[17] Szostak, M.; Spain, M.; Procter, D. J. *Org. Let.* **2012**, 14(3), 840-843.

[(M+H)-F], therefore low resolution mass spectrometry was used to confirm the molecular ion of the title compound.

R_f = 0.24 (pentane/Et_2O 11:9 (v/v)). NMR Spectroscopy: ^1H NMR (500 MHz, $CDCl_3$, 23 °C, δ): 7.17–7.13 (m, 2H), 6.99–6.94 (m, 2H), 3.67 (t, *J* = 6.4 Hz, 2H), 2.69 (t, *J* = 7.7 Hz, 2H), 1.90–1.84 (tdd, *J* = 8.6, 6.8, 5.3 Hz, 2H), 1.32 (s, 1H). ^{13}C NMR (125 MHz, $CDCl_3$, 23 °C, δ): 161.2 (d, *J* = 242 Hz), 137.4 (d, *J* = 2.8 Hz), 129.7 (d, *J* = 7.4 Hz), 115.0 (d, *J* = 20.9 Hz), 62.0, 34.2, 31.2. ^{19}F NMR (375 MHz, $CDCl_3$, 23 °C, δ): –120.7. LRMS-FIA(m/z) calcd for $C_9H_{11}FO$ $[M]^+$, 154.1; found, 154.1. HRMS-FIA(m/z) calcd for $C_9H_{11}FO$ [(M+H)-F], 136.0883; found, 136.0882.

2-(4-Fluorophenyl)acetic acid (2.3k)

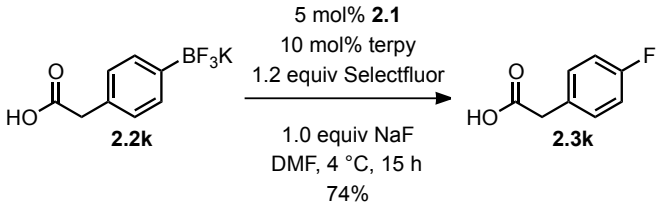

To a mixture of palladium precatalyst **2.1** (13.9 mg, 25.0 μmol, 0.0500 equiv), terpy (11.7 mg, 50.0 μmol, 0.100 equiv), aryl trifluoroborate **2.2k** (121 mg, 500 μmol, 1.00 equiv), Selectfluor (213 mg, 600 μmol, 1.20 equiv), and sodium fluoride (21.0 mg, 500 μmol, 1.00 equiv) was added dimethylformamide (5.0 mL, 0.1 M) at 23 °C. The reaction mixture was stirred for 15 hours at 4 °C and then transferred to a separatory funnel. Diethyl ether (20 mL) was added and the organic layer was washed with a 1 N aqueous HCl solution (20 mL). The aqueous layer was extracted with diethyl ether (3 × 20 mL). The combined organic layers were dried over sodium sulfate, filtered, and concentrated *in vacuo* to afford a yellow solid. The solid was purified by chromatography on silica gel

eluting with a solvent mixture of pentane/Et_2O/AcOH (70:30:1 (v/v)) to afford a colorless solid (60.1 mg) containing the title compound (57.1 mg, 370 μmol, 74% yield) and dichloromethane. The remaining solvent was not removed from the sample due to volatility of the product. The solvent content of the residue was determined by integration of the ^1H NMR spectrum of the mixture. Azeotropic evaporation of the trace solvent with $CDCl_3$ was performed prior to ^1H and ^{13}C NMR characterization.

R_f = 0.36 (pentane/Et_2O/AcOH 70:30:1 (v/v)). NMR Spectroscopy: ^1H NMR (600 MHz, $CDCl_3$, 23 °C, δ): 10.31 (bs, 1H), 7.27–7.24 (m, 2H), 7.05–7.01 (m, 2H), 3.64 (s, 2H). ^{13}C NMR (125 MHz, $CDCl_3$, 23 °C, δ): 178.1, 162.1 (d, J = 245 Hz), 130.9 (d, J = 8.3 Hz), 128.9 (d, J = 3.6 Hz), 115.5 (d, J = 21.9 Hz), 40.2. ^{19}F NMR (375 MHz, $CDCl_3$, 23 °C, δ): –118.2. HRMS-FIA(m/z) calcd for $C_8H_7FO_2$ $[M–H]^-$, 153.0357; found, 153.0353.

4-Fluorobenzamide (2.3l)

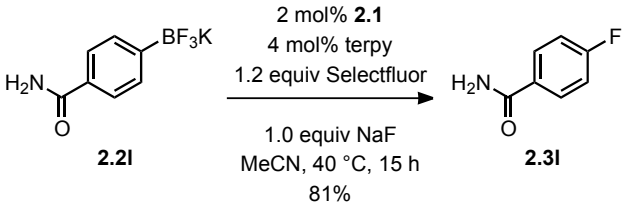

To a mixture of palladium precatalyst **2.1** (5.5 mg, 10 μmol, 0.020 equiv), terpy (4.7 mg, 20 μmol, 0.040 equiv), aryl trifluoroborate **2.2l** (114 mg, 500 μmol, 1.00 equiv), Selectfluor (213 mg, 600 μmol, 1.20 equiv), and sodium fluoride (21.0 mg, 500 μmol, 1.00 equiv) was added acetonitrile (5.0 mL, 0.1 M) at 23 °C. The reaction mixture was stirred for 15 hours at 40 °C, allowed to cool to 23 °C, and then transferred to a separatory funnel. Dichloromethane (20 mL) was added and the organic layer was

washed with water (20 mL). The aqueous layer was extracted with dichloromethane (3 × 20 mL). The combined organic layers were dried over sodium sulfate, filtered, and concentrated *in vacuo* to afford a yellow solid. The solid was purified by chromatography on silica gel eluting with a solvent mixture of dichloromethane/methanol (99:1 (v/v)) ramping to a solvent mixture of dichloromethane/methanol (97:3 (v/v)) to afford a colorless solid (64.2 mg) containing the title compound (56.0 mg, 403 μmol, 81% yield), 3-fluorobenzamide (3.88 mg, 27.9 μmol, 6% yield), 2-fluorobenzamide (2.22 mg, 15.9 μmol, 3% yield), water, pentane, and dichloromethane. The remaining solvent was not removed from the sample due to volatility of the product. The solvent content of the residue was determined by integration of the ^{1}H NMR spectrum of the mixture. Azeotropic evaporation of the trace solvent with $CDCl_3$ was performed prior to ^{1}H and ^{13}C NMR characterization.

R_f = 0.20 (dichloromethane/methanol 19:1 (v/v)). NMR Spectroscopy: ^{1}H NMR (600 MHz, $CDCl_3$, 23 °C, δ): 7.85–7.81 (m, 2H), 7.15–7.11 (m, 2H), 5.98 (bs, 1H), 5.67 (bs, 1H). ^{13}C NMR (100 MHz, DMSO-d_6, 23 °C, δ): 167.2, 163.9 (d, J = 249 Hz) , 130.3, 129.8 (d, J = 9.1 Hz), 114.6 (d, J = 21.4 Hz). ^{19}F NMR (375 MHz, $CDCl_3$, 23 °C, δ): –110.3. HRMS-FIA(m/z) calcd for C_7H_6FNO $[M+H]^+$, 140.0506; found, 140.0508.

1-Bromo-4-fluorobenzene (2.3m)

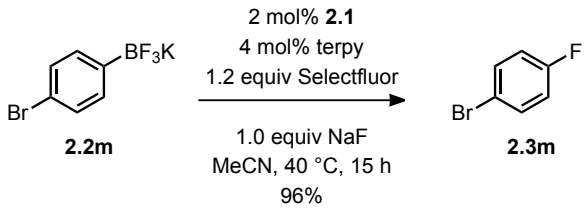

2.2m **2.3m**

To a mixture of palladium precatalyst **2.1** (5.5 mg, 10 μmol, 0.020 equiv), terpy (4.7 mg, 20 μmol, 0.040 equiv), aryl trifluoroborate **2.2m** (131 mg, 500 μmol, 1.00 equiv), Selectfluor (213 mg, 600 μmol, 1.20 equiv), and sodium fluoride (21.0 mg, 500 μmol, 1.00 equiv) was added acetonitrile (5.0 mL, 0.1 M) at 23 °C. The reaction mixture was stirred for 15 hours at 40 °C, allowed to cool to 23 °C, and then transferred to a separatory funnel. Pentane (20 mL) was added and the organic layer was washed with water (20 mL). The aqueous layer was extracted with pentane (3 × 20 mL). The combined organic layers were dried over sodium sulfate. The organic layer was filtered through silica gel (approx. 20 g) eluting with pentane (approx. 200 mL) and concentrated *in vacuo* at 0 °C to afford a colorless oil (130 mg) containing the title compound (84.4 mg, 482 μmol, 96% yield), pentane, and water. The remaining solvent was not removed from the sample due to volatility of the product. The solvent content of the residue was determined by integration of the ^{1}H NMR spectrum of the mixture.

R_f = 0.84 (pentane). NMR Spectroscopy: ^{1}H NMR (500 MHz, $CDCl_3$, 23 °C, δ): 7.47–7.42 (m, 1H), 6.98–6.93 (m, 1H). ^{13}C NMR (125 MHz, $CDCl_3$, 23 °C, δ): 161.8 (d, J = 245 Hz), 132.9 (d, J = 7.4 Hz), 117.2 (d, J = 22.8 Hz), 116.5 (d, J = 3.6 Hz). ^{19}F NMR (375 MHz, $CDCl_3$, 23 °C, δ): –118.4. HRMS-FIA(m/z) calcd for C_6H_4BrF $[M]^+$, 175.9455; found, 175.9452.

1-(4-Fluorophenyl)propan-2-one (2.3n)

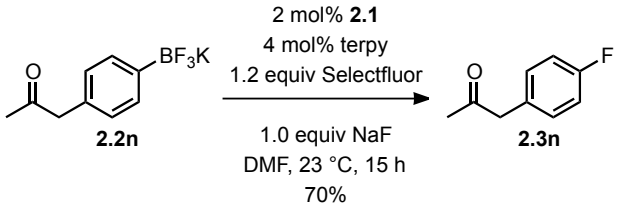

To a mixture of palladium precatalyst **2.1** (7.8 mg, 14 μmol, 0.020 equiv), terpy (6.5 mg, 28 μmol, 0.040 equiv), aryl trifluoroborate **2.2n** (168 mg, 700 μmol, 1.00 equiv), Selectfluor (298 mg, 840 μmol, 1.20 equiv), and sodium fluoride (29.4 mg, 700 μmol, 1.00 equiv) was added dimethylformamide (7.0 mL, 0.1 M) at 23 °C. The reaction mixture was stirred for 15 hours at 23 °C and then transferred to a separatory funnel. Pentane (20 mL) was added and the organic layer was washed with a 5% aqueous lithium chloride solution (20 mL). The aqueous layer was extracted with pentane (3 × 20 mL). The combined organic layers were dried over sodium sulfate, filtered, and concentrated *in vacuo* at 0 °C to afford a yellow oil. The residue was purified by chromatography on silica gel eluting with a solvent mixture of pentane/Et_2O (17:3 (v/v)) to afford a colorless oil (104 mg) containing the title compound (74.9 mg, 493 μmol, 70% yield), dichloromethane, pentane, and water. The remaining solvent was not removed from the sample due to volatility of the product. The solvent content of the residue was determined by integration of the ^1H NMR spectrum of the mixture. Azeotropic evaporation of the trace solvent with $CDCl_3$ was performed prior to ^1H and ^{13}C NMR characterization.

R_f = 0.28 (pentane/diethyl ether 17:3 (v/v)). NMR Spectroscopy: ^1H NMR (600 MHz, $CDCl_3$, 23 °C, δ): 7.18–7.14 (m, 2H), 7.04–7.00 (m, 2H), 3.68 (s, 2H), 2.17 (s, 3H). ^{13}C NMR (125 MHz, $CDCl_3$, 23 °C, δ): 206.0, 161.9 (d, J = 244 Hz), 130.9 (d, J = 8.3 Hz), 129.9 (d, J = 3.6 Hz), 115.5 (d, J = 21.0 Hz), 49.8, 29.2. ^{19}F NMR (375 MHz, $CDCl_3$, 23 °C, δ): –118.8. HRMS-FIA(m/z) calcd for C_9H_9FO $[M+H]^+$, 153.0710; found, 153.0709.

Aryl Fluoride 2.3o

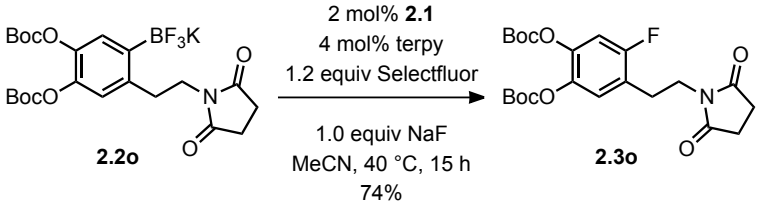

To a mixture of palladium precatalyst **2.1** (2.2 mg, 4.0 μmol, 0.020 equiv), terpy (1.9 mg, 8.0 μmol, 0.040 equiv), aryl trifluoroborate **2.2o** (108 mg, 200 μmol, 1.00 equiv), Selectfluor (85.0 mg, 240 μmol, 1.20 equiv), and sodium fluoride (8.40 mg, 200 μmol, 1.00 equiv) was added acetonitrile (2.0 mL, 0.1 M) at 23 °C. The reaction mixture was stirred for 15 hours at 40 °C, allowed to cool to 23 °C, and then transferred to a separatory funnel. Dichloromethane (20 mL) was added and the organic layer was washed with water (20 mL). The aqueous layer was extracted with dichloromethane (4 × 20 mL). The combined organic layers were washed with brine (20 mL), dried over sodium sulfate, filtered, and concentrated *in vacuo* to afford a yellow solid. The solid was purified by chromatography on silica gel eluting with a solvent mixture of hexanes/ethyl acetate (1:1 (v/v)) to afford the title compound (67.1 mg, 148 μmol, 74% yield) as a colorless crystalline solid.

R_f = 0.44 (hexanes/ethyl acetate 1:1 (v/v)). NMR Spectroscopy: ^{1}H NMR (600 MHz, $CDCl_3$, 23 °C, δ): 7.02 (d, J = 7.1 Hz, 1H), 7.00 (d, J = 9.6 Hz, 1H), 3.77 (t, J = 7.2 Hz, 2H), 2.93 (t, J = 7.2 Hz, 2H), 2.65 (s, 4H), 1.54 (s, 18H). ^{13}C NMR (125 MHz, $CDCl_3$, 23 °C, δ): 177.0, 158.0 (d, J = 245 Hz), 150.8, 150.1, 141.7 (d, J = 11.0 Hz), 138.3 (d, J = 3.6 Hz), 124.7 (d, J = 6.4 Hz), 122.7 (d, J = 18.3 Hz), 110.6 (d, J = 26.4 Hz), 84.1, 83.8,

37.9, 28.0, 27.5, 27.5, 26.7. ^{19}F NMR (375 MHz, $CDCl_3$, 23 °C, δ): –121.3. HRMS-FIA(m/z) calcd for $C_{22}H_{28}FNO_8$ $[M+NH_4]^+$, 471.2137; found, 471.2155.

6-Fluoro-4*H*-chromen-4-one (2.3p)

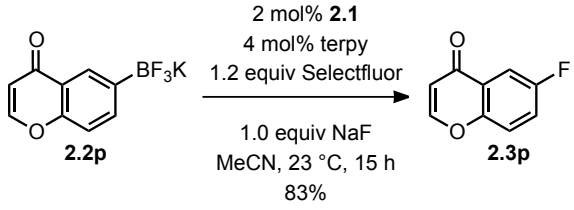

To a mixture of palladium precatalyst **2.1** (5.5 mg, 10 μmol, 0.020 equiv), terpy (4.7 mg, 20 μmol, 0.040 equiv), aryl trifluoroborate **2.2p** (126 mg, 500 μmol, 1.00 equiv), Selectfluor (213 mg, 600 μmol, 1.20 equiv), and sodium fluoride (21.0 mg, 500 μmol, 1.00 equiv) was added acetonitrile (5.0 mL, 0.1 M) at 23 °C. The reaction mixture was stirred for 15 hours at 23 °C and then transferred to a separatory funnel. Pentane (20 mL) was added and the organic layer was washed with water (20 mL). The aqueous layer was extracted with pentane (9 × 20 mL). The combined organic layers were dried over sodium sulfate, filtered, and concentrated *in vacuo* to afford a yellow solid. The solid was purified by chromatography on silica gel eluting with a solvent mixture of pentane/diethyl ether (7:3 (v/v)) to afford a colorless solid (72.8 mg) containing the title compound (67.9 mg, 413 μmol, 83% yield), dichloromethane, pentane, and water. The remaining solvent was not removed from the sample due to volatility of the product. The solvent content of the residue was determined by integration of the ^{1}H NMR spectrum of the mixture. Azeotropic evaporation of the trace solvent with $CDCl_3$ was performed prior to ^{1}H and ^{13}C NMR characterization.

R_f = 0.20 (pentane/diethyl ether 7:3 (v/v)). NMR Spectroscopy: ^{1}H NMR (600 MHz, $CDCl_3$, 23 °C, δ): 7.87 (d, *J* = 6.1 Hz, 1H), 7.85 (dd, *J* = 8.2, 3.1 Hz, 1H), 7.48 (dd, *J* = 9.2, 4.2 Hz, 1H), 7.40 (ddd, *J* = 9.2, 7.6, 3.1 Hz, 1H), 6.34 (d, *J* = 6.0 Hz, 1H). ^{13}C NMR (125 MHz, $CDCl_3$, 23 °C, δ): 176.7, 159.4 (d, *J* = 245 Hz), 155.4, 152.7 (d, *J* = 1.8 Hz), 125.9 (d, *J* = 7.3 Hz), 121.9 (d, *J* = 25.5 Hz), 120.3 (d, *J* = 7.3 Hz), 112.1, 110.5 (d, *J* = 23.6 Hz). ^{19}F NMR (375 MHz, $CDCl_3$, 23 °C, δ): –117.9. HRMS-FIA(m/z) calcd for $C_9H_5FO_2$ $[M+H]^+$, 165.0346; found, 165.0351.

Evaluation of other [Pd] pre-catalysts (Data pertaining to Table 2.2)

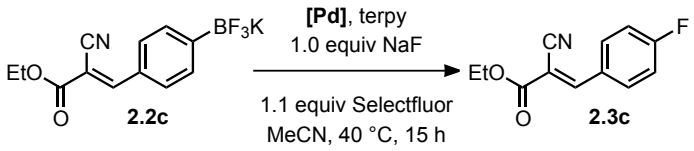

General Procedure:

To aryl trifluoroborate **2.2c** (31 mg, 0.10 mmol, 1.0 equiv), Selectfluor (39 mg, 0.11 mmol, 1.1 equiv), NaF (4.2 mg, 0.10 mmol, 1.0 equiv), the [Pd] source (2.0×10^{-3} mmol, 0.020 equiv), and terpy (1.0 mg, 4.0×10^{-3} mmol, 0.040 equiv) in a 4 mL glass vial was added MeCN (1.0 mL). The vial was sealed with a teflon-lined cap, and the reaction mixture was heated at 40 ºC with vigorous stirring. After 15 hours, the reaction mixture was cooled to room temperature, and then transferred to a separatory funnel, rinsing the reaction vial with additional MeCN (2 × 0.5 mL). H_2O (15 mL) was added, and the product was extracted from the aqueous mixture with CH_2Cl_2 (3 × 4 mL). The combined organic phases were dried over Na_2SO_4, filtered, and concentrated under vacuum to give an off-white solid. To the solid was added 2 mL of a 10% (v/v) Et_2O/pentane mixture, and the mixture was agitated using an ultrasonic bath. The resulting suspension was

filtered over a plug of SiO_2 (~1.5" in a Pasteur pipette), eluting with an additional 15 mL of 10% Et_2O/pentane. The filtrate was concentrated, and the product was further dried under vacuum, affording aryl fluoride **2.3c** as a colorless crystalline solid. Purity of the product was confirmed in each case via ^1H and ^{19}F NMR spectroscopy.

Specific details for each [Pd] source used are given in Table 2.S1 below:

Table 2.S1. Evaluation of Palladium Pre-Catalysts

[Pd] Source	**Commercial Supplier**	**Additive**	**Yield ArF 2.3c**
$[(terpy)_2Pd][BF_4]_3$ (**2.4**) (1.7 mg, 2 mol%)	*N/A*	None	21 mg, 95%
$[Pd(MeCN)_4][BF_4]_2$ (0.9 mg, 2 mol%)	Strem	None	21 mg, 95%
$Pd(OAc)_2$ (1.2 mg, 5 mol%)	Strem	$NaBF_4$ (22 mg, 2.0 equiv)	20 mg, 91%
$Pd(O_2CCF_3)_2$ (0.7 mg, 2 mol%)	Strem	$NaBF_4$ (11 mg, 1.0 equiv)	20 mg, 91%
$PdCl_2(MeCN)_2$ (1.3 mg, 5 mol%)	Sigma-Aldrich	$NaBF_4$ (22 mg, 2.0 equiv)	19 mg, 86% (as a mixture with ~10% ArCl)
$PdBr_2$ (1.3 mg, 5 mol%)	Sigma-Aldrich	$NaBF_4$ (22 mg, 2.0 equiv)	17 mg, 78% (as a mixture with ~10% ArBr)

Evaluation of other arylboron reagents (Data pertaining to Scheme 2.2)

Fluorination of [(*E*)-4-(2-cyano-2-ethoxycarbonylvinyl)phenyl]boronic acid pincol ester

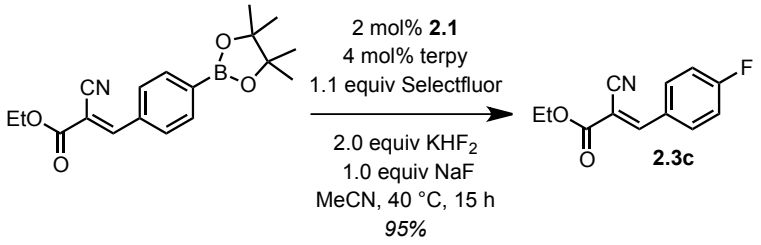

To [(*E*)-4-(2-cyano-2-ethoxycarbonylvinyl)phenyl]boronic acid pinacol ester (33 mg, 0.10 mmol, 1.0 equiv), Selectfluor (39 mg, 0.11 mmol, 1.1 equiv), KHF_2 (16 mg, 0.20 mmol, 2.0 equiv), NaF (4.2 mg, 0.10 mmol, 1.0 equiv), Pd complex **2.1** (1.1 mg, 2.0×10^{-3} mmol, 0.020 equiv), and terpy (1.0 mg, 4.0×10^{-3} mmol, 0.040 equiv) in a 4 mL glass vial was added MeCN (1.0 mL). The vial was sealed with a teflon-lined cap, and the reaction mixture was heated at 40 ºC with vigorous stirring. After 15 hours, the reaction mixture was cooled to room temperature, and then transferred to a separatory funnel, rinsing the reaction vial with additional MeCN (2×0.5 mL). H_2O (15 mL) was added, and the product was extracted from the aqueous mixture with CH_2Cl_2 (3×4 mL). The combined organic phases were dried over Na_2SO_4, filtered, and concentrated under vacuum to give an off-white solid. To the solid was added 2 mL of a 10% (v/v) Et_2O/pentane mixture, and the mixture was agitated using an ultrasonic bath. The resulting suspension was filtered over a plug of SiO_2 (~1.5" in a Pasteur pipette), eluting with an additional 15 mL of 10% Et_2O/pentane. The filtrate was concentrated, and the product was further dried under vacuum, affording 21 mg of aryl fluoride **2.3c** as a

colorless crystalline solid (95% yield). Purity of the product was confirmed via ^{1}H and ^{19}F NMR spectroscopy.

Fluorination of [(*E*)-4-(2-cyano-2-ethoxycarbonylvinyl)phenyl]boronic acid (2.S1)

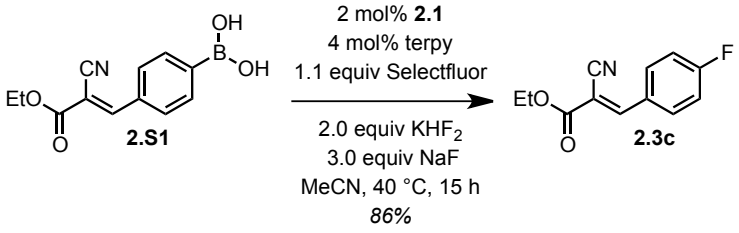

To [(*E*)-4-(2-cyano-2-ethoxycarbonylvinyl)phenyl]boronic acid (**2.S1**) (25 mg, 0.10 mmol, 1.0 equiv), Selectfluor (39 mg, 0.11 mmol, 1.1 equiv), KHF_2 (16 mg, 0.20 mmol, 2.0 equiv), NaF (13 mg, 0.30 mmol, 3.0 equiv), Pd complex **2.1** (1.1 mg, 2.0×10^{-3} mmol, 0.020 equiv), and terpy (1.0 mg, 4.0×10^{-3} mmol, 0.040 equiv) in a 4 mL glass vial was added MeCN (1.0 mL). The vial was sealed with a teflon-lined cap, and the reaction mixture was heated at 40 ºC with vigorous stirring. After 15 hours, the reaction mixture was cooled to room temperature, and then transferred to a separatory funnel, rinsing the reaction vial with additional MeCN (2×0.5 mL). H_2O (15 mL) was added, and the product was extracted from the aqueous mixture with CH_2Cl_2 (3×4 mL). The combined organic phases were dried over Na_2SO_4, filtered, and concentrated under vacuum to give an off-white solid. To the solid was added 2 mL of a 10% (v/v) Et_2O/pentane mixture, and the mixture was agitated using an ultrasonic bath. The resulting suspension was filtered over a plug of SiO_2 (~1.5" in a Pasteur pipette), eluting with an additional 15 mL of 10% Et_2O/pentane. The filtrate was concentrated, and the product was further dried under vacuum, affording 19 mg of aryl fluoride **2.3c** as a

colorless crystalline solid (86% yield). Purity of the product was confirmed via ^{1}H and ^{19}F NMR spectroscopy.

Fluorination of 4-phenoxyphenylboronic acid MIDA ester

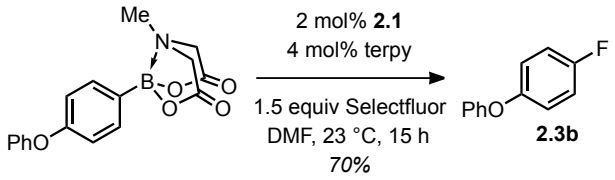

To 4-phenoxyphenylboronic acid MIDA ester (65 mg, 0.20 mmol, 1.0 equiv), Selectfluor (110 mg, 0.30 mmol, 1.5 equiv), Pd complex **2.1** (2.2 mg, 4.0×10^{-3} mmol, 0.020 equiv), and terpy (1.9 mg, 8.0×10^{-3} mmol, 0.040 equiv) in a 4 mL glass vial was added DMF (2.0 mL). The vial was sealed with a teflon-lined cap, and the reaction mixture was stirred at 23 ºC. After 15 hours, the reaction mixture was transferred to a separatory funnel. Brine (15 mL) was added, and the product was extracted from the resulting aqueous mixture with pentane (5 × 5 mL). The combined organic phases were dried over Na_2SO_4, and then filtered over a short pad of SiO_2 (~1 cm in a fritted funnel), eluting with an additional 20 mL of pentane. The filtrate was concentrated under vacuum at 0 °C, affording a colorless oil containing 27 mg of aryl fluoride **2.3b** (70% yield), along with water and pentane. The residual solvents were not further removed due to volatility of the product. The yield of **2.3b** was confirmed via ^{19}F and ^{1}H NMR spectroscopy using 1-fluoro-3-nitrobenzene (10. μL, 9.4×10^{-5} mol) as an internal standard.

No formation of aryl fluoride **2.3b** was observed in the reaction between 4-phenoxyphenylboronic acid MIDA ester and Selectfluor in the absence of Pd complex **2.1**.

Evaluation of other single-electron redox catalysts

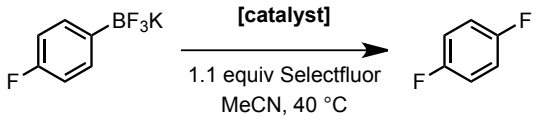

The proposed mechanism for the Pd-catalyzed fluorination reaction suggests the possiblity that other catalysts, capable of single-electron redox chemistry, may also be competent in the fluorination reaction. Therefore, we have performed a preliminary evaluation of other potential catalysts, summarized in Table 2.S2 below. The results indicate that other metal complexes are indeed competent to catalyze the fluorination reaction, but that the combination of Pd complex **2.1** and terpyridine is uniquely effective in providing high yields and selectivity.

General Procedure:

To the aryl trifluoroborate (25 mg, 0.11 mmol, 1.0 equiv), Selectfluor (50. mg, 0.14 mmol, 1.1 equiv), and the catalyst (see Table 2.S2) in a 4 mL glass vial was added MeCN (1.2 mL). The vial was sealed with a teflon-lined cap, and the reaction mixture was heated at 40 ºC with vigorous stirring. After 15 hours, the reaction mixture was cooled to room temperature, and then 1-fluoro-3-nitrobenzene (10. μL, 9.4×10^{-5} mol) was added as an internal standard. The yield of the aryl fluoride product, as well as unconsumed

aryl trifluoroborate and protodeborylated product, was determined via ^{19}F NMR spectroscopy, integrating against the internal standard peak at –112 ppm.

Table 2.S2. Evaluation of other single-electron redox catalysts

Catalyst	Additive	Yield ArF	Remaining $ArBF_3K$	Yield of Protodeborylation
$[(terpy)_2Ni][OTf]_2$ (2 mol%)	terpy (2 mol%)	19%	35%	22%
$[Ni(bpy)_3][BF_4]_2$ (2 mol%)	none	17%	51%	*not observed*
$[Ni(phen)_3][BF_4]_2$ (2 mol%)	none	13%	56%	< 2%
$[(terpy)Pt(MeCN)][BF_4]_2$ (2 mol%)	terpy (4 mol%)	17%	51%	*not observed*
Ferrocene (5 mol%)	none	9.5%	28%	42%

Evaluation of radical clock substrates

In order to probe the possibility of radical intermediates, we performed the Pd-catalyzed fluorination reaction on substrates **2.S4** and **2.S5**. Substrate **2.S4** probes the intermediacy of an aryl radical formed by homolysis of the C–B bond, and is known to undergo radical cyclization to afford dibenzofuran.[18] Substrate **2.S5** can undergo cyclopropane ring opening if a long-lived radical intermediate is formed via SET from the arene π-system. Both **2.S4** and **2.S5** underwent Pd-catalyzed fluorination to give a single major aryl fluoride product, in 54% and 62% yields, respectively (aryl fluoride yields determined by ^{19}F NMR spectroscopy, using 1-fluoro-3-nitrobenzene as internal standard). In the case of **2.S4**, radical cyclization was not observed; in the case of **2.S5**, no cyclopropane ring-opening was observed (the crude product mixtures were analyzed by ^{1}H NMR spectroscopy).

[18] Lockner, J. W.; Dixon, D. D.; Risgaard, R.; Baran, P. S. *Org. Lett*. **2011**, *13*, 5628–5631.

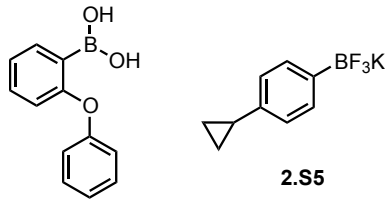

2.S4 **2.S5**

The lack of radical cyclization observed for **2.S4** is consistent with our mechanistic hypothesis, in which the C–F bond is formed prior to C–B bond cleavage. We note that the lack of cyclopropane ring opening for **2.S5** does not exclude the possibility of a radical mechanism, as the lifetime of the delocalized radical intermediate may be significantly shorter than the timescale of ring opening. In previous mechanistic investigations regarding SET reactivity with Selectfluor, computational evidence suggests that the lifetime of such intermediates are significantly shorter than the ring opening/closing timescale for radical clock substrates.[19]

Reaction Kinetics[20]

Kinetic Profile of Catalytic Reaction

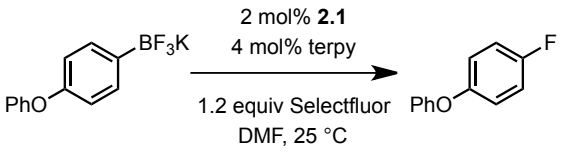

Solution A was prepared containing the aryl trifluoroborate (28 mg, 0.10 mmol, 1.0 equiv), Selectfluor (43 mg, 0.12 mmol, 1.2 equiv), and 1-fluoro-3-nitrobenzene (5.0 μL,

[19] Nyffeler, P. T.; Dur n, S. G.; Burkart, M. D.; Vincent, S. P. P.; Wong, C.-H. *Angew. Chem. Int. Ed.* **2005**, *44*, 192–212; and references therein.

[20] Many of the data plots resulting from these experimental procedures are shown in the main text of Chapter 2, and are not reproduced here.

4.7 × 10^{-5} mol) as internal standard, in 0.80 mL DMF. Solution B was prepared containing Pd(II) complex **2.1** (1.1 mg, 2.0 × 10^{-3} mmol, 0.020 equiv) and terpy (1.0 mg, 4.0 × 10^{-3} mmol, 0.040 equiv) in 0.20 mL DMF. Solution A was added to an NMR tube, followed by solution B, and the tube was shaken rapidly to mix the reagents. The reaction was monitored via ^{19}F NMR spectroscopy at 25 °C, following evolution of the product signal at –123 ppm and integrating against the internal standard peak at –112 ppm. The reaction was followed to greater than three half-lives, as determined by disappearance of the ^{19}F NMR signal corresponding to the aryl trifluoroborate. Because evolution of product was measured, linear natural log plots were obtained by using an infinite time point set to 100% yield, and data were fitted to a first order regression.

Initial Rate Kinetics of Pd Dependence

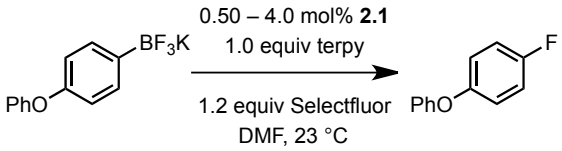

Three stock solutions were prepared: solution A, containing the aryl trifluoroborate (166 mg, 0.601 mmol), Selectfluor (255 mg, 0.720 mmol), and 1-fluoro-3-nitrobenzene (30.0 μL, 2.82 × 10^{-4} mol) as internal standard, in 3.00 mL DMF; solution B, containing Pd(II) complex **2.1** (5.5 mg, 1.0 × 10^{-2} mmol) in 0.50 mL DMF; and solution C, containing terpy (116 mg, 0.497 mmol) in 2.00 mL DMF. For each reaction, solution A (0.50 mL) was added to an NMR tube, followed by solution C (0.40 mL), DMF (100 – *x* μL), and finally solution B (*x* μL). Pd loadings in the range of 0.50–4.0 mol% were used. The tube was shaken rapidly to mix the reagents, and then the reaction was monitored via ^{19}F NMR spectroscopy at 25 °C, following evolution of the product signal at –123 ppm

and integrating against the internal standard peak at –112 ppm. Product formation was monitored up to ~10% yield, and data in the 3–10% yield range was used to determine the initial rates.

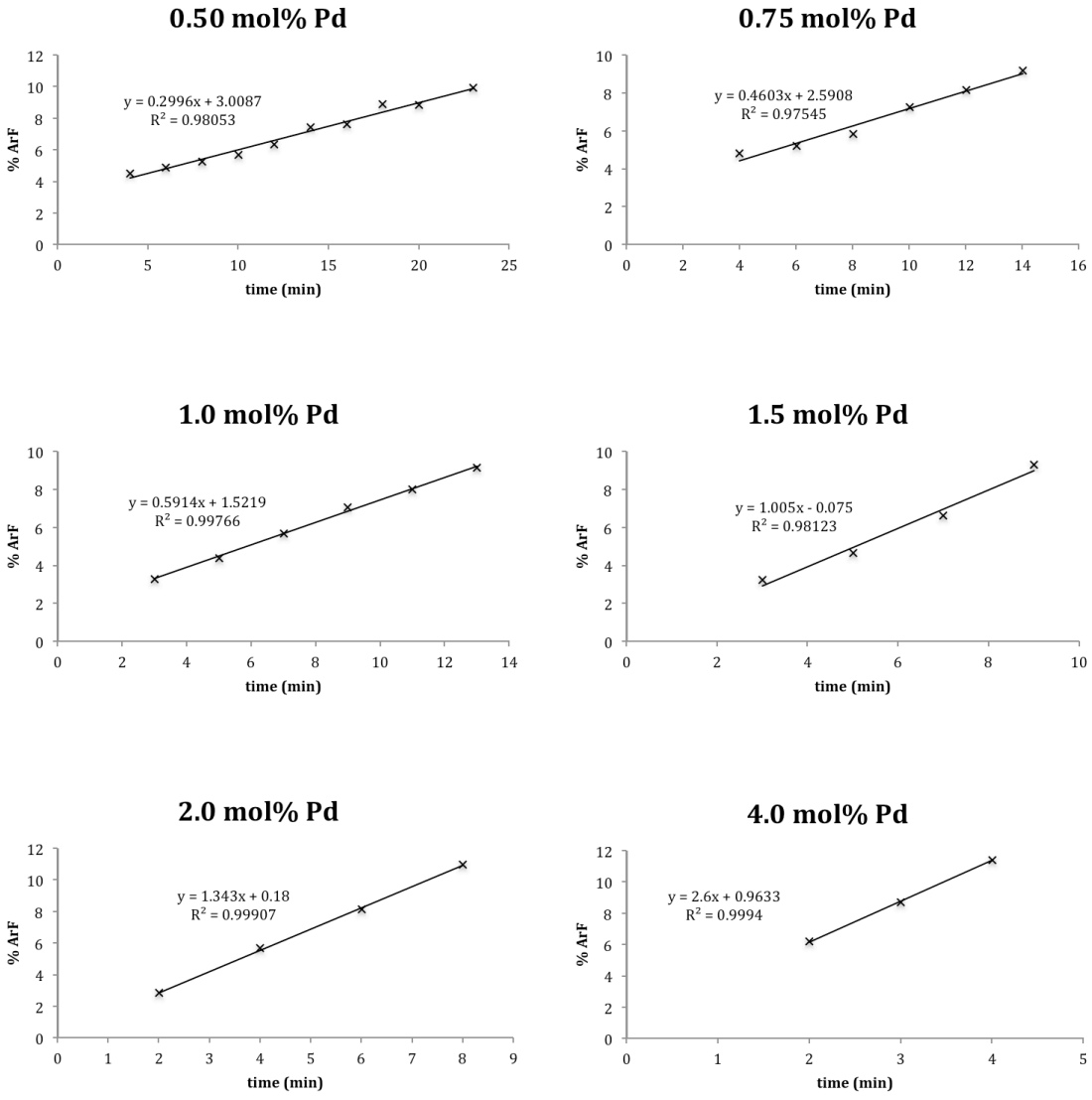

Initial Rate Kinetics of Terpyridine Dependence

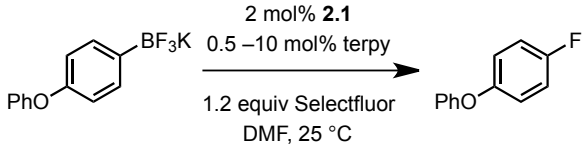

Three stock solutions were prepared: solution A, containing the aryl trifluoroborate (166 mg, 0.601 mmol), Selectfluor (255 mg, 0.720 mmol), and 1-fluoro-3-nitrobenzene (30.0 μL, 2.82×10^{-4} mol) as internal standard, in 3.00 mL DMF; solution B, containing Pd(II) complex **2.1** (3.3 mg, 6.0×10^{-3} mmol) in 0.60 mL DMF; and solution C, containing terpy (9.0 mg, 0.039 mmol) in 0.75 mL DMF. For each reaction, solution A (0.50 mL) was added to an NMR tube, followed by DMF (400 – *x* μL), solution C (*x* μL), and finally solution B (100 μL). Terpy loadings in the range of 0.5–10 mol% were used. The tube was shaken rapidly to mix the reagents, and then the reaction was monitored via ^{19}F NMR spectroscopy at 25 °C, following evolution of the product signal at –123 ppm and integrating against the internal standard peak at –112 ppm. Each reaction was monitored to approximately 5% yield, and yield was converted to an initial rate by dividing by the reaction time. The data obtained are presented in Figure 2.9.

Initial Rate Kinetics of Selectfluor Dependence

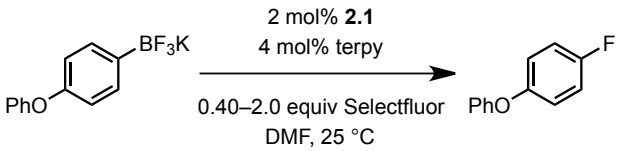

Three stock solutions were prepared: solution A, containing the aryl trifluoroborate (166 mg, 0.601 mmol) and 1-fluoro-3-nitrobenzene (30.0 μL, 2.82×10^{-4} mol) as internal

standard, in 2.40 mL DMF; solution B, containing Pd(II) complex **2.1** (6.7 mg, 1.2×10^{-2} mmol) and terpy (5.6 mg, 2.4×10^{-2} mmol) in 1.20 mL DMF; and solution C, containing Selectfluor (176 mg, 0.500 mmol) in 1.00 mL DMF. For each reaction, solution A (0.40 mL) was added to an NMR tube, followed by DMF (400 – *x* μL), solution C (*x* μL), and finally solution B (0.20 mL). Selectfluor concentrations in the range of 0.040–0.20 M were used. The tube was shaken rapidly to mix the reagents, and then the reaction was monitored via ^{19}F NMR spectroscopy at 25 °C, following evolution of the product signal at –123 ppm and integrating against the internal standard peak at –112 ppm. Product formation was monitored up to ~10% yield, and data in the 2–10% yield range was used to determine the initial rates. The data obtained are presented below.

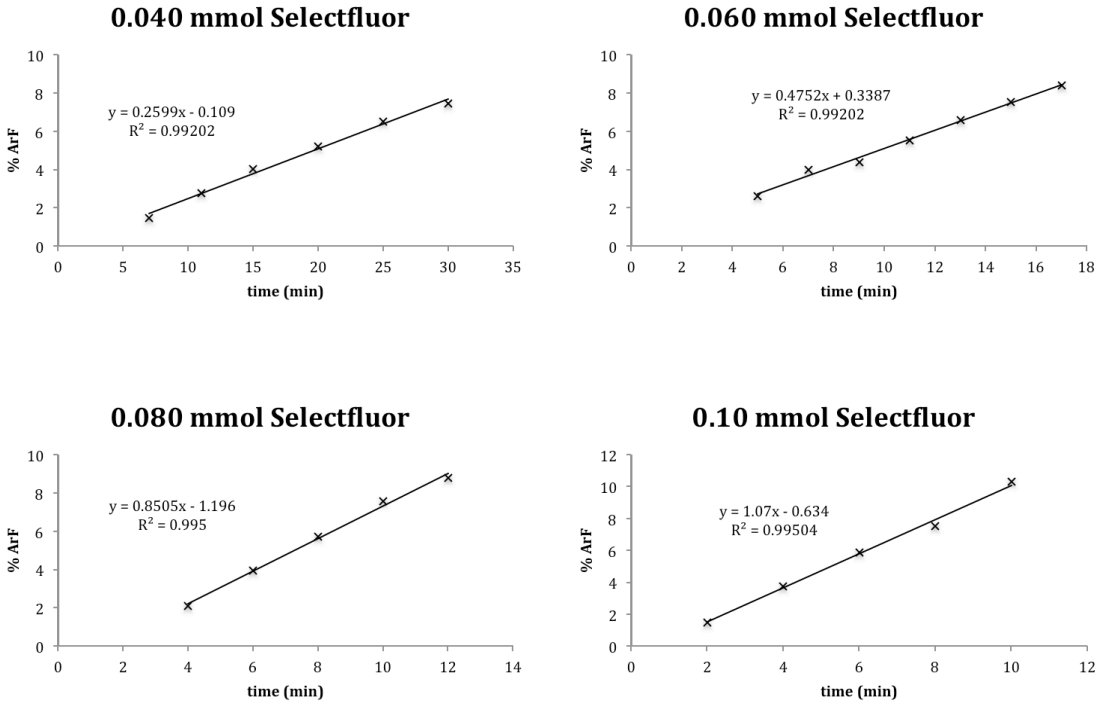

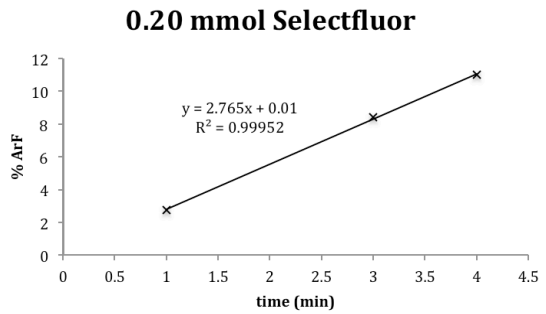

Initial Rate Kinetics of Aryl Trifluoroborate Dependence

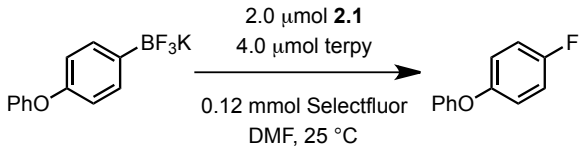

Three stock solutions were prepared: solution A, containing the aryl trifluoroborate (166 mg, 0.601 mmol) in 0.900 mL DMF; solution B, containing Pd(II) complex **2.1** (6.7 mg, 1.2×10^{-2} mmol) and terpy (5.6 mg, 2.4×10^{-2} mmol) in 1.20 mL DMF; and solution C, containing Selectfluor (255 mg, 0.720 mmol) and 1-fluoro-3-nitrobenzene (30.0 μL, 2.82×10^{-4} mol) as internal standard, in 3.00 mL DMF. For each reaction, solution A (x μL) was added to an NMR tube, followed by DMF ($300 - x$ μL), solution C (500 μL), and finally solution B (200 μL). Aryl trifluoroborate concentrations in the range of 0.020–0.20 M were used. The tube was shaken rapidly to mix the reagents, and then the reaction was monitored via ^{19}F NMR spectroscopy at 25 °C, following evolution of the product signal at –123 ppm and integrating against the internal standard peak at –112 ppm. Each reaction was monitored to approximately 6% yield, and yield was converted to an initial rate by dividing by the reaction time. The data obtained are presented in Figure 2.7.

Binding Constant Analysis

The equilibrium between **2.1** and **2.5** was probed experimentally using UV-vis spectroscopy. Exogenous terpy was added to a solution of **2.1** in DMF, and absorbance at 400 nm was measured. 400 nm was chosen based on the fact that neither **2.1** nor terpy display a significant absorption feature at this wavelength, but the absorption value at 400 nm displayed a notable increase when terpy was added to **2.1**. A titration experiment was carried out, and the measured binding isotherm is shown below (the plot shows overlaid data from two separate experiments):

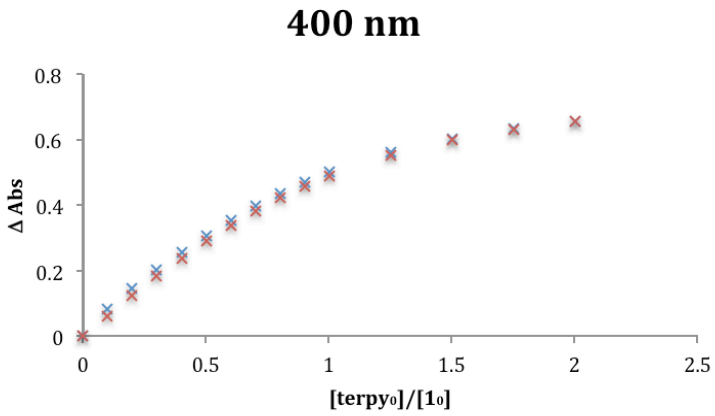

Fitting of the binding isotherm was performed using a 1:1 binding model between **2.1** and terpyridine,[21] which provided satisfactory results. The fitting gave an association constant (K_a) of 3×10^3 (± 19%). The output from the fitting program is given below, with K_a and the associated error analysis highlighted in red.

[21] Thordarson, P. *Chem. Soc. Rev.* **2011**, *40*, 1305.

Results from 1:1 fitting		
sum of squares (ss)	Standard error (SEy)	covariance of fit
0.001395689	0.007189728	0.001107889
Results for Ka	Results for other fitted parameters	
2711.11372	441.678802	432.3025342
%confidence interval on parameters (from asymptotic error):		
19.49414486	3.812721295	3.817393058

Isotopic Labeling Experiment[22]

Radiochemistry General Methods and Procedures

No-carrier-added [^{18}F]fluoride was produced from water 97% enriched in ^{18}O (Sigma-Aldrich®) by the nuclear reaction ^{18}O(p,n)^{18}F using a Siemens Eclipse HP cyclotron and a silver-bodied target at MGH Athinoula A. Martinos Center for Biomedical Imaging. The produced [^{18}F]fluoride in water was transferred from the cyclotron target by helium push. In the analysis of the ^{18}F-labeled compounds, isotopically unmodified reference substances were used for identification. Radioactivity was measured in a Capintec, Inc. CRC-25PET ion chamber. *Solvents and reagents for radiochemical experiments:* Acetonitrile, extra dry, (AcroSeal®) was purchased from Acros® and used as received. *N*,*N*-dimethylformamide was distilled from 4Å molecular sieves and stored under inert atmosphere. Water was obtained from a Millipore Milli-Q Integral Water Purification System. 18-crown-6 was sublimed. Potassium carbonate (≥99.99%) was purchased from Sigma-Aldrich® and used as received.

[^{18}F]Fluoride solution obtained from a cyclotron was loaded onto a Macherey-Nagel SPE Chromafix 30-PS-HCO3 cartridge that had been previously washed with 2.0 mL of 5.0 mg/mL K_2CO_3 in Millipore Milli-Q water and then 20 mL of Millipore Milli-Q water.

[22] Thanks to Constanze Neumann for performing the radiochemistry experiments.

After loading, the cartridge was washed with 2 mL of Millipore Milli-Q water. [^{18}F]Fluoride was eluted with 2.0 mL of a 5.0 mg/mL K_2CO_3 in Millipore Milli-Q water solution. The solution was diluted with 8.0 mL of acetonitrile providing 10 mL of 4:1 MeCN:H_2O solution containing 1.0 mg/mL K_2CO_3. 1.0 mL of this solution was then put in a conical vial that had been washed with acetone and deionized water and dried at 150 °C prior to use. 0.50 mL of a stock solution containing 18-crown-6 (26.2 mg/mL MeCN) was then added. The solution was evaporated at 108 °C with a constant nitrogen gas stream. At dryness, 0.5 mL of acetonitrile was added and evaporated at 108 °C with a constant nitrogen gas stream. Another 0.5 mL of acetonitrile was added and evaporated at 108 °C with a constant nitrogen gas stream to leave a white precipitate around the bottom and sides of the vial. The vial was purged with nitrogen, and sealed with a cap fitted with a septum. 0.4 mL of *N*,*N*-dimethylformamide was added and the conical vial was sonicated for 30 seconds before the solution was taken up in a syringe.

Procedure for Labeling Experiment

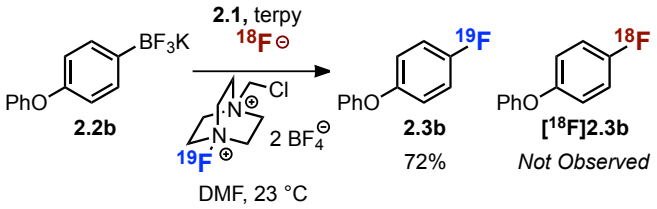

A 4 mL vial was charged with aryl trifluoroborate **2.2b** (5.0 mg, 0.018 mmol, 1.0 equiv), Selectfluor (6.4 mg, 0.018 mmol, 1.0 equiv), Pd(II) complex **2.1** (2.5 mg, 4.5×10^{-3} mmol, 0.25 equiv) and terpy (2.1 mg, 9.1×10^{-3} mmol, 0.50 equiv), and sealed with a cap fitted with a septum. A DMF solution (0.4 mL) of [^{18}F]fluoride, prepared and dried as described above, was added to the vial via the septum. The mixture was allowed to

stir for 15 minutes at 23 °C, and then a capillary tube was used to spot the solution on a silica gel TLC plate. The TLC plate was eluted with a 10% (v/v) mixture of Et_2O/pentane. The TLC plate was scanned with a Bioscan AR-2000 Radio TLC Imaging Scanner to determine [^{18}F]fluoride incorporation into the aryl fluoride product (**2.3b**), using an authentic sample of **2.3b** as a reference. The radio TLC scan is shown below, and indicates no [^{18}F]fluoride incorporation into the organic product:

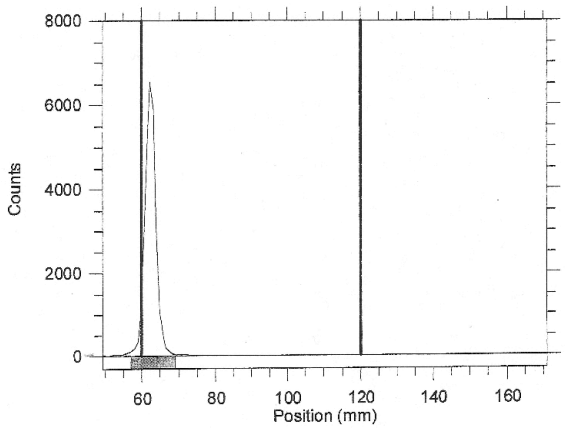

The radioactivity was allowed to decay over the course of 3 days, and then 1-fluoro-3-nitrobenzene (5.0 μL, 4.7×10^{-5} mol) was added to the vial as internal standard. The mixture was transferred to an NMR tube, and then the yield of aryl fluoride **2.3b** was determined to be 0.013 mmol (72%) via ^{19}F NMR spectroscopy, integrating against the internal standard peak at –112 ppm.

The result of the isotopic labeling experiment suggests that C–F bond formation in the Pd-catalyzed fluorination reaction does not occur via nucleophilic attack by fluoride.

Electrochemical Data

General Methods

Cyclic Voltammetry (CV) was performed using approximately 2 mg/mL solutions of the analyte in MeCN, with Bu_4NPF_6 (0.1 M) as the electrolyte. A glassy carbon working electrode was used, along with a Pt wire counter electrode and a non-aqueous Ag/Ag^+ reference electrode. CVs were obtained at a scan rate of 0.1 V/s or 0.05 V/s (indicated for each sample), and ferrocene was used as an external reference. All reported potentials are vs Fc/Fc^+ unless otherwise noted.

CV of $[(terpy)_2Pd][BF_4]_3$ (2.4)

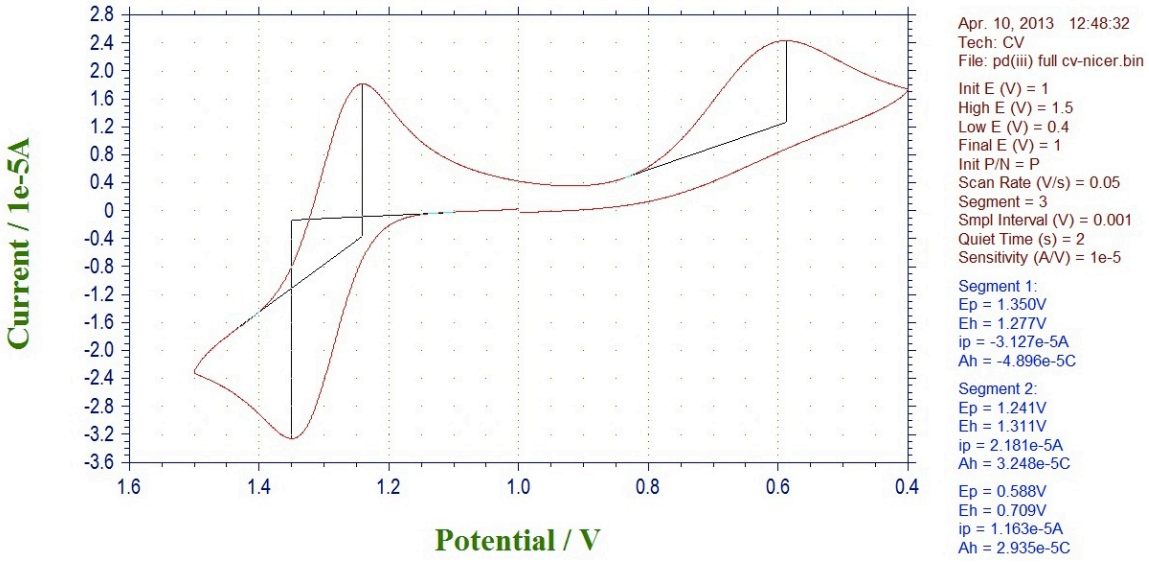

The reversible oxidation at 1.17 V (vs Fc/Fc^+) is assigned as the Pd(III)/Pd(IV) redox couple while the irreversible reduction wave at 460 mV (vs. Fc/Fc^+) is assigned as the Pd(III)/Pd(II) redox couple.

CV of [(terpy)Pd(MeCN)][BF_4]$_2$ (2.1) with added terpyridine

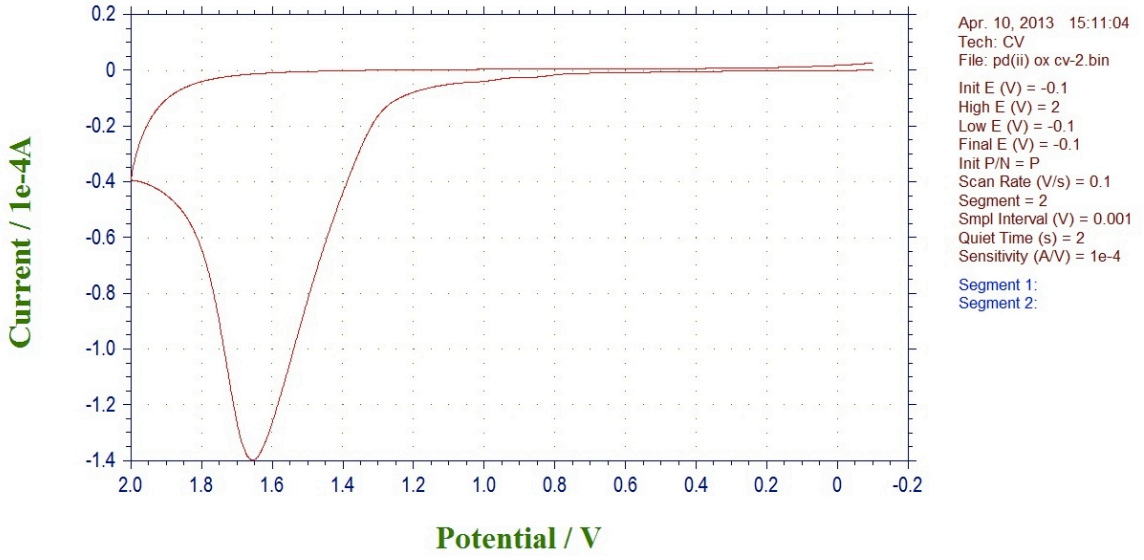

The only observed feature is an irreversible oxidation wave at 1.5 V (vs. Fc/Fc^+).

CV of terpyridine

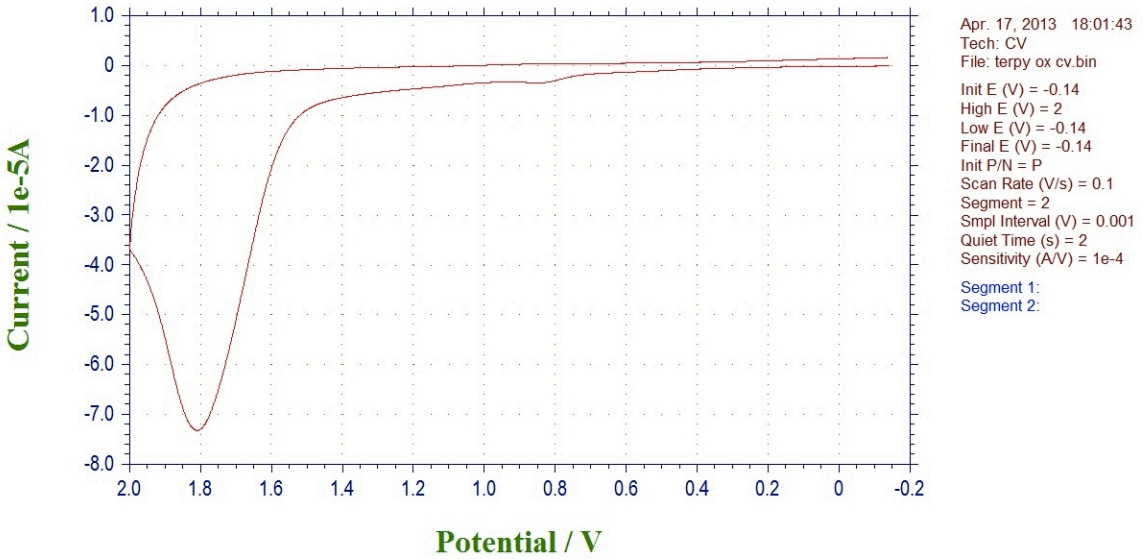

The only observed feature is an irreversible oxidation wave at 1.7 V (vs. Fc/Fc^+).

Discussion of electrochemical data

The absence of any reversible oxidation waves for the mixture of $[(terpy)Pd(MeCN)]^{2+}$ (**2.1**) and terpyridine, and the observation of an irreversible reduction wave at 460 mV for $[(terpy)_2Pd]^{3+}$ (**2.4**) indicates that the oxidation of **2.1** to **2.4** in the presence of terpyridine and Selectfluor does not occur via an outer-sphere S.E.T. pathway.

General Procedure for DFT Calculations

Density functional theory (DFT) calculations were performed using Gaussian09[23] at the Odyssey cluster at Harvard University. Geometry optimizations were carried out using the atomic coordinates from crystal structures as starting points. The unrestricted wave function was used for ground state optimizations. BS I includes SDD quasirelativistic pseudopotentials on Pd (MWB28) and Cl (MWB10) with basis sets (Pd: (8s7p6d)/[6s5p3d][24]; Cl: (4s5p)/[2s3p][25]) extended by polarization functions (Pd: f, 1.472[26]; Cl: d, 0.640[27]), and 6-31G(d,p)[28] on H, C, O, N, F. All geometry optimizations

[23] Frisch, M. J.; Trucks, G. W.; Schlegel, H. B.; Scuseria, G. E.; Robb, M. A.; Cheeseman, J. R.; Scalmani, G.; Barone, V.; Mennucci, B.; Petersson, G. A.; Nakatsuji, H.; Caricato, M.; Li, X.; Hratchian, H. P.; Izmaylov, A. F.; Bloino, J.; Zheng, G.; Sonnenberg, J. L.; Hada, M.; Ehara, M.; Toyota, K.; Fukuda, R.; Hasegawa, J.; Ishida, M.; Nakajima, T.; Honda, Y.; Kitao, O.; Nakai, H.; Vreven, T.; , J. A. Montgomery, J.; Peralta, J. E.; Ogliaro, F.; Bearpark, M.; Heyd; J. J. Brothers, E.; Kudin, K. N.; Staroverov, V. N.; Normand; J. Raghavachari, K.; Rendell, A.; Burant, J. C.; Iyengar, S. S.; Cossi, J. M.; Rega, N.; Millam, J. M.; Klene, M.; Knox, J. E.; Cross, J. B.; Bakken, V.; Adam, C.; Jaramillo, J.; Gomperts, R.; Stratmann, R. E.; Yazyev, O.; Austin, A. J.; Cammi, R.; Pomelli, C.; Ochterski, J. W.; Martin, R. L.; Morokuma, K.; Zakrzewski, V. G.; Voth, G. A.; Salvador, P.; Dannenberg, J. J.; Dapprich, S.; Daniels; A. D. Farkas, O.; Foresman, J. B.; Ortiz, J. V.; Cioslowski; J. Fox, D. J. *Gaussian 09, Revision A.02*; Gaussian, Inc.: Wallingford CT, 2009.

[24] (a) Andrae, D.; Häussermann, U.; Dolg, M.; Stoll, H.; Preuss, H. *Theor. Chim. Acta* **1990**, *77*, 123-141. (b) Andrae, D.; Häussermann, U.; Dolg, M.; Stoll, H.; Preuss, H. *Theor. Chim. Acta* **1991**, *78*, 247-266.

[25] Bergner, A.; Dolg, M.; Küchle, W.; Stoll, H.; Preuss, H. *Mol. Phys*. **1993**, *30*, 1431-1441.

[26] Ehlers, A. W.; Böhme, M.; Dapprich, S.; Gobbi, A.; Höllwarth, A.; Jonas, V.; Köhler, K. F.; Stegmann, R.; Veldkamp, A.; Frenking, G. *Chem. Phys. Lett*. **1993**, *208*, 111-114.

were performed using either the B3PW91 or the M06 functional with the BS I basis set. Molecular orbitals were generated using an isosurface value of 0.03 with M06/BS I or B3PW91/BS I. Calcuation of atomic contributions to the frontier molecular orbitals (Mulliken contribution), as well as analysis of simulated UV-vis spectra, was performed using Chemissian.[29] Images were generated using Chem3D or GaussView5.[30]

General Procedure for X-ray Crystallographic Analysis

A crystal was mounted on a nylon loop using Paratone-N oil, and transferred to a Bruker APEX II CCD diffractometer (MoKα radiation, λ=0.71073 Å) equipped with an Oxford Cryosystems nitrogen flow apparatus. The sample was held at 100 K during the experiment. The collection method involved 0.5° scans in ω at 28° in *2*θ. Data integration down to 0.82 Å resolution was carried out using SAINT V7.46 A (Bruker diffractometer, 2009) with reflection spot size optimisation. Absorption corrections were made with the program SADABS (Bruker diffractometer, 2009). The structure was solved by the direct methods procedure and refined by least-squares methods against F^2 using SHELXS-97 and SHELXL-97 (Sheldrick, 2008). Non-hydrogen atoms were refined anisotropically, and hydrogen atoms were allowed to ride on the respective atoms. Restraints on bond lengths and constraints of the atomic displacement parameters on each pair of disorder fragments (SADI and EADP instructions of SHELXL97), as well as the restraints of the atomic displacement parameters (SIMU/DELU instructions of

---

[27] Höllwarth, A.; Böhme, M.; Dapprich, S.; Ehlers, A. W.; Gobbi, A.; Jonas, V.; Köhler, K. F.; Stegmann, R.; Veldkamp, A.; Frenking, G. *Chem. Phys. Lett*. **1993**, *208*, 237-240.

[28] Hariharan, P. C.; Pople, J. A. *Theor. Chim. Acta* **1973**, *28*, 213-222.

[29] *Chemissian*, Version 3.3; © Skripnikov Leonid 2005-2012; www.chemissian.com

[30] Dennington, R., II; Keith, T. A.; Millam, J. M. *GaussView*, Version 5.0.8; Semichem, Inc.

SHELXL97) if necessary, have been applied for the disorder refinement. Graphics were produced using the CystalMaker 8.6 software program (©1994-2012 CrystalMaker Software Ltd.).

Computer programs: *APEX2* v2009.3.0 (Bruker-AXS, 2009), *SAINT* 7.46A (Bruker-AXS, 2009), *SHELXS97* (Sheldrick, 2008), *SHELXL97* (Sheldrick, 2008), Bruker *SHELXTL*.